NAM

Experimental campaign on Reinforced Concrete buildings typical of the Groningen region

Cyclic testing of a full-scale two-storey Reinforced Concrete precast wall-slab-wall structure representative of the Groningen building stock (EUC-BUILD4).

Eucentre

Brunesi E., Peloso S., Pinho R. and Nascimbene R.

Date June 2017

Editors Jan van Elk & Dirk Doornhof

General Introduction

The experimental and study program into the seismic response of buildings initially focussed on masonry buildings (Ref. 1 to 8), with many tests and experiments on masonry building material, walls and full-scale buildings. Both a terraced house and a detached house have been tested by EUcentre in Pavia (Italy), with follow-up experiments on the first floor and roof of the terraced house by LNEC in Lisbon (Portugal).

However, in Groningen, many buildings have been constructed using pre-cast concrete elements. Often these buildings are not easily recognized as the pre-cast concrete elements making up the structural system are behind masonry veneers, giving the building a masonry appearance.

To better understand the seismic behaviour of the precast concrete panels commonly used in construction in The Netherlands (e.g. Heembeton and Alvon panels and Dycore floors) experiments were conducted. Especially, the connections between the panels are important to understand the seismic response of a pre-cast concrete building (Ref. 9).

The current report describes experimental cyclic testing of a reinforced precast concrete prototype. The test structure (EUC-BUILD4 specimen) was designed to combine several common features of this type of structures and it was built directly on the shaking table of EUCENTRE laboratory by a Dutch contractor.

This document describes the testing campaign performed at EUCENTRE laboratory in 2017, executed in collaboration with the DICAr Laboratory of the University of Pavia (UNIPV). The experimental programme included thus:

- Compression testing of concrete samples;
- Tensile testing of steel connectors;
- Friction testing of felt material (triplet specimens);
- Quasi-static cyclic testing of full-scale specimen in as-built and “retrofitted” configurations.

The results of these experiments are used in the preparation of fragility curves for these buildings (Ref. 10).

References

1. Eucentre Shake-table Test of Terraced House Modelling Predictions and Analysis Cross Validation, staff from ARUP, Eucentre (Pavia) and TU Delft, November 2015 [this document also includes; (1) Instruments full-scale test-house Eucentre Laboratory, (2) Protocol for Shaking Table Test on Full Scale Building (Eucentre) V_1, and (3) Selection of Acceleration Time-Series for Shake Table Testing of Groningen Masonry Building at the EUCENTRE, Pavia, all three by staff from Eucentre (Pavia)],
2. Collapse shake-table testing of terraced house (LNEC-BUILD1), Eucentre and LNEC (U. Tomassetti, A. A. Correia, F. Graziotti, A.I. Marques, M. Mandirola, P.X. Candeias), 1st September 2017.
3. LNEC-BUILD1: Modelling predictions and analysis cross-validation, ARUP, TU Delft, Eucentre and Mosayk (several staff members from all four institutions), 8th September 2017.
4. Using the Applied Element Method to model the collapse shake-table testing of a URM cavity wall structure (LNEC-BUILD1), Mosayk (D. Malomo, R. Pinho), 31st October 2017.
5. Using the Applied Element Method to model the collapse shake-table testing of a terraced house roof substructure (LNEC-BUILD2), Mosayk (D. Malomo, R. Pinho), 31st October 2017.
6. Experimental campaign on a clay URM full-scale specimen representative of the Groningen building stock (EUC-BUILD2), Eucentre (F. Graziotti, U. Tomassetti, A. Rossi, B. Marchesi, S. Kallioras, M. Mandirola, A. Fragomeli, E. Mellia, S. Peloso, F. Cuppari, G. Guerrini, A. Penna, G. Magenes, G), 20th July 2016.
7. EUC-BUILD2: Modelling predictions and analysis cross-validation of detached single-storey URM Building, ARUP, TU Delft, Eucentre and Arcadis (several staff members from all four institutions), 30th September 2016
8. Shake-table test up to collapse on a roof substructure of a Dutch terraced house (LNEC-BUILD2), Eucentre and LNEC (A.A. Correia, A.I. Marques, V. Bernardo, L. Grottoli, U. Tomassetti, F. Graziotti), 31st October 2017.
9. Cyclic testing of precast panel connections for RC precast wall-slab-wall structures representative of the Groningen building stock. Eucentre (E. Brunesi, R. Nascimbene), 22nd October 2015.
10. Report on the v5 fragility and consequence models for the Groningen Field, H. Crowley and R. Pinho, 31st October 2017.

NAM

Title	**Experimental campaign on Reinforced Concrete buildings typical of the Groningen region** **Cyclic testing of a full-scale two-storey Reinforced Concrete precast wall-slab-wall structure representative of the Groningen building stock (EUC-BUILD4).**		**Date**	June 2017
			Initiator	NAM
Autor(s)	**Brunesi E., Peloso S., Pinho R. and Nascimbene R.**	**Editors**	Jan van Elk and Dirk Doornhof	
Organisation	EUcentre	**Organisation**	NAM	
Place in the Study and Data Acquisition Plan	Study Theme: Seismic Response Buildings Comment: The experimental and study program into the seismic response of buildings initially focussed on masonry buildings (Ref. 1 to 8), with many tests and experiments on masonry building material, walls and full-scale buildings. Both a terraced house and a detached house have been tested by EUcentre in Pavia (Italy), with follow-up experiments on the first floor and roof of the terraced house by LNEC in Lisbon (Portugal). However, in Groningen, many buildings have been constructed using pre-cast concrete elements. Often these buildings are not easily recognized as the pre-cast concrete elements making up the structural system are behind masonry veneers, giving the building a masonry appearance. To better understand the seismic behaviour of the precast concrete panels commonly used in construction in The Netherlands (e.g. Heembeton and Alvon panels and Dycore floors) experiments were conducted. Especially, the connections between the panels are important to understand the seismic response of a pre-cast concrete building (Ref. 9). The current report describes experimental cyclic testing of a reinforced precast concrete prototype. The test structure (EUC-BUILD4 specimen) was designed to combine several common features of this type of structures and it was built directly on the shaking table of EUCENTRE laboratory by a Dutch contractor. This document describes the testing campaign performed at EUCENTRE laboratory in 2017, executed in collaboration with the DICAr Laboratory of the University of Pavia (UNIPV). The experimental programme included thus: ▪ Compression testing of concrete samples; ▪ Tensile testing of steel connectors; ▪ Friction testing of felt material (triplet specimens); ▪ Quasi-static cyclic testing of full-scale specimen in as-built and “retrofitted” configurations.			

	The results of these experiments are used in the preparation of fragility curves for these buildings (Ref. 10).
Directliy linked research	(1) Shake Table Tests (2) Risk Assessment
Used data	Full experimental and Modelling program into seismic response URM & non-URM buildings.
Associated organisation	NAM
Assurance	Independent Assurance Panel

Nederlandse Aardolie Maatschappij B.V.

Schepersmaat 2, Postbus 28000, 9400 HH Assen

Experimental campaign on RC buildings typical of the Groningen region: cyclic testing of a precast specimen

EUCENTRE
FOR YOUR SAFETY.

Via Ferrata 1, 27100 Pavia, Italy
Tel. +39.0382.516911 Fax. +39.0382.529131
http://www.eucentre.it
email: info@eucentre.it

LAB AND TESTS RESPONSIBLE	DOCUMENT AUTHOR	REVIEWER
Filippo Dacarro	Emanuele Brunesi	Rui Pinho
Signature	Signature	Signature
Issue: 22/06/2017	Document type:	File name: EUC_BUILD4-test_campaign_report.pdf
Revision: 31/08/2017	Technical report	
Revision: 24/09/2017	pages: 257	Protocol 173/2017U
Revision:		

Cite as:

Brunesi E., Peloso S., Pinho R., Nascimbene R. (2017). *Cyclic testing of a full-scale two-storey RC precast wall-slab-wall structure representative of the Groningen building stock*. Report EUC173/2017U, European Centre for Training and Research in Earthquake Engineering (EUCENTRE), Pavia, Italy.

EUCENTRE FOUNDATION
European Centre for Training and Research in Earthquake Engineering

Table of contents

1 Preamble

As discussed in Arup report *229746_031_NOT2008_Rev0.05_Issue EUC-BUILD-4 Prototype building description*, reinforced concrete buildings in the Groningen region largely consist of what are herein termed wall-slab-wall structures, featuring no columns or beams, but only slabs and walls.

These structures can be found in both cast-in-place (tunnel construction or not) as well as precast configurations, and this report deals with the experimental programme aimed at cyclically testing the latter (please refer to Arup set of drawings *229746_031.0_DRW2007_Rev0.05_Issue_EUC-BUILD-4_5 SWb Specimen drawings* for construction details on the selected prototype structure).

Dynamic testing of another precast specimen (EUC-BUILD5) and cyclic testing of a cast-in-place prototype (EUC-BUILD3) are described in two separate companion reports.

2 Introduction

2.1 Description of test programme

This report describes experimental testing activities that were undertaken within the framework of the research programme for hazard and risk of induced seismicity in Groningen sponsored by the Nederlandse Aardolie Maatschappij BV. As part of NAM data acquisition and analysis programme aimed at developing a seismic hazard and risk model for induced seismicity in the Groningen area, pseudostatic cyclic tests were performed on a full-scale reinforced precast concrete wall-slab-wall structure, representative of a building typology that was found to be very common in that region. Auxiliary characterization tests were carried out as well.

Laboratory tests were thus performed on a full-scale two-storey one-bay reinforced precast concrete prototype, which was adapted to the needs imposed by laboratory constraints. The index building, namely EUC-BUILD4 specimen, was designed to combine several common features of this type of structures (please refer to Arup report: *229746_031_NOT2008_Rev0.05_Issue EUC-BUILD-4 Prototype building description* for details on the selected design concept) and it was built directly on the strong floor of EUCENTRE laboratory by a Dutch contractor.

This document describes the testing campaign performed at EUCENTRE laboratory in 2017. Some of the tests listed above were also conducted by EUCENTRE technicians at the DICAr Laboratory of University of Pavia (UNIPV). The experimental programme included:

- Compression testing of concrete samples;
- Tensile testing of steel connectors;
- Friction testing of felt material (triplet specimens);
- Quasi-static cyclic testing of full-scale specimen in as-built and “retrofitted” configurations.

The complete list of the tests carried out at EUCENTRE laboratory is reported in Table 1.

Table 1. Summary table of tests and dates.

Laboratory	Activity name	Test type	Day of test
UNIPV	Concrete cubes	Compression – Characterization	Apr 03, 2017
UNIPV	Concrete cubes	Compression – Characterization	Apr 11, 2017
UNIPV	Felt material (triplet test)	Friction – Characterization	Apr 11-13, 2017
EUCENTRE	EUC-BUILD4 (as-built)	Cyclic full-scale specimen	Apr 11-13, 2017
EUCENTRE	EUC-BUILD4 (retrofitted)	Cyclic full-scale specimen	Apr 18-19, 2017
UNIPV	Steel connectors	Tensile – Characterization	June 06, 2017

3 Nomenclature

Symbol	Definition
μ	Static friction coefficient of felt material
σ	Compressive stress applied to triplet specimen
τ	Shear stress computed by means of triplet test results
A_l	Lateral surface of triplet specimens, parallel to the vertical shear force
F_H	Horizontal force applied to triplet specimen
F_V	Vertical force imposed to triplet specimen and measured during testing

4 Auxiliary material characterization tests

As normally foreseen during all experimental campaigns, auxiliary material tests were performed to characterise the behaviour of concrete, steel connectors and felts. In more detail:

- Cubic concrete samples underwent standard tests for determining the compressive resistance of concrete. Tests were performed on both the concrete cubes delivered by the producer of precast wall panels and the ones corresponding to the slab topping concrete. Six specimens were indeed prepared during the casting of concrete for floor finishing;
- Tensile tests were carried out to define the ultimate strength and the ultimate deformation of the smooth steel bars/connectors used for panel-to-panel connections. The complete stress-strain relationship up to rupture could not be recorded because of their short length;
- Triplet tests were performed to evaluate the friction coefficient of felt material under three different levels of axial load that were selected to be representative of the range of axial load values present in the walls of EUC-BUILD4 specimen.

As mentioned above, in addition to standard characterization tests for concrete and steel anchors, the latter being used for wall-to-wall three-way connections, nine triplet specimens such as the one shown in Figure 1, were each tested under three different levels of axial load, for a total of 27 tests, so as to estimate, with a good level of confidence, the mechanical/frictional properties of the felt material that was found to be dominating in the response of the full-scale specimen, as expected and discussed later on.

Figure 1. Triplet test for friction testing of felt material.

As shown in Figure 1, each triplet specimen consists of three concrete blocks and two layers of felt material placed in-between them. The specimen is positioned in the testing apparatus, between two steel plates, while it is supported by roller bearings. A compression force (representative of the range of axial load values present in EUC_BUILD4 walls) is applied at the two lateral faces of the specimen, before the application of vertical action by means of a MTS actuator in displacement control. The horizontal/axial load is kept constant during each single test and the vertical shear force is applied to the central concrete block. Three different levels of axial load were selected to be imposed for each single triplet specimen. The only aim of the 27 tests planned is to determine the level of shear force corresponding to the activation of sliding, which in turn allows determination of the static friction coefficient of the felt material. As specified later on, the force-time response recorded for each one of the specimens is provided in the following paragraphs, even though the only information one can actually derive within the framework of this type of experimental test is the friction coefficient, in a static fashion. Force-displacement relationships are thus not informative, especially after the sudden activation of the sliding mechanism.

4.1 Tests for materials characterization of concrete and steel anchors

Mechanical properties of steel connectors and concrete were measured by means of characterization tests performed in compliance with current European standards (i.e. UNI EN ISO 15630-1 and UNI EN 12390-3-4-7). It is worthwhile to mention that concrete class C35/45 according to Eurocode 2 was used for precast concrete walls of EUC-BUILD4 full-scale prototype, whilst concrete strength class C53/65 was adopted for the hollow core slabs. The steel type that was chosen for the anchors of the three-way panel-panel joints is apparently S355. Noteworthy is that the compressive strength values obtained by the characterization tests reported in the following section have little bearing on the response of the full-scale specimen, which is instead dominated by issues of friction/sliding and connection behaviour (see Chapter 6).

4.1.1 Compressive strength of concrete

Standard compressive tests were performed on concrete cubes corresponding to both the wall panels and the slab topping concrete. Those tests were carried out on concrete samples after a minimum 28 days curing period so that one can characterise the full compressive resistance of concretes pertaining to both portions of the full-scale specimen. In particular, six concrete samples were prepared during the casting of slab concrete topping, whilst another fifteen cubes were delivered by the producer of the precast wall panels. The latter were tested on April 3rd (i.e. after 40 days of casting) and on April 11th (i.e. first day of testing of EUC-BUILD4 specimen).

4.1.1.1 Cubic specimens – Wall panels

Standard compression tests were performed on three concrete cubes (wall panels) after 40 days of casting, at least, and the results are reported below (see Table 2), for reference. The characterization tests were carried out following the European Norm 12390 – “Testing Hardened Concrete” (UNI EN 12390-3-4-7).

Table 2. Material characterization tests: cubic samples after 40 days of casting (i.e. April 3rd).

ID	Size [mm^3]	Mass [kg]	Mass/Vol. [kg/m^3]	Load [kN]	Resistance [N/mm^2]	Type of failure
1	148.5 x 149.8 x 150.0	7.65	2293	1422	63.94	S
2	148.5 x 149.8 x 149.9	7.71	2312	1334	59.97	S
3	149.2 x 149.8 x 149.9	7.85	2343	1472	65.84	S

It is worth noting that S stands for satisfactory. Moreover, other twelve cubic samples were tested on April 11th (i.e. first day of testing of EUC-BUILD4 specimen) and the obtained concrete strength of the additional concrete cubes are collected in Table 3. It can be noted that the values of strength indicated in Table 2 and Table 3 for the concrete samples refer to the actual resistance measured on those cubes (i.e. applied force divided by the area of the concrete cube), and not to their cylindrical equivalent, which is instead typically estimated by multiplying the cubic strength with a reduction factor in the 0.80-0.85 range.

Table 3. Material characterization tests: cubic samples tested on April 11th – wall panels.

ID	Size [mm^3]	Mass [kg]	Mass/Vol. [kg/m^3]	Load [kN]	Resistance [N/mm^2]	Type of failure
1	149.5 x 149.8 x 149.9	7.74	2306	1373	61.33	S
2	148.6 x 150.0 x 150.1	7.72	2307	1452	65.14	S
3	150.3 x 149.3 x 149.4	7.88	2350	1413	62.95	S
4	150.1 x 150.4 x 150.5	7.89	2322	1432	63.44	S
5	148.6 x 149.7 x 149.8	7.69	2308	1422	63.94	S
6	149.0 x 149.7 x 149.8	7.69	2301	1521	68.17	S
7	148.8 x 149.7 x 149.7	7.74	2321	1315	59.01	S
8	151.3 x 149.7 x 149.8	7.89	2325	1452	64.10	S
9	149.3 x 149.8 x 149.9	7.77	2318	1403	62.72	S
10	149.9 x 149.7 x 149.7	7.80	2322	1324	59.02	S
11	149.5 x 149.7 x 149.8	7.81	2330	1324	59.18	S
12	149.1 x 149.8 x 149.9	7.83	2339	1432	64.13	S

The differences in compressive strength are almost negligible. The additional twelve cubic samples (Table 3) present results that are very much aligned with those of the three samples tested on April 3rd (Table 2), for which an average compressive strength of about 63.2 MPa can be established. The average compressive resistance computed from the values reported in Table 3 is equal to 62.8 MPa, whilst the average strength computed from the fifteen cubes is approximately 62.9 MPa. Moderate standard deviations is also observed.

4.1.1.2 Cubic specimens – slab topping

Compression tests were carried out on six samples corresponding to the slab topping concrete, for an average resistance of 51.1 MPa. Noteworthy is that three cubes per each floor were tested and the obtained values of concrete resistance are reported below (see Table 4).

Table 4. Material characterization tests: cubic samples tested on April 11th – slab topping.

ID	Size [mm^3]	Mass [kg]	Mass/Vol. [kg/m^3]	Load [kN]	Resistance [N/mm^2]	Type of failure
1	148.9 x 149.7 x 149.8	7.77	2327	1030	46.21	S
2	148.5 x 149.7 x 149.8	7.77	2333	1256	56.48	S
3	148.8 x 150.3 x 150.2	7.76	2310	1187	53.08	S
4	150.2 x 150.2 x 150.1	7.79	2300	1246	55.22	S
5	150.1 x 149.8 x 149.9	7.80	2314	1050	46.68	S
6	150.1 x 150.7 x 150.6	7.90	2319	1109	49.01	S

It is worth noting that, also in this case, use was made of the European Norm 12390 – "Testing Hardened Concrete" (UNI EN 12390-13). The first three cubic samples refer to the slab topping of the second floor, whereas the remaining ones refer to the topping of the first floor level. As mentioned above, an average compressive strength of approximately 51.1 MPa can be established from the six cubes tested. The differences in compressive strength are once again relatively moderate, although slightly higher than those observed in the case of concrete samples corresponding to wall panels.

As a general consideration, it is recalled that concrete properties will have a minor influence on the behaviour of EUC-BUILD4 specimen, which is instead governed by the flexural response of steel connectors and the frictional force transfer between the slabs and the walls. Characterization tests of anchors (see Section 4.1.2) and felts (Section 4.2) are thus more significant.

4.1.2 Tensile tests of steel anchors for panel-to-panel connections

Precast concrete technology in the Netherlands (and worldwide) is highly-standardised, in terms of both the building system and the construction process. The same applies to the connections between the elements, that, in this construction system, are primarily constituted by mortar and welded joints (conform to NEN-EN 287-1), as well as felts and mechanical anchors (please refer to Arup report: *229746_031_NOT2008_Rev0.05_Issue EUC-BUILD-4 Prototype building description* for details on the selected design concept and to Eucentre report: *NAM_Project-precast_panels_testing_report – EUC319/2015U*). In particular, wall-to-wall joints are constituted by mechanical connections that can be either two-way or three-way anchorages, depending on if two contiguous panels are linked or not with a perpendicular stability/shear wall.

As shown in Figure 2 and Figure 3, small niches are usually created in correspondence to the inner edge of each wall segment in order to arrange the panel-to-panel connections at different positions up to the height of the panel. Figure 2 and Figure 3 present photographs of mechanical connectors and anchoring system that is composed of bolts and steel plates that are typically used to fasten the hook reinforcement to the external longitudinal rebar of each panel segment. After the anchors are lodged into the niches, a low-strength mortar is adopted for the injection grout. An example of the execution of these joints is provided in Figure 3 as well.

Of paramount importance is therefore the characterization of mechanical properties of those anchors that were observed to fail, by a flexural mechanism, during the testing of EUC-BUILD4 specimen. Standard tensile tests on those smooth steel rebars were undertaken at the DICAr Laboratory of the University of Pavia on June 6th, and the corresponding stress-strain relationships

(not up to rupture) are presented in Figure 4. Furthermore, Table 5 collects the prevailing information obtained by this auxiliary testing campaign.

Figure 2. Representative example of anchoring system for wall-to-wall connection.

Figure 3. Arrangement of hook reinforcement in EUC-BUILD4 specimen and flexural failure mechanism.

Six samples were tested on June 6th. As one may notice, the yield strength is roughly equal to 600 MPa, which, perhaps coincidentally, corresponds to the yield strength of previously tested steel samples from one of the buildings in Groningen (which was also around 600 MPa) and to the yield strength of the smooth reinforcing bars that were used for EUC-BUILD3 specimen. It can also be noted that the stress-strain relationships reported in Figure 4 reveal a fairly stable behaviour with pronounced and well-rounded post-incipient-yielding branch.

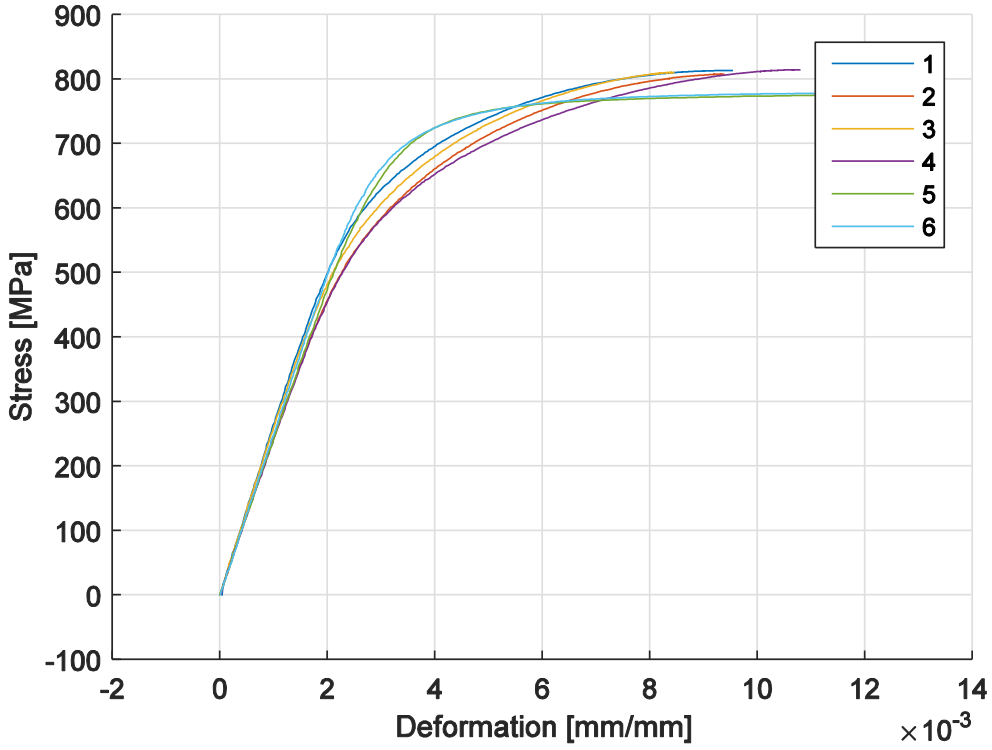

Figure 4. Tensile tests of steel anchors: stress-strain relationships of 10 mm diameter bars.

As reported in Table 5, two types of connectors, each of which having a specific length, were tested and the following values of maximum stress and elastic modulus are obtained. The Young modulus was computed as a secant value evaluated between 100 MPa and 300 MPa.

Table 5. Material characterization tests: steel connectors tested on June 6th.

Sample	Length of sample [mm]	Elastic Modulus(*) [MPa]	Maximum stress [MPa]
1	100	262.30 x10^3	812.82
2	100	237.98 x10^3	807.41
3	100	250.39 x10^3	809.81
4	100	236.20 x10^3	814.05
5	70	236.99 x10^3	775.86
6	70	249.29 x10^3	777.57
Mean values		245.53 x10^3	799.59

(*) Secant value evaluated between 100 MPa and 300 MPa

Noteworthy is that the material testing of the connectors and, hence, the corresponding stress-strain curves could be affected by the short length of the available bars (which prevents appropriate fixing

to the uniaxial testing machine). Although this might imply an increase of the measured modulus of elasticity, yield strength (and stress counterparts, more in general) can be on the other hand referred to as slightly more reliable estimates.

The above being stated, it also turns out from the stress-strain relationships reported in Figure 4 that 70 mm- and 100 mm-long anchors are characterised by different responses. Whilst long connectors have shown a well-rounded post-yielding branch, short ones have a steeper branch for strains in the range $2 \cdot 10^{-3}$ – $4 \cdot 10^{-3}$. After the latter value is exceeded, the stress-strain relationship suddenly drops, featuring an almost flat post-yielding branch. As also clarified in Table 5, this discrepancy becomes evident in terms of maximum stress.

As discussed above, these characterization tests have not been carried out in ideal conditions, given the impossibility of extracting from the connectors steel samples with the necessary length (50 cm), which might explain why the Young Modulus' values are higher than what is typically found in the literature for steel. For the same reason, it is believed that the stress-strain curves reported in Figure 4 are not necessarily fully reliable and the same applies to the trends obtained for larger levels of strain that in the end are not shown therein.

4.2 Triplet tests for characterization of felt material

Considering that the experimental response of EUC-BUILD4 specimen is supposed to be dominated since the early stages of cyclic testing by issues of sliding and connection behaviour (the latter ones being expected for drift levels larger than those corresponding to the former), friction testing of felt material is a key activity of this campaign of tests because it allows an estimate of the force transfer between the hollow core slabs and the precast walls underneath them. Needless to say that, in the full-scale specimen, like in several existing buildings of this type, no steel rebars connect the first with the second-story walls through the floor, and the same applies to the wall-slab connection at the roof level. Slabs are simply supported onto the precast walls without any rationally-conceived (or not) mechanical device, which in turn implies that the entire lateral-force resisting system merely relies on the shear friction transferred by the felts.

In light of this, nine triplet specimens consisting of concrete bricks and felt layers of the same thickness of that used for the full-scale specimen were each tested under three different levels of axial load, for a total of 27 tests (which in reality ended up by being 25, since in two cases the test could not be successfully completed). Such an approach was meant to assess variations in the friction coefficient of the felt material under consideration as a consequence of changes in the imposed axial/horizontal load, in any case selected to be representative of the range of axial load values present in the walls of EUC-BUILD4 specimen. Worthwhile to mention is also that different combinations of axial force were applied in such way that any eventual sensitivity to the loading sequence could be determined as well.

Despite the fact that testing of triplets is based on well-known and established methods, it is mostly applied to the case of masonry structures. As such, some key aspects of both experimental setup and procedure are presented in the following as background information for interested readers. The full set of experimental results is then reported in Paragraph 4.2.2, whereas the main trends derived are discussed in Paragraph 4.2.3 along with a summary of key data.

4.2.1 Experimental setup and procedure

Figure 5 shows a schematic of triplet specimens that consist of three concrete bricks and two layers of felt material placed in-between them. As presented in Figure 6, the specimen is positioned in the testing apparatus, between two steel plates, while it is supported by roller bearings. Steel rods are used to post-tension the specimen, applying a compression (representative of the range of axial load values present in EUC_BUILD4 walls) to the two lateral faces of it. Figure 6 and Figure 7 present a view of testing apparatus and details of the adopted experimental setup. The horizontal/axial load is kept constant during each single test and the vertical shear force is applied, in displacement control, to the central concrete block by means of an MTS actuator.

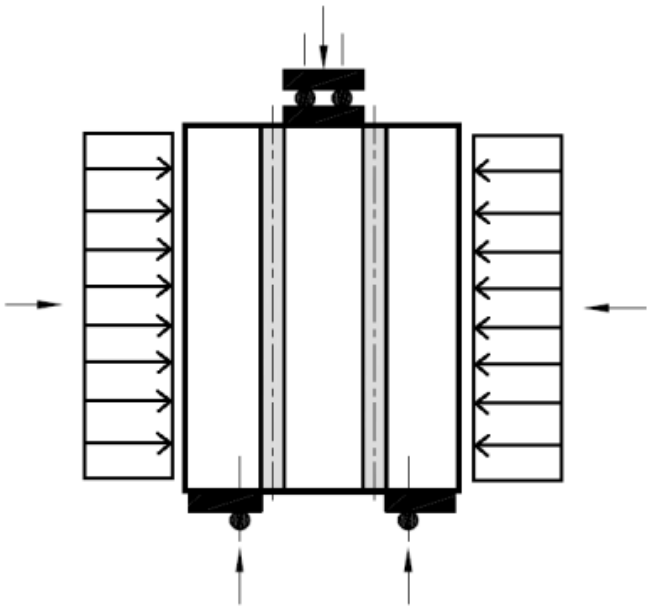

Figure 5. Friction testing of felt material: application of horizontal and vertical forces.

As previously mentioned, three levels of horizontal/axial load, corresponding to 0.2 MPa, 0.4 MPa and 0.6 MPa, were chosen for each single triplet specimen, with the sequence of their application being also varied from one test to the other. The compressive load is meant to be uniformly distributed on the faces of the specimen and the vertical shear force is applied with a very low velocity. The horizontal force (F_H) and the vertical force (F_V) were measured during the tests and permitted one to determine both the shear stress (τ) and friction coefficient of felt material (μ), for a given compressive stress (σ).

The main aim of this type of test is to determine the level of shear force corresponding to the activation of sliding (see e.g. Figure 8), which in turn allows determination of the static friction coefficient of the felt material. Noteworthy is that, in two cases (out of the 27 planned), the test was not successfully completed because of the disassembling of the triplet specimen when the axial load was changed from one level to another.

Figure 6. Experimental setup for friction testing of felt material.

Figure 7. Testing apparatus and installed/assembled triplet specimen.

Figure 8. Examples of relative block-to-block sliding mechanism during one of the triplet test.

The shear stress τ, for a given compressive stress σ (imposed by the lateral load on the specimen, F_H), can be expressed as:

$$\tau = \frac{F_V}{2A_l}$$

where A_l is the lateral surface of the specimens parallel to the vertical shear force, and which was equal to 194 x 80 mm^2. The static friction coefficient μ can be determined as:

$$\mu = \frac{F_V}{2F_H}$$

The force-time response for each specimen is provided in the following Section, although the key information that can be derived within the framework of this type of tests is the static friction coefficient.

4.2.2 Test results

Figure 9 presents the vertical shear force-pseudotime response of triplet specimens #01, #02 and #03, the testing of which was carried out imposing increasing levels of horizontal/axial force that correspond to 0.2 MPa, 0.4 MPa and 0.6 MPa. Response graphs like the one shown in Figure 9 permits one to identify the drops in strength corresponding to the activation of sliding (see Figure 8).

Figure 10 and Figure 11 depict the vertical shear force-pseudotime history of the other specimens (i.e. triplet specimen #04 to triplet specimen #09).

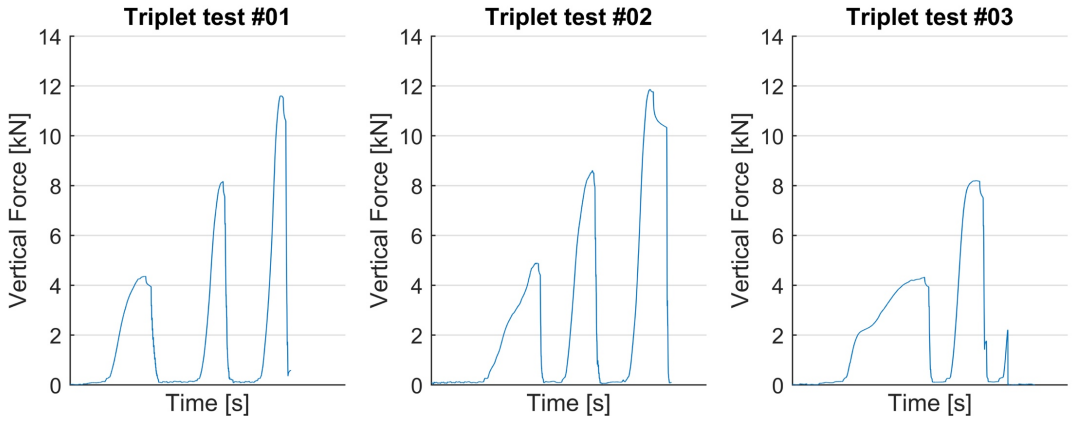

Figure 9. Triplet tests #01, #02 and #03: vertical force-pseudotime response – σ = 0.2 - 0.4 - 0.6 MPa.

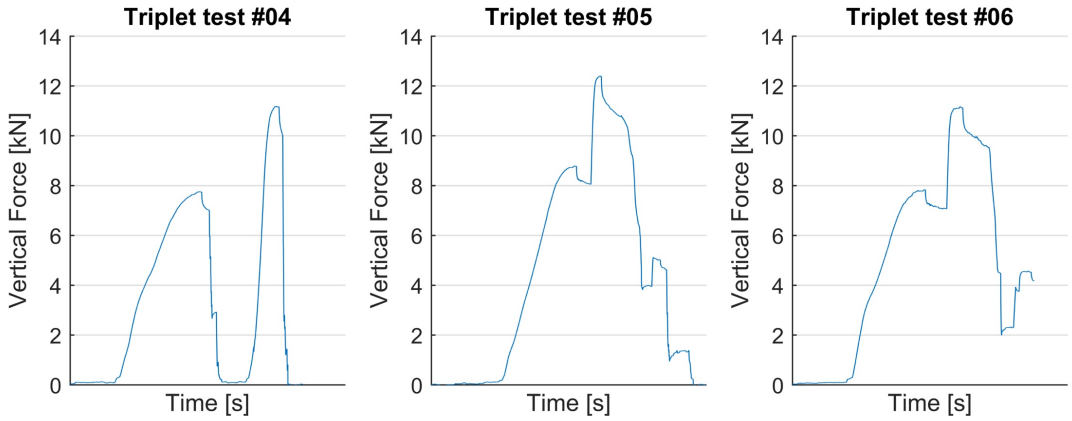

Figure 10. Triplet test #04, #05 and #06: vertical force-pseudotime response – σ = 0.4 - 0.6 - 0.2 MPa.

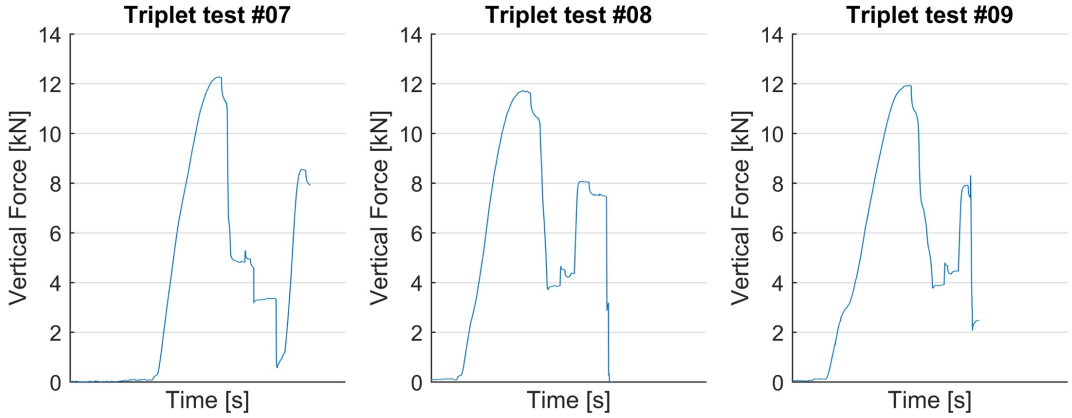

Figure 11. Triplet test #07, #08 and #09: vertical force-pseudotime response – σ = 0.6 - 0.2 - 0.4 MPa.

Key values obtained from the force-time plots reported above (Figure 9 to Figure 11) are collected in a series of tables presented below. For instance, Table 6 summarises the results of triplet test #01, in terms of vertical shear force, shear stress and friction coefficient determined for each level of the imposed horizontal/axial load.

Table 6. Triplet test #01: shear force and friction coefficient.

Triplet test #01				
Horizontal		Vertical		
σ [Mpa]	F_H [kN]	F_V [kN]	τ [Mpa]	μ [-]
0.20	3.2	4.4	0.14	0.37
0.40	6.3	8.2	0.26	0.38
0.60	9.2	11.6	0.37	0.40

As done before for the response graphs, the results of the other triplet specimens (i.e. specimen #02 to specimen #09) are reported in their entirety below, from Table 7 to Table 14.

Table 7. Triplet test #02: shear force and friction coefficient.

Triplet test #02				
Horizontal		Vertical		
σ [Mpa]	F_H [kN]	F_V [kN]	τ [Mpa]	μ [-]
0.20	3.2	4.9	0.16	0.33
0.40	6.3	8.6	0.28	0.37
0.60	9.4	11.9	0.38	0.40

Table 8. Triplet test #03: shear force and friction coefficient.

Triplet test #03				
Horizontal		Vertical		
σ [Mpa]	F_H [kN]	F_V [kN]	τ [Mpa]	μ [-]
0.20	3.2	4.3	0.14	0.36
0.40	6.1	8.2	0.26	0.37
-	-	-	-	-

Table 9. Triplet test #04: shear force and friction coefficient.

Triplet test #04				
Horizontal		Vertical		
σ [Mpa]	F_H [kN]	F_V [kN]	τ [Mpa]	μ [-]
0.40	6.2	7.8	0.25	0.40
0.60	9.3	11.2	0.36	0.42
-	-	-	-	-

Table 10. Triplet test #05: shear force and friction coefficient.

Triplet test #05				
Horizontal		Vertical		
σ [Mpa]	F_H [kN]	F_V [kN]	τ [Mpa]	μ [-]
0.40	6.2	8.8	0.28	0.35
0.60	9.3	12.4	0.40	0.37
0.20	3.3	5.1	0.17	0.33

Table 11. Triplet test #06: shear force and friction coefficient.

Triplet test #06				
Horizontal		Vertical		
σ [Mpa]	F_H [kN]	F_V [kN]	τ [Mpa]	μ [-]
0.40	6.2	7.8	0.25	0.39
0.60	9.2	11.2	0.36	0.41
0.20	3.4	4.6	0.15	0.38

Table 12. Triplet test #07: shear force and friction coefficient.

Triplet test #07				
Horizontal		Vertical		
σ [Mpa]	F_H [kN]	F_V [kN]	τ [Mpa]	μ [-]
0.60	9.2	12.2	0.39	0.38
0.20	3.2	5.3	0.17	0.31
0.40	6.2	8.6	0.28	0.36

Table 13. Triplet test #08: shear force and friction coefficient.

Triplet test #08				
Horizontal		Vertical		
σ [Mpa]	F_H [kN]	F_V [kN]	τ [Mpa]	μ [-]
0.60	9.4	11.7	0.38	0.40
0.20	3.3	4.7	0.15	0.35
0.40	6.4	8.1	0.26	0.39

Table 14. Triplet test #09: shear force and friction coefficient.

Triplet test #09				
Horizontal		Vertical		
σ [Mpa]	F_H [kN]	F_V [kN]	τ [Mpa]	μ [-]
0.60	9.5	11.9	0.38	0.40
0.20	3.4	4.8	0.15	0.36
0.40	6.1	7.9	0.26	0.38

Analysing each triplet test result singularly, it can be noticed that the static friction coefficient of the felt material under investigation is almost insensitive to changes in the imposed compressive load and in the applied loading sequence, which in turn implies that the standard deviation computed using the full dataset available is extremely low. The values of μ were thus found to range between 0.31 and 0.40, whereas an average of 0.37 with a standard deviation of 0.03 can be established.

4.2.3 Summary

To further verify the abovementioned trends with regards to the imposed axial force and loading sequence, the results collected in Table 6 to Table 14 are now presented in terms of (τ, σ) couples by superimposing the results obtained from specimens characterised by the same loading strategy. For instance, Figure 12 shows the τ-σ curves of triplet tests #01, #02 and #03 that were performed by imposing increasing compressive loads corresponding to compressive stresses of 0.2 MPa, 0.4 MPa and 0.6 MPa. The latter loading sequence was referred to as combination #01 and the related values of friction coefficient under the three levels of compressive stress are summarised in Table 15.

A small variation of the static friction coefficient between a lower value of 0.33 and a higher value of 0.40 was noticed. An average of about 0.37 can be established with a standard deviation roughly equal to 0.02.

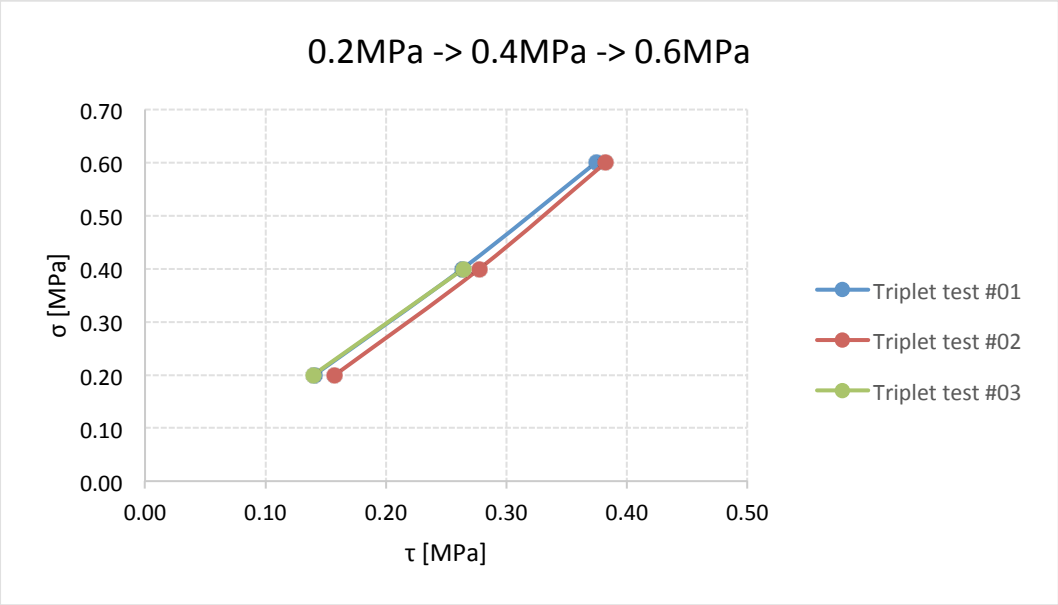

Figure 12. Triplet test results for different combinations of horizontal/axial load – combination #01.

Table 15. Triplet test results: compressive stress and friction coefficient – combination #01.

σ [MPa]	triplet #01	triplet #02	triplet #03
0.20	0.37	0.33	0.36
0.40	0.38	0.37	0.37
0.60	0.40	0.40	-

The results obtained according to the other two loading strategies, namely combination #02 (i.e. 0.4 MPa - 0.6 MPa - 0.2 MPa) and combination #03 (i.e. 0.6 MPa - 0.2 MPa - 0.4 MPa), are presented in Figure 13 and Figure 14. Accordingly, the series of friction coefficients are collected in Table 16 and Table 17.

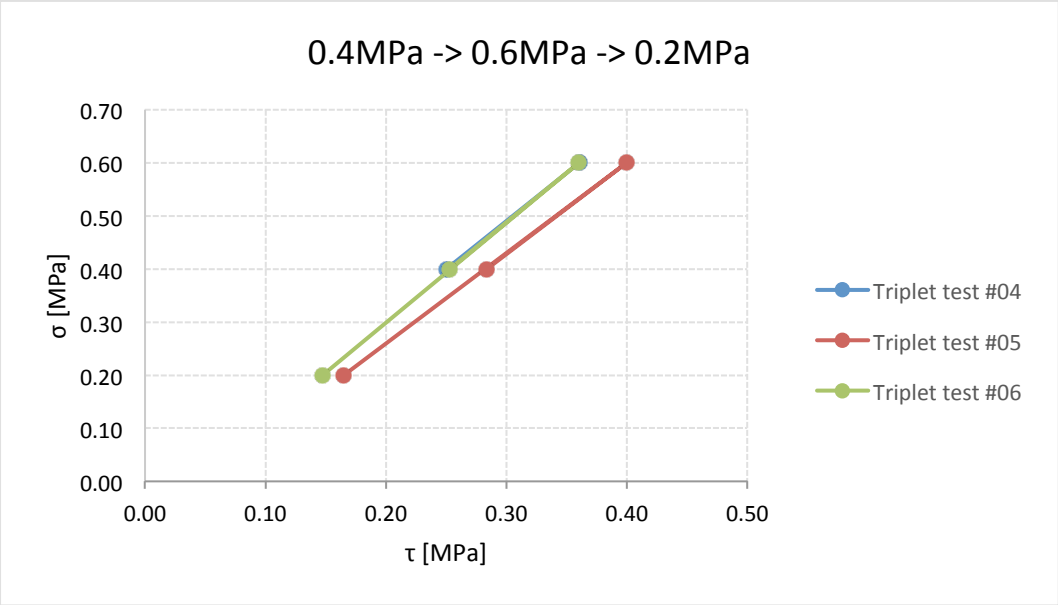

Figure 13. Triplet test results for different combinations of horizontal/axial load – combination #02.

Table 16. Triplet test results: compressive stress and friction coefficient – combination #02.

σ [MPa]	triplet #04	triplet #05	triplet #06
0.40	0.40	0.35	0.39
0.60	0.42	0.37	0.41
0.20	-	0.33	0.38

As far as the so-called combination #02 is concerned, the friction coefficient was again observed to be in the range 0.33-0.40. In this case, the average of μ is equal to 0.38, and the standard deviation computed for this set of results is 0.03. Similar considerations can be drawn for combination #03, as the average of the static friction coefficient is 0.37 with a low standard deviation of approximately 0.03. More in detail, a slightly greater variation in the friction coefficient can be noticed in this case, given that this parameter was found to range between 0.31 to 0.40.

As previously mentioned, if the overall 25 tests performed are considered, an average of 0.37 with a standard deviation equal to 0.03 can be computed. The set of τ-σ curves were observed to be linear regardless of the imposed loading sequence, which also means that the static friction coefficient of the felt material under study is moderately sensitive to the compressive load. These are likely to be dominating factors for what concerns the response of EUC-BUILD4 specimen.

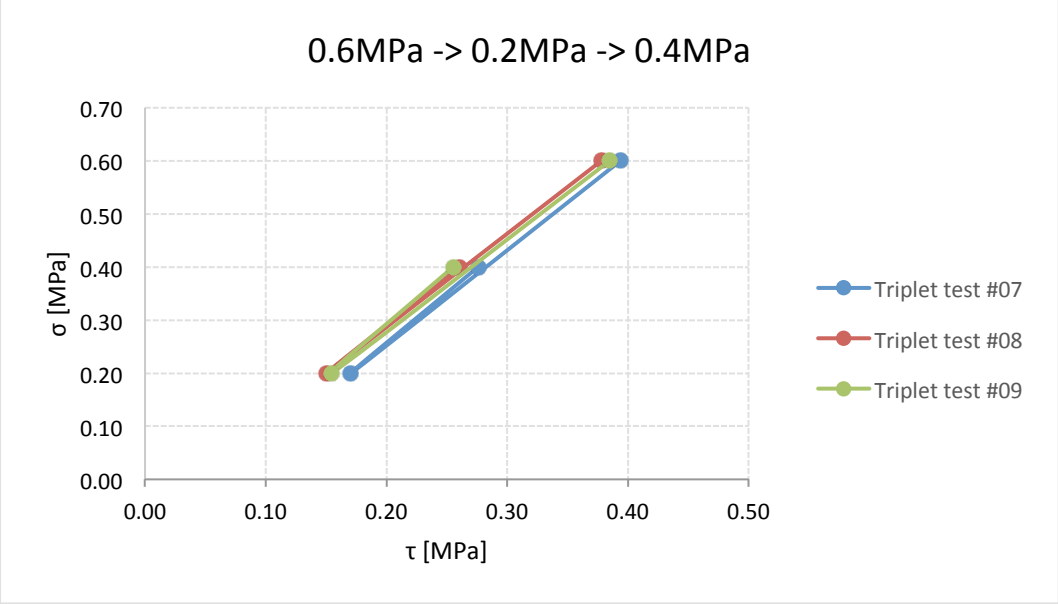

Figure 14. Triplet test results for different combinations of horizontal/axial load – combination #03.

Table 17. Triplet test results: compressive stress and friction coefficient – combination #03.

σ [MPa]	triplet #07	triplet #08	triplet #09
0.60	0.38	0.40	0.40
0.20	0.31	0.35	0.36
0.40	0.36	0.39	0.38

5 Full-scale test specimen, setup and instrumentation

5.1 Preamble and selection of test specimen

The full-scale test specimen, namely EUC-BUILD4, was defined featuring the main characteristics of the existing buildings under study and standard details of reinforced precast concrete technology employed in the Dutch construction practice. The index building, a full-scale two-storey reinforced precast concrete wall-slab-wall structure representative of the Groningen building stock, was selected and designed based on an iterative process that consisted of:

- "ad hoc" selection of the candidate specimen among three possible solutions representative of different design criteria/concepts;
- refinement of the selected candidate in order to comply with laboratory-related issues/needs for what concerns test execution (i.e. experimental setup and procedure).

Key aspects concerning the latter part of this process are presented and discussed in the following sections, as background information for interested readers. In addition to the information contained herein, one may and should also consider Arup's *229746_031_NOT2008_Rev0.05_Issue EUC-BUILD-4 Prototype building description*, as a valuable companion and complementary document. It is also worth mentioning that construction details regarding the selected prototype structure can also be found in *229746_031.0_DRW2007_Rev0.05_Issue_EUC-BUILD-4_5 SWb Specimen drawings*. This set of Arup drawings is, in any case, reflecting the final design and hence it is not meant as an as-built version representative of the actual mock-up building (though the only minor difference is the type of hollow core slab, which however did not play any role in the response of the specimen).

5.2 Description of selected case-study structure

This section is concerned with the iterative refinement process towards the identification/definition of a candidate specimen in terms of geometrical characteristics, mechanical properties of materials and design assumptions compliant with Dutch building practice for this type of houses.

As mentioned in Section 1, reinforced concrete buildings in the Groningen region largely consist of wall-slab-wall structures, featuring no columns or beams, but only slabs and walls. These structures are a common form of housing and can be found in both cast-in-place (tunnel construction or not) as well as precast configurations. A brief overview of the main characteristics of the latter is given so as to motivate the selection of the candidate specimen, bearing also in mind that the construction process and details of these houses are very specific to the Netherlands as for instance confirmed by the photographic sequence presented in the following section.

This type of low-rise residential terraced buildings is usually constructed with precast floors, precast party/gable walls and precast walls in the longitudinal direction. The precast walls are erected first and shored up by steel diagonal props; the floor is then settled on the walls and supported by steel rebars that connect the first with the second-storey wall, through the floor. Noteworthy is that, however, these dowels are not always present in this type of construction scheme/technology. The most common precast slabs for this structural typology are hollow core sections presenting circular voids in accordance with their moderate thickness (i.e. 200-250 mm). A

thickness in the range 200-250 mm and 120-150 mm is typically assumed for party walls and inner leaf gable walls, respectively.

Front and back façades of these multiple-unit buildings are generally cavity walls. The most common concrete grade used for these structures is C35/45 and the reinforcing steel is usually formed by a wiremesh. One layer of reinforcement in the precast walls is most likely used for small residential houses and two layers for the apartments. During the construction phase, use is made of cranes to erect and set in place the precast walls that rest directly on the foundations or on the ground floor slab, which in turn rests on the foundations. The latter option is anyway either less frequent or in non-standard configurations. Once the connections between the elements are realised, the temporary props used to ensure the stability of the structure against the horizontal wind actions are removed. Starter rebars are usually not present in this construction system, and the wall-to-foundation connections merely consist of mortar joints. Mechanical anchors and felts are used as well, the latter being provided at the bottom of the hollow core slabs, which are not necessarily connected together through concrete topping. Discrete L-shaped metal restraints can sometimes be found in existing buildings to prevent the unseating of prefabricated wall-elements. Wall-to-wall joints are standardised solutions and are mainly constituted by mechanical connections that can be either two-way or three-way anchorages, depending on if two contiguous panels are linked or not with a perpendicular stability wall.

EUC-BUILD4 specimen, designed to combine several common features of this type of structures, was meant to feature stability walls, perpendicular to the lateral loadbearing walls, since these lightly reinforced wall-panels tend to be crucial elements for this structural scheme. The geometry of the tentative specimen was re-designed by varying the length of the stability walls according to three different criteria, which resulted in the corresponding three candidates:

- 229746_031.0_DRW2006_Rev0.05_Issue_EUC-BUILD-4_5 SWa Specimen drawings;
- 229746_031.0_DRW2007_Rev0.05_Issue_EUC-BUILD-4_5 SWb Specimen drawings;
- 229746_031.0_DRW2008_Rev0.05_Issue_EUC-BUILD-4_5 SWc Specimen drawings.

The second candidate (i.e. option b), which features half-span long stability walls, was selected and the corresponding structural drawings were then further refined. Such a selection was due to on one hand the excessive slenderness of option a, in which these walls are assumed to be 2 m long, and on the other the fact that having stability walls squat like the ones assumed for the third candidate (i.e. 3.75 m long) is not representative of the median properties of the building stock of interest. In fact, the third option was designed by taking the length of the stability walls as two-thirds of the slab spans, which is a rare upper bound that can be referred to as the maximum length possible. Option b, in which the length of the stability walls is equal to the inter-storey height and approximately one half of the slab span as per existing buildings, is the most “reliable” and suitable structural prototype for the purposes of this experimental study. The choice was also consistent with the original design of the reference building and confirmed by preliminary computations of overturning moment (please refer to Arup’s *229746_031_NOT2008_Rev0.05_Issue EUC-BUILD-4 Prototype building description* for other and more specific details).

The initial design concept was refined and a few adjustments were made with respect to the existing configurations and the assumptions based on which the index building was derived. This process is needed to fully comply with testing requirements in terms of both design of the setup and

prevention of collapses during the execution of pseudostatic cyclic testing. In particular, it is noteworthy that:

- EUC-BUILD4 prototype, formerly designed as a two-bay (two-unit), two-storey RC precast building with dimensions in plane of 4.0 x 11.2 m and an inter-storey net height of 2.66 m, was modified to be a single-bay, two-storey structure with plane dimensions equal to 4.0 x 5.5 m, the latter being intended as the centre-to-centre wall spacing. This was due to the fact that the two contiguous units, separated by a cavity, are connected to each other by means of steel rods at the level of the floors and embedded in the hollow core slabs. According to that, no continuity can be ensured between the two units in terms of lateral force transfer. Hence, it was decided to split the original prototype into two nominally identical prefabricated one-bay, two-floor specimens. The two twin specimens are meant to be tested at Eucentre Lab, one of them cyclically, in pseudostatic fashion, and the other one dynamically, on the shake table of the laboratory.
- taking the decision of testing a one-unit mock-up allowed to increase the slabs span to 5.5 m (centre-to-centre) in order to better resemble the existing building sizes, anyway complying with the assembly of the set of actuators on the strong wall of the laboratory. It is also worth noting that an intermediate configuration was studied, in which the span bay was adjusted to a value of 4.2 m. That configuration was nonetheless abandoned, since it was decided not to shorten the span bay to take advantage of the same anchorage points to mount the actuators on the strong wall of the laboratory. As discussed in section 5.4, this was achieved by simply attaching the four actuators controlling the specimen in the transverse direction to the slabs. The chosen span bay fits well with the dimensions of Eucentre shake table, and hence the same geometry can be assumed for the twin prototype, namely EUC-BUILD5 specimen.
- the hollow core slabs of each floor were selected to protrude in order to execute the tests in a safe manner with regards to the unseating of slabs in correspondence to the wall-slab joints. In more detail, the slabs are designed to overhang the wall-slab joints (i.e. 250 mm on each side of the specimen) so as (i) to prevent their unseating and (ii) to host L-shaped restrainers that inhibit out-of-plane collapses of wall-elements and sliding after an aprioristically fixed gap is taken up. A 30 mm gap was assumed to carry out the testing of EUC-BUILD4 mock-up in its as-built configuration. Use can also be made of the abovementioned stoppers/restrainers to “retrofit” the damaged specimen by simply preventing sliding from occurring in wall-slab joints that merely consists of fabric felts.

A three-dimensional drawing of EUC-BUILD4 full-scale specimen is shown in Figure 15, and other key assumptions regarding the selected building are discussed hereafter. The reference prototype is a single-bay, two-floor precast RC mock-up building with dimensions in plane of 4.0 x 5.5 m, and an inter-storey net height of 2.66 m. The flooring system consists of 200 mm thick hollow core slab elements. Hollowcore K200, spanning 5.5 m to the transversal walls (i.e. centre-to-centre distance), were selected. Most of the floor elements are type K200-6, whilst only the 400 mm wide elements (one for each floor) are K200-6D. Although concrete topping is not always present in this structural typology, a 50 mm thick concrete screed was considered, so as to ensure more stiffness in the transversal direction (with respect to the direction of the slab span) and also to prevent any possible slab disassembly during large deformation testing stages.

The prototype features two stability walls (one per each floor), perpendicular to the lateral load-bearing walls, placed in the central line of the specimen and half-span long. The lateral walls consist of 2.00 x 2.66 m contiguous panels connected together by means of two-way anchorages (Figure 2). By contrast, three-way anchorages are provided to connect the lateral wall panels with the stability wall, as shown in Figure 16. According to common Dutch practice, each panel wall accommodates four anchorages. The transversal walls and the stability walls were assumed to be 120 mm thick and to have the same reinforcement layout, which is composed of a steel grid Ø5/250 of ribbed rebars.

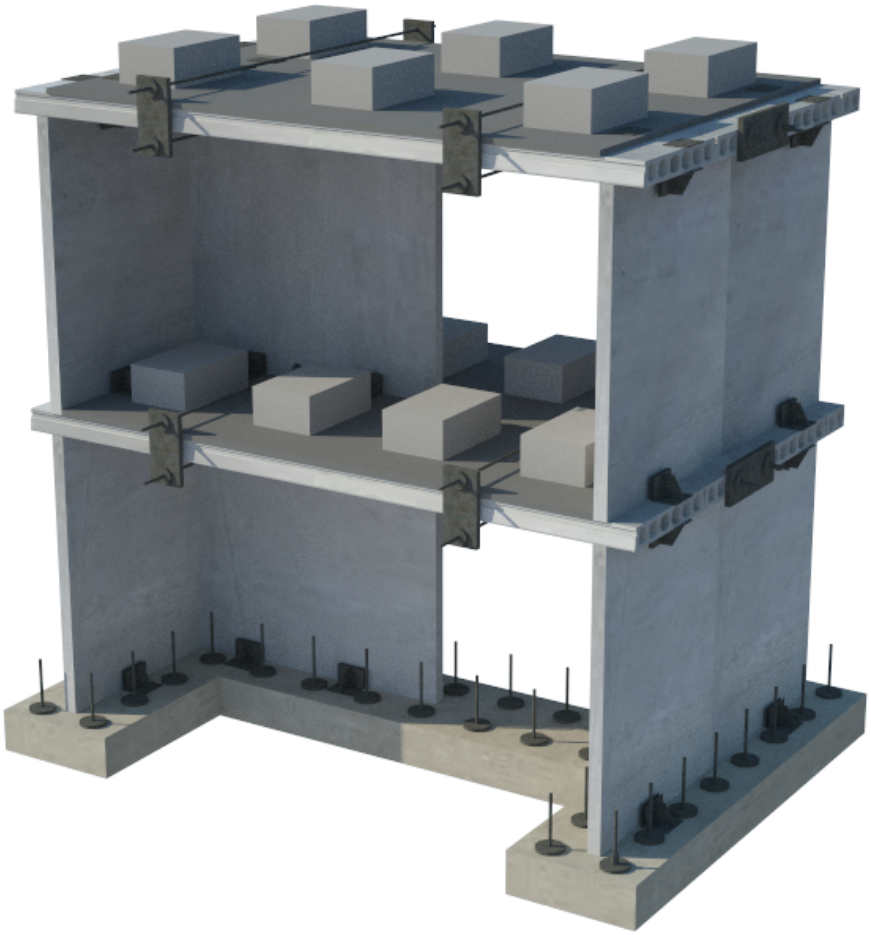

Figure 15. Isometric view of EUC-BUILD4 specimen.

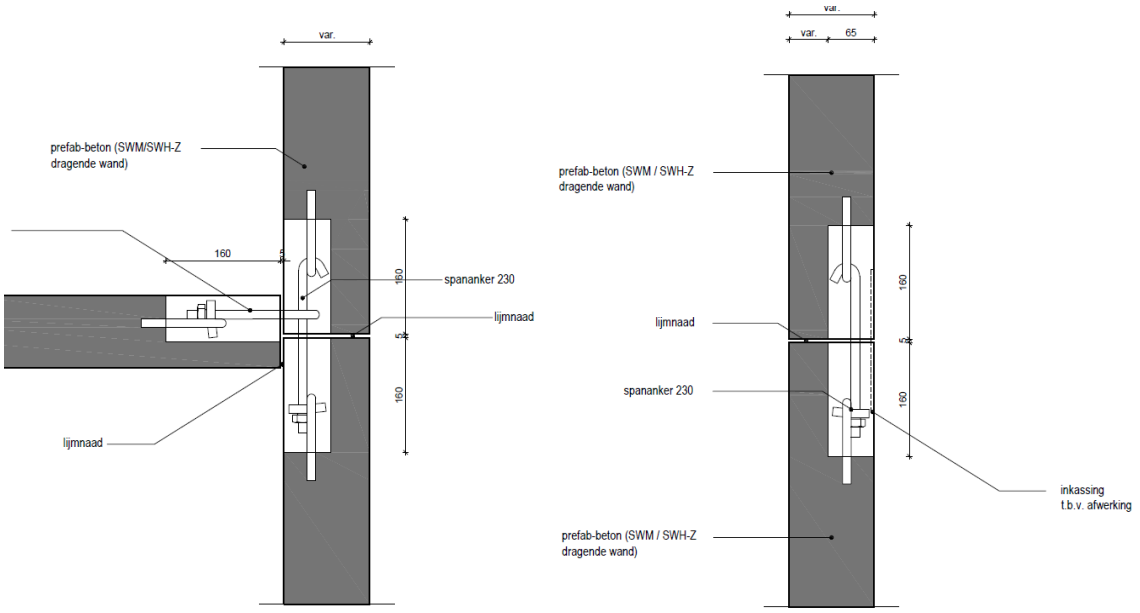

Figure 16. Examples of three-way and two-way anchorages for panel-to-panel connection. Courtesy of Arup (please refer to *229746_031_NOT2008_Rev0.05_Issue EUC-BUILD-4 Prototype building description*)

According to conventional practice for such structures, design loads were defined as follows:

- First floor: 1 kN/m^2 and 2 kN/m^2 for dead and live loads, respectively;
- Second floor: 1 kN/m^2 and 1.5 kN/m^2 for dead and live loads, respectively;
- Wind load: 0.85 kN/m^2 according to Dutch National Annex of Eurocode.

It is noteworthy that testing will take into account only downward gravity loads, the effect of which can be simulated within the framework of pseudostatic and shake table tests through either concrete masses or a further layer of non-collaborating concrete topping, the former being in the end used for the sake of simplicity.

As previously mentioned, no starter rebars protruding from the concrete foundations are used in this building typology, and hence the walls rest on the underneath foundations by means of mortar joints without mechanical connection. A similar construction scheme is assumed for the first floor as well. In accordance with common Dutch building practice, the slabs are simply supported onto the walls underneath them through fabric felts like those studied via triplet testing in section 4.2. Instead of L-shaped metal restraints/strips, use was made of concrete topping, thus ensuring a minimum stiffness in the transversal direction of the slabs. By the same token, unseating-induced collapse mechanisms were controlled and prevented from occurring through rationally-conceived external devices.

Needless to say that gable walls and front/back façades (i.e. longitudinal non-loadbearing walls) are not included in the prototype, as the testing is chiefly concerned with the assessment of the structure itself (i.e. structural and loadbearing elements) without consideration of secondary non-loadbearing elements and components, for subsequent validation and calibration of numerical models.

5.3 Construction process and details

As previously discussed, EUC-BUILD4 prototype was meant and designed to be representative of a particular typology of Dutch buildings. Hence, it was decided that a Dutch contractor (i.e. Bouwborg) would be in charge of the construction process. Under controlled laboratory conditions, the specimen was thus built in accordance with common Dutch practice. EUC-BUILD4 prototype was assembled/built directly on the foundations mounted onto the strong floor of EUCENTRE Laboratory, to avoid any eventual/unintended damage due to transportation (if the specimen had been built outside of the lab).

In the following, the details involved in the construction of the building prototype are described in some extent. These details concern both the unloading of precast panels and construction material more in general and the assemblage of precast elements, as well as the arrangement of connections and the casting of concrete topping. A photographic sequence addressing these crucial aspects is shown and some considerations are given as needed to highlight key points.

In Figure 17 to Figure 22, one may find details regarding the precast elements delivered by the local Dutch contractor and the crane-driven uplifting system used in the laboratory. Photographs showing the process adopted by Dutch workers to assemble the specimen are collected in Figure 23 to Figure 45, in which it is described how precast wall panels and hollow core slabs were set in place. Further photos showing casting of concrete topping – Figure 46 to Figure 60 – and the completed EUC-BUILD4 specimen after levelling and finishing – Figure 61 to Figure 64 – are reported as well.

Figure 17. Uplift of precast wall-elements by means of cranes.

Figure 18. Uplift and transportation of precast wall-elements by means of cranes – detail 1.

Figure 19. Uplift and transportation of precast wall-elements by means of cranes – detail 2.

Figure 20. Uplift and transportation of precast wall-elements by means of cranes – detail 3.

Figure 21. Detail of pre-cracked stability wall – crack running through the entire wall width and depth.

Figure 22. Examples of the two typologies of precast hollow core slabs.

Figure 23. Uplift and installation of precast hollow core slabs composing the first floor.

Figure 24. Installation of a precast hollow core slabs of the first floor.

Figure 25. Execution of a mortar joint at the base of EUC-BUILD4 specimen – lateral wall.

Figure 26. Detail of a mortar joint at the base of EUC-BUILD4 specimen – lateral wall.

Figure 27. Detail of filling in contiguous precast panels – lateral wall.

Figure 28. Detail of temporary steel diagonal props for stability purposes – lateral wall.

Figure 29. Detail of mortar in a panel-to-panel two-way connection – lateral wall.

Figure 30. Detail of temporary props – stability and lateral walls.

Figure 31. Detail of panel-to-panel three-way connections – stability wall.

Figure 32. Detail of the mortar joint at the base of the opposite lateral wall – global view.

Figure 33. Detail of the mortar joint at the base of the opposite lateral wall – enlarged view.

Figure 34. Global view of EUC-BUILD4 specimen after assembling of the first storey.

Figure 35. Detail of fabric felt underneath precast slabs, as well as of 250 mm overhang in wall-slab joints.

Figure 36. Detail of three-way joint and filling in stability wall-lateral wall connection.

Figure 37. Detail of base mortar joint after dismantling of plywood beams.

Figure 38. Installation of safety measures and preparation of mock-up for assemblage of second storey.

Figure 39. Assemblage of precast wall-elements of the second storey.

Figure 40. Installation of the stability wall of the second storey.

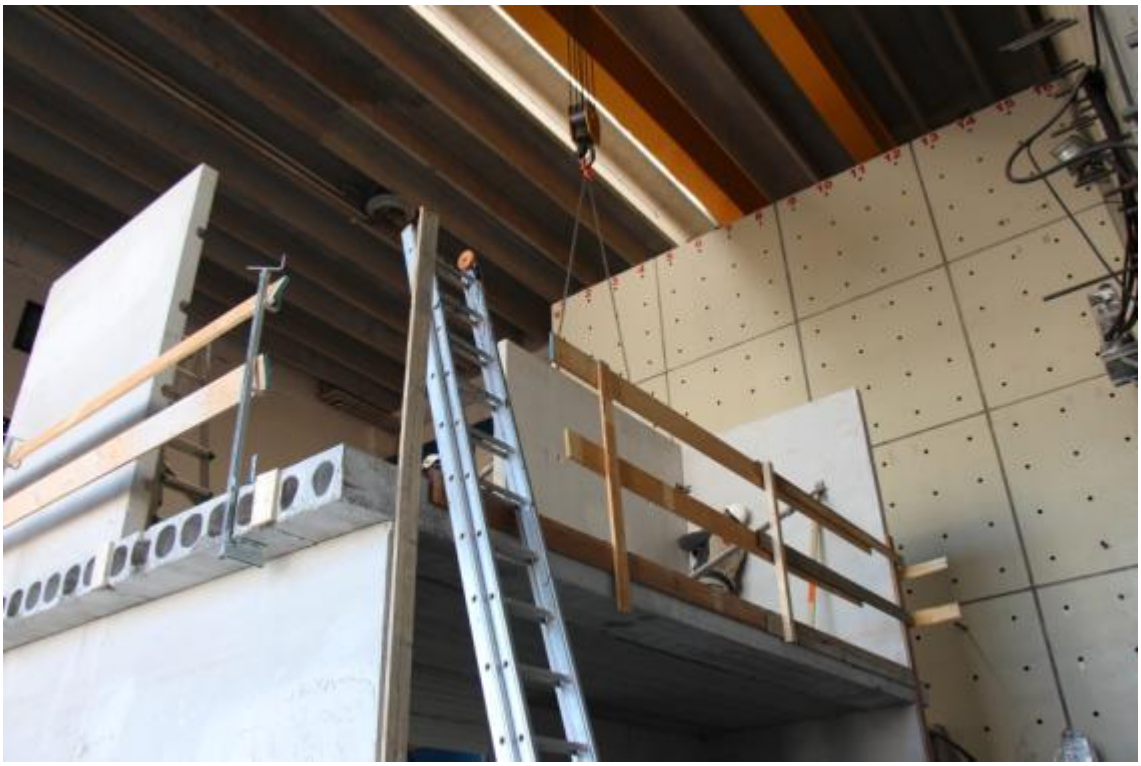

Figure 41. Crane-driven installation of the stability wall of the second storey.

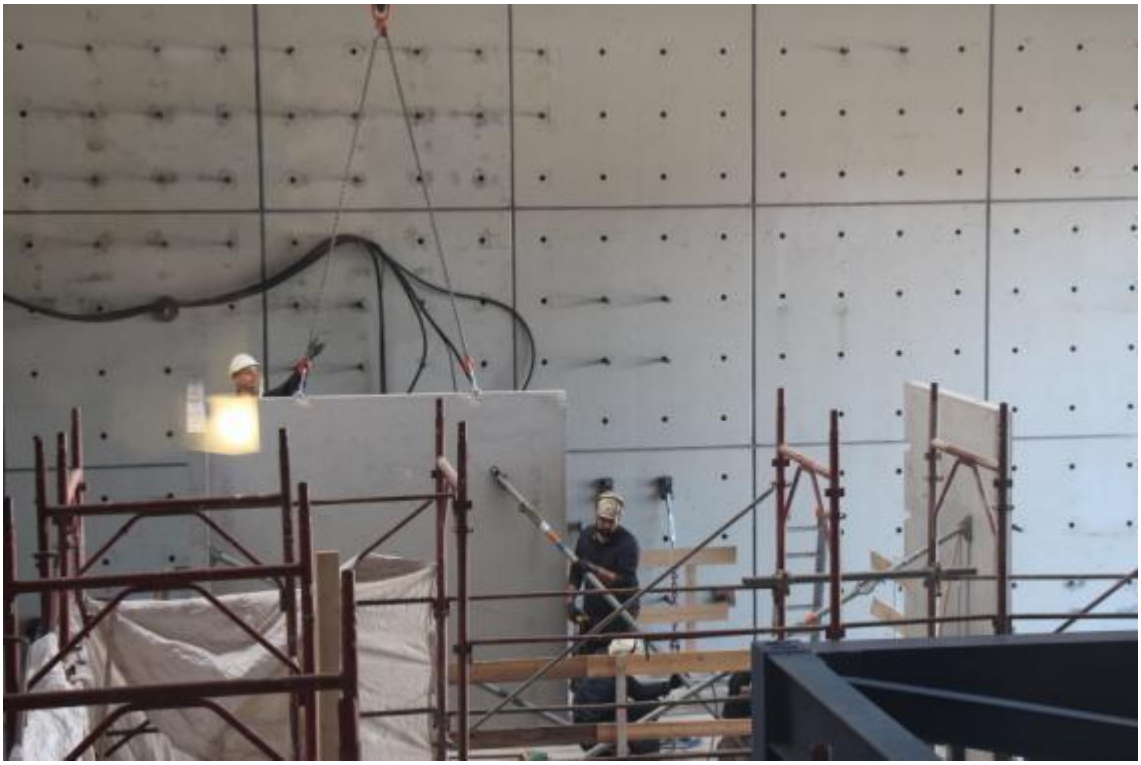

Figure 42. Panel lifting and fixing of the stability wall panel.

Figure 43. Installation of flooring system at the second floor level – side view.

Figure 44. Installation of hollow core slabs of the second storey – top view.

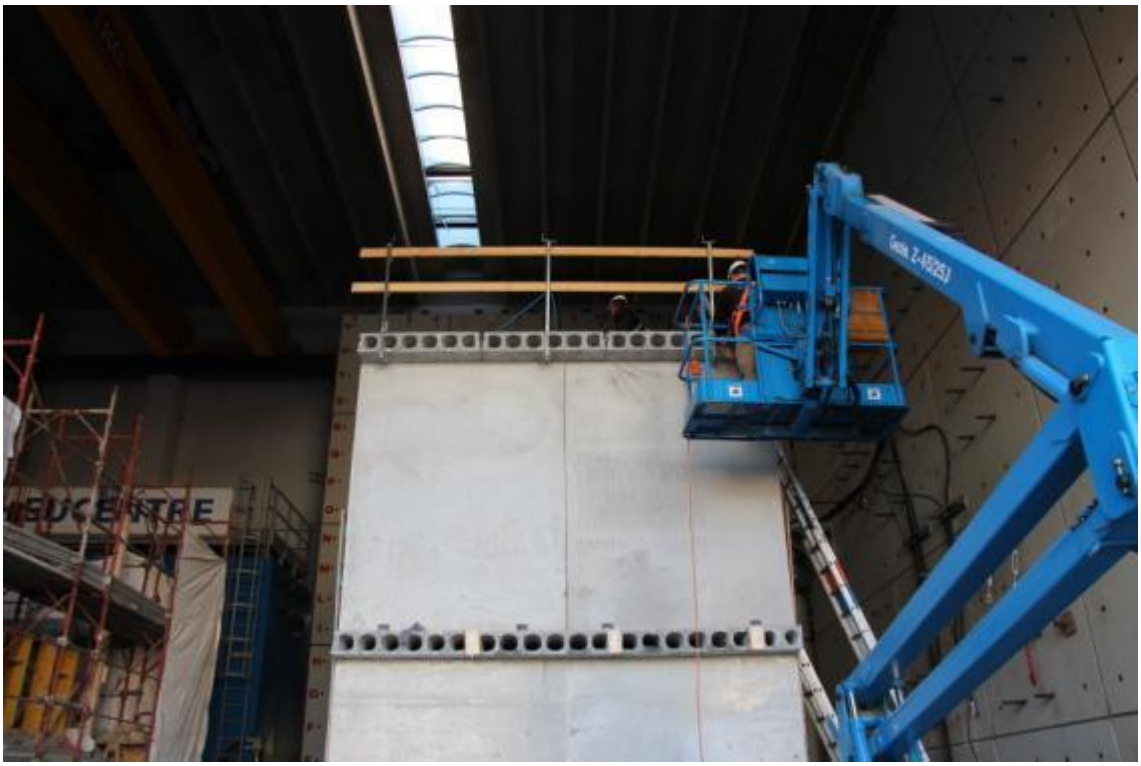

Figure 45. Installation of safety barriers and plywood plates for slab finishing.

Figure 46. Preparation of the second storey for slab finishing.

Figure 47. Detail of slab finishing via injection grout between the precast slab-elements.

Figure 48. Detail of injection grout and final levelling.

Figure 49. Arrangement of steel reinforcement before casting of concrete topping – second floor.

Figure 50. Steel reinforcement of concrete slab topping – second floor.

Figure 51. Arrangement of steel reinforcement before casting of concrete topping – second floor.

Figure 52. Steel reinforcement of concrete slab topping – first floor.

Figure 53. Casting of concrete slab topping – second storey, detail 1.

Figure 54. Casting of concrete slab topping – second storey, detail 2.

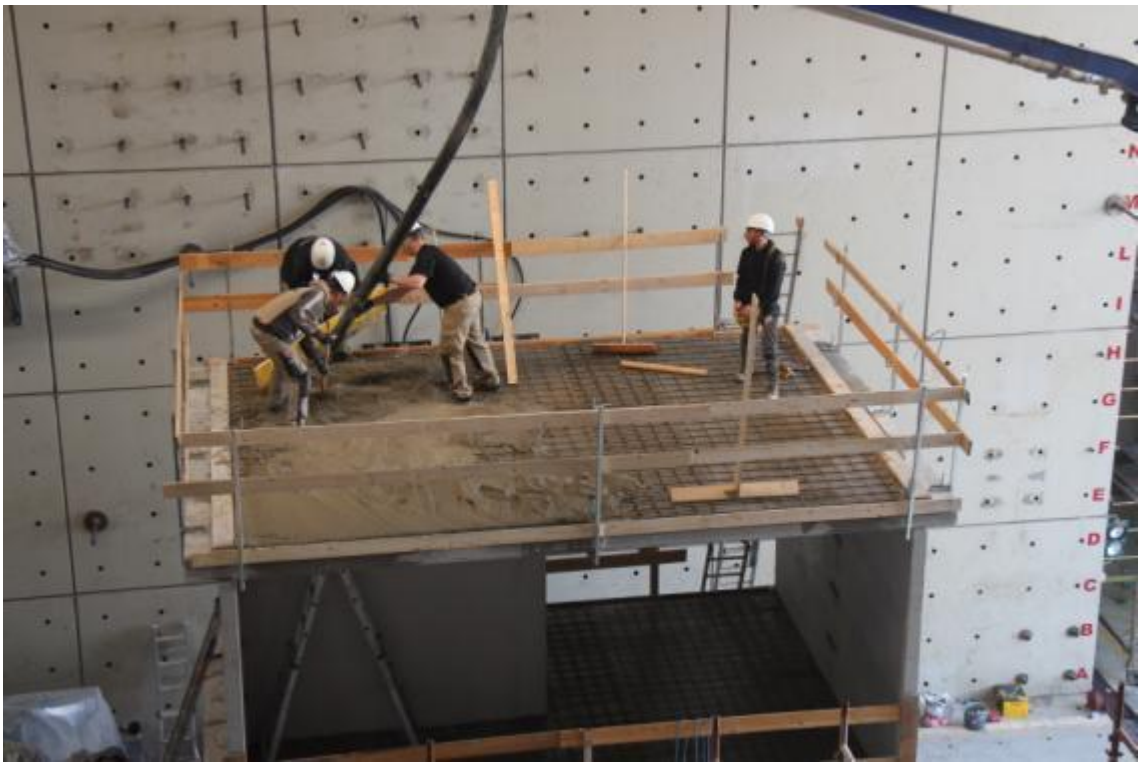

Figure 55. Casting of concrete slab topping – second storey, detail 3.

Figure 56. Casting of concrete slab topping – second storey, detail 4.

Figure 57. Casting of concrete – detail of levelling and finishing.

Figure 58. Casting of concrete slab topping – first storey, detail 1.

Figure 59. Casting of concrete slab topping – first storey, detail 2.

Figure 60. Casting of concrete slab topping – first storey, detail 3.

Figure 61. Detail of mortar joint at the base of the lateral wall at the second storey.

Figure 62. Detail of mortar joint and injection grout between precast hollow core slab members.

Figure 63. Overall view of EUC-BUILD4 specimen after levelling and finishing – top view.

Figure 64. Overall view of EUC-BUILD4 specimen after levelling and finishing – side view.

One of the panels (for the stability walls) arrived cracked, as shown in Figure 21. The diagonal crack runs through the entire width of the panel and also through its entire depth, which in turn suggested the pertinence of monitoring the crack width during the testing of EUC-BUILD4 prototype. Worthwhile to mention is that the panel was employed on the second floor, where the shear forces will be lower than those at the base.

Furthermore, it can be noted that, although hollow core slabs 'D200 type K-200-6D' were supposed to be employed, the very vast majority of slab panels that arrived to Pavia were actually 'N200 Type K200-6', which are lighter than what had been envisaged in the design phase. Hence, test-rig setup was adjusted accordingly. A photo of the hollow core slab elements adopted for construction can be seen in Figure 22.

5.4 Test setup and loading protocol

In this Section, the main aspects regarding the test procedure are presented in detail. First of all, a brief overview concerning the rationale behind the design of the test setup and the definition of the tentative loading protocol is proposed to highlight the primary assumptions that were considered for the execution of the test. Also, photographs showing the actual setup and tables summarizing the loading steps/sequence are provided and collected in separate sub-paragraphs, one per each item.

5.4.1 Rationale

Figure 65 and Figure 66 show two isometric views of EUC-BUILD4 specimen together with the key components of the experimental setup conceived for pseudostatic cyclic testing of the mock-up, whereas a set of two-dimensional schematics presenting the installation of MTS actuators and the foundation system is provided in Figure 67, Figure 68 and Figure 69. As usually foreseen during

this type of tests, the concrete foundations were designed to remain elastic and were post-tensioned to the strong floor of the laboratory so as to completely inhibit any relative motion during the tests.

Two actuators, one for each floor, were used to cyclically apply the horizontal load to the specimen in its longitudinal direction, whilst four actuators in the transverse direction were employed to prevent possible torsion or uneven displacement of the specimen during testing in its weak longitudinal direction (see Figure 65); it is noted that relatively low forces, of the order of 3-5 kN, had to be developed by the transverse actuators in order to prevent transverse deformations. Although such an experimental setup permits bi-directional testing of the building, it was decided to carry out cyclic push-pull testing only in mono-directional fashion considering that (i) the dynamic counterpart test (i.e. EUC-BUILD5) will also not feature testing in transverse direction; (ii) the response in the strong-transverse direction of the specimen will be one of wall rocking, thus providing no particularly new findings; (iii) it would be difficult to control and monitor (due to the non-monolithic characteristics of the specimen and the presence of the stability walls).

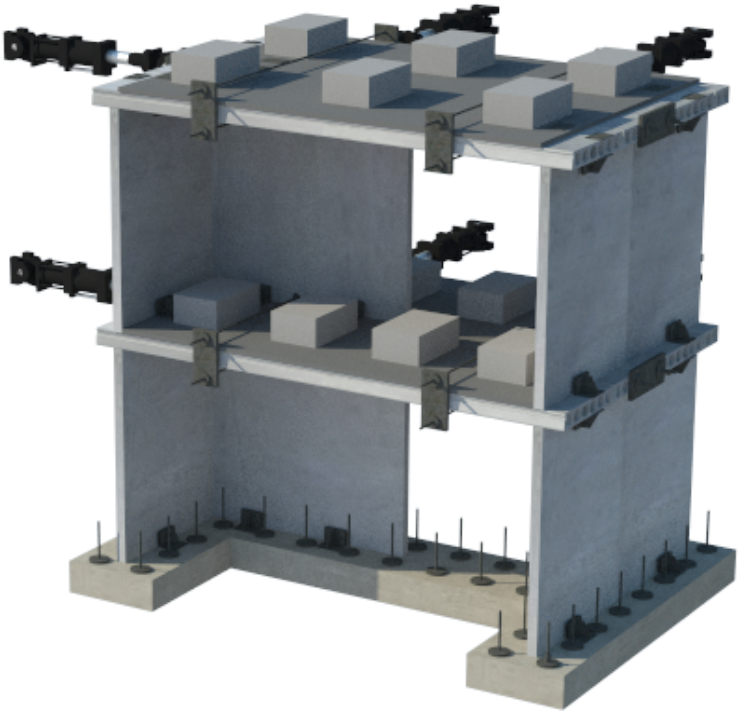

Figure 65. Isometric view of EUC-BUILD4 specimen and installation of experimental setup – North side.

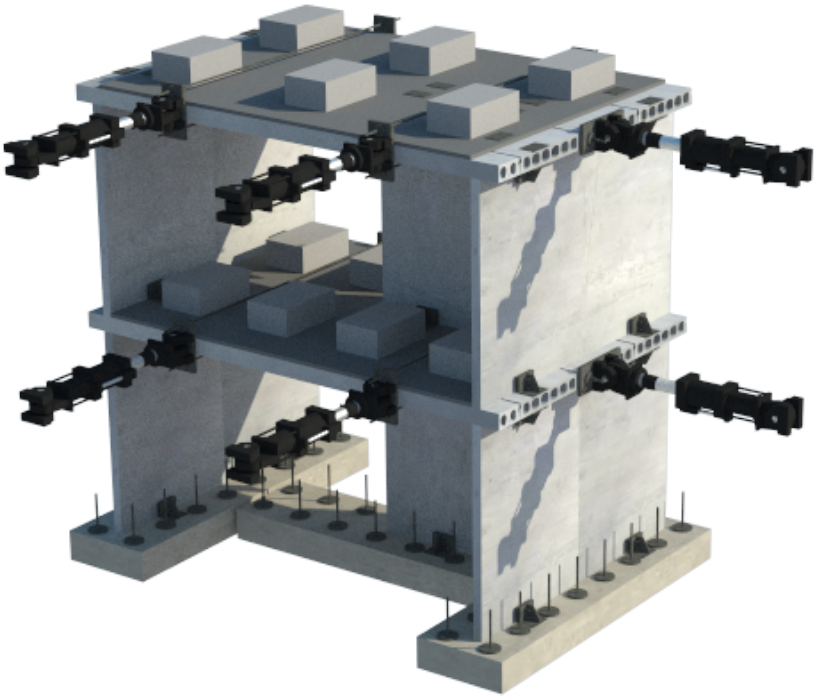

Figure 66. Isometric views of EUC-BUILD4 specimen and installation of experimental setup – South side.

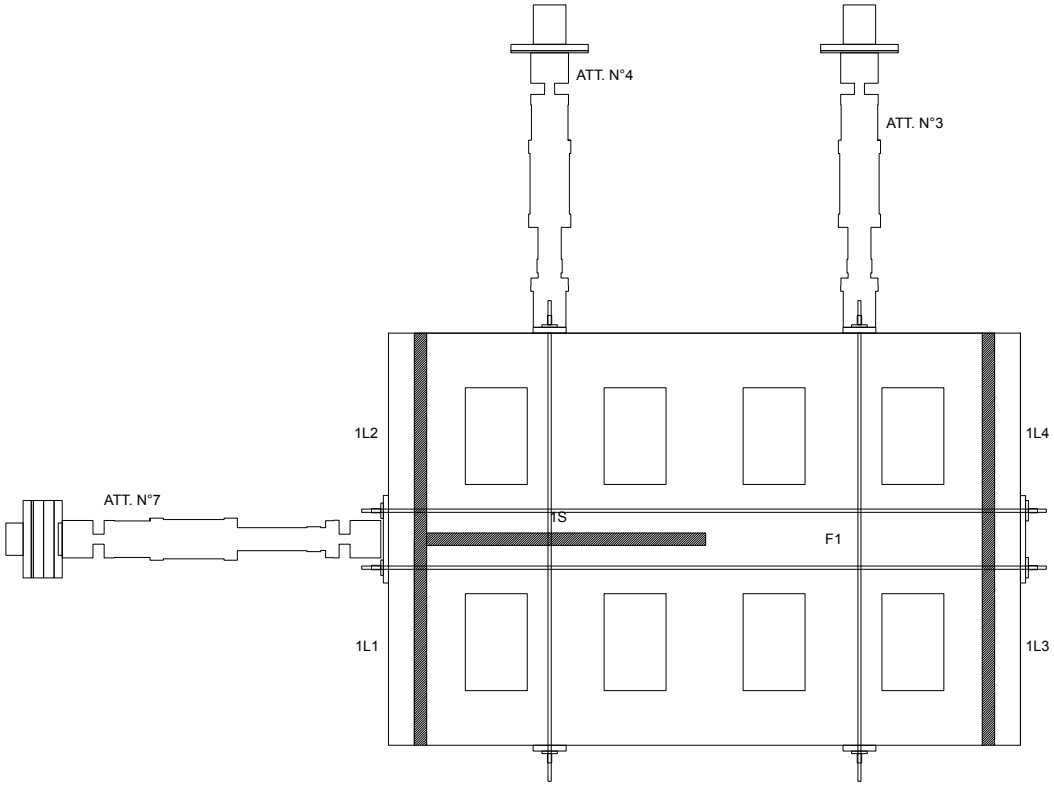

Figure 67. Schematic of the experimental setup – top view of the first floor slab.

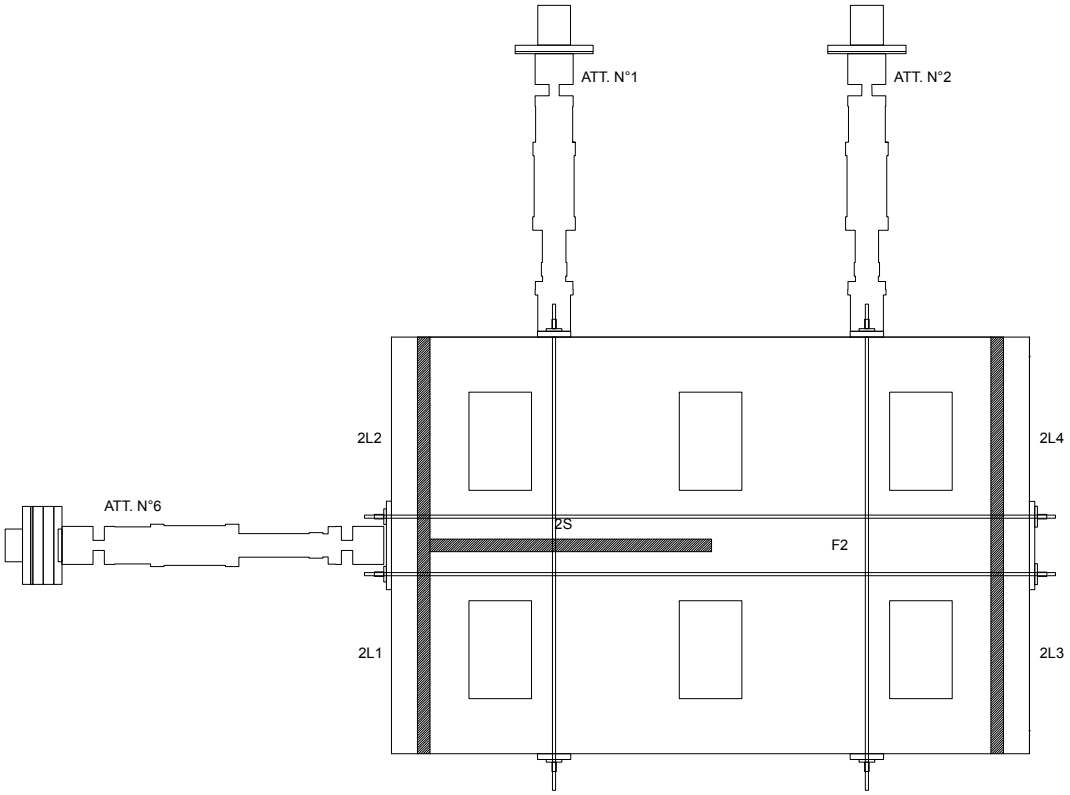

Figure 68. Schematic of the experimental setup – top view of the first floor slab.

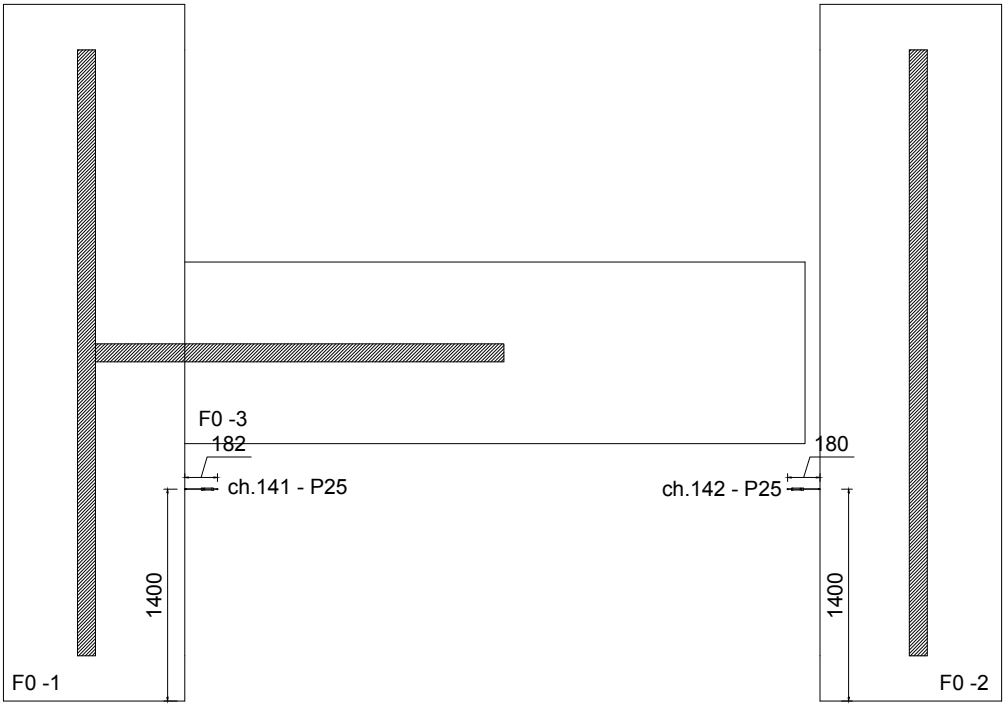

Figure 69. Schematic of foundation beams – top view and nomenclature.

A tentative loading protocol (that could be adapted during the test as a function of the observed structural response) was defined for the longitudinal direction of the specimen. Table 18 summarises the main steps and assumptions behind the proposal. As typically adopted in quasi-static tests, two cycles per force/drift amplitude were considered, so that any potential cycle-to-cycle degradation phenomenum may be quantified.

Table 18. EUC-BUILD4 prototype: loading protocol for pseudostatic testing.

Test run #	Test Name	Main DoF	Control Type	MAX Ampl.	MIN Ampl.	Drift Ampl.	Load Shape	Load Rate	Cycles
			(Force or Displ.)	[kN] [mm]	[kN] [mm]	[%]		[kN/s] [mm/s]	[#]
01	Step#01-FC	Long	Force	30	-30	-	triang.	0.1	2
02	Step#02-FC	Long	Force	45	-45	-	triang.	0.2	2
03	Step#03-DC	Long	Displ.	2.8	-2.8	0.05	triang.	0.02	2
04	Step#04-DC	Long	Displ.	3.9	-3.9	0.07	triang.	0.028	2
05	Step#05-DC	Long	Displ.	5.6	-5.6	0.10	triang.	0.04	2
06	Step#06-DC	Long	Displ.	11.2	-11.2	0.20	triang.	0.08	2
07	Step#07-DC	Long	Displ.	16.8	-16.8	0.30	triang.	0.08	2

It is worthwhile to mention that:

- the values of force planned for the first two steps (i.e. 30 kN and 45 kN) refer to the sum of forces applied to the test-structure by the two actuators, given the assumption of an inverted triangular distribution (i.e. proportional to the first mode of vibration). The planned proportion between the forces at the second and the first floor is 1.0:0.5. Thus, the planned values for these force-controlled cycles can be expressed as 30 (20+10) kN and 45 (30+15) kN.
- Once those force-controlled cycles will have been performed, displacement-controlled cycles could be calibrated or adapted in accordance with the observed/monitored structural response. The values reported above have been planned so far taking as reference the displacement of the actuator mounted at the second storey (i.e. mid-depth of the floor slab). The corresponding drifts were computed as the target displacement normalised by the total structure height, the latter being assumed as 5.62 m (i.e. level of the actuator at the second floor with respect to the foundation).
- The additional vertical gravity loads can be simulated through either concrete masses/blocks or a further layer of non-collaborating concrete topping. As one may notice in Figure 67 and Figure 68, use was made of the former solution for simplicity and reproducibility during the dynamic counterpart test (i.e. EUC-BUILD5). Figure 70 and Figure 71 show the number and the exact position of concrete masses on the first and second floor slabs, respectively. Eight and six concrete blocks were placed on the first and second floor levels before testing.

As a general observation concerning the setup described in this Section, it can be stated that it was designed to interfere as least as possible with the response of EUC-BUILD4 specimen. On the other hand, pseudostatic tests intrinsically imply the need of effectively transfer the loads from the setup to the specimen. As such, measures were indeed taken to keep this interaction to the minimum when horizontal forces are transferred to the structure. A few considerations can thus be made on that:

- A constant prestressing force, at the floors, has to be exerted so that the actuators can apply lateral loads to the specimen. No alternatives are available within this type of experimental framework, and a choice was therefore made to keep the prestressing force constant and slightly higher than the horizontal peak force that has to be applied during the test. This was to avoid a stepwise increase with cycles.
- As far as the application of the prestressing force is concerned, it was decided that the same system will be applied in the two principal directions. Because of the fact that each actuator needs to be solidly connected to the test-specimen, at each actuator location there are two steel plates and two steel rebars applying to the specimen a constant compression. A clear example of the adopted system is shown in Figure 65. Whilst in the transverse direction it was decided to arrange a hole at the top of each stability wall to allow the post-tensioned bars for passing through it without coming in contact with the wall-element, advantage was taken in the longitudinal direction of the holes of the slab panels, which were chosen to be clear from one end to the other, so as to permit the test-rig bars to pass all the way through.
- Nothing is foreseen to monitor the prestressing force because no variations are expected. Indeed, once a concrete element is prestressed (in this case with a very small level of force), there is no reason to expect variation of that force without concrete crushing. On the other hand, if the concrete crushes, there is no point on monitoring the prestressing force as probably there will be a complete disruption of the test-specimen.
- The tests will start without sliding restrainers, which can be considered as a safety measure for prevention of collapse mechanisms and damages to the instrumentation and setup itself. After testing of the as-built configuration, stoppers are meant to be “activated” for testing of the retrofitted configuration.

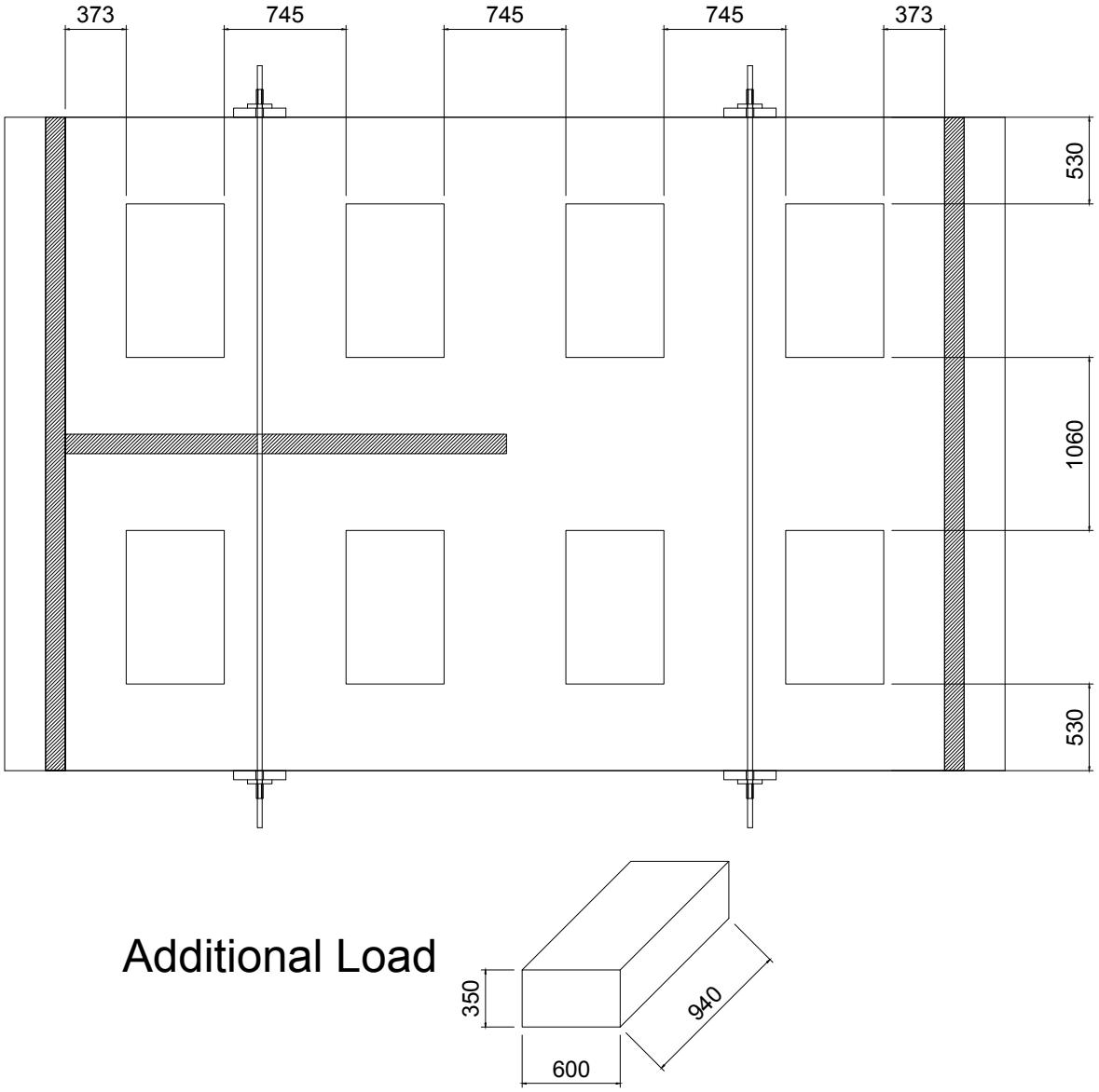

Figure 70. Number and position of concrete masses for additional gravity load – first floor slab.

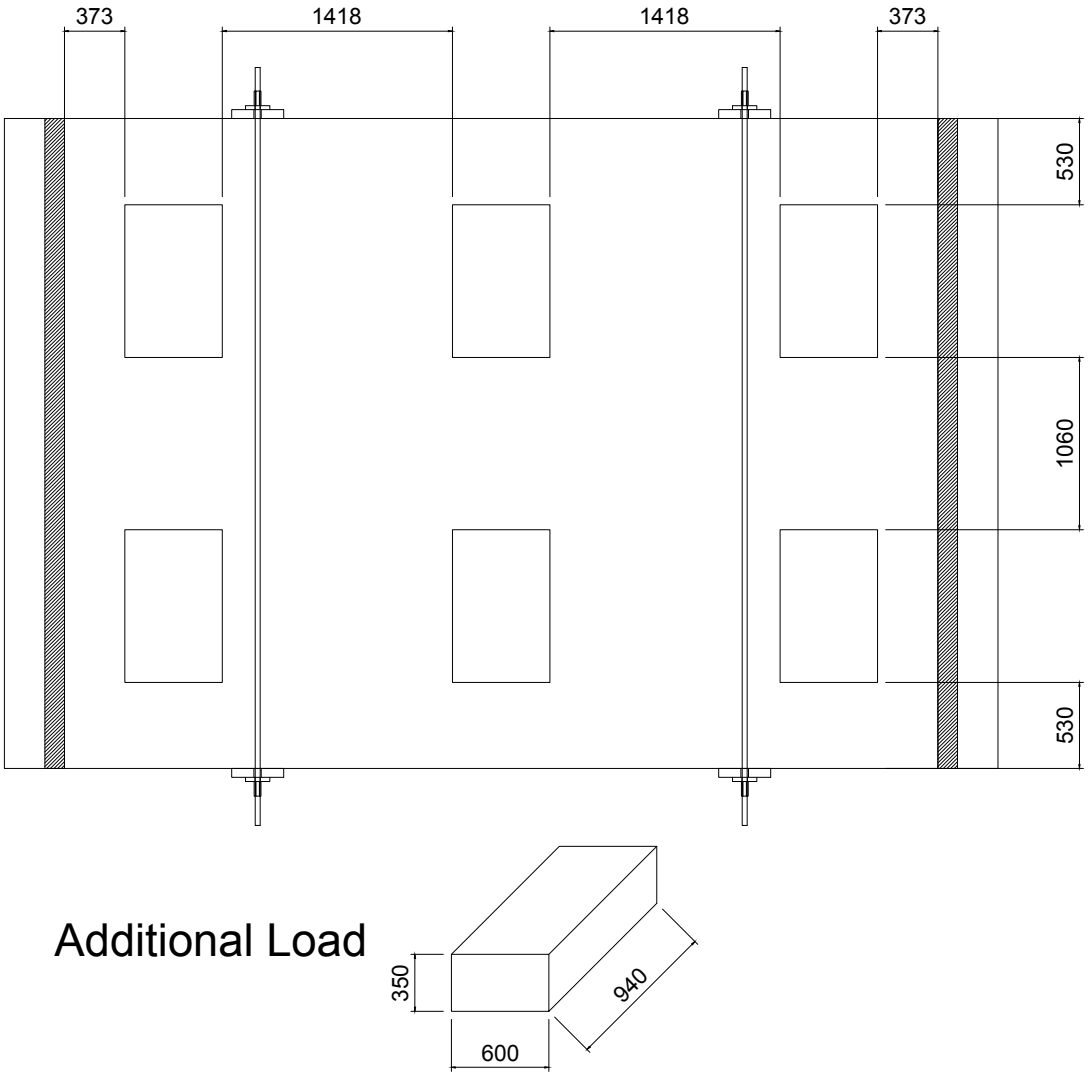

Figure 71. Number and position of concrete masses for additional gravity load – second floor slab.

5.4.2 Actual setup

A set of photos showing the actual setup used to test EUC-BUILD4 specimen is provided in Figure 72 to Figure 77. An overall view of the installed devices is presented therein together with details of specific components such as actuators and prestressing cables for the application of horizontal load in cyclic fashion.

In particular, Figure 73 shows the type of steel rebars used to post-tension the concrete foundation to the strong floor of the lab, whereas Figure 74 presents an example of the hole that was employed to allow the post-tensioned bar for passing through the stability wall without coming in contact with it.

As highlighted in Figure 75 and Figure 76, advantage was taken of post-tensioned bars and steel plates to connect the actuators to the specimen in the longitudinal direction as well. In this case, use was made of the slab panels holes, some of which designed to be clear all the way through. A detail of the sliding restrainers in their inactive configuration is shown in Figure 77. Worthwhile to note is

that, before the testing of EUC-BUILD4 specimen in as-built configuration, all the restrainers were set to have a 300 mm clearance with respect to the counterpart structural elements.

As previously mentioned, that 300 mm gap will then be eliminated before testing EUC-BUILD4 specimen in retrofitted configuration (after being damaged by mono-directional testing in its as-built scheme). An example of active restrainers for testing the retrofitted specimen is shown in Figure 78. Further details regarding the retrofitting scheme adopted will be given in Section 6.3.

Figure 72. Photographs of the experimental set-up mounted before testing the as-built configuration.

Figure 73. Detail of bars post-tensioned to the concrete foundation.

Figure 74. Detail of post-tensioned bars and clearance with respect to the stability wall panel.

Figure 75. Detail of steel plates and post-tensioned bars – longitudinal direction.

Figure 76. Detail of post-tensioned bars for application of lateral load in the longitudinal direction.

Figure 77. Detail of sliding restrainers – inactive configuration for testing the as-built specimen.

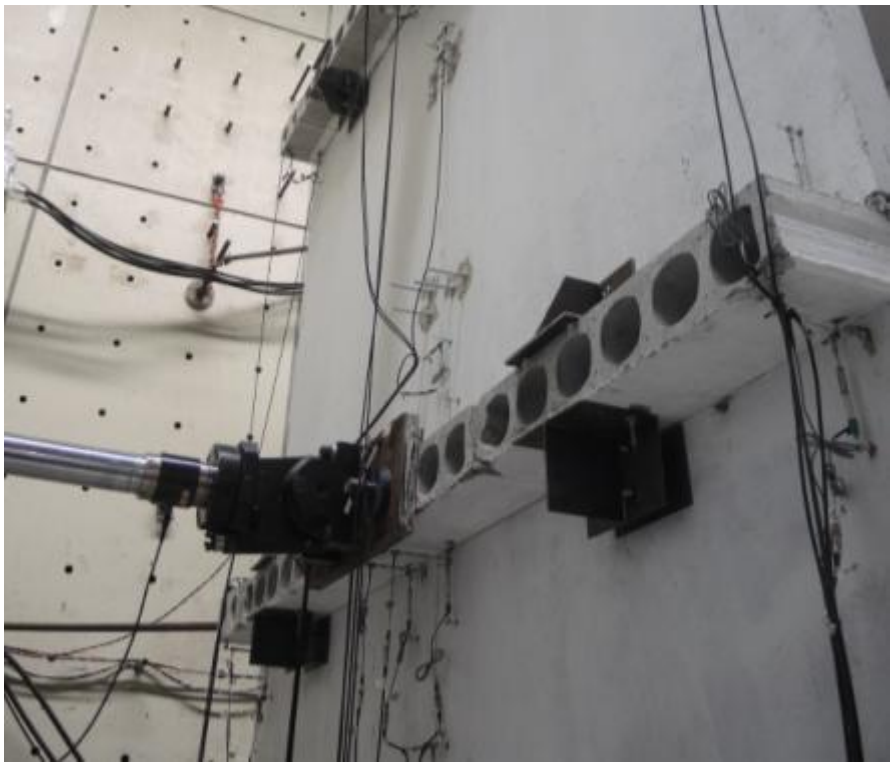

Figure 78. Detail of sliding restrainers – active configuration for testing the retrofitted specimen.

5.4.3 Execution of the test and loading protocol for as-built and retrofitted specimen

As reported in Table 1, pseudostatic mono-directional cyclic tests on EUC-BUILD4 specimen in as-built configuration and retrofitted configurations were performed on 11-13 April 2017 and 18-19 April 2017, respectively. Table 19 summarises the loading protocol that was effectively followed during the tests.

Table 19. EUC-BUILD4: loading protocol for testing as-built and retrofitted prototype.

AS-BUILT CONFIGURATION

Test run #	Test Name	Main DoF	Control Type	MAX Ampl.	MIN Ampl.	Drift Ampl.	Load Shape	Load Rate	Cycles
			(Force or Displ.)	[kN] [mm]	[kN] [mm]	[%]		[kN/s] [mm/s]	[#]
01	Step#01-FC	Long	Force	30	-30	-	triang.	0.1	2
02	Step#02-FC	Long	Force	45	-45	-	triang.	0.2	2
03	Step#03-DC	Long	Displ.	2.8	-2.8	0.05	triang.	0.02	2
04	Step#04-DC	Long	Displ.	3.9	-3.9	0.07	triang.	0.028	2
05	Step#05-DC	Long	Displ.	5.6	-5.6	0.10	triang.	0.04	2
06	Step#06-DC	Long	Displ.	11.2	-11.2	0.20	triang.	0.08	2
07	Step#07-DC	Long	Displ.	16.8	-16.8	0.30	triang.	0.08	2

RETROFITTED CONFIGURATION

Test run #	Test Name	Main DoF	Control Type	MAX Ampl.	MIN Ampl.	Drift Ampl.	Load Shape	Load Rate	Cycles
			(Force or Displ.)	[kN] [mm]	[kN] [mm]	[%]		[kN/s] [mm/s]	[#]
01R	Step#01R-FC	Long	Force	30	-30	-	triang.	0.1	2
02R	Step#02R-FC	Long	Force	45	-45	-	triang.	0.2	2
03R	Step#03R-FC	Long	Displ.	2.8	-2.8	0.05	triang.	0.02	2
04R	Step#04R-DC	Long	Displ.	3.9	-3.9	0.07	triang.	0.028	2
05R	Step#05R-DC	Long	Displ.	5.6	-5.6	0.10	triang.	0.04	2
06R	Step#06R-DC	Long	Displ.	11.2	-11.2	0.20	triang.	0.08	2
07R	Step#07R-DC	Long	Displ.	16.8	-16.8	0.30	triang.	0.08	2
08R	Step#08R-DC	Long	Displ.	33.7	-33.7	0.60	triang.	0.16	2

As previously mentioned, the cyclic testing of the as-built configuration was carried out without the sliding restrainers coming into play, in order not to alter the response of the specimen by preventing sliding from occurring in critical portions of the structure.

Table 19 summarises the loading protocol that, in the end, was effectively followed during the tests of EUC-BUILD4 “as-built” specimen. Initially, the horizontal actuators were kept unloaded and the concrete masses were set in place on the first- and second-storey floor slabs to simulate the vertical

gravity loads. Once the additional loads were applied, the horizontal loading history was applied in a mixed force-controlled and displacement-controlled procedure. It is worth noting that the duration of each cycle was kept almost constant, incrementing the displacement rate almost proportionally to the target displacement of the cycle. It was decided to begin testing by pulling rather than pushing, and this sign convention (i.e. positive stands for pulling stages) was also assumed for the discussion of the obtained results (Chapter 6).

The force-controlled cycles at ± 30 kN and ± 45 kN were performed in the longitudinal direction of the specimen, and, after those cycles were completed, it was decided to switch the control of the testing into a displacement-based one. As reported in Table 19, two cycles per amplitude were performed in such way that one may gather not only information on potential degradation from amplitude to amplitude but also from cycle to cycle. Only the first two force-controlled loading cycles were carried out on 12th April 2017, whilst it was proceeded with the (displacement-controlled) cycling of the specimen on 13th April 2017.

Cyclic inelastic tests were performed (only) in the longitudinal direction up to a total storey drift of 0.3%, which is lower than what had been initially envisaged because of the premature failure of three-way joints at the first storey of the building, as discussed in Chapter 6, laid evident by visual inspection of the structure (a decision to stop the test was made, since the specimen was clearly not able to sustain any additional horizontal load of relevance). It was then decided to "tighten" some of the sliding restrainers to the precast walls to simulate a likely retrofitting strategy, and then re-test the specimen, with a view to gather not only further potentially useful information (for the numerical calibration) on the behaviour of EUC-BUILD4 specimen, but also appreciate if and how a simple retrofitting measure may or not improve the seismic resistance of this type of structures.

This "simulated retrofitting" was implemented by Eucentre technicians during the day of April 14th, with a view to allow for testing on April 18th or 19th. The technicians applied the retrofitted scheme, and it was tried as much as possible to get the specimen back to an undeformed stage, although this was in the end not fully possible, since the damage was too extensive and a permanent gap of about 2.5 cm remained between the stability and transverse walls of the ground floor. The aforementioned "retrofitting" efforts prevented technicians from re-testing the specimen on 18th April.

Cyclic testing of EUC-BUILD4 "retrofitted" specimen was executed on 19th April 2017. Although the building mock-up was "not-fully-effectively-retrofitted", it was possible to push the structure up to a roof displacement level (33.7 mm) that was double the displacement that had instead taken the original specimen EUC-BUILD4 to incipient collapse. The applied loading protocol, together with the one adopted for the as-built configuration, are summarised in Table 19. The testing was stopped at the end of the fifth envisaged set of displacement-controlled cycles, when not only very extensive damage was seen spreading throughout the specimen (including a full-depth/full-width/mid-height horizontal crack in the transverse wall), but also in-cycle and between-cycle strength degradation started being observed. This final test run did confirm that, by guaranteeing (through steel angles) a sturdier wall-slab connection, a better response could be readily obtained (see Chapter 6).

5.5 Instrumentation of tested specimen

5.5.1 Rationale

Monitoring of displacements and forces applied to the test-specimen is of paramount importance to understand and model the structural behaviour. The load cells on the actuators will measure the horizontal forces applied to the structure. In order to summarise both the number and the type of instruments used to monitor the tests on EUC-BUILD4 specimen, tables are reported in the following, along with the nomenclature assumed for panel-elements. Furthermore, schematics are also presented in Section 5.5.2 to provide a clear picture of the position of those instruments. Reference front views (South and North ones) are shown in Figure 79. In addition, one side (East) view is presented in Figure 80, whereas three plan views corresponding to each floor level of interest are collected in Figure 81.

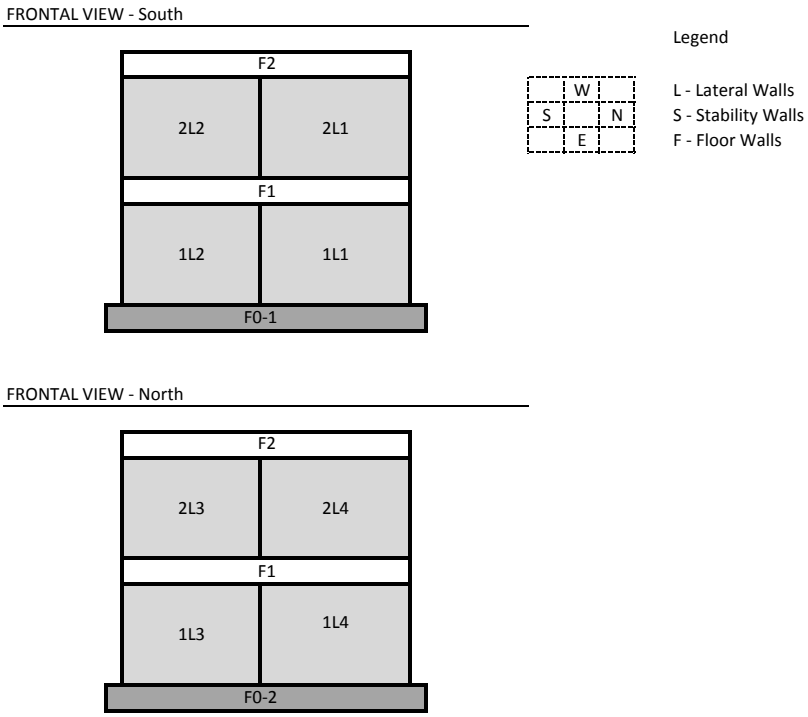

Figure 79. EUC-BUILD4 specimen: reference front (South-North) views for instrumentation.

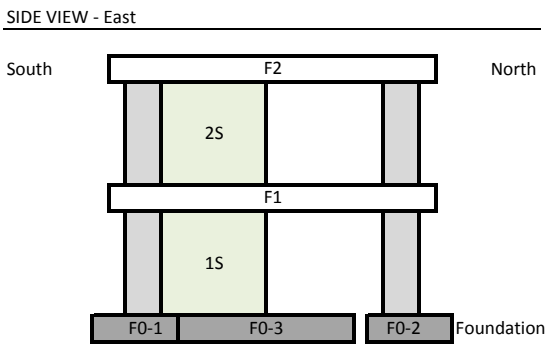

Figure 80. EUC-BUILD4 specimen: reference side (East) views for instrumentation.

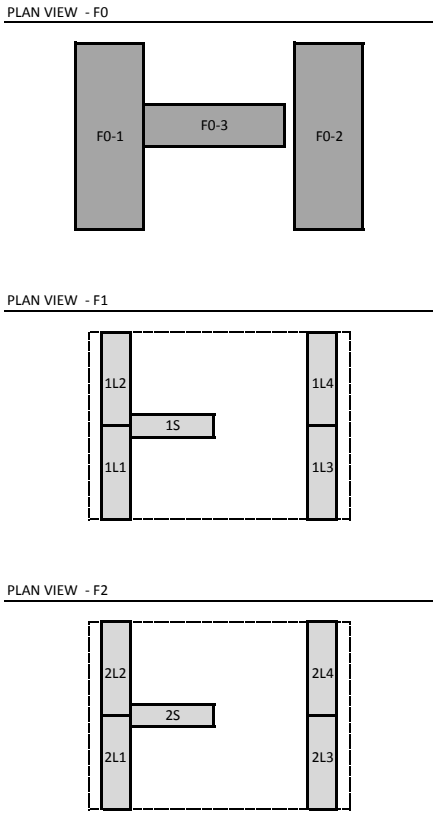

Figure 81. EUC-BUILD4 specimen: reference plan views for instrumentation (ground, first and second floors).

A number of displacement transducers connected to a fixed reference monitor global displacements of the specimen at both floor levels. In addition, the displacements parallel to the weakest direction of the specimen are monitored on both sides of each floor slab in order to check its possible torsion or uneven displacement of it. Table 20 presents the number of instruments installed to monitor global displacements of the two floor slabs.

As described in Table 21, the out-of-plane displacement of lateral walls is monitored at both base and top, and the same applies to the monitoring of the in-plane rocking and the transversal rocking of those elements (see Table 22 to Table 27). Furthermore, Table 28 collects the set of instruments that are positioned to measure the sliding of the lateral walls at their top and bottom. Particular care was also paid to the two stability walls, in terms of relative sliding with respect to the corresponding lateral walls (see Table 29), as well as for what concerns in-plane deformation, transversal rocking and out-of-plane displacement (see Table 30 to Table 33). As presented in Table 34 and Table 35, it was also decided to take track of both the possible in-plane deformation of the precast slab-elements and the eventual sliding of concrete foundations, even though these were naturally very unlikely deformation mechanisms. Lastly, two instruments with very high accuracy were placed in correspondence to the second-story stability wall so as to monitor the eventual opening of the pre-crack running through the entire width of the panel and also through its entire depth.

Table 20. Instrumentation: global displacement of first and second floors.

General note	Instrument #	Type	Stroke	Description
Global Displacement -F1	1	Tast.	25	(W-E) - Ext. Displacement - F1 - Position (WS)
	2	Tast.	25	(W-E) - Ext. Displacement - F1 - (WN)
	3	Pot.	100	(S-N) - Ext. Displacement - F1 - (NW)
	4	Pot.	100	(S-N) - Ext. Displacement - F1 - (N)
	5	Pot.	100	(S-N) - Ext. Displacement - F1 - (NE)
Global Displacement -F2	6	Tast.	25	(W-E) - Ext. Displacement - F2 - (WS)
	7	Tast.	25	(W-E) - Ext. Displacement - F2 - (WN)
	8	Pot.	250	(S-N) - Ext. Displacement - F2 - (NW)
	9	Pot.	250	(S-N) - Ext. Displacement - F2 - (N)
	10	Pot.	250	(S-N) - Ext. Displacement - F2 - (NE)
Global Displacement -F1	11	Pot.	25	(S-N) - Ext. Displacement - F1 - (N)
Global Displacement -F2	12	Pot.	25	(S-N) - Ext. Displacement - F2 - (N)

Table 21. Instrumentation: out-of-plane displacement of lateral walls.

General note	Instrument #	Type	Stroke	Description
Lateral Wall - 1L1	13	Pot.	50	W1L1 - SE - Out-of-Plane Displ. @Top
Out-of-plane displacement	14	Pot.	50	W1L1 - SW - Out-of-Plane Displ. @Top
	15	Pot.	50	W1L1 - SE - Out-of-Plane Displ. @Base
	16	Pot.	50	W1L1 - SW - Out-of-Plane Displ. @Base
Lateral Wall - 1L2	17	Pot.	50	W1L2 - SE - Out-of-Plane Displ. @Top
Out-of-plane displacement	18	Pot.	50	W1L2 - SW - Out-of-Plane Displ. @Top
	19	Pot.	50	W1L2 - SE - Out-of-Plane Displ. @Base
	20	Pot.	50	W1L2 - SW - Out-of-Plane Displ. @Base
Lateral Wall - 1L3	21	Tast.	50	W1L3 - North - Out-of-Plane Displ. @Top
Out-of-plane displacement	22	Tast.	50	W1L3 - N - Out-of-Plane Displ. @Base
Lateral Wall - 1L4	23	Tast.	50	W1L4 - N - Out-of-Plane Displ. @Top
Out-of-plane displacement	24	Tast.	50	W1L4 - N - Out-of-Plane Displ. @Base
Lateral Wall - 2L1	25	Pot.	50	W2L1 - SE - Out-of-Plane Displ. @Top
Out-of-plane displacement	26	Pot.	50	W2L1 - SW - Out-of-Plane Displ. @Top
	27	Pot.	50	W2L1 - SE - Out-of-Plane Displ. @Base
	28	Pot.	50	W2L1 - SW - Out-of-Plane Displ. @Base
Lateral Wall - 2L2	29	Pot.	50	W2L2- SE - Out-of-Plane Displ. @Top
Out-of-plane displacement	30	Pot.	50	W2L2 - SW - Out-of-Plane Displ. @Top
	31	Pot.	50	W2L2 - SE - Out-of-Plane Displ. @Base
	32	Pot.	50	W2L2 - SW - Out-of-Plane Displ. @Base
Lateral Wall - 2L3	33	Tast.	50	W2L3 - N - Out-of-Plane Displ. @Top
Out-of-plane displacement	34	Tast.	50	W2L3 - N - Out-of-Plane Displ. @Base
Lateral Wall - 2L4	35	Pot.	50	W2L4 - N - Out-of-Plane Displ. @Top
Out-of-plane displacement	36	Pot.	50	W2L4 - N - Out-of-Plane Displ. @Base

Table 22. Instrumentation: in-plane and transversal rocking of lateral wall 1L1.

General note	Instrument #	Type	Stroke	Description
Lateral Wall - 1L1	37	Pot.	50	Wall 1L1 -South East - Rocking @Top
In-plane rocking	38	Pot.	50	W1L1-SW - Rocking @Top
	39	Pot.	50	W1L1-SE - Rocking @Base
	40	Pot.	50	W1L1-SW - Rocking @Base
Lateral Wall - 1L1	41	Pot.	50	W1L1-NE - Rocking @Top
Transversal Rocking	42	Pot.	50	W1L1-NW - Rocking @Top
	43	Pot.	50	W1L1-NE - Rocking @Base
	44	Pot.	50	W1L1-NW - Rocking @Base

Table 23. Instrumentation: in-plane and transversal rocking of lateral wall 1L2.

General note	Instrument #	Type	Stroke	Description
Lateral Wall - 1L2	45	Pot.	50	W1L2-SE - Rocking @Top
In-plane rocking	46	Pot.	50	W1L2-SW - Rocking @Top
	47	Pot.	50	W1L2-SE - Rocking @Base
	48	Pot.	50	W1L2-SW - Rocking @Base
Lateral Wall - 1L2	49	Pot.	50	W1L2-NE - Rocking @Top
Transversal Rocking	50	Pot.	50	W1L2-NW - Rocking @Top
	51	Pot.	50	W1L2-NE - Rocking @Base
	52	Pot.	50	W1L2-NW - Rocking @Base

Table 24. Instrumentation: in-plane and transversal rocking of lateral walls 1L3 and 1L4.

General note	Instrument #	Type	Stroke	Description
Lateral Wall - 1L3	53	Pot.	50	W1L3-N - Rocking @Top
Transversal Rocking	54	Pot.	50	W1L3-N - Rocking @Base
Lateral Wall - 1L3	55	Pot.	50	W1L3-S - Rocking @Top
Transversal Rocking	56	Pot.	50	W1L3-S - Rocking @Base
Lateral Wall - 1L4	57	Pot.	50	W1L4-N - Rocking @Top
Transversal Rocking	58	Pot.	50	W1L4-N - Rocking @Base
Lateral Wall - 1L4	59	Pot.	50	W1L4-S - Rocking @Top
Transversal Rocking	60	Pot.	50	W1L4-S - Rocking @Base

Table 25. Instrumentation: in-plane and transversal rocking of lateral wall 2L1.

General note	Instrument #	Type	Stroke	Description
Lateral Wall - 2L1	61	Pot.	50	W2L1-SE - Rocking @Top
In-plane rocking	62	Pot.	50	W2L1-SW - Rocking @Top
	63	Pot.	50	W2L1-SE - Rocking @Base
	64	Pot.	50	W2L1-SW - Rocking @Base
Lateral Wall - 2L1	65	Pot.	50	W2L1-NE - Rocking @Top
Transversal Rocking	66	Pot.	50	W2L1-NW - Rocking @Top
	67	Pot.	50	W2L1-NE - Rocking @Base
	68	Pot.	50	W2L1-NW - Rocking @Base

Table 26. Instrumentation: in-plane and transversal rocking of lateral wall 2L2.

General note	Instrument #	Type	Stroke	Description
Lateral Wall - 2L2	69	Pot.	50	W2L2-SE - Rocking @Top
In-plane rocking	70	Pot.	50	W2L2-SW - Rocking @Top
	71	Pot.	50	W2L2-SE - Rocking @Base
	72	Pot.	50	W2L2-SW - Rocking @Base
Lateral Wall - 2L2	73	Pot.	50	W2L2-NE - Rocking @Top
Transversal Rocking	74	Pot.	50	W2L2-NW - Rocking @Top
	75	Pot.	50	W2L2-NE - Rocking @Base
	76	Pot.	50	W2L2-NW - Rocking @Base

Table 27. Instrumentation: in-plane and transversal rocking of lateral walls 2L3 and 2L4.

General note	Instrument #	Type	Stroke	Description
Lateral Wall - 2L3	77	Pot.	50	W2L3-N - Rocking @Top
Transversal Rocking	78	Pot.	50	W2L3-N - Rocking @Base
Lateral Wall - 2L3	79	Pot.	50	W2L3-S - Rocking @Top
Transversal Rocking	80	Pot.	50	W2L3-S - Rocking @Base
Lateral Wall - 2L4	81	Pot.	50	W2L4-N - Rocking @Top
Transversal Rocking	82	Pot.	50	W2L4-N - Rocking @Base
Lateral Wall - 2L4	83	Pot.	50	W2L4-S - Rocking @Top
Transversal Rocking	84	Pot.	50	W2L4-S - Rocking @Base

Table 28. Instrumentation: sliding of lateral walls.

General note	Instrument #	Type	Stroke	Description
Lateral Wall - 1L1 / 1L2	85	Pot.	25	W 1L1 / 1L2 - S - Sliding @Top
Wall sliding	86	Pot.	25	W 1L1 / 1L2 - S - Sliding @Base
Lateral Wall - 1L3 / 1L4	87	Pot.	25	W 1L3 / 1L4 - N - Sliding @Top
Wall sliding	88	Pot.	25	W 1L3 / 1L4 - N - Sliding @Base
Lateral Wall - 2L1 / 2L2	89	Pot.	25	W 2L1 / 2L2 - S - Sliding @Top
Wall sliding	90	Pot.	25	W 2L1 / 2L2 - S - Sliding @Base
Lateral Wall - 2L3 / 2L4	91	Pot.	25	W 2L3/ 2L4 - N - Sliding @Top
Wall sliding	92	Pot.	25	W 2L3/ 2L4 - N - Sliding @Base

Table 29. Instrumentation: lateral wall-to-stability wall sliding.

General note	Instrument #	Type	Stroke	Description
Lateral Wall / Stability Wall _ 1L1 - 1S	93	Pot.	50	1S-ES - Relative Sliding @Center |
Lateral Wall / Stability Wall _ 1L2 - 1S	94	Pot.	50	1S-WS - Relative Sliding @Center |
Lateral Wall / Stability Wall _ 2L1 - 2S	95	Pot.	50	2S-ES - Sliding @Center |
Lateral Wall / Stability Wall _ 2L2 - 2S	96	Pot.	50	2S-WS - Sliding @Center |

Table 30. Instrumentation: out-of-plane displacement of stability walls.

General note	Instrument #	Type	Stroke	Description
Stability Wall - 1S	97	Pot.	50	1S - ES - Out-of-Plane Displ. @Top
Out-of-plane displacement	98	Pot.	50	1S - EN - Out-of-Plane Displ. @Top
	99	Pot.	50	1S - ES - Out-of-Plane Displ. @Base
	100	Pot.	50	1S - EN - Out-of-Plane Displ. @Base
Stability Wall - 2S	101	Pot.	50	2S - ES - Out-of-Plane Displ. @Top
Out-of-plane displacement	102	Pot.	50	2S - EN - Out-of-Plane Displ. @Top
	103	Pot.	50	2S - ES - Out-of-Plane Displ. @Base
	104	Pot.	50	2S - EN - Out-of-Plane Displ. @Base

Table 31. Instrumentation: in-plane deformation and transversal rocking of stability wall 1S.

General note	Instrument #	Type	Stroke	Description
Stability Wall - 1S	105	Pot.	50	1S-ES - Rocking @Top
In-plane deformation	106	Pot.	50	1S-EN - Rocking @Top
	107	Pot.	50	1S-ES - Rocking @Base
	108	Pot.	50	1S-EN - Rocking @Base
	109	Pot.	50	1S-E - Sliding @Top ---
	110	Pot.	50	1S-E - Sliding @Base ---
Stability Wall - 1S	111	Pot.	50	1S-WS - Rocking @Top
Transversal Rocking	112	Pot.	50	1S-WN - Rocking @Top
	113	Pot.	50	1S-WS - Rocking @Base
	114	Pot.	50	1S-WN - Rocking @Base

Table 32. Instrumentation: in-plane deformation and transversal rocking of stability wall 2S.

General note	Instrument #	Type	Stroke	Description
Stability Wall - 2S	115	Pot.	50	2S-ES - Rocking @Top
In-plane deformation	116	Pot.	50	2S-EN - Rocking @Top
	117	Pot.	50	2S-ES - Rocking @Base
	118	Pot.	50	2S-EN - Rocking @Base
	119	Pot.	50	2S-E - Sliding @Top ---
	120	Pot.	50	2S-E - Sliding @Base ---
Stability Wall - 2S	121	Pot.	50	2S-WS - Rocking @Top
Transversal Rocking	122	Pot.	50	2S-WN - Rocking @Top
	123	Pot.	50	2S-WS - Rocking @Base
	124	Pot.	50	2S-WN - Rocking @Base

Table 33. Instrumentation: out-of-plane displacement (stability wall-to-lateral wall).

General note	Instrument #	Type	Stroke	Description
Lateral Wall / Stability Wall _ 1L1 - 1S	125	Tast.	25	W1L1/1S - SE - Out-of-Plane Displ. @Top
Out-of-plane displacement	126	Tast.	25	W1L1/1S - SE - Out-of-Plane Displ. @Base
Lateral Wall / Stability Wall _ 1L2 - 1S	127	Tast.	25	W1L2/1S - SW - Out-of-Plane Displ. @Top
Out-of-plane displacement	128	Tast.	25	W1L2/1S - SW - Out-of-Plane Displ. @Base
Lateral Wall / Stability Wall _ 2L1 - 2S	129	Tast.	25	W2L1/2S - SE - Out-of-Plane Displ. @Top
Out-of-plane displacement	130	Tast.	25	W2L1/2S - SE - Out-of-Plane Displ. @Base
Lateral Wall / Stability Wall _ 2L2 - 2S	131	Tast.	25	W2L2/2S - SW - Out-of-Plane Displ. @Top
Out-of-plane displacement	132	Tast.	25	W2L2/2S - SW - Out-of-Plane Displ. @Base

Table 34. Instrumentation: in-plane deformation of slab-elements.

General note	Instrument #	Type	Stroke	Description
F1 - Floor	133	Pot.	25	F1- E - Defomation
In-plane deformation	134	Pot.	25	F1- Center - Defomation
	135	Pot.	25	F1- W - Defomation
F2 - Floor	136	Pot.	25	F2- E - Defomation
In-plane deformation	137	Pot.	25	F2- Center - Defomation
	138	Pot.	25	F2- W - Defomation

Table 35. Instrumentation: sliding of foundations and crack monitoring of stability wall S2.

General note	Instrument #	Type	Stroke	Description
F0 - Foundation	139	Pot.	25	F0- SE - Sliding
	140	Pot.	25	F0- NE - Sliding
Stability Wall - 2S	141	Pot.	25	S2 -W - Deformation /
S2 - Crack Monitoring	142	Ωgage	2	S2 -W - Deformation /

Considering that the response/behaviour of the lateral walls is controlled by phenomena/mechanisms of rocking (both in-plane one and transversal one), the in-plane deformation of these precast walls was not monitored during the tests of EUC-BUILD4 specimen. On the other hand, both sliding and out-of-plane deformations were measured. Twelve instruments per each storey were used for the latter mechanisms, whereas two potentiometers per each panel were used to measure sliding relative to the other companion lateral wall (see Table 28). It is also noteworthy that sliding of the lateral walls with respect to the companion stability wall, if present, is monitored as summarised in Table 29. The out-of-plane displacements (i.e. lateral wall-to-stability wall) at the top and bottom of the two different wall-elements were monitored as well (Table 33).

The in-plane deformation of the two stability walls is monitored according to the rationale and scheme reported in Table 31 and Table 32, and the same applies to the transversal rocking and the out-of-plane displacements experienced by these elements. Four instruments were indeed considered, for each mechanism, in each one of the two stability walls. Given that these are supposed to carry the higher shear forces, the presence of a crack running through the entire width and depth of one of them was monitored very carefully during the execution of the testing sequence. In fact, two additional instruments having a high accuracy were placed close to the vertical edge of

the second-storey wall to monitor the above-mentioned crack and its evolution during the imposed cycles (see Table 35).

When pulling/pushing the structure in its weakest direction, sliding of the floor slabs with respect to the walls above and underneath them is expected. Global displacements of the first and the second floors are thus of paramount importance and are hence monitored by means of twelve instruments, six per each storey. Two transducers monitor possible displacement between the walls and the floor and the base of the wall and the foundation. As sliding is also expected to occur at the second storey, the same scheme was applied therein. Worthwhile to mention is also that the relative displacements between the hollow core slab panels composing the two floors will be measured so as to verify the effectiveness of the slab topping or, alternatively, to take track of any local mechanism that might eventually occur.

In addition to the tables collected above, a set of CAD drawings of the instrumentation used for EUC-BUILD4 specimen is shown in the following paragraph.

5.5.2 Identification of the position of potentiometers

As planned and discussed in the previous paragraph, a total of 142 instruments were considered to measure crucial structural response parameters at key locations throughout the specimen. Figure 82 shows a few plan views of EUC-BUILD4 specimen that can be considered as a helpful reference for the identification of the position of the installed instrumentation. In particular, Figure 83 to Figure 86 depict front views of the instrumented structure, showing the number and position of each single instrument mounted onto the lateral walls at both South and North sides. Furthermore, in Figure 87 and Figure 88, East and West side views of EUC-BUILD4 specimen are provided in order to clarify the position of the instrumentation installed onto the two stability walls. The information contained therein could then be merged also with the details collected in Figure 89 and Figure 90, which instead identify the set of displacement transducers placed in correspondence to the first- and second-storey slabs, respectively. Three-dimensional drawings of the instrumented building mock-up are finally given in Figure 91, Figure 92, Figure 93 and Figure 94.

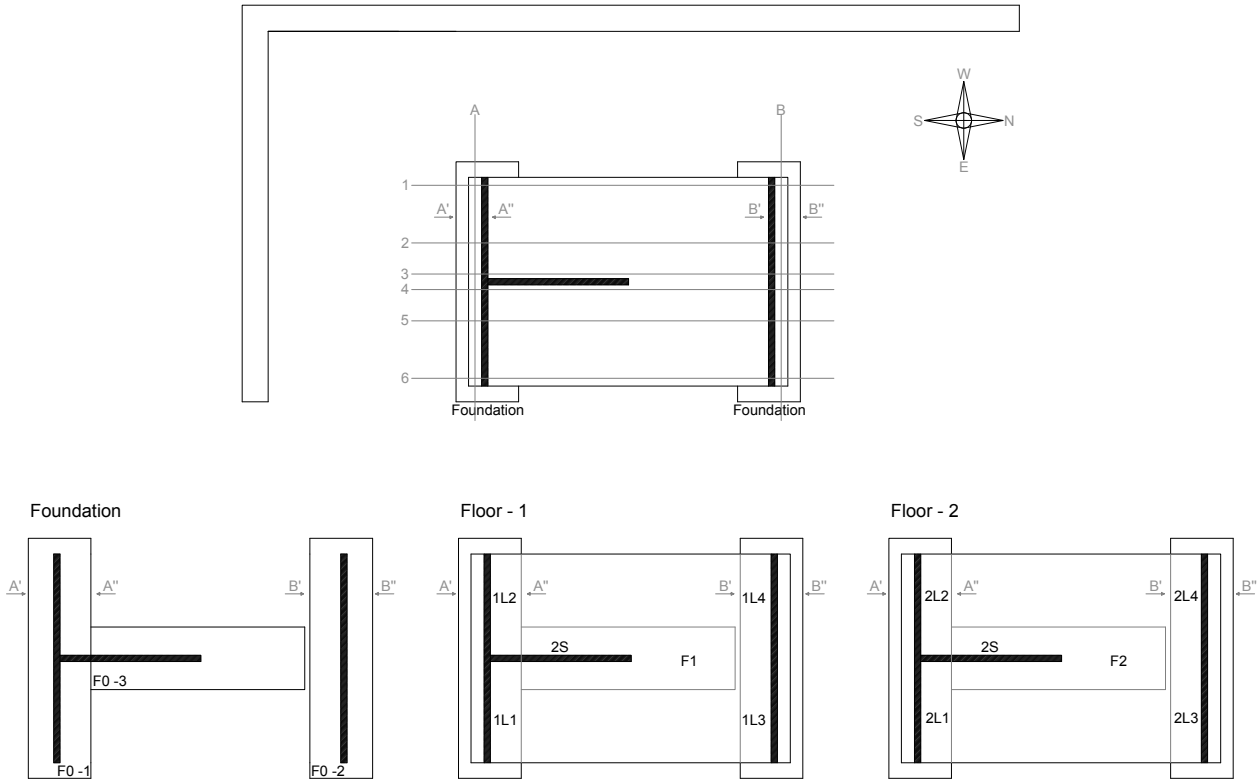

Figure 82. Plan views of EUC-BUILD4 specimen – position of the installed instrumentation.

A'

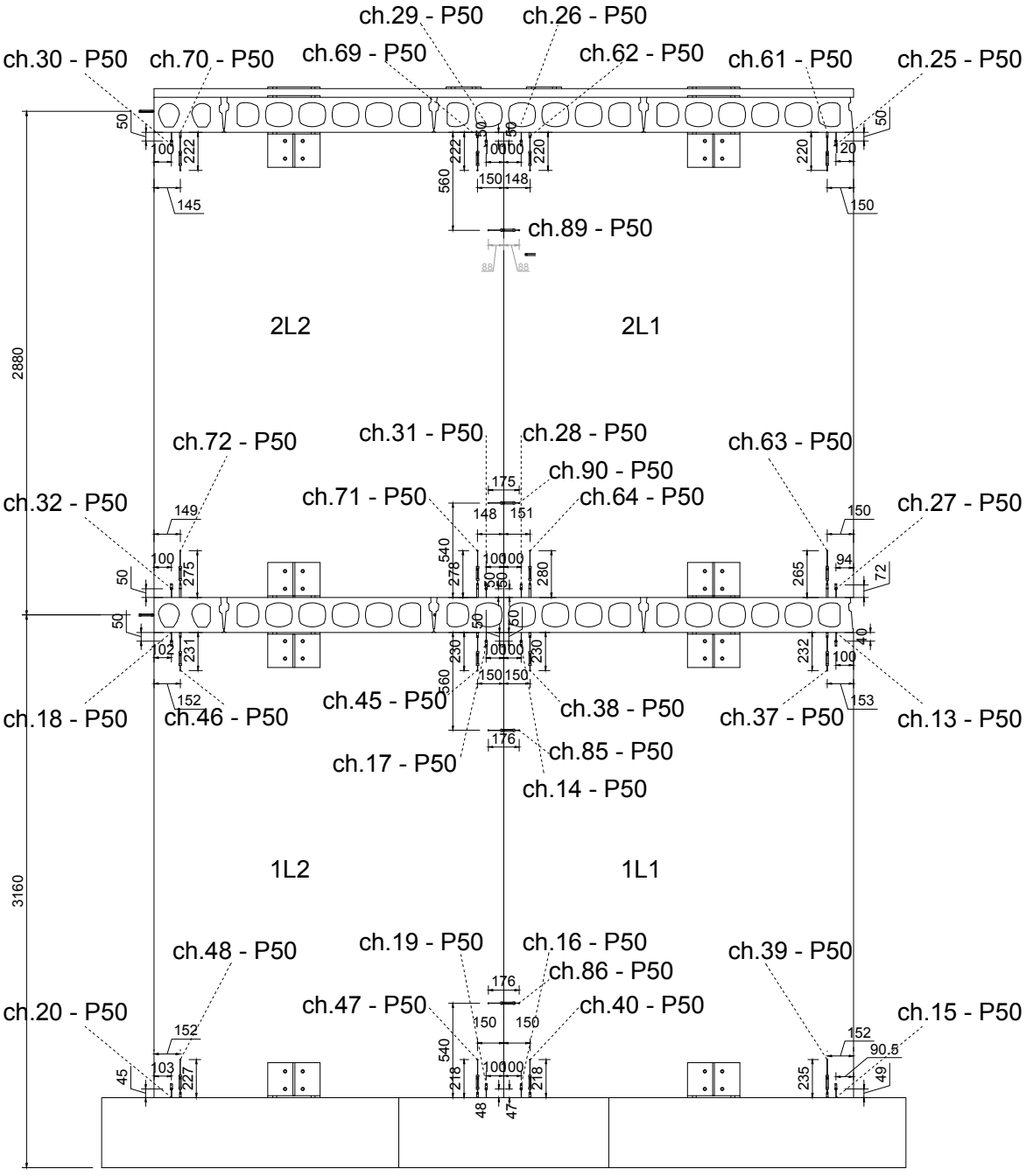

Figure 83. Schematic of the installed instrumentation: front views of the specimen – Lateral walls, A'.

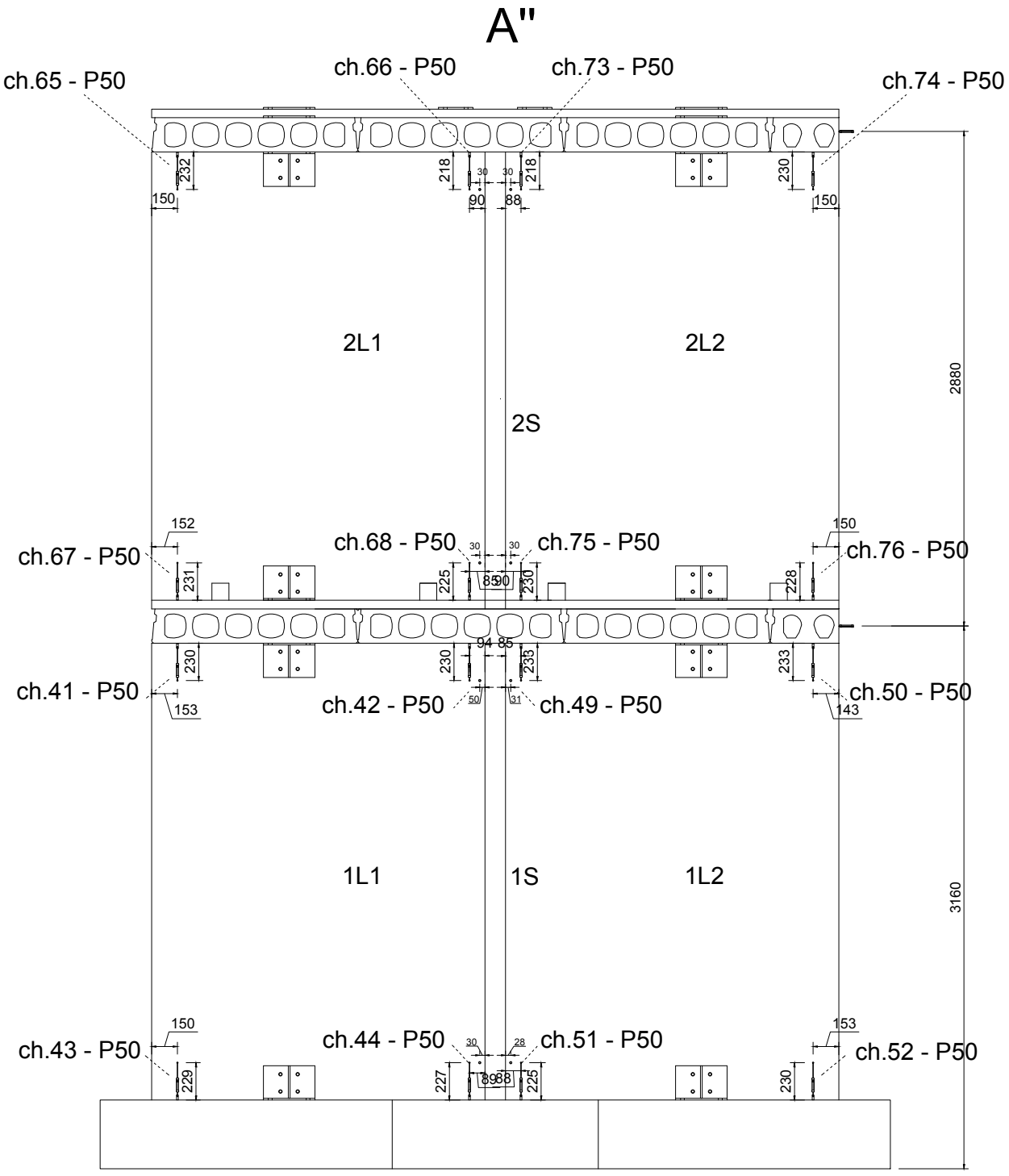

Figure 84. Schematic of the installed instrumentation: front views of the specimen – Lateral walls, A''.

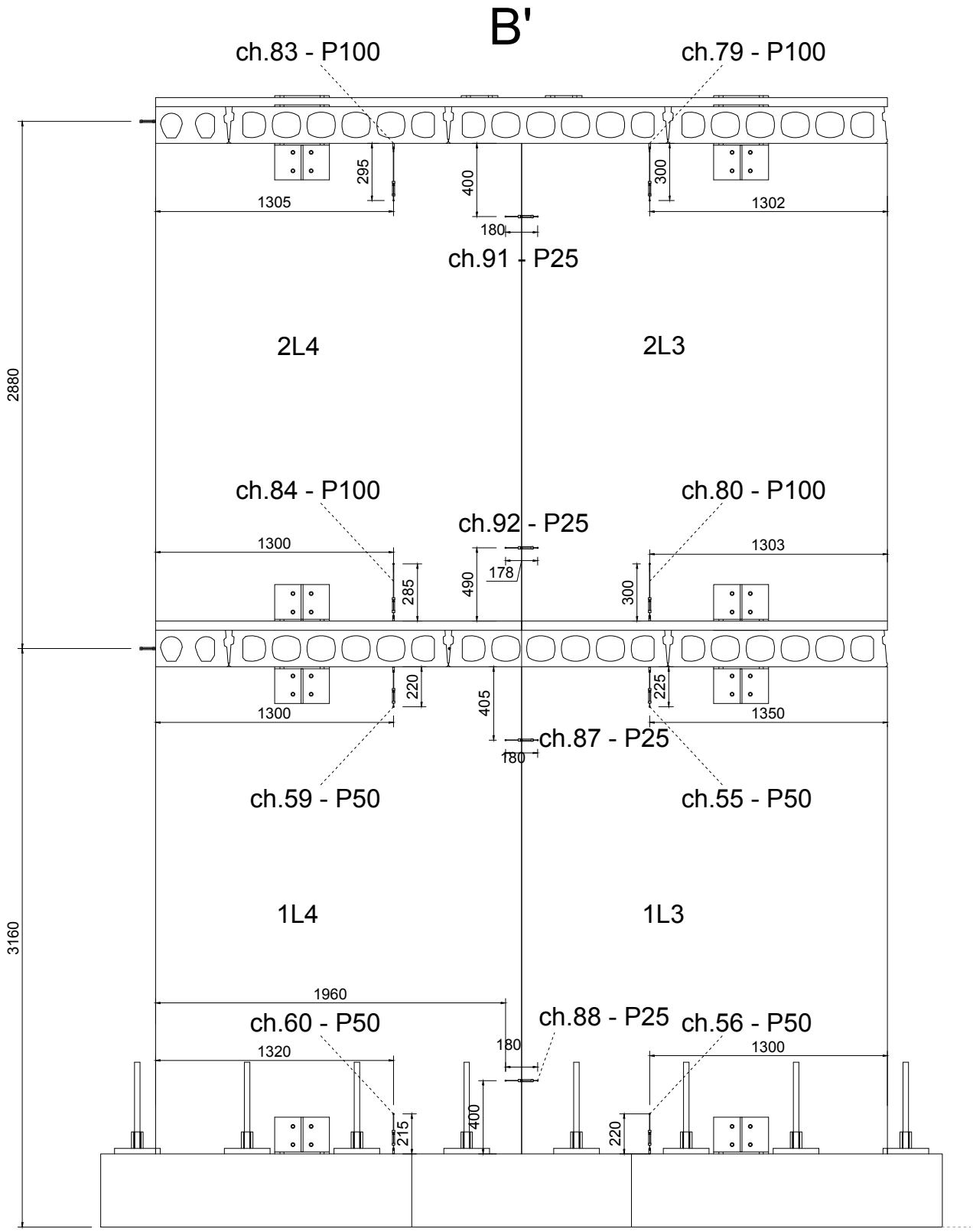

Figure 85. Schematic of the installed instrumentation: front views of the specimen – Lateral walls, B'.

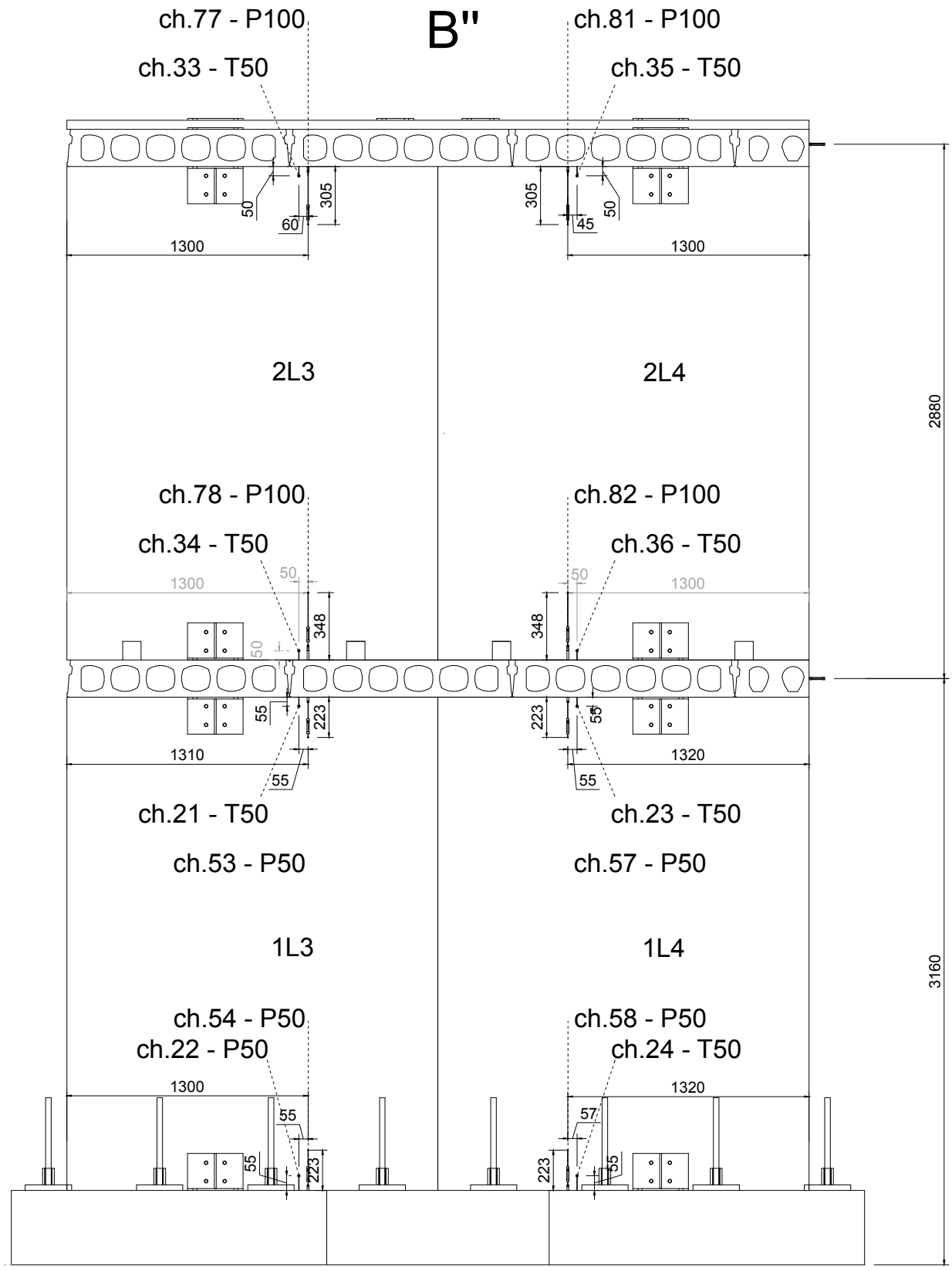

Figure 86. Schematic of the installed instrumentation: front views of the specimen – Lateral walls, B''.

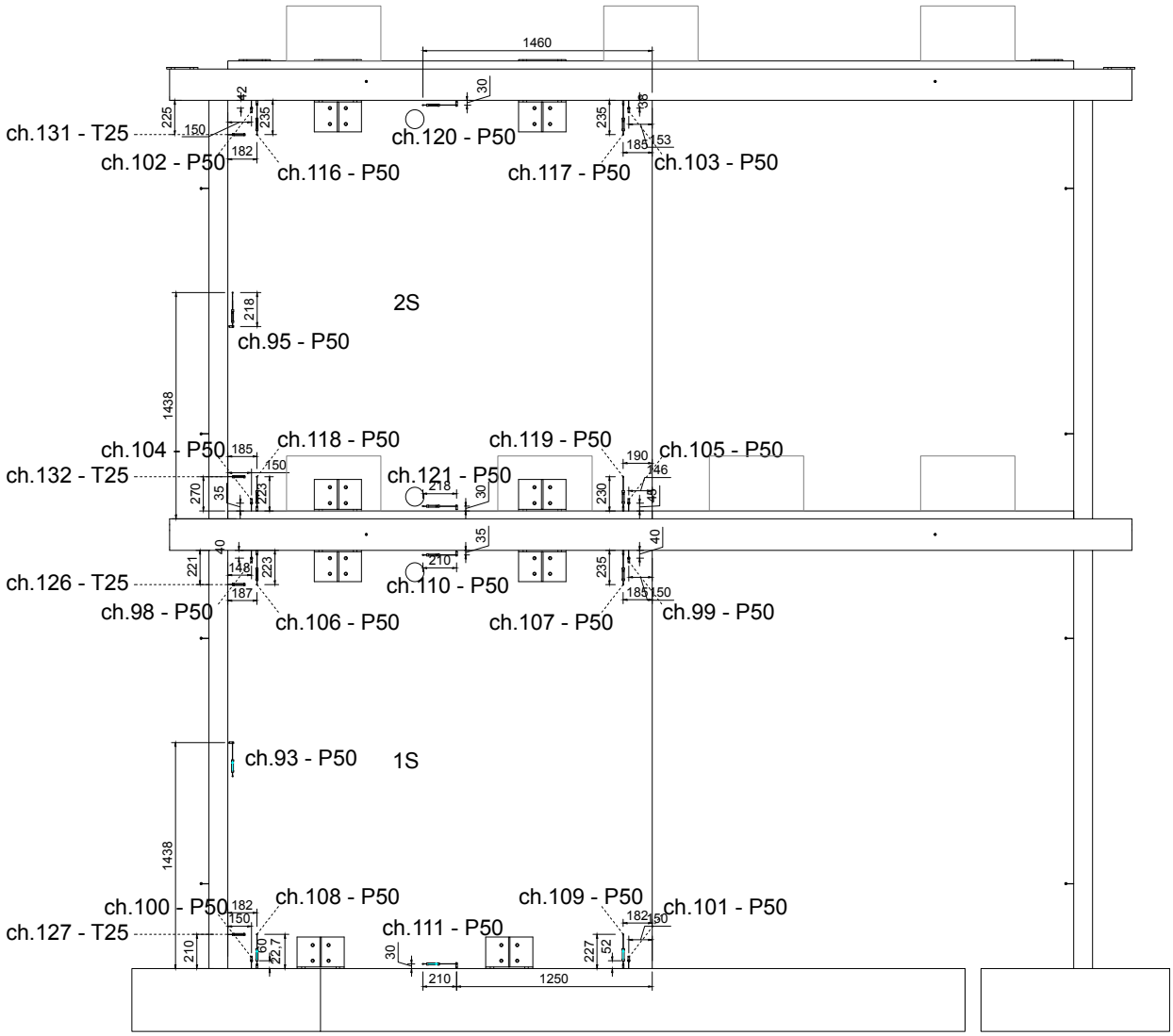

Figure 87. Installed instrumentation: side views of the specimen – Stability walls, East.

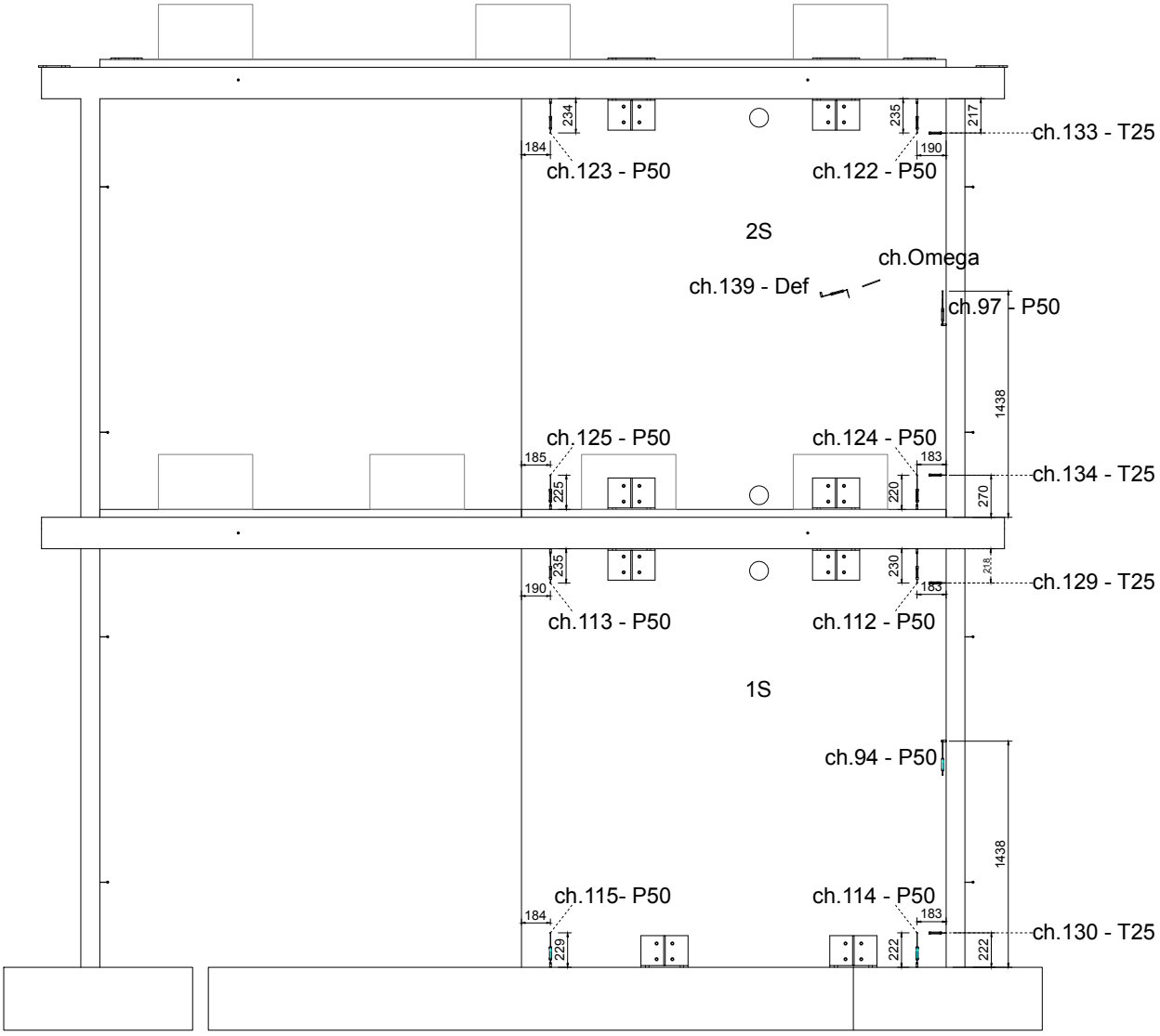

Figure 88. Installed instrumentation: side views of the specimen – Stability walls, West.

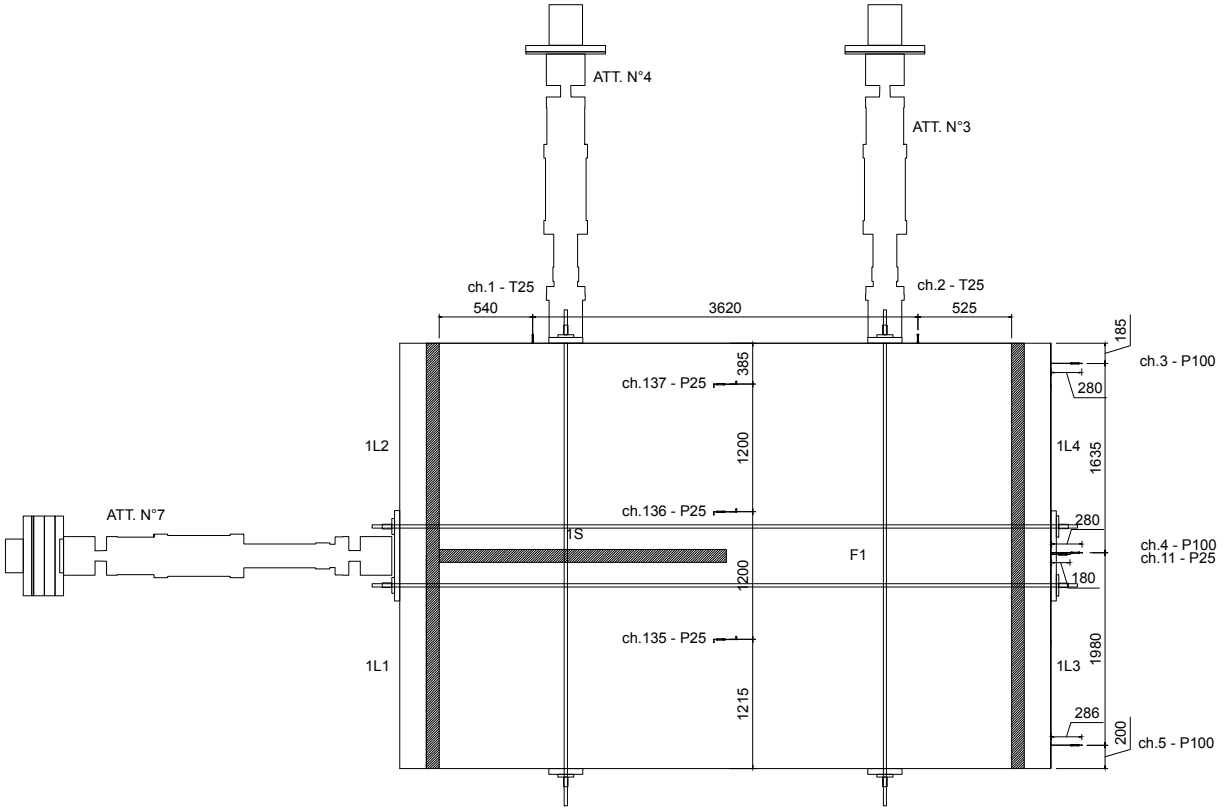

Figure 89. Schematic of the installed instrumentation: plan view of the specimen – Floor Slab, 1.

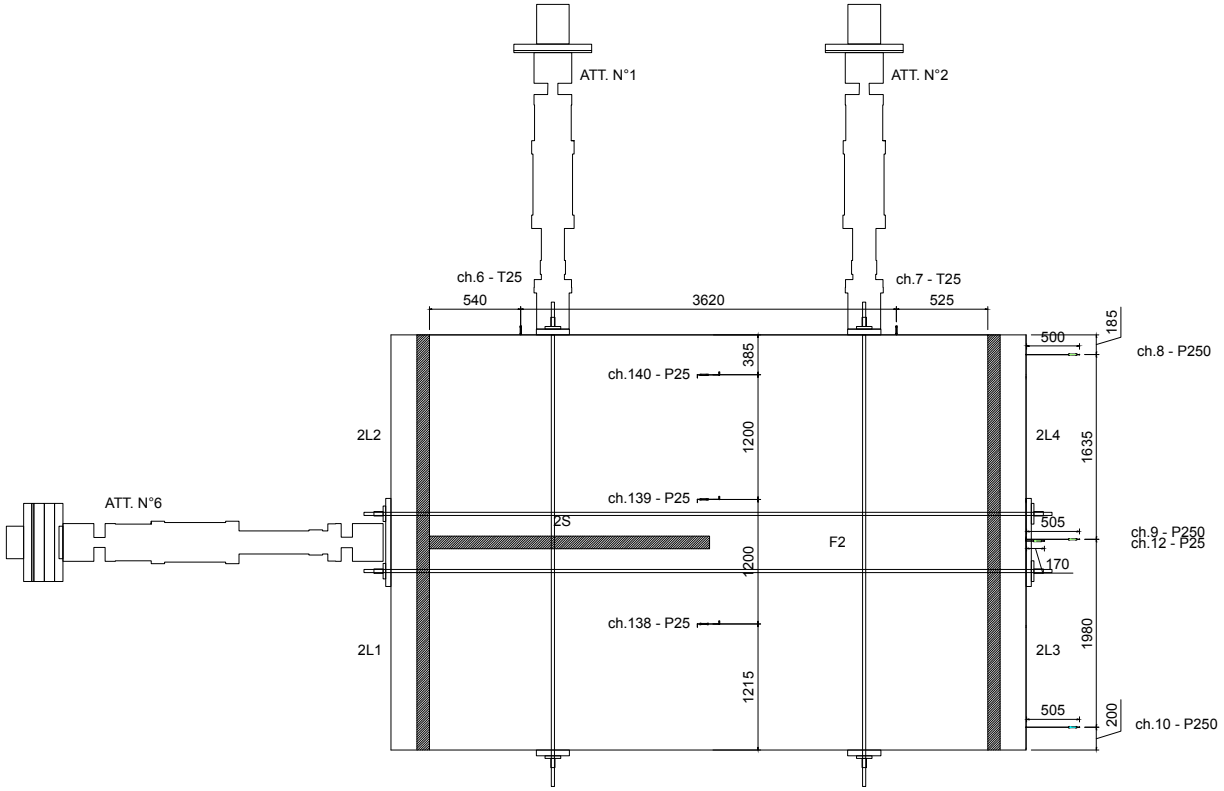

Figure 90. Schematic of the installed instrumentation: top view of the specimen – Floor Slab, 2.

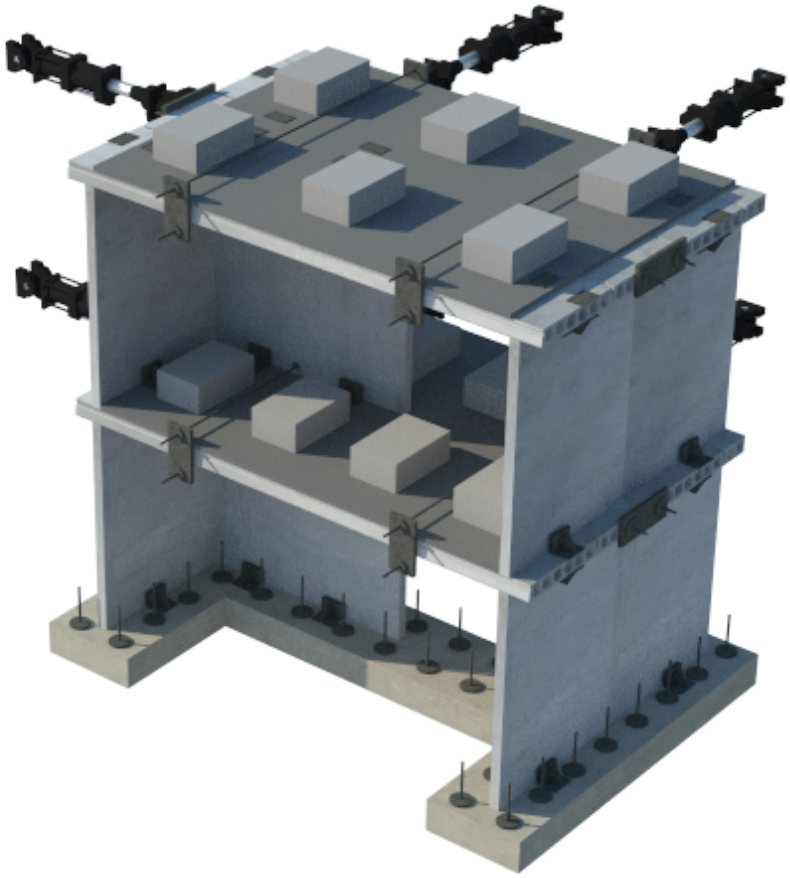

Figure 91. Isometric views of the installed instrumentation – Top side, front view.

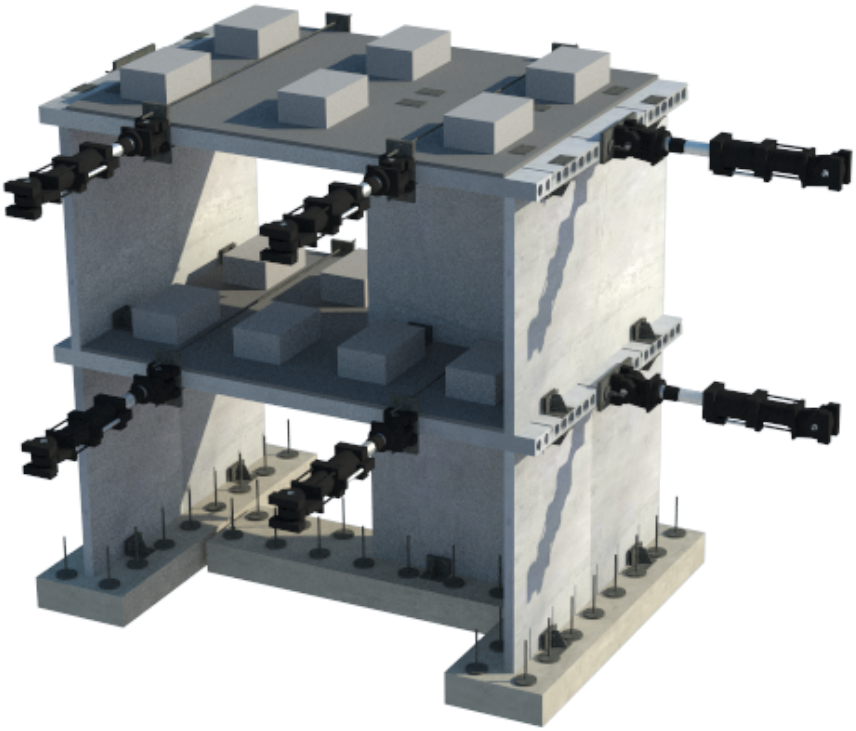

Figure 92. Isometric views of the installed instrumentation – Top side, back view.

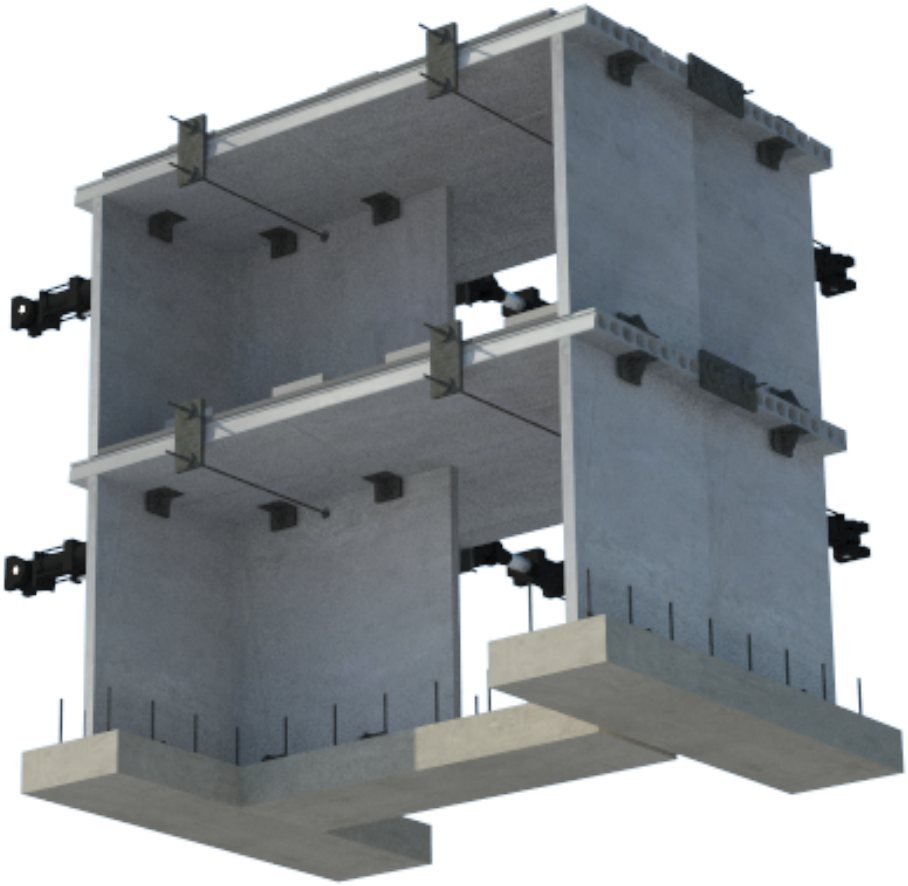

Figure 93. Isometric views of the installed instrumentation – Bottom side, front view.

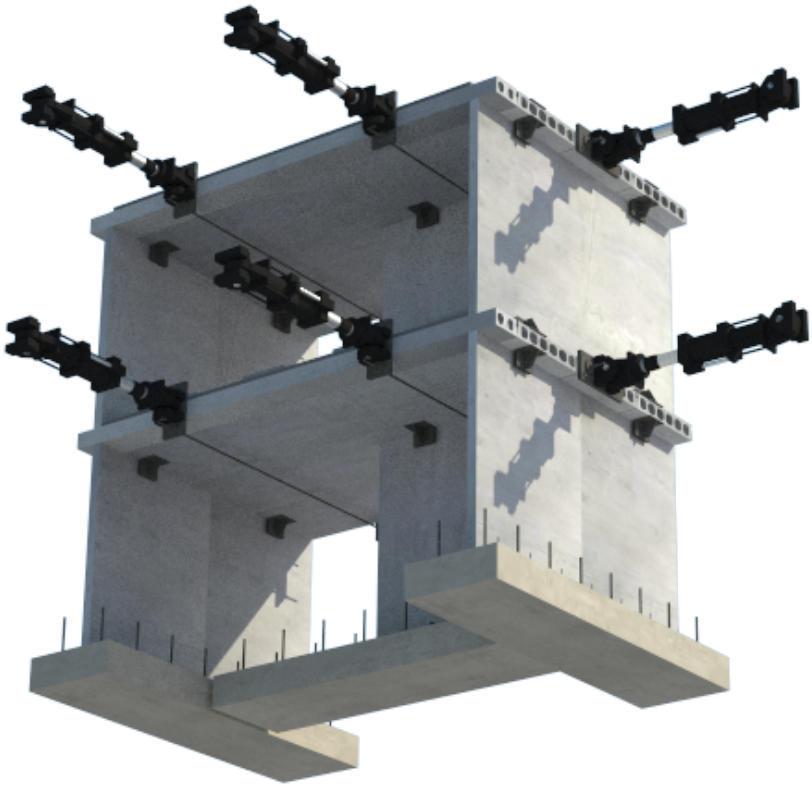

Figure 94. Isometric views of the installed instrumentation – Bottom side, back view.

As noticeable in the series of drawings collected above, the global displacements of both the two floor slabs are monitored; four potentiometers per each floor were employed to measure the displacements in the direction of cyclic loading, whereas two additional instruments per each floor were utilised to check possible torsion or uneven displacement of each floor slab. According to the expected in-plane displacements, instruments with different strokes were used at the first storey and at the second storey of the specimen. Figure 89 and Figure 90 present the set of instruments for the absolute displacements of the slabs, as well as those meant to verify whether spurious mechanisms (i.e. torsion, uneven displacement of floor slab, relative displacement of slab panels composing each floor) took place during the cyclic testing or not. Three 25 mm-stroke potentiometers per each floor slab were used in this latter case.

As shown in Figure 83 and Figure 86, the lateral walls of both North and South sides of the building were monitored in terms of out-of-plane displacement at the top and bottom of the first- and second-storey panels, as well as in respect to the in-plane and transversal rocking mechanisms. As far as the lateral walls connecting to the stability wall by means of three-way anchorages are concerned, four 50 mm-stroke potentiometers were used for each wall panel to measure out-of-plane displacements at their four corners, whereas two instruments were considered for the out-of-plane displacements of those placed at the North side of the structure because they are just connected together without an additional link to a stability wall. Eight instruments per each wall panel were utilised to monitor the in-plane and transversal rocking mechanism of lateral walls featuring a three-way connection with a stability wall. By constrast, only two potentiometers were used to take track of the above-mentioned resisting mechanisms in lateral walls placed on the opposite side of the specimen. Obviously, it was decided to install them at the top of the wall and in correspondence to the wall base. Two 25 mm-stroke potentiometers were also mounted onto each lateral wall in order to monitor sliding of those precast wall-elements.

Figure 87 and Figure 88 provide a clear view of the instrumentation installed onto the two sides of the first-storey and second-storey stability walls. In this case, four 50 mm-stroke potentiometers were used for each stability wall of the structure in order to obtain its in-plane deformation. The same type and number of displacement transducers were considered for transversal rocking and out-of-plane displacements of this element typology, whereas use was made of only two 50 mm-stroke potentiometers for what concerns sliding. One of them was placed at the top of the wall, whilst the other one was installed at the wall base. Other twelve linear variable displacement transducers (LVDTs) were used to monitor local relative mechanisms that might occur between the stability wall and the corresponding lateral walls. More in detail, four 50 mm-stroke instruments were installed with respect to sliding and other eigth 25 mm-stroke LVDTs were mounted for what concerns the out-of-plane displacements. In this way, it becomes possible for one to decouple the different mechanisms that these walls are likely to undergo during the testing in the weakest direction of the specimen.

Finally, sliding of the foundations was monitored using two 25 mm-stroke potentiometers and other two instruments (25 mm- and 2 mm-stroke ones) were considered to monitor any propagation of the crack present in the second-storey stability wall of the specimen. Photos of the instrumentation used are collected in Figure 95 to Figure 131.

Figure 95. Detail of instrumentation for global displacement of the first storey – Central slab panel.

Figure 96. Detail of instrumentation for global displacement of the first storey – Lateral slab panel.

Figure 97. Detail of a potentiometer for global displacement of the first storey – Opposite lateral slab panel.

Figure 98. Detail of the instrumentation installed for uneven displacement in the transverse direction.

Figure 99. Detail of the instrumentation for global displacement of the second storey – Lateral slab panel.

Figure 100. Instruments for global displacement of the second storey – Central slab panel.

Figure 101. Instrumentation for global displacement of the second storey – Opposite lateral slab panel.

Figure 102. Global displacement of the second storey – short and long stroke potentiometers.

Figure 103. Detail of short and long stroke potentiometers for global displacement of the second storey.

Figure 104. Instrumentation installed onto lateral walls – top of the wall.

Figure 105. Instrumentation mounted onto the lateral walls – panel-to-panel connection.

Figure 106. Instrumentation at the base of lateral walls – Central zone.

Figure 107. Instrumentation at the top of lateral walls – Central zone.

Figure 108. Instrumentation installed onto lateral walls – top of the wall, opposite side.

Figure 109. Instrumentation at the base of lateral walls – Opposite side of the specimen.

Figure 110. Instrumentation at the top of lateral walls – Opposite side of the specimen.

Figure 111. Instrumentation installed onto lateral walls – top of the wall, second storey.

Figure 112. Instrumentation installed on lateral walls – Top of the wall, second storey, central zone.

Figure 113. Detail of potentiometers at the base of lateral walls – External edge zone, second storey.

Figure 114. Potentiometers at the base of the lateral walls – Central zone, second storey.

Figure 115. Potentiometers installed onto the top of the lateral walls - Second storey, opposite side.

Figure 116. Instrumentation at the base of the lateral walls – Central zone, second storey, adjacent panel.

Figure 117. Detail of the instrumentation installed at the base of a lateral wall.

Figure 118. Instrumentation in correspondence to lateral wall-to-stability wall connection – Top of the walls.

Figure 119. Detail of the instrumentation installed at the base of a lateral wall – Opposite panel.

Figure 120. Detail of a potentiometer installed in correspondence to a panel-to-panel connection.

Figure 121. Detail of potentiometers installed at the base of a lateral wall.

Figure 122. Instrumentation for slab-to-stability wall sliding – First floor slab, top of the wall.

Figure 123. First-storey stability wall – Instrumentation for in-plane rocking at the top of the wall.

Figure 124. First-storey stability wall – Instrumentation for in-plane rocking at the base of the wall.

Figure 125. First-storey stability wall – Instrumentation for out-of-plane displacement at the wall base.

Figure 126. Instrumentation for slab-to-stability wall sliding – Second floor slab, top of the wall.

Figure 127. Potentiometer for monitoring of slab-to-stability wall sliding – Second floor slab, wall base.

Figure 128. Detail of a 25 mm-stroke for monitoring relative displacements between slab panels.

Figure 129. Instrumentation installed for relative displacement between slab panels – Opposite side.

Figure 130. Potentiometer for monitoring of crack opening – 25 mm-stroke instrument.

Figure 131. Detail of omegagage instrument for monitoring of crack opening – 2 mm-stroke instrument.

6 Test results

EUC-BUILD4 specimen was subjected to a loading history that consists of a series of progressively increased displacement levels planned to study the structural response/behaviour of the prototype in the longitudinal/weak direction of the specimen. Given that the dynamic counterpart test (i.e. EUC-BUILD5) will not feature testing in the transverse/strong direction, it was decided to focus the study only on the weakest direction of the specimen. Such an assumption was also motivated by the fact that testing the transverse/strong direction will not result in particularly new experimental findings because the response will inevitably be one of wall rocking. Monitoring and controlling tests in this direction would also be difficult, due to the non-monolithic characteristics of the specimen and the presence of the stability wall, and, hence, testing in the strong direction was not carried out.

The building mock-up was separately tested in two different configurations: as-built and "retrofitted". The EUC-BUILD4 test started on 11 April 2017 and was completed on 13 April 2017. A "retrofitted" version of the specimen featuring improved connection between the walls was then tested with a view to assess the potential ensuing gain in seismic resistance. Testing of the retrofitted specimen started on 18 April 2017 and was completed the day after (19 April 2017). In both the two cases, cyclic tests were carried out in pseudostatic fashion, and the following main stages can thus be identified:

- cyclic inelastic testing of as-built specimen in longitudinal direction up to a storey drift of 1.15%. This value is the absolute maximum (positive or negative) storey drift measured during the testing sequence (i.e. Test run #7 – Imposed top displacement of ± 16.8 mm).
- cyclic inelastic testing of retrofitted specimen in longitudinal direction up to a storey drift of 1.04%. This value is the absolute maximum (positive or negatve) storey drift measured during the testing sequence (i.e. Test run #8R – Imposed top displacement of ± 33.7 mm).

It is worth noting that the aforementioned storey drifts were obtained as the maximum inter-storey displacement normalised by the storey height. For both as-built and "retrofitted" configurations, the maximum values of drift reported above and pertaining to the last test run were recorded at the first storey of the specimen, although this consideration does not apply necessarily to all the other stages of the testing sequence. In light of this and to lead to a readily interpretation of the results presented in the following Sections, Table 36 collects the maximum storey drift for each test run as well as the floor level at which it was recorded. Considering that floor displacements were used to compute the storey drifts summarised therein, these values result from a combination of (i) rocking of the precast wall-elements, and (ii) sliding of the floor slabs on the fabric felts placed underneath the walls.

For the sake of clarity, and also to facilitate the possible quantification of damage state thresholds, the maximum storey drift computed as explained above will be referred to as the main structural response parameter when presenting the building damage evolution throughout the testing sequence, regardless of whether the maximum value is recorded at the first or second storey. Nonetheless, additional information on the effects of the two mechanisms mentioned before can be found in the sub-Sections addressing displacement profiles.

Table 36. EUC-BUILD4: maximum storey drift for each test run.

AS-BUILT			RETROFITTED		
Test run #	Drift [%]		Test run #	Drift [%]	
	1st Floor	2nd Floor		1st Floor	2nd Floor
01	0.004	**0.008**	01R	0.004	**0.021**
02	0.010	**0.019**	02R	0.027	**0.033**
03	0.048	**0.076**	03R	0.049	**0.055**
04	0.093	**0.105**	04R	**0.085**	0.083
05	0.142	**0.148**	05R	**0.141**	0.140
06	**0.503**	0.444	06R	**0.333**	0.208
07	**1.153**	0.852	07R	**0.514**	0.260
			08R	**1.045**	0.347

In what follows, once an overview of the experimental response/behaviour observed in the above two cases is given, separate sub-sections, one per each configuration, are presented to collect the main findings of these experimental investigations in a synthetic and systematic manner.

6.1 Overview of specimen's response

As expected, the response of the specimen, in its as-built configuration, was dominated by issues of friction/sliding and connection behaviour. These two were definitely the dominating mechanisms as sliding of the floor slabs on the fabric felts placed underneath the precast walls was recorded at the early stages of the tests in correspondence to both storey floors. Furthermore, the connectors between the transverse and stability ground-floor walls were not able to sustain much load, leading to a relatively early failure of the specimen (after only four displacement-controlled loading cycles).

More specifically, and for what concerns the connectors behaviour, permanent bending of the connector bar embedded in the transverse walls is the observed failure mode encountered during the test of EUC-BUILD4 full-scale specimen in its as-built configuration. At the end of this initial testing sequence, the grout around one of such connectors was removed, showing that the connector bars in the stability wall were intact, which implies that dislodgement did not occur. When the specimen was dismantled, at the end of the testing campaign, a more detailed inspection of these failed connectors was undertaken, confirming bending of the anchors arranged in the connections between the transverse walls to be the failure mechanism experienced by the three-way anchorage composing the joint between the stability wall and the two corresponding lateral walls. A photographic sequence on the dismantling of the specimen will be provided in this chapter so as to clarify the observed connectors behaviour even further.

Considering that after failure occurring in panel-to-panel connections between the lateral and stability ground-floor walls the specimen is clearly not able to sustain any additional horizontal load of relevance, a "simulated retrofitting" was implemented by Eucentre technicians during the day of

Friday 14th, with a view to allow for a further test run. In accordance with the scheme discussed in a separate section (i.e. sub-Section 6.3), some of the sliding restrainers were "tightened" to the walls to simulate a sturdier wall-slab connection. It is also worth noticing that attempts were made to get the building into its original/undeformed configuration, trying to close the gap that had open between the stability and transverse walls before the implementation of the "retrofitting strategy" mentioned above. Notwithstanding the fact that none of the two operations could be fully achieved, due to the excessive damage the "as-built" specimen had sustained, the testing of the EUC-BUILD4 "retrofitted" specimen was still executed, pushing the structure up to a displacement level (33.7 mm) that was double the displacement that had instead taken the original specimen to incipient collapse. This final test run did confirm that the lack of adequate connection between the stability walls and the slabs/transverse walls was the principle cause for the deficient response of the original specimen. Indeed, by guaranteeing (through bolted steel angles) a sturdier wall-slab connection, a much more symmetric response of the specimen could be readily obtained (sliding no longer occurred), ensuing larger energy dissipation and thus equally higher seismic force resistance. The testing was stopped at the end of the fifth envisaged set of displacement-controlled cycles, when not only very extensive damage could be seen spreading throughout the specimen (including a full-depth/full-width/mid-height horizontal crack in the lateral wall), but also in-cycle and between-cycle strength degradation started being observed.

The testing sequence has also confirmed that the crack running through the entire width and depth of the second-storey stability wall did not play any noticeable or important role in the response of the specimen, since damage was observed in other zones of the building mock-up.

A more detailed account of the main experimental findings obtained by the testing of EUC-BUILD4 specimen in as-built and retrofitted configurations are presented in the following sub-Sections, one per each structural configuration of testing.

6.2 As-built configuration

Pseudostatic cyclic tests on EUC-BUILD4 specimen, in the as-built configuration, were carried out, and experimental results are discussed in the following. Please refer to Section 5 for details on both geometrical characteristics of the prototype structure and refinements to make the original building scheme compliant with laboratory-related needs. In addition to the information contained there, one should consider Arup's *229746_031_NOT2008_Rev0.05_Issue EUC-BUILD-4 Prototype building description*, as a valuable companion and complementary document. Worthwhile to mention is that construction details regarding the selected prototype structure can also be found therein.

At the end of every stage of the testing sequence, detailed surveys of the crack patterns developed were carried out for the detection of every possible sign of damage having affected the structure. As emerged from those surveys, the behaviour of the tested building was mainly governed by sliding. Concrete cracking was observed to take place at the base of the ground-floor stability wall and also in correspondence to the connections between the first-floor stability wall and the transverse-lateral walls.

The following section reports the building damage evolution throughout the sequence of increasing drifts imposed in terms of the cracks patterns developed together with response graphs, showing the main behavioural characteristics of the specimen and of key portions of it. Separate sub-paragraphs

were prepared to present the global response of the specimen, the local response of walls in terms of base rocking and vertical sliding and the observation of damage caused by the most significant steps of testing. Deformed shapes and displacement profiles of the tested structure are given as well.

6.2.1 Global response of the specimen

In Figure 132, the total base shear-roof top displacement response curve of EUC-BUILD4 specimen is shown with a view to clarify the response for each single displacement amplitude imposed during cyclic testing of the prototype building in its longitudinal/weak direction, whilst the backbone curve from cyclic tests is a bit more clearly reported and compared to hysteresis loops in Figure 133. Care was also paid to the response of each single storey, so as to chiefly decouple the behaviour observed for each one of them. As one may notice in Figure 134 to Figure 137, the same approach was used to present results with respect to the cyclic curve and the envelope of cyclic response in both pulling and pushing directions of testing.

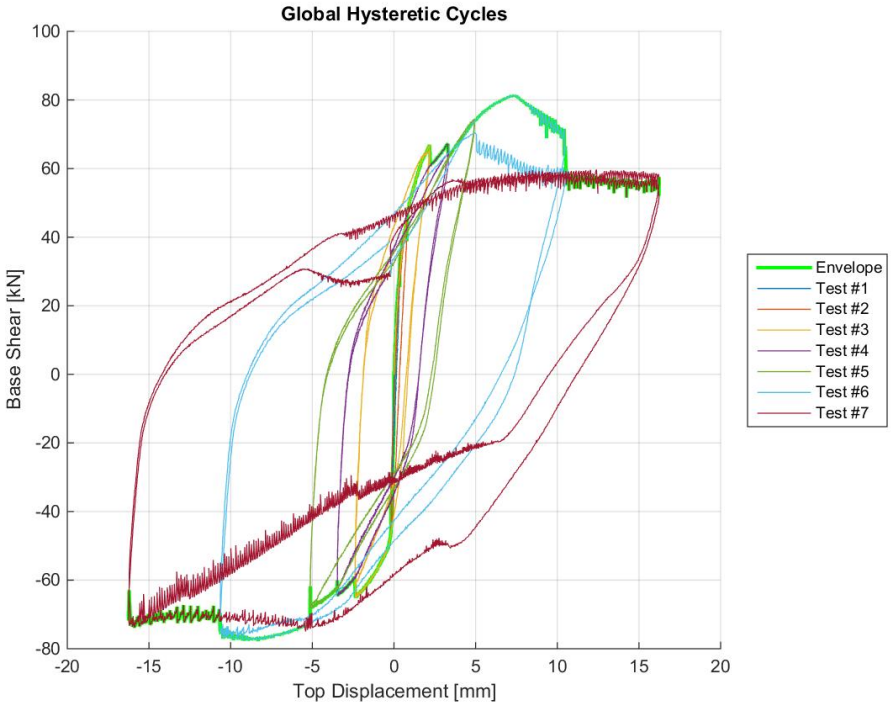

Figure 132. Cyclic total base shear-top displacement response of EUC-BUILD4 specimen.

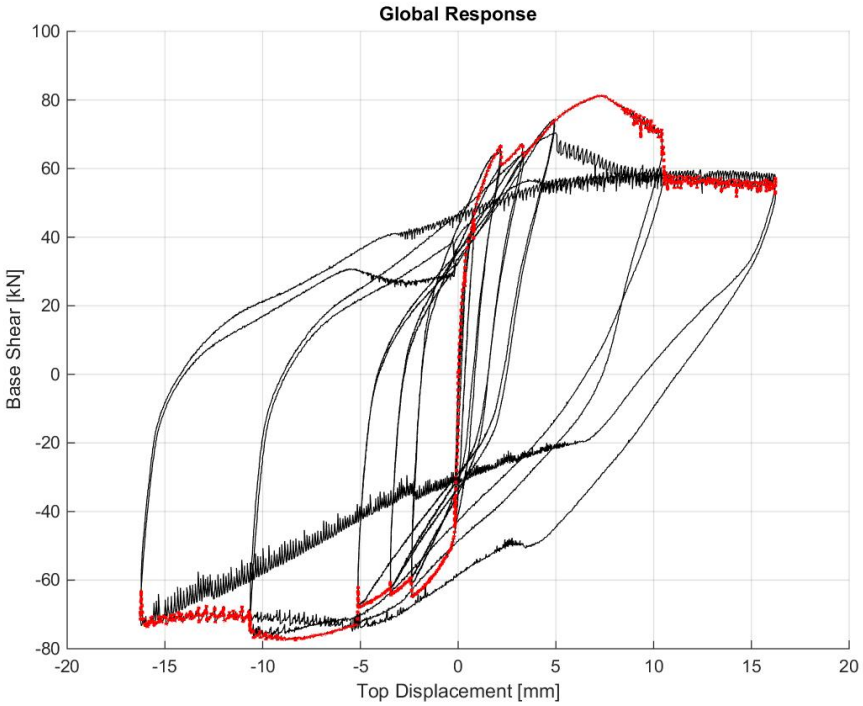

Figure 133. Base shear-top displacement response of EUC-BUILD4 specimen – Backbone and cyclic curves.

First of all, it is noteworthy that the behaviour of the building mock-up is not symmetric in pulling and pushing directions, given that EUC-BUILD4 resisted a peak base shear of approximately 82 kN and 78 kN in the case of pulling and pushing, respectively. The maximum base shear when pulling was experienced for a top displacement of about 6 mm, whilst the peak lateral loadcarrying capacity in the opposite direction of testing (i.e. pushing – negative displacements/forces) was undergone for a displacement roughly equal to 8 mm. Data shown in Figure 132 (and obviously in Figure 133 as well) were not filtered mostly because of the fact that the noisy branch of the experimental response observed, when reloading the specimen in both pulling and pushing directions, can be strictly associated with the actual characteristics of the structural behaviour itself rather than with disturbance and/or noisy signals, more in general. Indeed, frictional transfer mechanisms evident from visual observations of the full-scale building prototype appear to be portreited, even more clearly, by the shape and type of the obtained hysteretic loops. Sliding of the precast hollow core slab panels on the underneath felts and corresponding floor scratching on the precast wall-elements underneath is therefore the likeliest reason for that. This mechanism far outstripped any of the other ones experienced by the specimen, during cyclic testing, apart from issues related to the connectors behaviour, as clearly highlighted by the series of damage patterns collected after each single set of cycles (see Sections 6.2.5 to 6.2.9).

The non-negligible strength drop depicted in Figure 132 after the peak force is experienced is indeed attributable to pronounced damage in the four three-way connections between the ground-floor stability walls and the corresponding South-sided transversal walls of the structure. It is worthwhile to mention that the above resistance decay is much more pronounced in the pulling direction simply because of the flexural failure mechanism of the connectors embedded in the niche of the transversal walls, which in turn were pulled and bent permanently (towards the North side of

the building) by the counterpart anchors installed into the niches of the stability wall, merely owing to shear transfer mechanisms in the precast wall-elements of this portion of the structure. In contrast to pulling direction, the post-peak softening in pushing direction was relatively modest, even though actually present. For the sake of clarity, the peak base shear recorded at peak roof displacement for the last cycles was roughly equal to 59 kN in pulling direction, which in turn implies a nearly 30% strength degradation and hence a suggestion to stop testing because of both safety precautions in lab environment and the fact that, in that condition, the specimen cannot withstand any further load of relevance nor experience larger displacement demands also because of the accumulation of residual displacement during testing.

The latter aspect can be clearly seen in the storey shear versus inter-storey displacement response of the two floor levels, which are separately shown in Figure 134 and Figure 135. As mentioned earlier and reminded here for interested readers, Figure 136 and Figure 137 collect the counterpart curves (i.e. cyclic vs. envelope ones) of the first storey and second storey, respectively. Despite the slightly different peak base shear forces observed in the two directions of testing, the shape of the hysteretic response depicted in Figure 132, in terms of global/structural behaviour, was still very similar as far as the pulling and pushing directions are compared. It can be nonetheless noticed that in-cycle and between-cycle strength degradation becomes slightly different in the two directions, after extensive damage took place in correspondence to the three-way wall-to-wall connections of the first storey. With respect to the similarity in shape of the pulling/pushing responses, different considerations can be drawn whether the response curves of the two floors are examined.

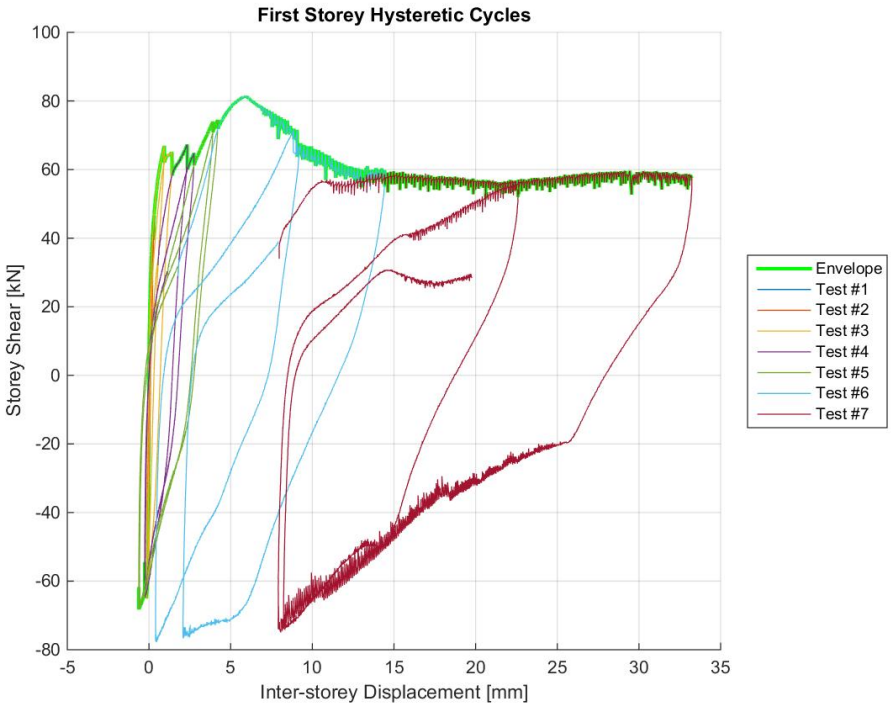

Figure 134. Storey shear vs. inter-storey displacement response – First storey.

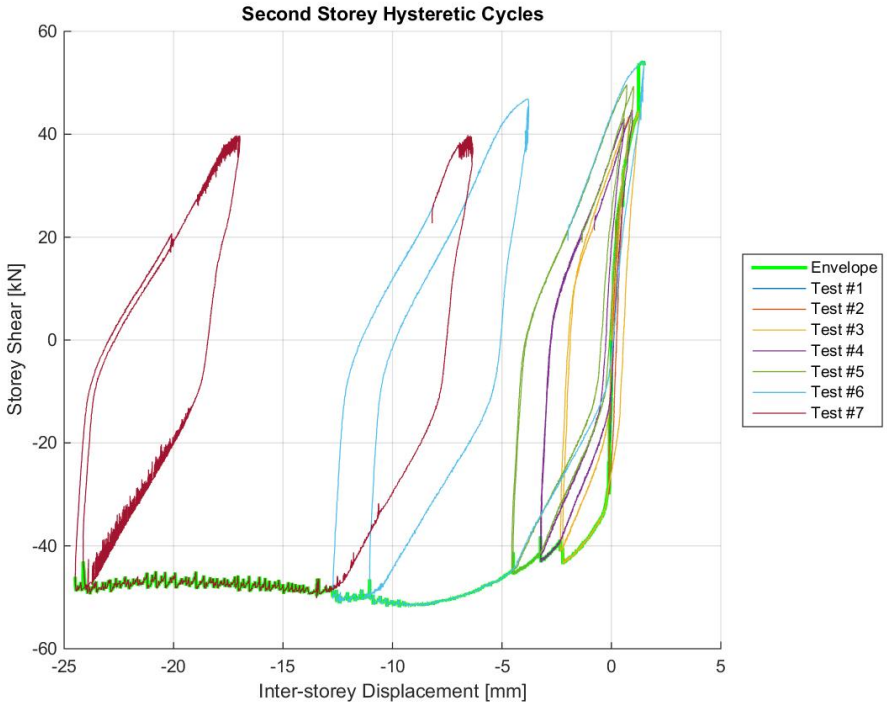

Figure 135. Storey shear vs. inter-storey displacement response – Second storey.

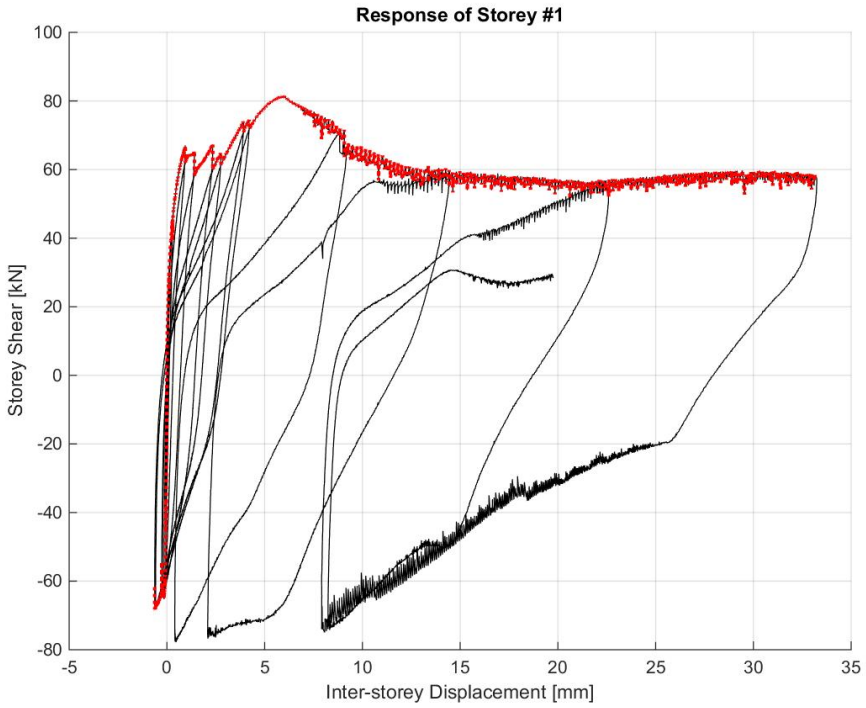

Figure 136. Storey shear vs. inter-storey displacement response – First storey, backbone and cyclic curves.

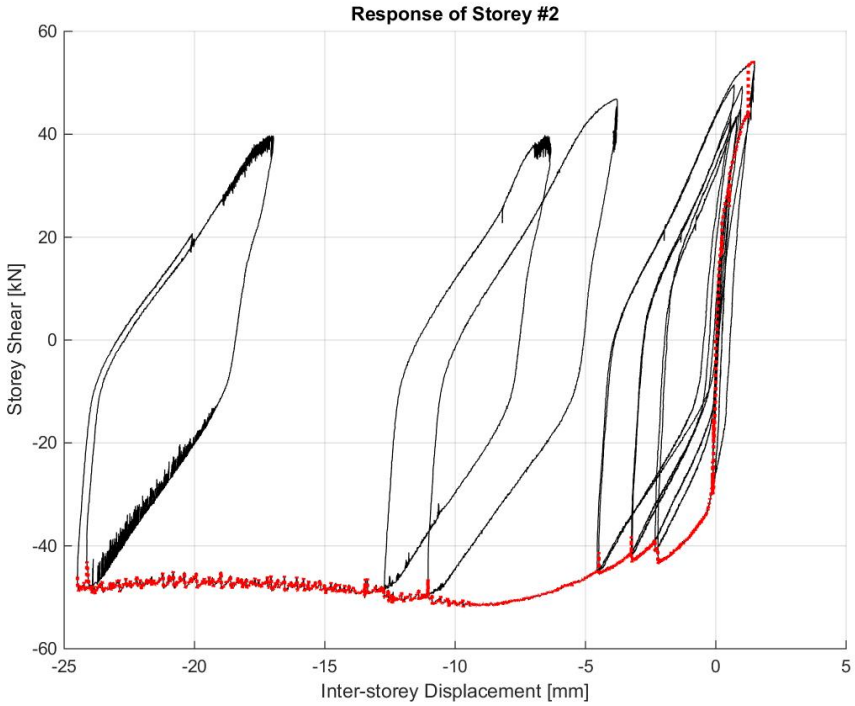

Figure 137. Storey shear vs. inter-storey displacement response – Second storey, backbone and cyclic curves.

By taking a look at the respose curves reported in Figure 134 and Figure 135, it becomes clear that the first storey experienced maximum positive inter-storey displacement of up to 34 mm, whilst the second storey was found to undergo peak negative inter-storey displacements slightly lower than 25 mm for a nearly 40% lower storey shear force. Sliding and accumulation of residual displacements can be clearly observed, especially in correspondence to the second storey (see Figure 135 or Figure 137). The response curves of the first and second storey floors are thus heavily unsymmetric and are also opposed in phase, if they are compared together.

As shown in Figure 137, the backbone curve obtained by the cyclic storey shear versus inter-storey displacement response of the second floor is characterised a relatively moderate post-peak softening, which agrees well with the fact that EUC-BUILD4 specimen was observed to be almost undamaged at the second storey except for few minor cracks in correspondence to the three-way panel-to-panel joints close to the top of the stability wall and at the base of the transversal walls opposite to it (North side of the specimen). On the contrary, the strength degradation shown by the global response curve of the structure (Figure 133) is a direct consequence of damage at the first-storey elements and connections, which is thus confirmed by the cyclic loops collected in Figure 136. Accumulation of residuals and corresponding non-re-centering response are evident after the achievement of the maximum base shear experienced during Test run #6. Before that step of the testing sequence, the strength decay – from cycle to cycle – was observed to be minor. This can be attributable to the type of resisting mechanism that took place – sliding of the concrete surfaces on fabric felts – and to almost non-degrading frictional/mechanical properties of this latter material.

Sliding of the two floor slabs on the walls underneath is found to be a key mechanism, together with the out-of-phase/out-of-plane rocking of transversal walls of the first and second storey. As such,

this uneven mode is discussed later on, in more details (Sections 6.2.2 and 6.2.3 for qualitative deformed shapes and displacement profiles of the test-specimen).

Friction is thus one of the most dominating resisting mechanism observed during the tests of this full-scale prototype, as also clarified by the set of equivalent viscous damping ratios collected in Figure 138. As previously done for the hysteretic response, the contribution of each storey is decoupled also in terms of energy dissipation (see Figure 139 and Figure 140). It becomes clear from the three sets of equivalent viscous damping ratio-displacement relationships that high levels of energy dissipation can be ensured by this building mock-up since the early stages of inelastic cyclic testing, purely because of friction. Values ranging between roughly 12% and 25% were observed for roof top displacements of up to 5.6 mm (see Figure 138). Even higher values (i.e. 32-39%) can be computed from the total base shear-top displacement curve of the specimen for the last two displacement-controlled amplitudes. In this case, a higher energy dissipation is achieved as a result of the combination of friction and damage in the specimen at the level of the four three-way connections.

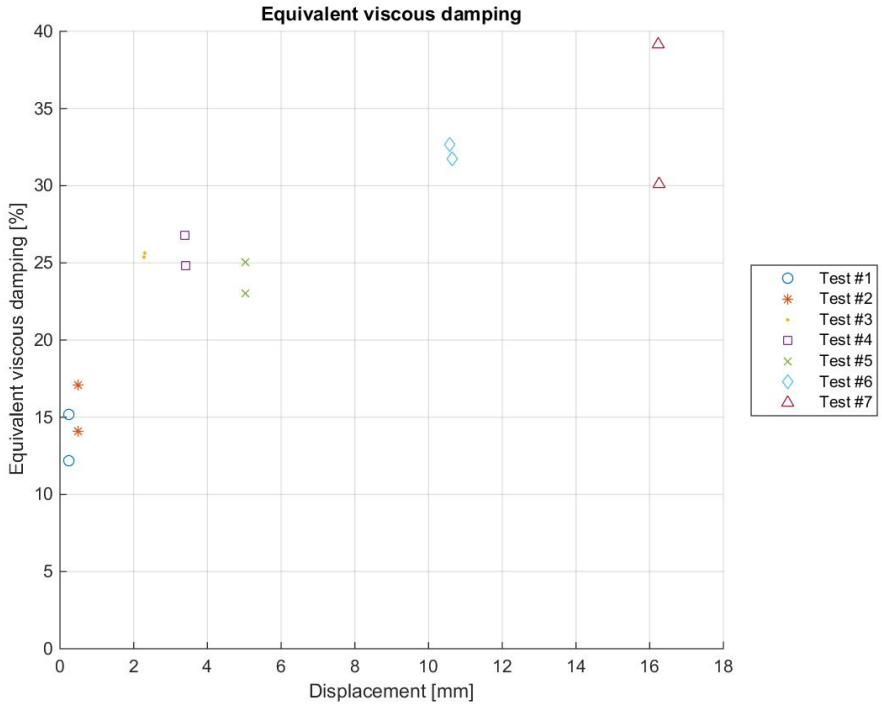

Figure 138. Equivalent viscous damping-displacement relationships – computed from overall response.

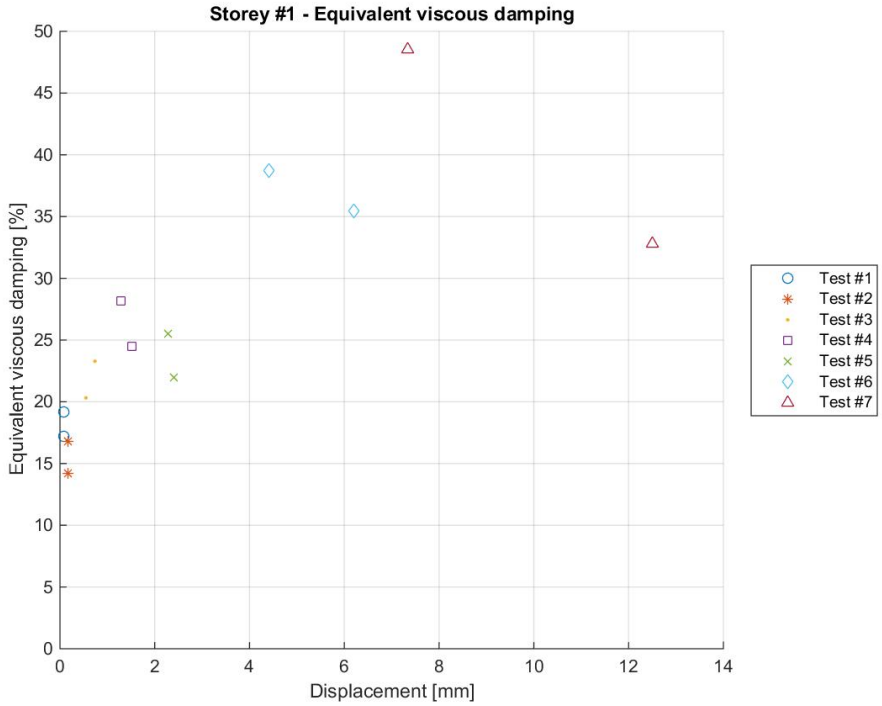

Figure 139. Equivalent viscous damping-displacement relationships – computed from first storey response.

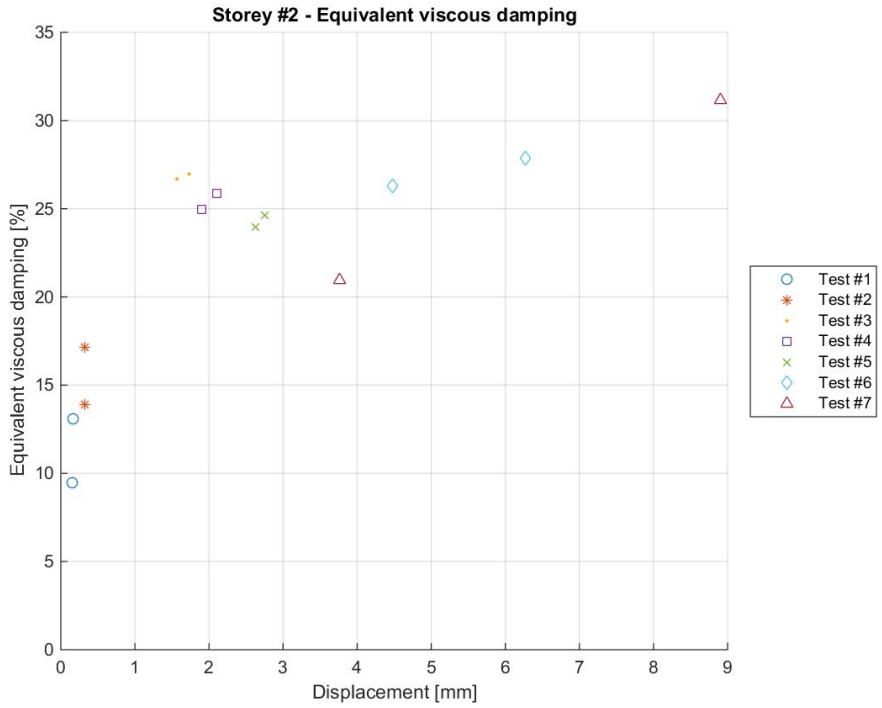

Figure 140. Equivalent viscous damping-displacement relationships – computed from second storey response.

A direct comparison between Figure 139 and Figure 140 renders evident that some major sources of energy dissipation are driven by the first storey, which is indeed the one that has experienced most

of the damage caused by the application of lateral forces. It is also worth noting that the equivalent viscous damping-displacement relationship revealed a fairly linear trend, regardless of the approach used for its computation (i.e. Figure 138, Figure 139 or Figure 140). Needless to say that the most visible degradation with the number of cycles is observed to occur during the last two steps of testing, and this is also reflected by the sets of equivalent viscous damping estimates collected above. Moreover, it can be concluded that, although quite high levels of energy dissipation can be computed from the response curves of the specimen and hence can be associated with it (and perhaps with structures of similar type), those latter sources are not necessarily driven by a rationally-controlled mechanically-conceived earthquake-resistant mechanism, considering that they mostly come from mere frictional force transfer in fabric felts without any sort of mechanical wall-to-slab connection and partly from damage in vital panel-to-panel joints lacking adequate execution and seismic-resistant design. These are thus crucial considerations that can be drawn towards the upgrade of such an early prefabricated technology.

Response pseudo-time histories obtained for the testing sequence in the longitudinal/weak direction of the specimen are collected in Figure 141 to Figure 147. The horizontal forces imposed at the two floor levels and the corresponding horizontal displacements recorded during the stages of testing are collected therein, together with the hysteretic cycles.

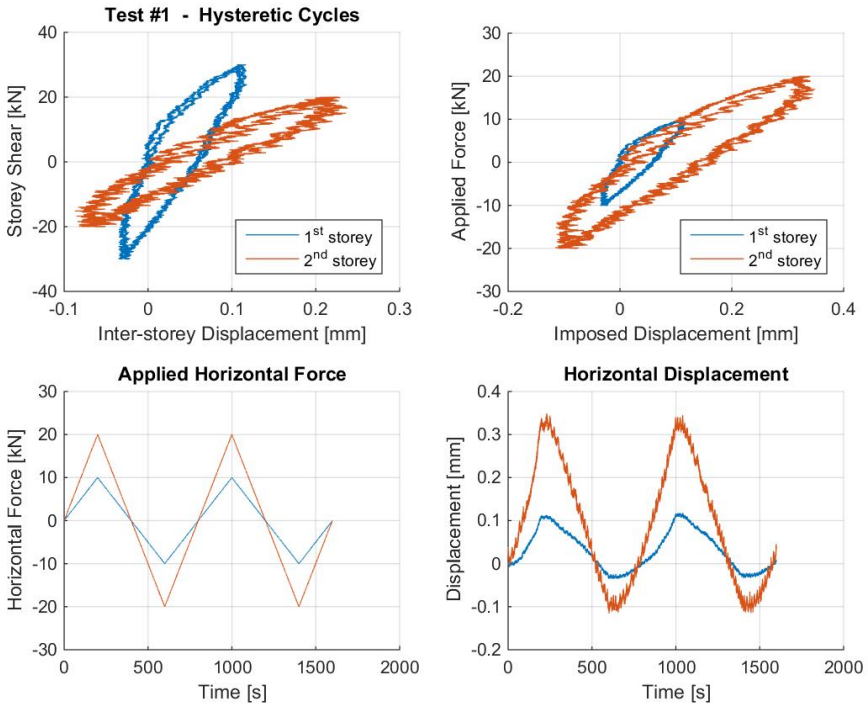

Figure 141. Response time histories: force, displacement and storey shear – Test run #1.

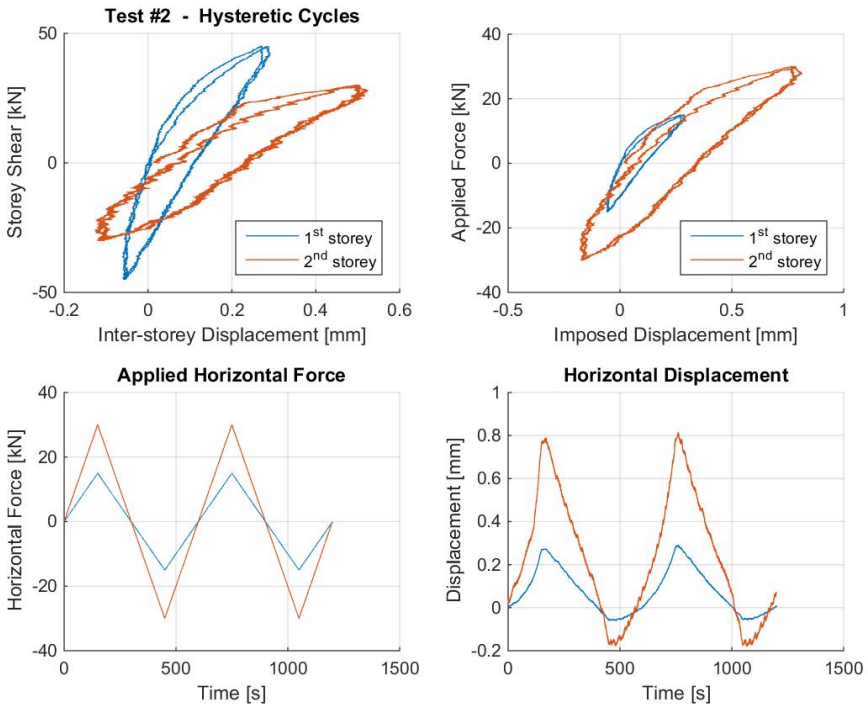

Figure 142. Response time histories: force, displacement and storey shear – Test run #2.

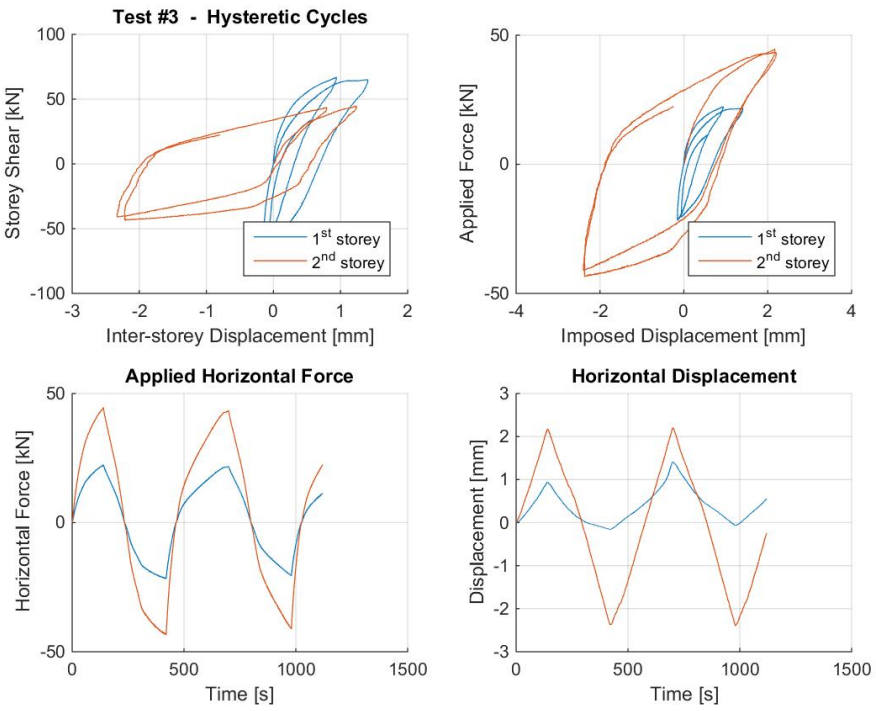

Figure 143. Response time histories: force, displacement and storey shear – Test run #3.

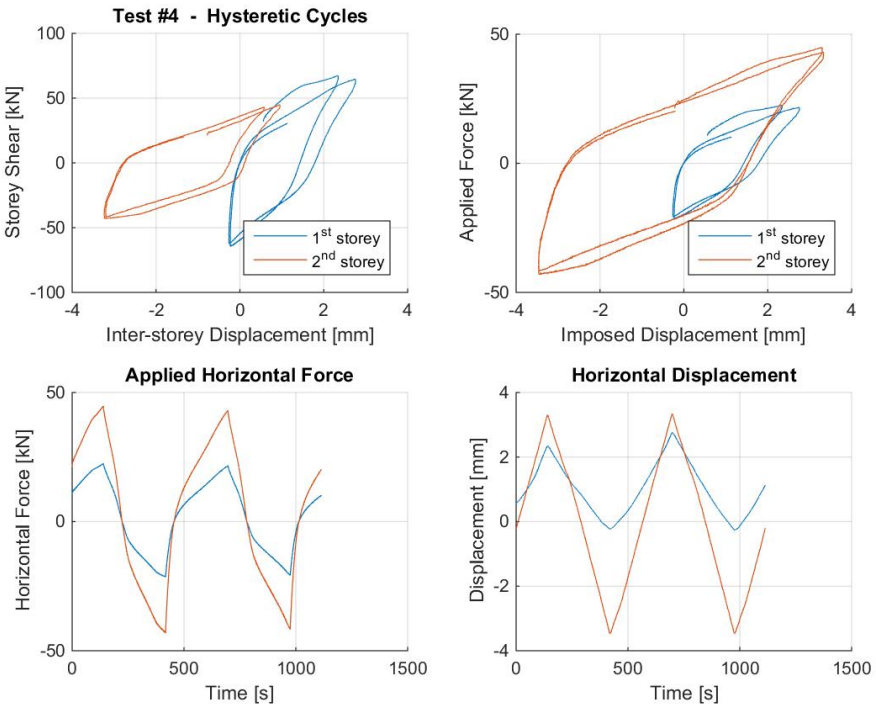

Figure 144. Response time histories: force, displacement and storey shear – Test run #4.

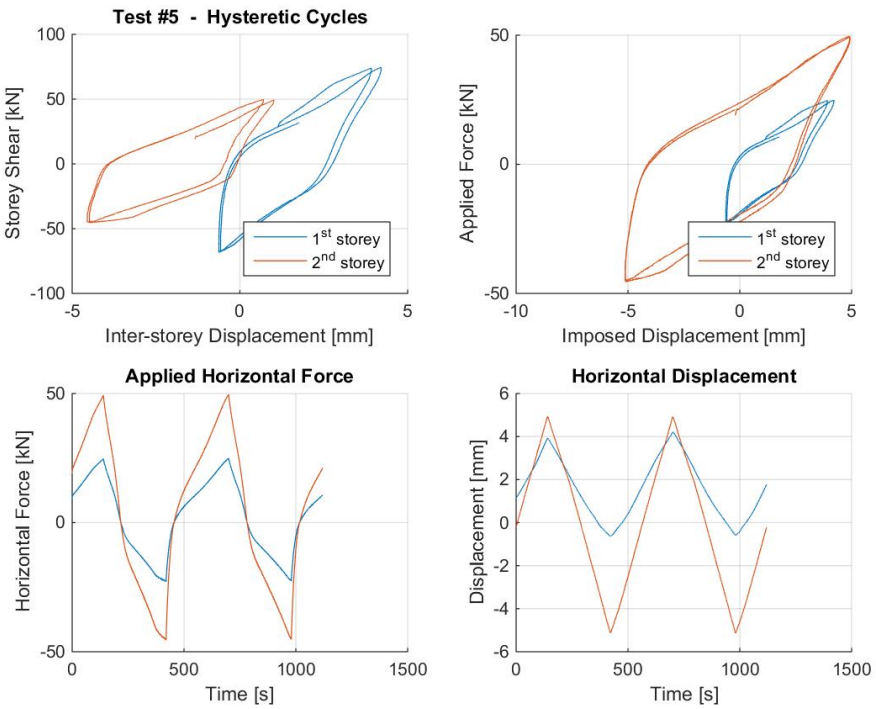

Figure 145. Response time histories: force, displacement and storey shear – Test run #5.

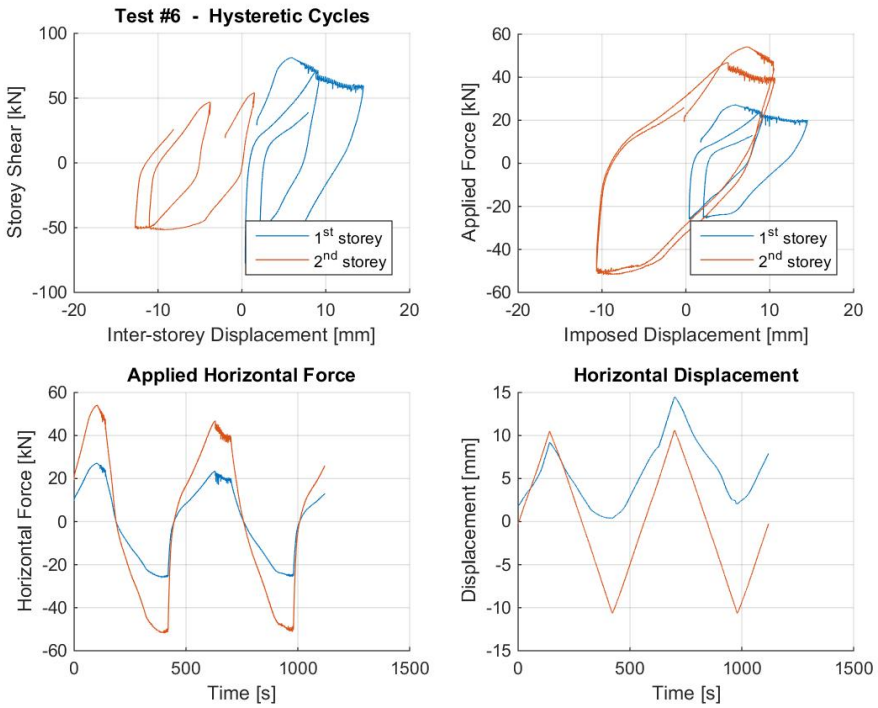

Figure 146. Response time histories: force, displacement and storey shear – Test run #6.

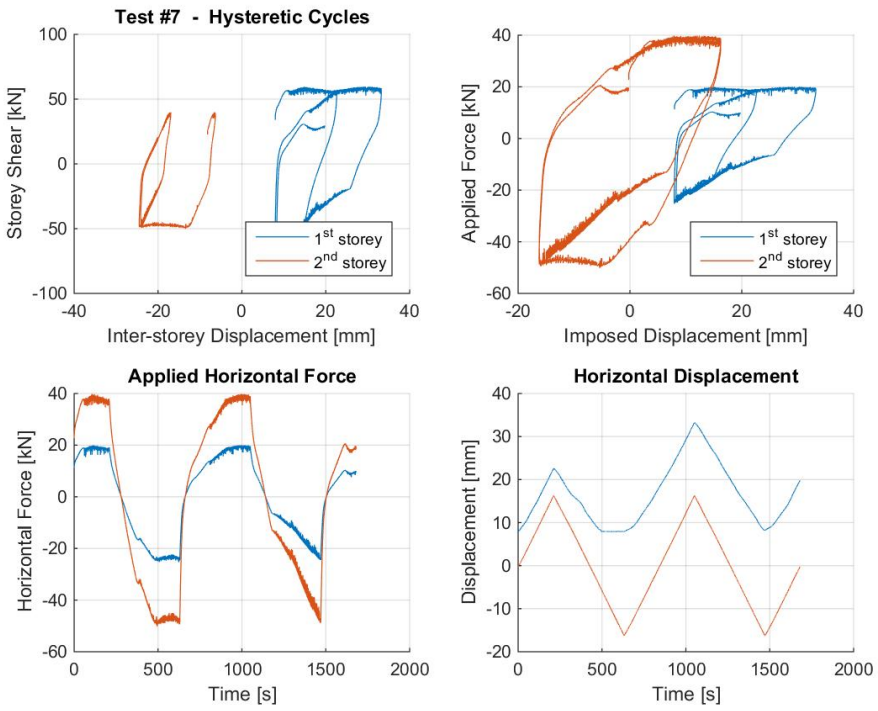

Figure 147. Response time histories: force, displacement and storey shear – Test run #7.

The above response graphs, showing the hysteretic response of each imposed amplitude in terms of storey shear versus inter-storey displacement as well as applied force versus imposed displacement with reference to each one of the two floor levels, are presented for interested readers with the main aim of clarifying even further some aspects of the experimental response. In addition to the response curves shown in this section and the set of deformed shapes discussed in the next one, they provide the reader with insights into specific behavioural characteristics of the specimen like accumulation of residual displacements during the testing sequence.

The first two force-controlled cycles revealed a fairly elastic response, whereas sliding started being observed at both the two floors since the first displacement-controlled stage of testing. A fairly bilinear response can be observed as far as storey shear versus inter-storey displacement response is concerned, which allows one to argue that during Test run #3, Test run #4 and Test run #5 the response of the specimen is simply governed by friction and hence by sliding of the floor slabs on the walls underneath. As will be mentioned later on when addressing damage patterns, only minor concrete cracking was observed for these steps of the testing sequence. It becomes also evident, from hysteresis loops and displacement pseudo-time histories, that residual displacements were accumulated cycle after cycle. Up to these stages of testing, response curves are characterised by hardening because of the frictional properties of the adopted felt material. Damage and subsequent post-peak softening was found to occur in the three-way connections during Test run #6 and this is visible in the hysteretic loops of the first storey. Residuals were getting higher and higher during the cycles of both this step and the last one imposed (i.e. Test run #7 – Figure 147).

6.2.2 Qualitative deformed shapes

This section is chiefly concerned with the analysis and discussion of the observed deformed shapes at positive and negative displacement peaks imposed during each stage of testing. A series of plots, shown in Figure 148 to Figure 154, are thus presented to shed light on this aspect in a synthetic and systematic manner. An example of these plots is given below, with reference to the first step of the cyclic testing (i.e. Test run #1 – Figure 148), whilst a few considerations regarding the approach used to create and present them can be given as listed below.

The dataset obtained from the instrumentation was examined in such way that absolute and relative displacements of the specimen and key portions of it can be identified. Sliding of the two floor slabs can thus be determined and taken as reference for the development of qualitative deformed shapes, which are, of course, amplified with respect to actual displacements red by potentiometers installed onto the specimen. To lead to a readily interpretation of these deformed shapes, they are all graphed together with the undeformed configuration of EUC-BUILD4 specimen.

The set of graphs collected below confirms the resisting mechanisms commented in the previous Sections, in terms of asymmetric response of the test-specimen and sliding of each one of the two floor slabs on the walls underneath; the same applies to the detachment of the ground-storey stability wall from the corresponding transversal wall panels because of damage in the connections between them (see Figure 153 and Figure 154). The out-of-plane rocking of the opposite transversal walls is confirmed as well.

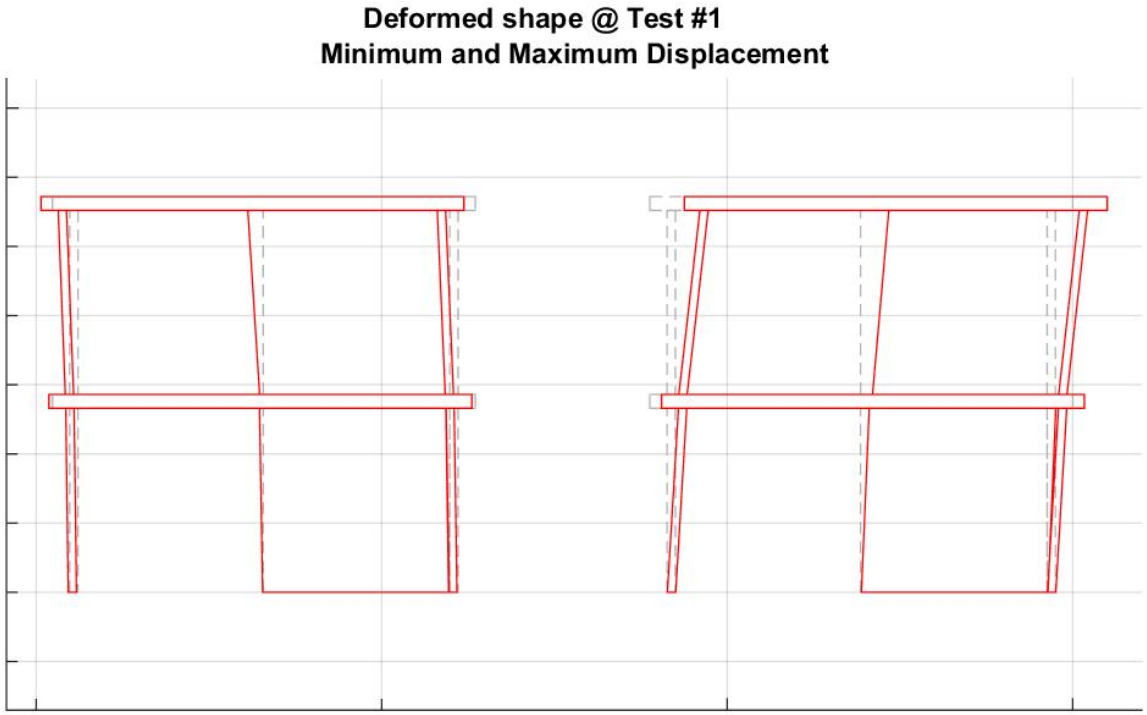

Figure 148. Deformed shape of EUC-BUILD4 specimen (max and min) – Test run #1.

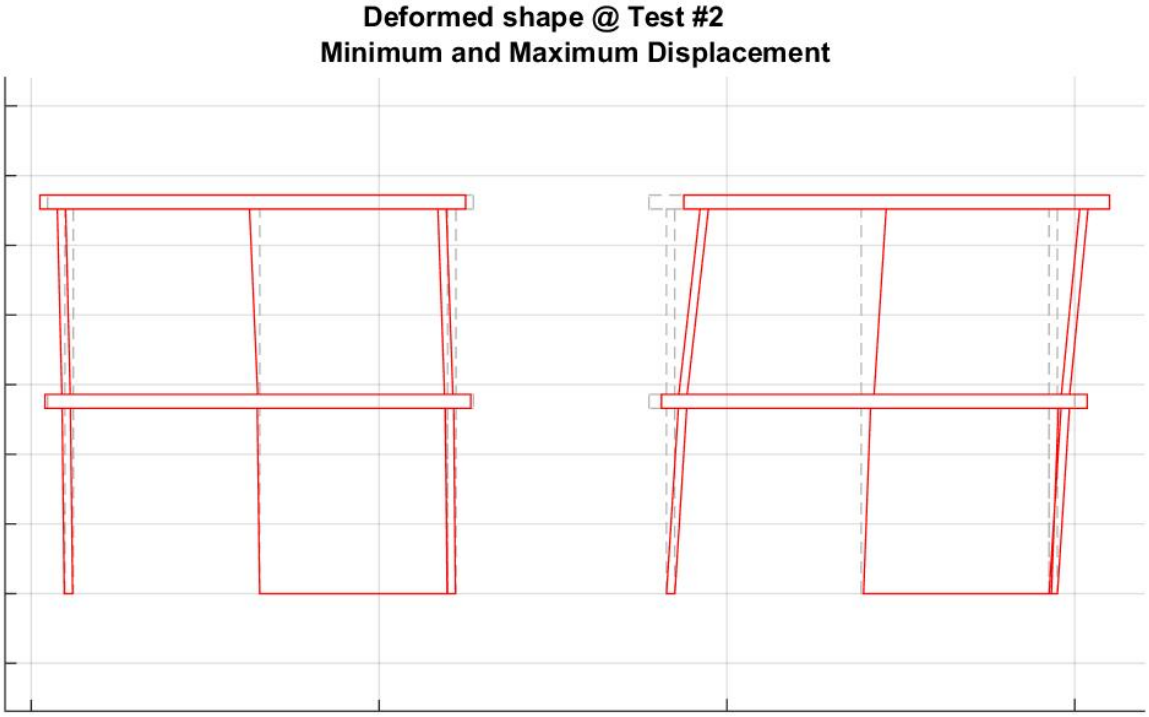

Figure 149. Deformed shape of EUC-BUILD4 specimen (max and min) – Test run #2.

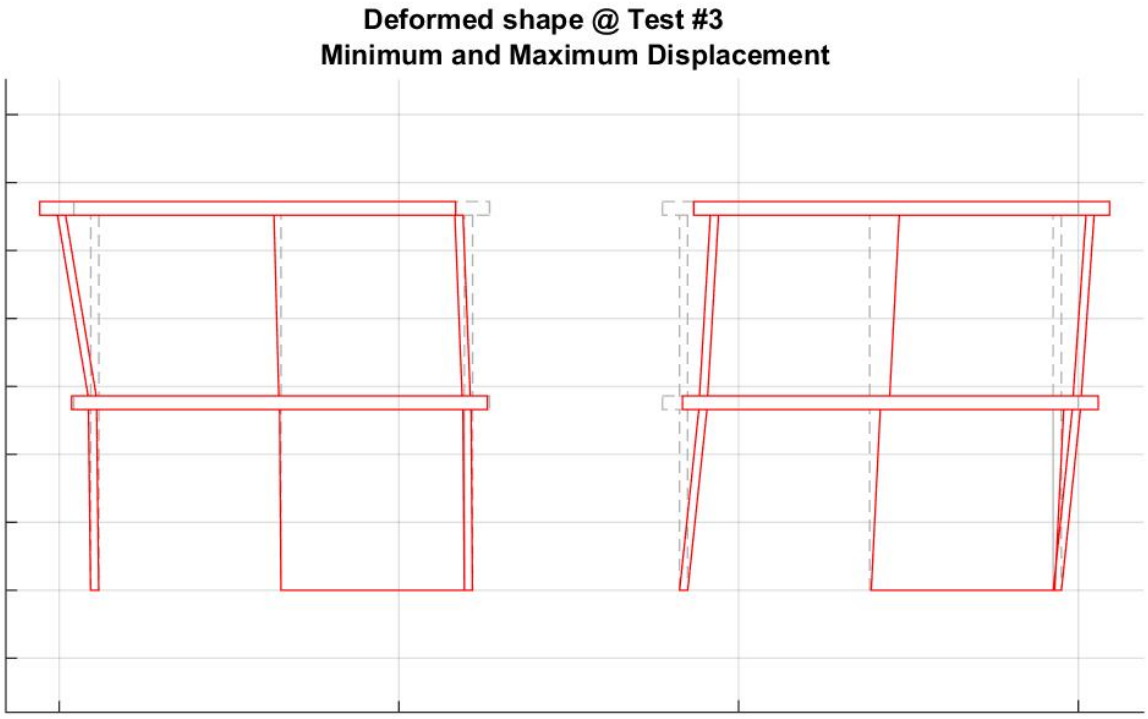

Figure 150. Deformed shape of EUC-BUILD4 specimen (max and min) – Test run #3.

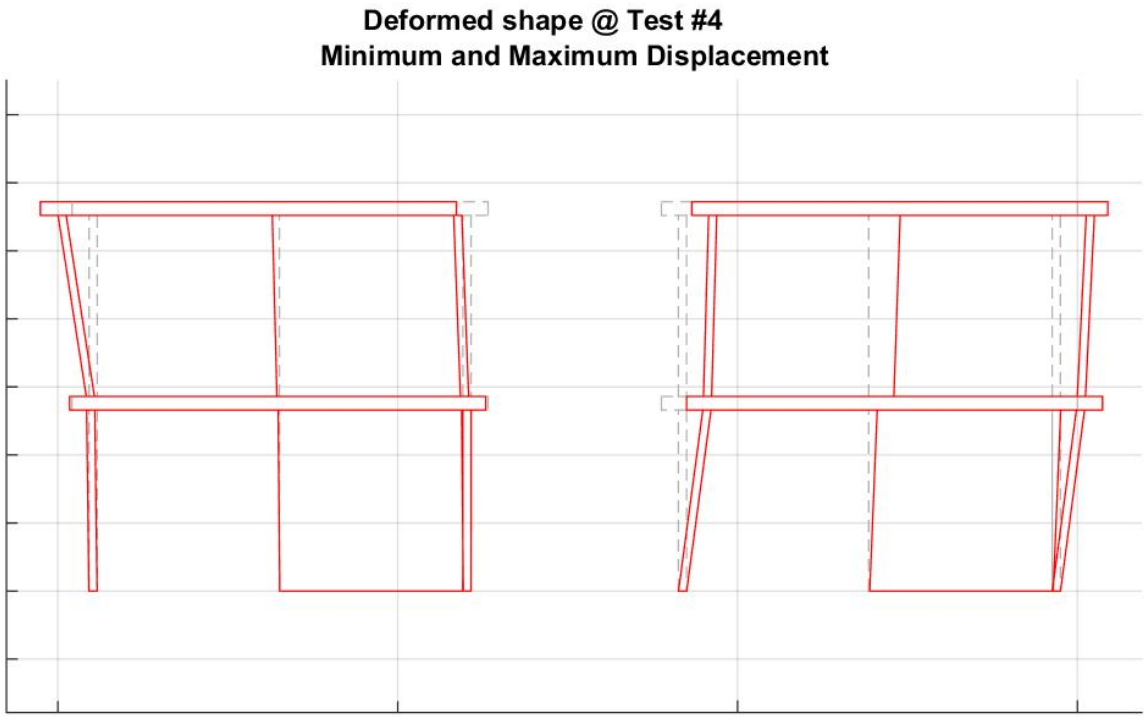

Figure 151. Deformed shape of EUC-BUILD4 specimen (max and min) – Test run #4.

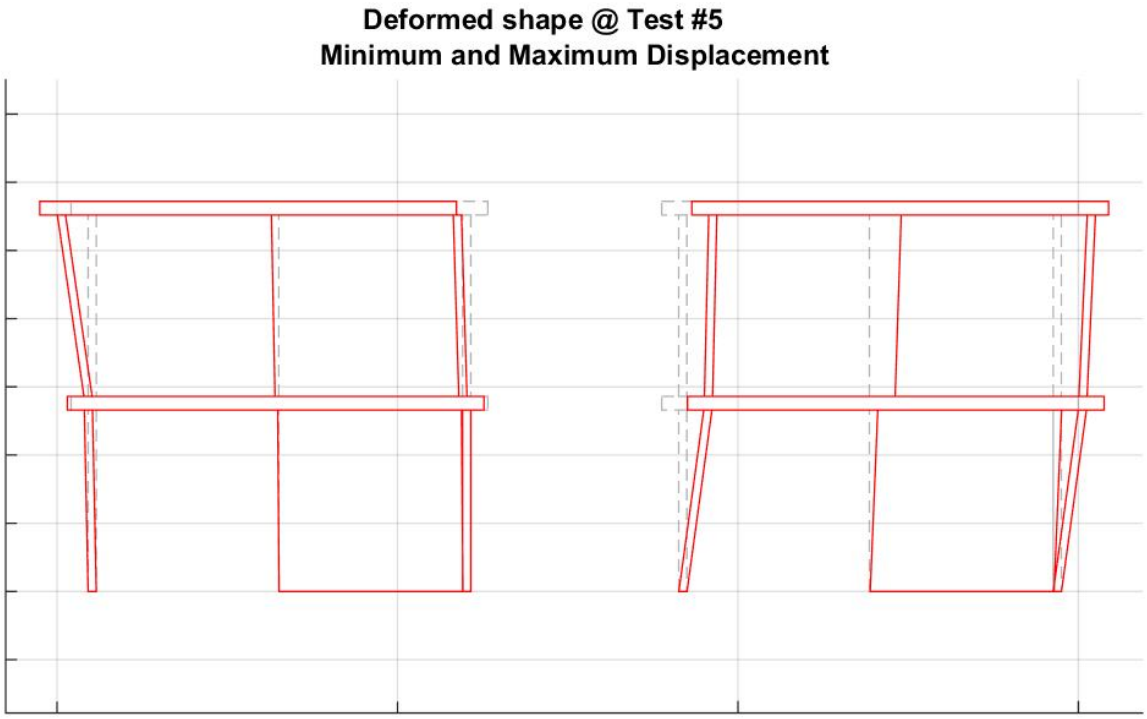

Figure 152. Deformed shape of EUC-BUILD4 specimen (max and min) – Test run #5.

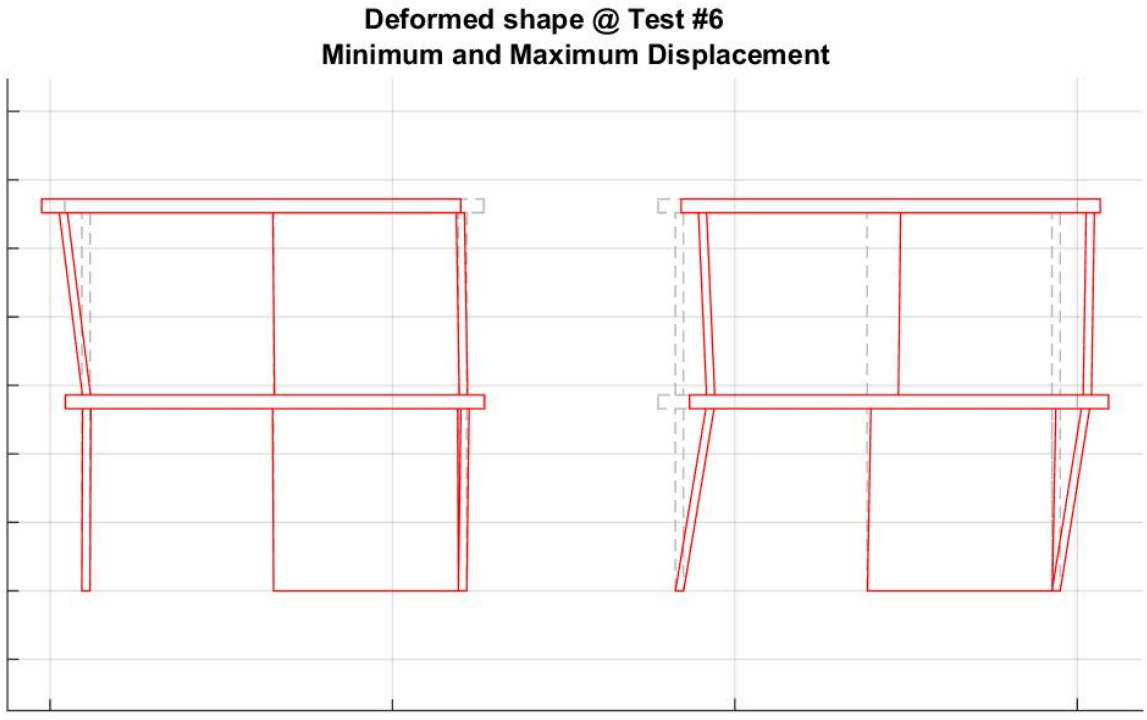

Figure 153. Deformed shape of EUC-BUILD4 specimen (max and min) – Test run #6.

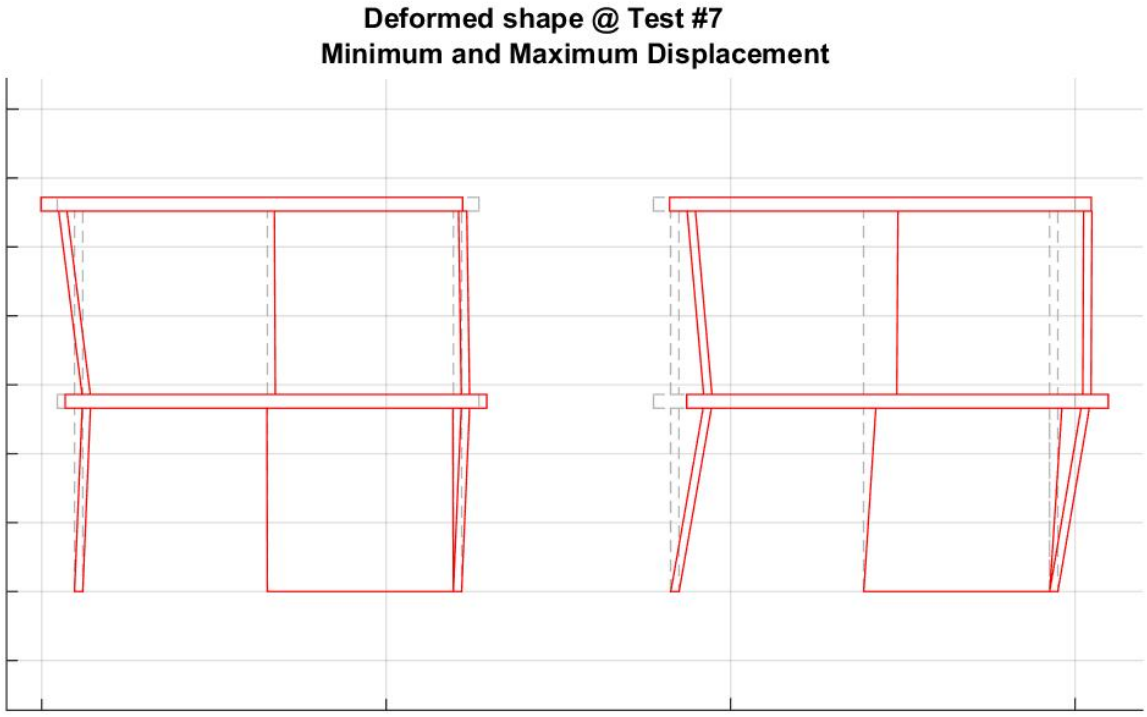

Figure 154. Deformed shape of EUC-BUILD4 specimen (max and min) – Test run #7.

6.2.3 Displacement profiles

In what follows, the displacement profiles recorded at positive and negative displacement peaks of each step of testing are plotted together with the initial position at the beginning of that stage, which means with respect to the deformed configuration at the end of the previous stage of testing. Data of the North-sided and South-sided transversal walls are presented, along with the results obtained for the stability walls. It is also worth noticing that these graphs also consider the relative sliding of the floor slabs with respect to the wall-elements above and underneath. The latter mechanisms can thus be seen therein, in addition to the displacement profile of the wall-elements themselves. It was then decided to present the three profiles obtained from each stage of testing by assuming the same scale, which implies that a direct comparison between the three structural wall-elements can be even more clearly appreciated.

Though quite modest in magnitude, sliding was observed since the beginning of the testing sequence, particularly in one of the two directions. As depicted in Figure 160 and Figure 161, the out-of-plane rocking of the first-storey and second-story lateral walls, which were opposed in phase during the last two steps of cyclic testing, can be reaffirmed. For sake of clarity, this latter consideration refers to the transversal walls placed in correspondence to the North side of the mock-up building, whereas those at the South side of EUC-BUILD4 exhibited a completely different type of response, which is obviously much more aligned with that undergone by the stability walls. More in detail, the displacement profile of the South-sided transversal walls and that of the stability ones differ from each other mostly at the first storey, given that the former displaced more than the latter one. This difference tends to increase as the roof top displacement applied to the structure increases and is particularly evident for the stage of major damage to the specimen in its three-way joints.

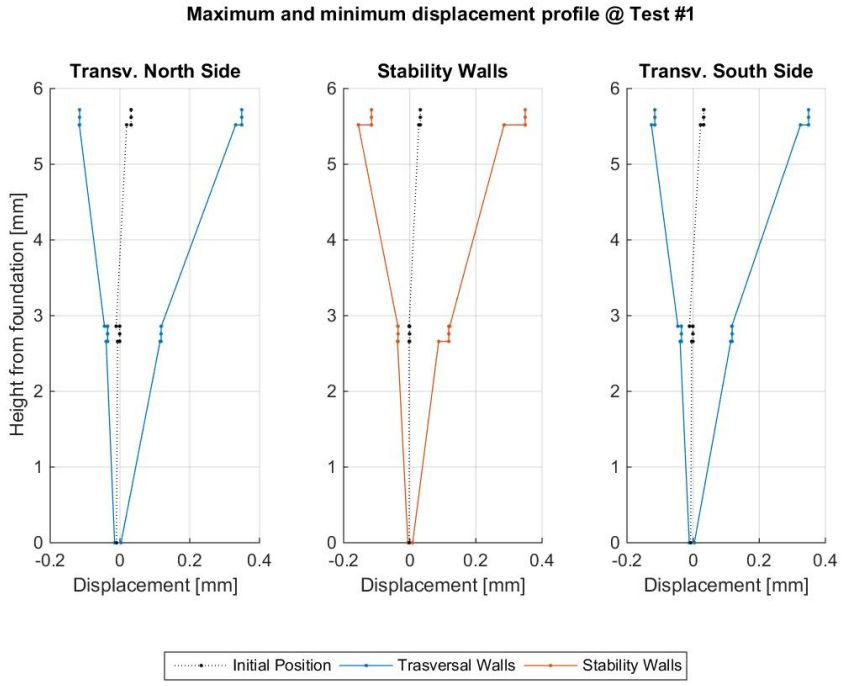

Figure 155. EUC-BUILD4 as-built specimen: displacement profiles of structural walls – Test run #1.

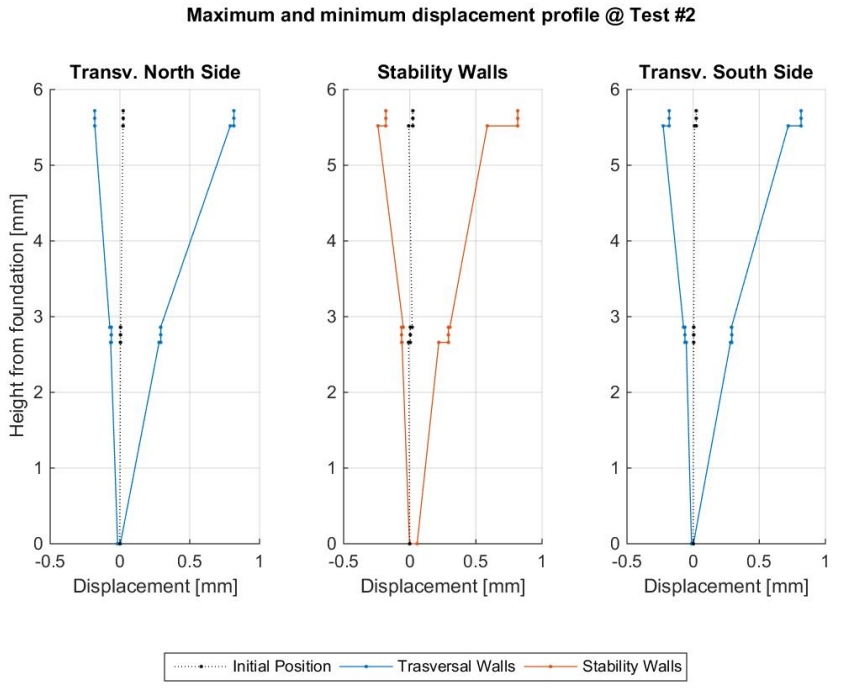

Figure 156. EUC-BUILD4 as-built specimen: displacement profiles of structural walls – Test run #2.

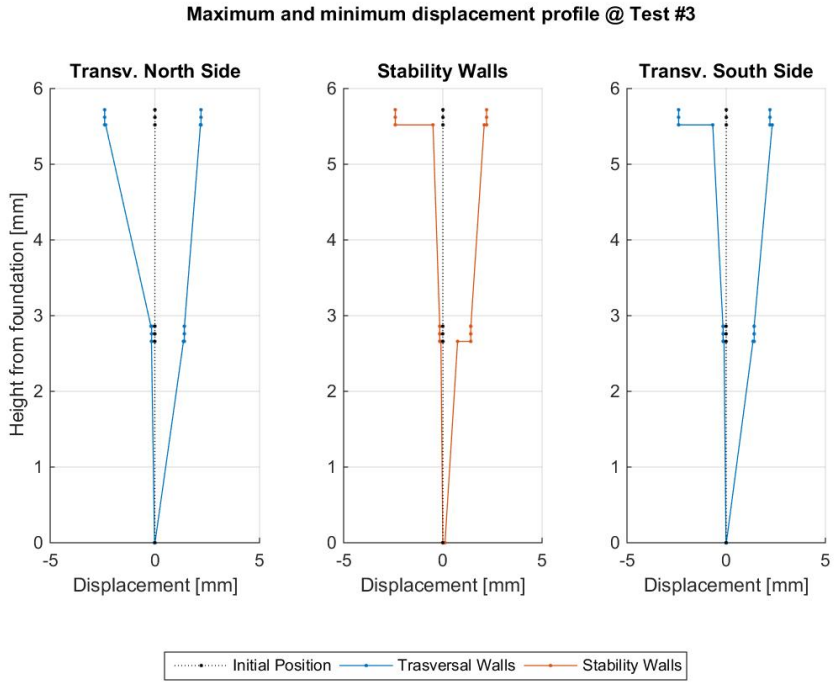

Figure 157. EUC-BUILD4 as-built specimen: displacement profiles of structural walls – Test run #3.

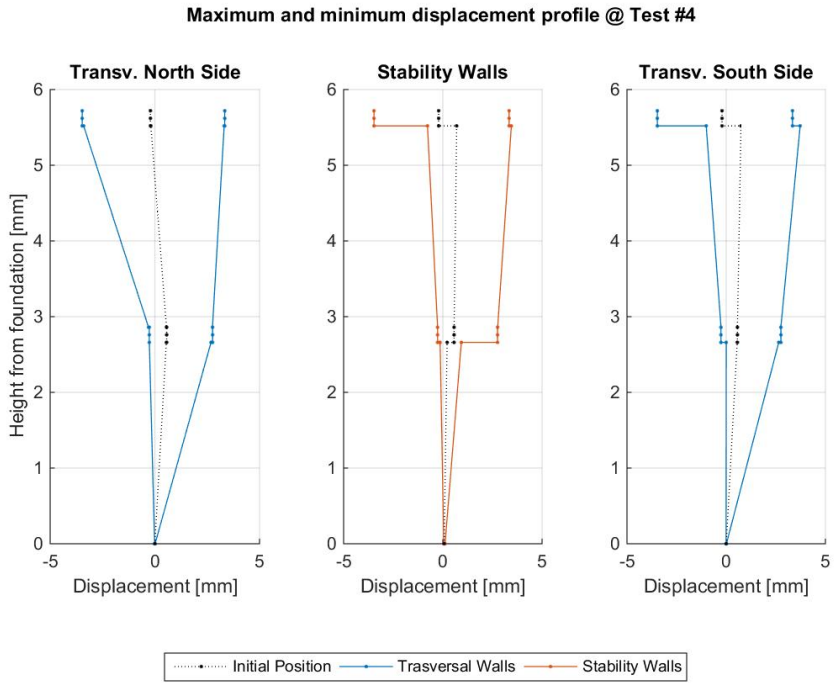

Figure 158. EUC-BUILD4 as-built specimen: displacement profiles of structural walls – Test run #4.

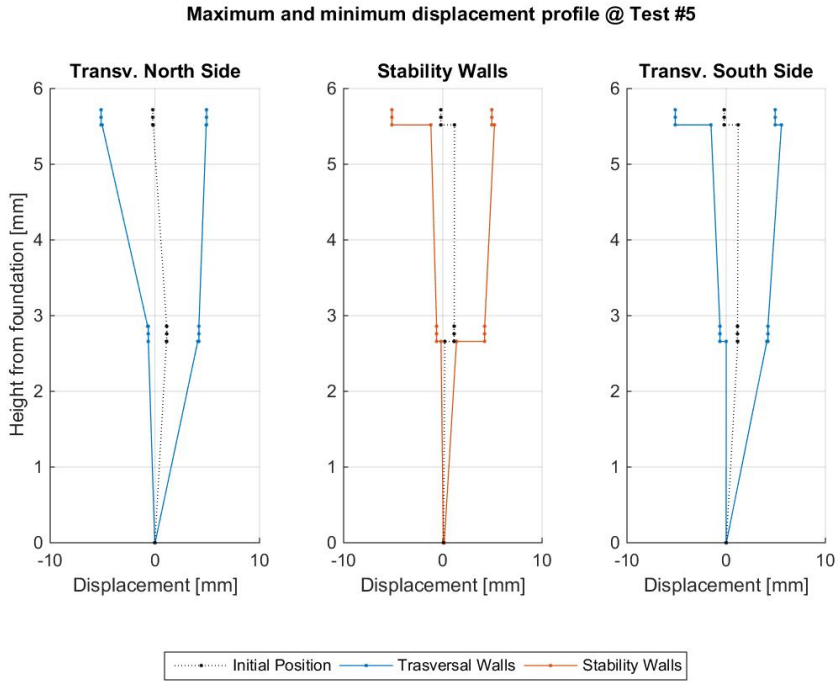

Figure 159. EUC-BUILD4 as-built specimen: displacement profiles of structural walls – Test run #5.

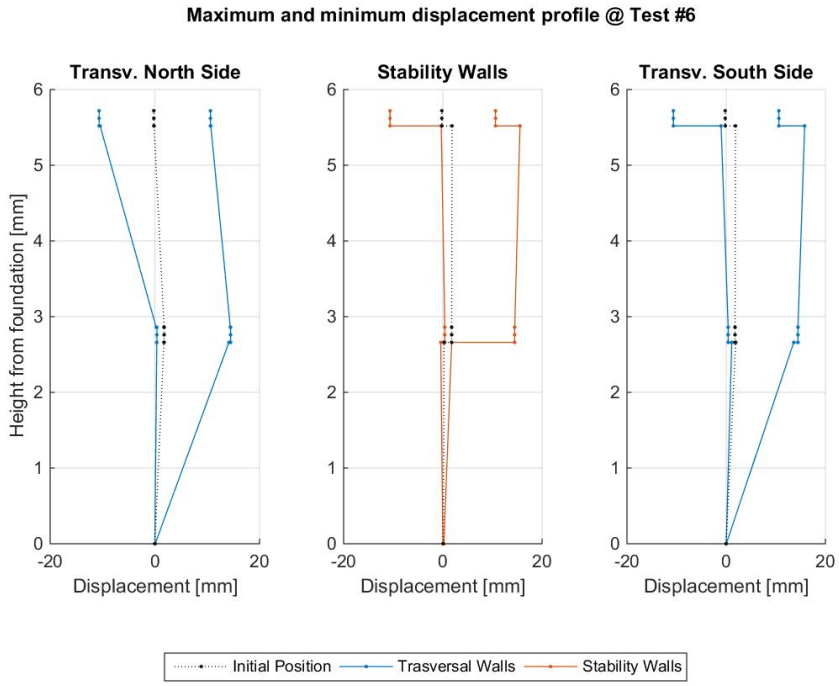

Figure 160. EUC-BUILD4 as-built specimen: displacement profiles of structural walls – Test run #6.

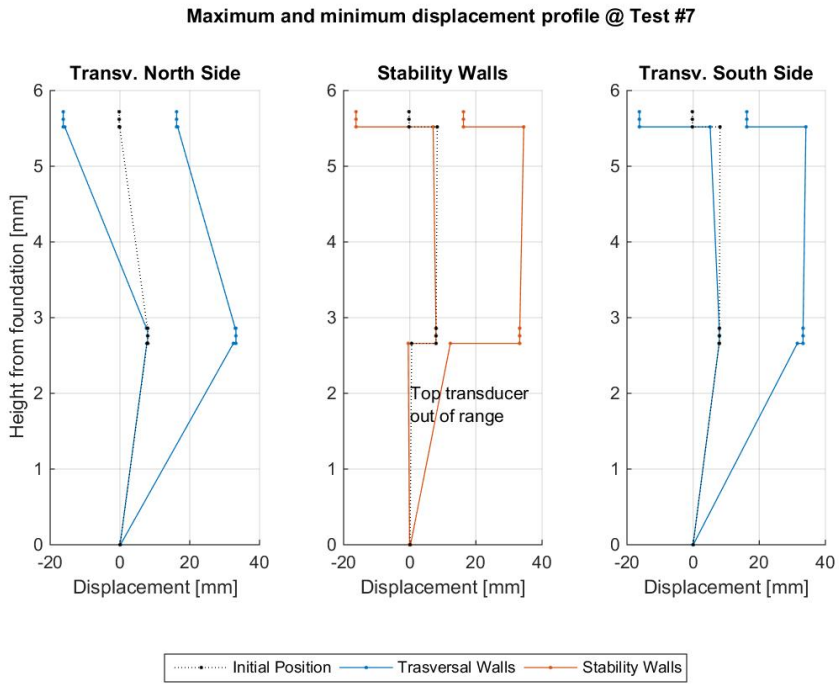

Figure 161. EUC-BUILD4 as-built specimen: displacement profiles of structural walls – Test run #7.

6.2.4 Local response of key structural portions

Rotation response data were examined in detail, placing particular emphasis on the base rotation due to rocking of the first-storey and second-storey stability walls. In both cases, that parameter was of course evaluated using the in-plane displacement transducers installed according to what was shown and discussed in Section 5.5.2. Accordingly, the plots given below were created by means of the instruments placed on West and East sides separately. The average of them was presented as well, thus resulting in a total of three response graphs per each wall. The same approach was used to assess the vertical sliding of the first-storey and second-storey stability walls, which was determined by taking as reference the corresponding transversal walls. Therefore, three plots per each storey are presented.

The rocking response of the ground-floor stability wall is provided in Figure 162 and Figure 163, in which it is graphed against the storey shear force. Furthermore, Figure 164 and Figure 165 highlight the experimental behaviour of this panel wall in terms of observed vertical sliding. Finally, response graphs of the second-storey stability wall are collected in Figure 166 to Figure 169. None of the two mechanisms was found to be particularly pronounced, and this applies to both the first-floor and the second-floor walls. Rocking was clearly more significant in the ground-floor stability wall, and this mechanism was not symmetric in pulling and pushing directions (see Figure 162 and Figure 163). A similar conclusion can be drawn as far as the second-storey stability wall is concerned (Figure 166 and Figure 167). The response curves of both walls present fairly regular trends, despite the fact that they are not necessarily smooth. Rotation maxima of about $6 \cdot 10^{-4}$ rad were obtained in the ground-floor stability wall, whilst peaks much lower (i.e. one order of magnitude) can be observed at the second storey.

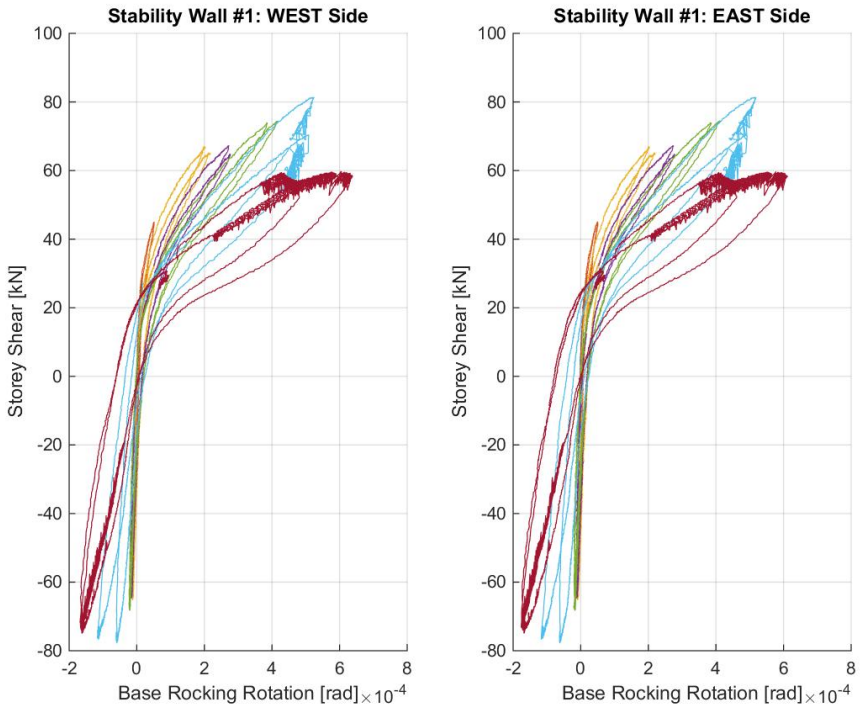

Figure 162. First-storey stability wall: base rotation due to rocking (as-built specimen) – West and East sides.

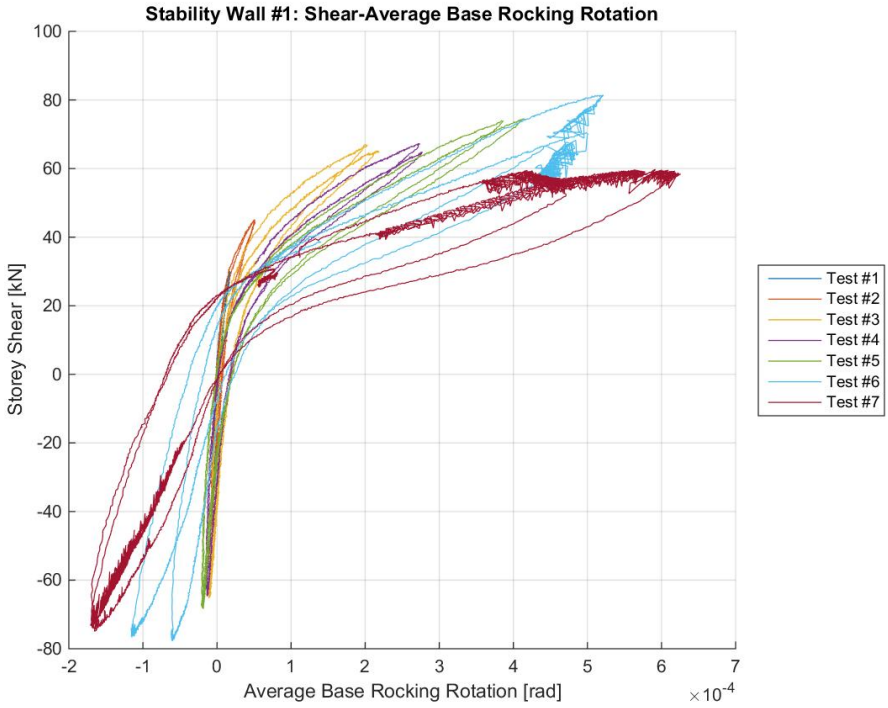

Figure 163. First-storey stability wall: base rotation due to rocking (as-built specimen) – Average.

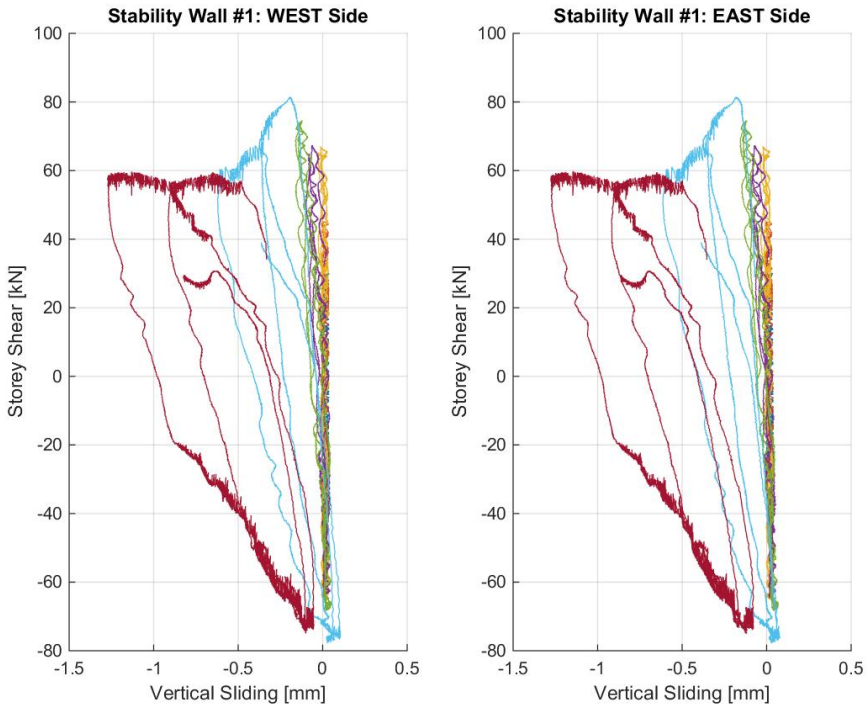

Figure 164. Vertical sliding of first-storey stability wall (as-built specimen) – West and East sides.

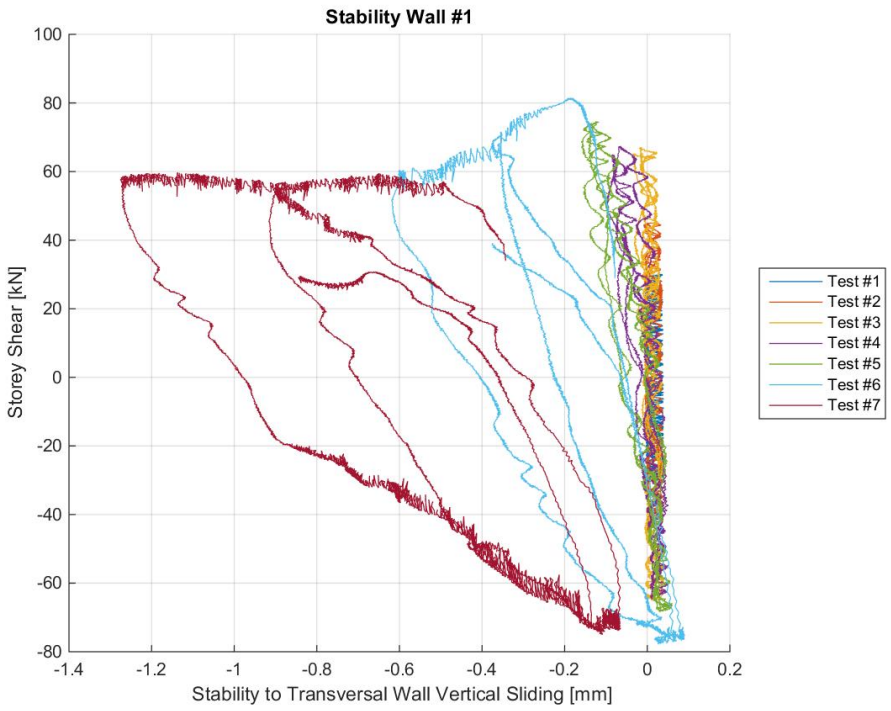

Figure 165. Vertical sliding of first-storey stability wall (as-built specimen) – Average.

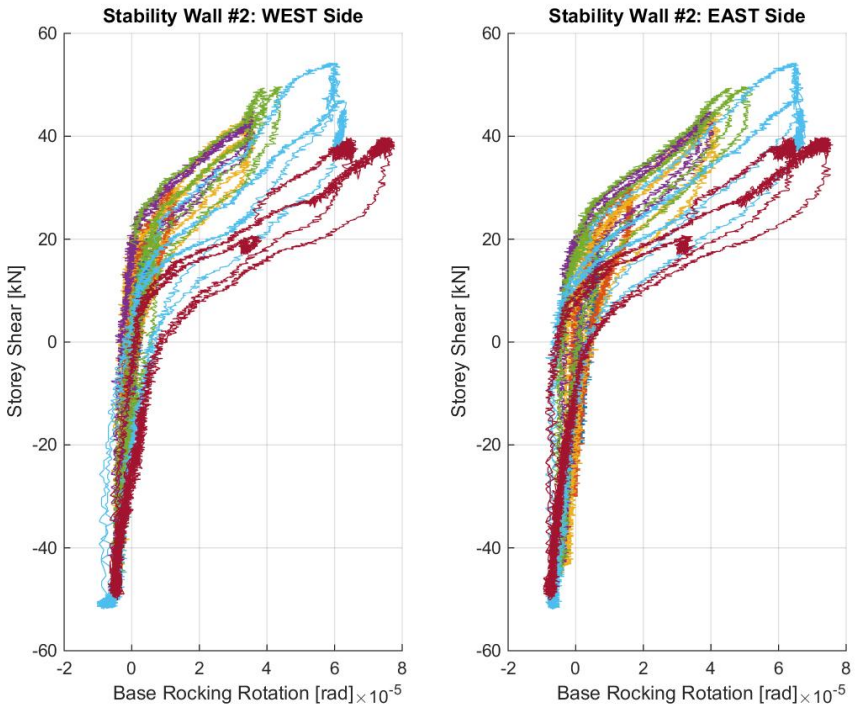

Figure 166. Second-storey stability wall: base rotation due to rocking (as-built specimen) – West and East sides.

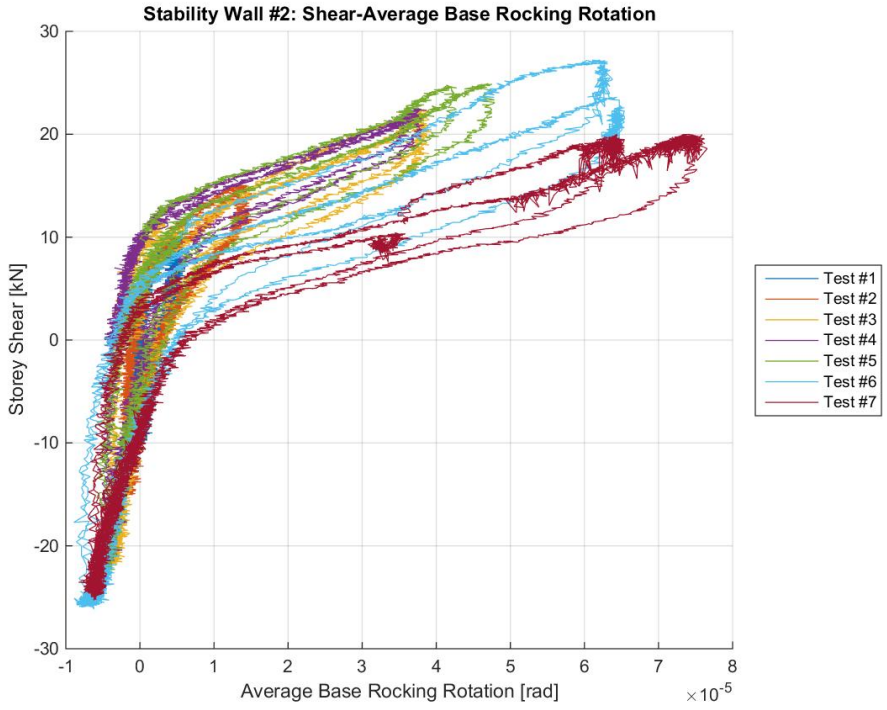

Figure 167. Second-storey stability wall: base rotation due to rocking (as-built specimen) – Average.

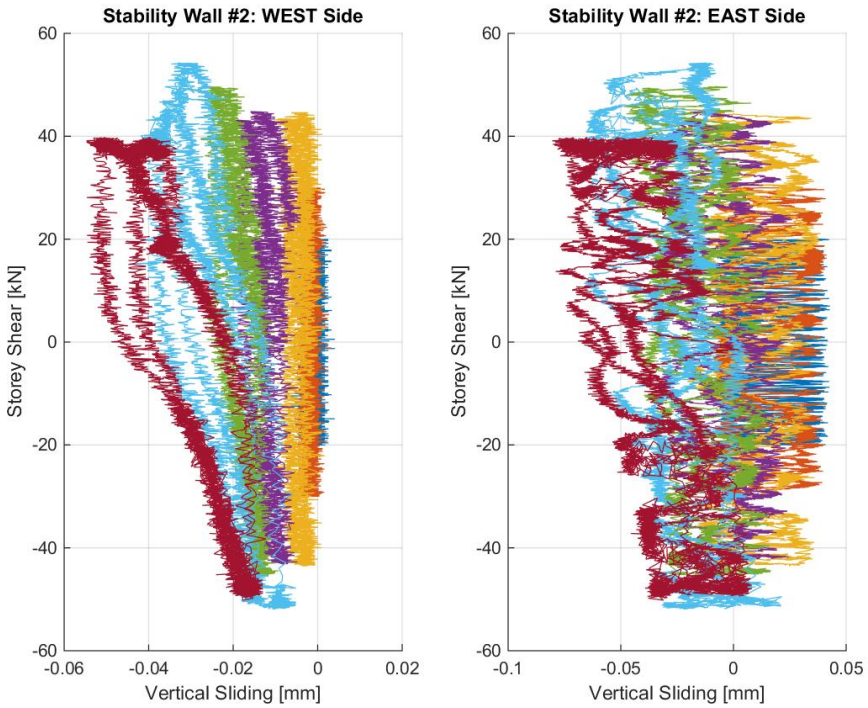

Figure 168. Vertical sliding of second-storey stability wall (as-built specimen) – West and East sides.

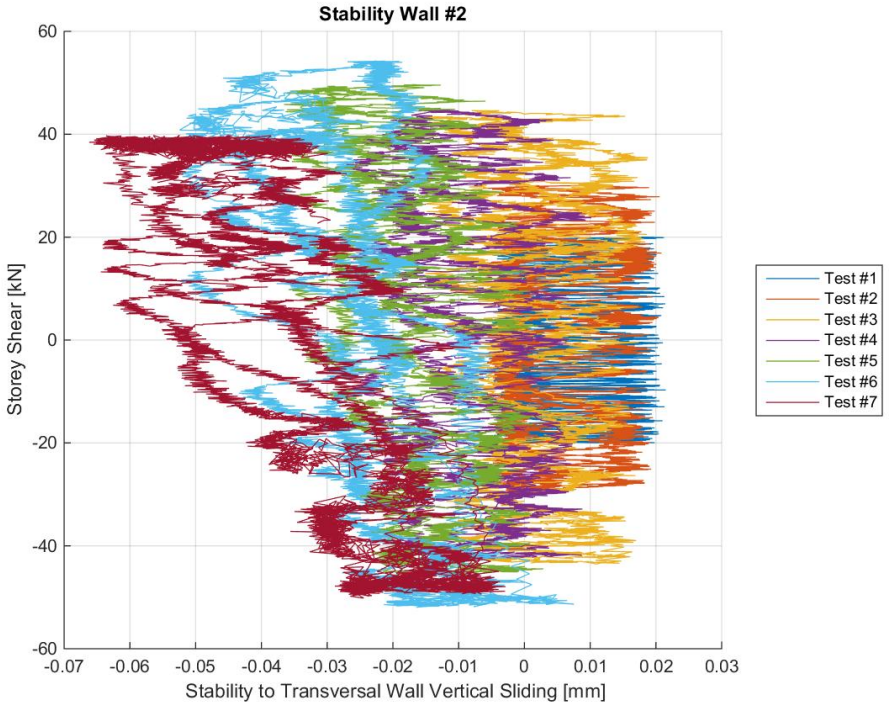

Figure 169. Vertical sliding of second-storey stability wall (as-built specimen) – Average.

For what concerns vertical sliding, it can be seen from both Figure 164 and Figure 165 that peaks of up to 1.2 mm were obtained between the stability and transversal walls at the first floor. However, it is evident that sliding was almost negligible, as is also in the second storey, before any type/sort of incipient damage took place in the three-way panel-to-panel joints (Test run #6 and Test run #7). As shown in Figure 168 and Figure 169, the second-storey stability wall underwent a maximum sliding of roughly 0.06 mm, and very similar values can be found whether displacement transducers on the East and West sides are considered separately.

6.2.5 Observed damage after Test run #3 – Imposed top displacement = 2.8 mm (max storey drift of 0.08% measured)

The first sign of damage that affected EUC-BUILD4 full-scale specimen was detected at the end of Test run #3, which consisted of two displacement-controlled cycles for a top displacement of up to 2.8 mm (see Table 19). At the end of testing for the first two preliminary force-controlled cycles, the mock-up building did not experience any type of "eye-catching" damage. On the other hand, minor cracks formed at the base of the ground-floor stability wall as well as in correspondence to the connections between the latter structural element and the lateral walls. Figure 170 to Figure 175 collect the most noticeable observations. More in detail, the development of minor cracks in correspondence to the North corner of the stability wall is reported in Figure 170, Figure 171 and Figure 172, noting also that such cracks formed on both East and West sides of the wall. Figure 173 and Figure 174 then present the crack pattern in the joint between the stability wall and the orthogonal walls. Also in this case, the crack propagated on both sides of the stability wall, along its top half. Another minor crack opened up in one of the two South-sided transversal wall, as shown in Figure 175.

Figure 170. Development of cracks in the ground-floor stability wall.

Figure 171. Crack pattern at the base of the first-floor stability wall – Edge of the wall.

Figure 172. Crack pattern at the base of the first-floor stability wall – Opposite side.

Figure 173. Crack opening in correspondence to the connection between stability and lateral walls – Top.

Figure 174. Crack opening in the connection between stability and lateral walls – Opposite side.

Figure 175. Development of a crack at the base of one of the transversal walls at the South side.

Therefore, the most remarkable observations collected after the first run of displacement-controlled cycles regard the development of those minor flexural/tensile cracks. Whilst they formed on each of the two wall sides, the width of these cracks was nonetheless moderate and additionally they did not propagate along the entire wall depth/height.

6.2.6 Observed damage after Test run #4 – Imposed top displacement = 3.9 mm (max storey drift of 0.10% measured)

EUC-BUILD4 suffered further damage during Test run #4, as presented in Figure 176 to Figure 179. In detail, minor flexural/tensile cracks caused by the application of the previous series of cycles were observed to evolve and propagate along the depth of the ground-floor stability wall (Figure 176 and Figure 177) and the same consideration can be drawn from Figure 178, in which the development of the vertical crack opened up in the three-way connection between the stability and transversal walls can be appreciated. Both the East and West side views confirm the propagation of this vertical crack down the storey height. It can also be noted that a new crack opened up at the base of one of the two ground-floor transversal walls, as shown by the West side view reported in Figure 179. However, the latter crack did not develop at both sides of these 120 mm-thick walls, nor along their entire width.

Other signs of damage were not detected during visual inspections undertaken at the end of Test run #4, which consisted of two displacement-controlled cycles for applied top displacements of up to 3.9 mm. As also commented for Test run #3, the width of these flexural/tensile cracks was very moderate and, more in general, it can be concluded that the building mock-up did not undergo any severe “eye-catching” damage also at this stage of cyclic testing. This totally agrees well with the fact that the dominating response mechanism for moderate drift amplitudes such as those imposed

up until Test run #4 is chiefly concerned with issues of friction/sliding, as previously mentioned with reference to response curves and displacement profiles.

Figure 176. Propagation of horizontal cracks along the depth of the ground-floor stability wall – Wall base.

Figure 177. Propagation of horizontal cracks along the depth of the ground-floor stability wall – Opposite side.

Figure 178. Development of vertical crack in the three-way panel connection (stability-to-lateral walls).

Figure 179. Formation of a new crack at the base of transversal walls – South side of the specimen.

It is also worthwhile to note that, apart from the aforementioned occurrence (Figure 179), the South transversal walls of the first storey did not present any type of damage at the end of Test run #4, whilst different considerations can be made as far as the next stage of testing is considered, as discussed in the following section. No cracks were found to form for these cycles in the North lateral walls as well.

6.2.7 Observed damage after Test run #5 – Imposed top displacement = 5.6 mm (max storey drift of 0.15% measured)

Cyclic testing for top displacements of up to 5.6 mm was observed to cause slightly more damage than what had been discussed in Sections 6.2.5 and 6.2.6. A complete photographic sequence of the main observations collected at the end of this test is provided in Figure 180 to Figure 184.

As depicted in Figure 180 to Figure 182, first signs of new damage were found in the North ground-floor transversal walls of EUC-BUILD4 specimen. Indeed, a new crack formed in correspondence to the two-way panel-to-panel connection and propagated along the height of these walls (see Figure 180). In addition to that, some other cracks developed at the wall base, as pointed out in Figure 181 and in Figure 182, which present the South and East faces of the first-storey transversal wall, respectively. Once again, the width of these cracks was relatively moderate; noteworthy is that they did not form on both the two sides of the wall, which means that North and West faces of these wall panels remained intact. Finally, it can be noticed that cracks developed along the wall height in the joints of the two adjacent lateral walls simply because they are disconnected with each other, niches/joints apart. As presented in Figure 184, a similar occurrence was observed in the South lateral walls.

Figure 180. Development of a new crack along the two-way connection between lateral walls – North side.

Figure 181. Crack pattern at the base of lateral wall W1L4 – North side, internal edge.

Figure 182. Crack pattern at the base of lateral wall W1L3 – North side, external edge.

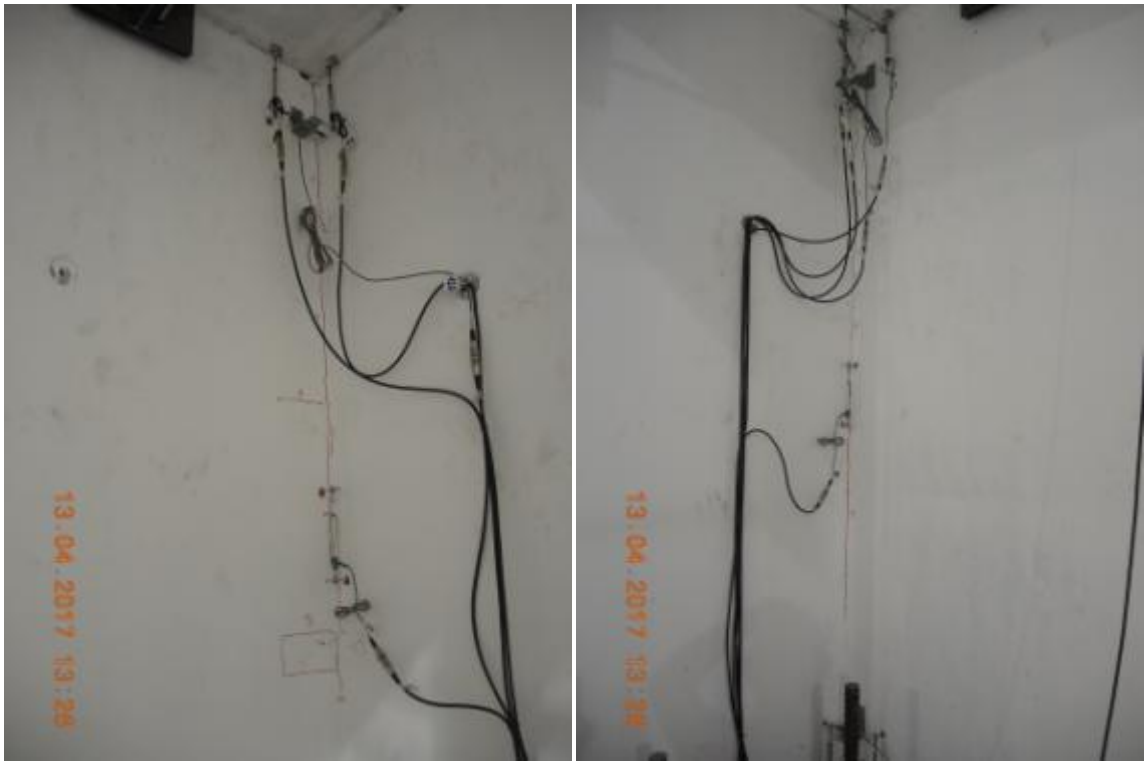

Figure 183. Three-way connection: propagation of crack pattern in the niches and along the wall height.

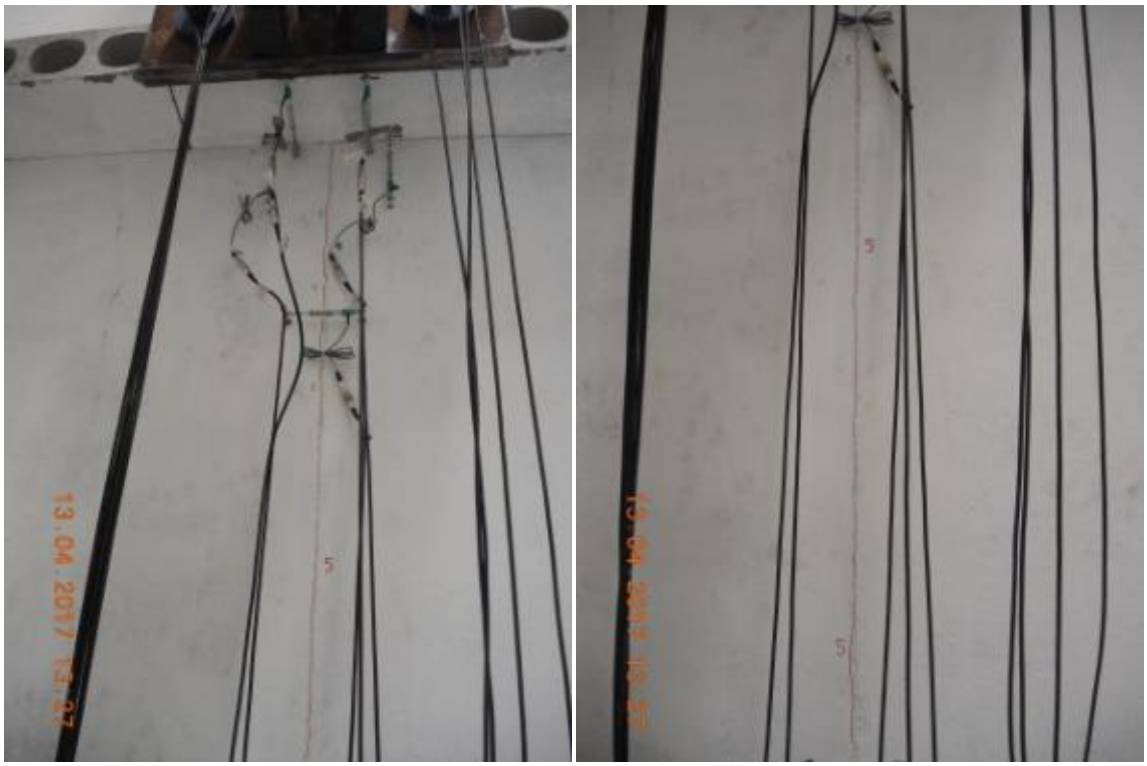

Figure 184. Three-way connection: development of a new crack at the two adjacent lateral walls.

Figure 184 shows the formation/propagation of cracks all along the top half of the wall height in the South transversal wall, which is composed of two contiguous panels completely unengaged except

for the four anchorages. Particular attention was paid to the survey of the stability wall, considering that it is the most critical element of the lateral-force resisting system. As clearly reported in Figure 183, new cracks opened up and those already present developed even further. In detail, visual inspections revealed that previous vertical cracks propagated even further and that the first signs of an incipient damage in the niches of the three-way connection between the stability and lateral walls are clearly evident at this stage of the testing sequence.

6.2.8 Observed damage after Test run #6 – Imposed top displacement = 11.2 mm (max storey drift of 0.50% measured)

As pointed out by the cyclic curves shown in Section 6.2.1 and also reaffirmed by the displacement profiles presented in Paragraph 6.2.3, Test run #6, which consisted of two push/pull cycles for imposed top displacements of 11.2 mm, was characterised by a significant evolution of damage in the four three-way connections between the ground-floor stability wall and the transversal walls. This in turn caused a visible drop in strength, due to the fact that the relatively poor sources of nonlinearity of those joints are now fully in use. Permanent flexural deformations in the connectors between the two transversal walls started being observed, which results in post-peak softening, as the specimen is no longer able to ensure higher loadbearing capacity against the force imposed by the actuators. It is worthwhile to note that first signs of damage took place at the base of the second-storey lateral walls, especially in the North side ones. The outcome of visual inspections is shown in Figure 185 to Figure 197.

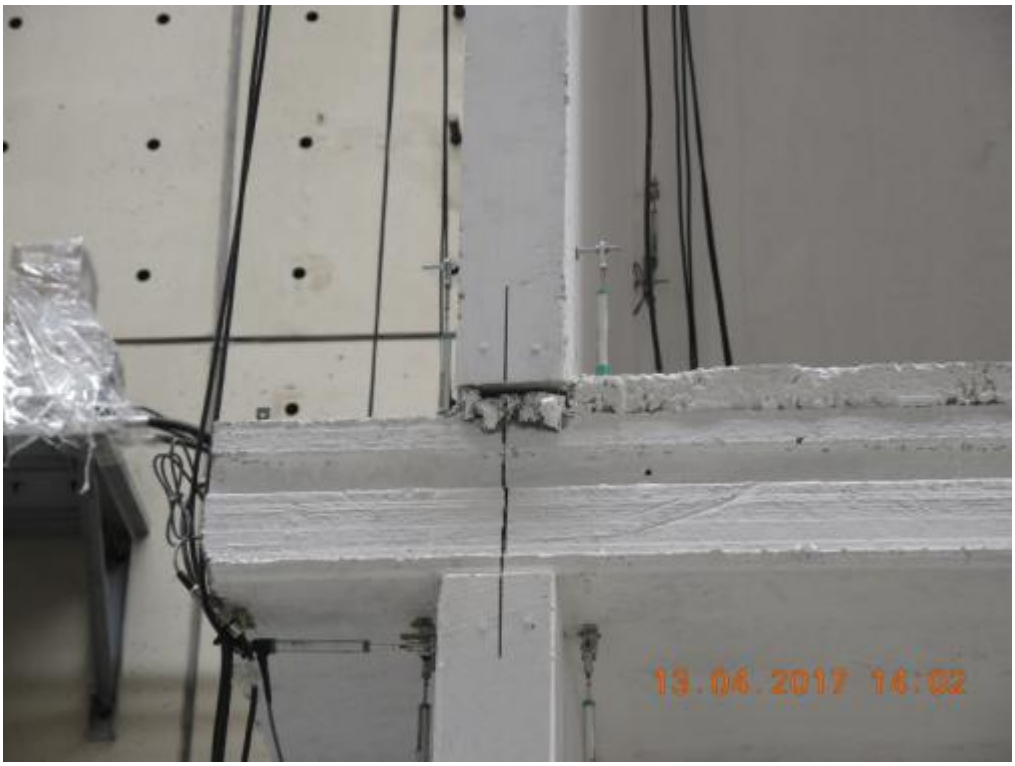

Figure 185. Detail of the first-storey floor slab after Test run #6 – top displacement = 11.2 mm.

Figure 186. Detail of the second-storey floor slab after Test run #6 – accumulation of displacement residuals.

Figure 187. Crack pattern at the base of lateral wall W1L1 – South side, internal edge.

Figure 188. Three-way connection: propagation of vertical crack along the entire height of the stability wall.

Figure 189. Three-way connection: propagation of crack along the entire wall height – Opposite side.

Figure 190. Detachment of stability wall with respect to lateral walls – global view and detail at the top.

Figure 191. Extensive damage of the top three-way joint – detail of niches and grout, lateral walls.

Figure 192. Detail of the crack pattern at the base of the transversal walls – South side.

Figure 193. Formation of horizontal cracks at the base of the transversal walls – North side.

Figure 194. Formation of horizontal cracks at the base of the transversal walls – North side, opposite edge.

Figure 195. Horizontal cracks at the base of the transversal walls – North side, internal edge.

Figure 196. Propagation of vertical crack in the grout of panel-to-panel joint and loss of verticality.

Figure 197. Crack pattern at the base of the second-storey transversal walls – North side, internal face.

Figure 186 confirm that sliding of slabs on the walls underneath was pronounced as far as this stage of the testing sequence is regarded. According to that, the accumulation of residual displacements was non-negligble. Flexural cracks developed at the base of the South transversal walls mostly in correspondence to the internal/North face, as presented in Figure 187 and Figure 192. The crack/damage pattern of the North lateral walls evolved as well. In particular, Figure 193 and Figure 194 show the propagation of horizontal flexural cracks at the base of the North face of those lateral walls because of their out-of-plane rocking. This resisting mechanism was nearly symmetric during cyclic reversals and hence cracks were also found to propagate at the base of the South face of these walls (Figure 195). The propagation of a previously formed vertical crack in the grout of a panel-to-panel joint was then observed in the North transversal walls (see Figure 196). Such a damage mode is reported therein along with the loss of verticality of these transversal walls at the end of this stage of cyclic testing. Observations regarding the transversal walls of the structure are then completed by Figure 197, which reports the horizontal crack at the base of the second-storey lateral walls opposite to the stability wall (i.e. North side ones).

As evidenced by Figure 188 to Figure 191, the most remarkable observation regards the development of very severe cracks running through the entire height of the ground-floor stability and lateral walls in correspondence to their three-way connections. As pointed out in Figure 188 and Figure 189, this vertical crack propagated all over the whole wall storey height with very extensive damage in joints lacking properly conceived mechanical connectors. Global and enlarged views of cracks on both the two wall sides, as well as some further details of the complete detachment between the stability and transversal walls, are also shown in Figure 190 and Figure 191.

6.2.9 Observed damage after Test run #7 – Imposed top displacement = 16.8 mm (max storey drift of 1.15% measured)

The previously discussed damage modes/patterns were found to develop even further, as confirmed by the very detailed surveys undertaken at the end of Test run #7; the prevailing observations of damage/failure that were collected during visual inspections are shown in Figure 198 to Figure 212.

As a general comment on what happened during this last step of the testing sequence, it can be seen from Figure 198 to Figure 212 that no mechanisms other than those produced by the previous stage were observed to occur, but obviously the ones already activated evolved even further. This progressive evolution of damage (associated with the previously shown decay in the load carrying capacity) was nonetheless very notable, given (i) the small increment of top displacement compared to that of the previous step and, (ii) more in general, the relatively modest imposed drift amplitude.

Figure 198 and Figure 199 present the detail of a slab-wall joint of the first and second storey, thus confirming that residual displacements were mostly accumulated at the second floor of the mock-up building. Sliding of slabs on the fabric felts was significant and this, in addition to the accumulation of displacements during the previous steps, caused a few potentiometers to go out-of-range.

Figure 198. Detail of the first-storey floor slab after Test run #7 – top displacement = 16.8 mm.

Figure 199. Accumulation of displacement residuals due to sliding – Detail of the second-storey floor slab.

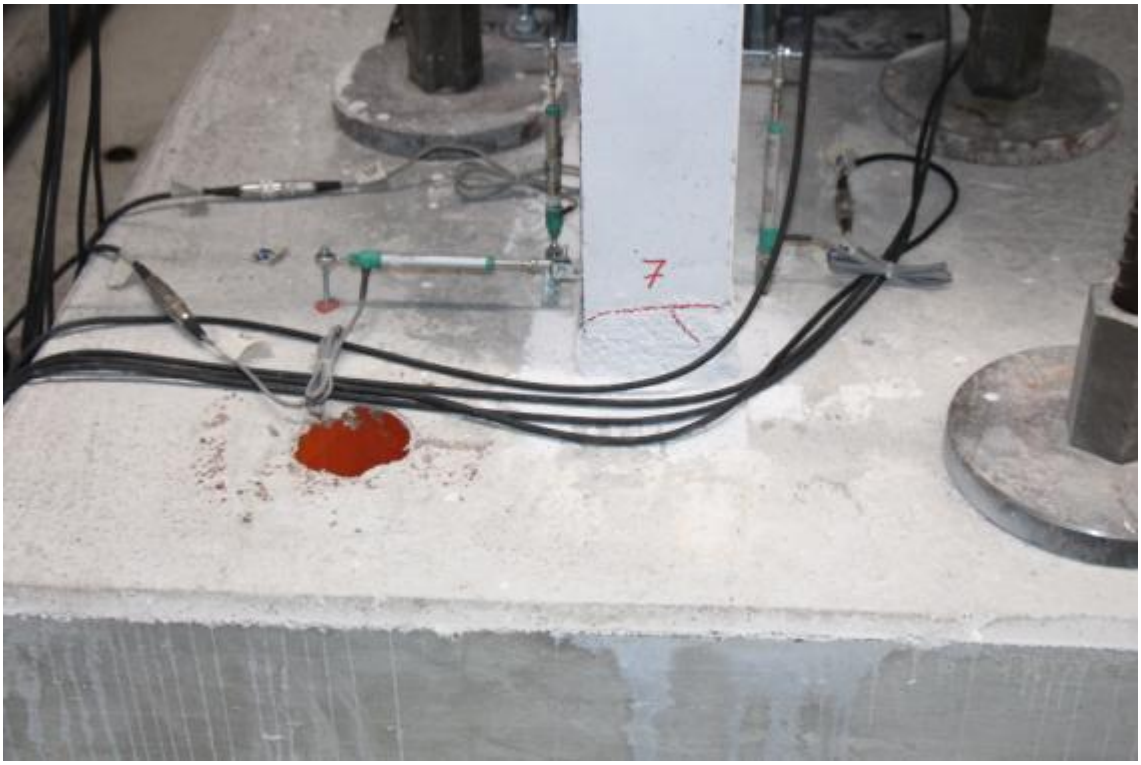

Figure 200. Detail of the crack pattern at the base of transversal walls – South side of the specimen.

Figure 201. Failure of three-way connection and complete gap opening between the stability and lateral walls.

Figure 202. Detail of the complete gap opening between the stability and lateral walls – Top.

Figure 203. Damage pattern at the base of the ground-floor stability wall – East face.

Figure 204. Gap opening between the stability and lateral walls – Top and mid-height, opposite side.

Figure 205. Detail of gap opening between the stability and lateral walls – Mid-height, West side.

Figure 206. Detail of gap opening between the stability and lateral walls – Top, West side.

Figure 207. Evolution of crack pattern at the base of the transversal walls – North side of the specimen.

Figure 208. Crack pattern at the base of the transversal walls – North side, second floor, internal face.

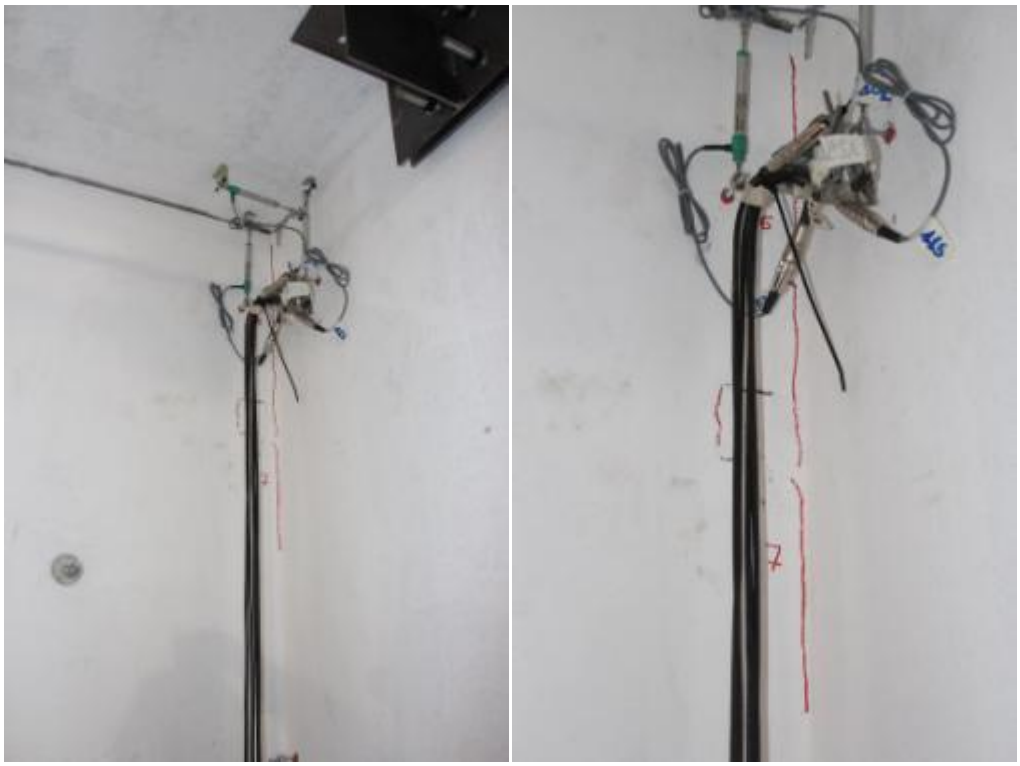

Figure 209. Vertical crack in the top three-way joint between the stability and lateral walls – Second floor.

Figure 210. Accumulation of residuals due to sliding of the second-storey slabs – Bottom view.

Figure 211. Flexural failure mode of the anchors embedded in the transversal walls – Top three-way joint.

Figure 212. Damage of the three-way joint at the end of testing – Global and enlarged views.

Before paying attention to both the connection behaviour and the ground-floor stability wall, a few considerations can be made regarding the damage patterns observed in the transversal walls. In Figure 200, details of the flexural crack developed at the base of a South transversal wall because of its out-of-plane rocking are presented, pointing out that the latter horizontal crack was running over the entire wall thickness. By the same token, Figure 207 shows the evolution of cracks at the base of a North transversal wall of the first storey. As can be seen in Figure 208, similar cracks were found in the second-storey transversal walls of the specimen (i.e. North side). Furthermore, a bottom view of the second-storey floor slabs is given in Figure 210, by which it can be reaffirmed that sliding of them on the underneath walls induced a significant accumulation of displacement residuals.

The response of three-way connections between the stability and transversal walls can be examined in a more detailed manner. First of all, it can be noticed that, although very moderate in width, a few vertical cracks developed in the top three-way joint between the stability wall and the corresponding lateral walls of the second floor. As depicted in Figure 209, they are on one hand relatively minor, if compared to the ones of the first storey (see e.g. Figure 211 or Figure 212), but on the other they are very similar to those observed at the ground floor during the first stages of the testing sequence.

In Figure 201 and Figure 202, details regarding the complete detachment between the lateral walls and the stability wall are provided. As shown in Figure 203, the latter wall-element was also the one that underwent more damage at the base. At the end of Test run #7, the horizontal crack due to rocking was running through the entire wall depth. Other global and enlarged views of the gap opening between the stability and lateral walls are presented in Figure 204, Figure 205 and Figure 206. Damage was very severe, as all four anchorages of the wall-panel were observed to collapse. It

is noteworthy that the maximum gap opened in the top connection and was approximately 25-30 mm wide. Figure 211 and Figure 212 are finally presented to confirm the type and nature of failure mechanism undergone by these joints. As previously explained and now shown in such photos, connections were found to fail in the hook reinforcement embedded in the niches of the transversal wall. No dislodgement was observed after the removal of the grout around these anchors, and the mechanism was reaffirmed to be a flexural one that was induced by the hook embedded in the stability wall.

6.3 Retrofitted configuration

As discussed before, after the initial test sequence, a decision was made to try to simulate and test a potential retrofitting strategy through the:

- firstly, the (attempted) closure of the gap that had opened up between the stability and transverse walls (i.e. trying to get the specimen back to its original configuration);
- the full connection through steel angles of the stability walls to the transverse walls and the slabs in order to obtain sturdier connections between precast panels.

The second of these operations involved "tightening" some of the sliding restrainers to the walls; in Figure 213 it is shown which sliding restrainers were simply "tightened" (i.e. yellow-boxed ones) and which were "moved and clamped" (i.e. red-boxed ones), thus leading to the final configuration seen in Figure 214. This "retrofitting" was rigged out by Eucentre technicians during the day of Friday 14th, which implied that the second test sequence started on April 18th and it was then completed the day after (April 19th).

It is however important to note that none of the two operations described above could be fully achieved, since:

- damage was too extensive and a permanent gap of approximately 25 mm remained between the stability and transverse walls at the top of the ground floor, as can be seen in some of the photos collected below (i.e. Figure 215 to Figure 217). By contrast, at the bottom of the wall the gap could be closed.
- again as can be seen in the photos that are presented below (Figure 215 - Figure 219), not all bolts that tie the steel angles to the precast walls could be screwed-in. Normally one would have liked to use four bolts per plate, but instead only two could often be employed because of the presence of existing rebars internal to the walls (if a proper retrofitting design would have been carried out, this would have obviously been avoided).

As a consequence of the above, it is expected that these steel angles will not be as effective as they would have been if they had been properly designed as a structural upgrading measure for an intact, undamaged structure. On the other hand, it was felt that the testing of this "not-fully-effectively-retrofitted" damaged structure will further highlight (through comparison with the response of the initial specimen) how much of a weakness the original connections are in this type of buildings, and also how additional seismic resistance can be mobilised by appropriately connecting their structural elements together.

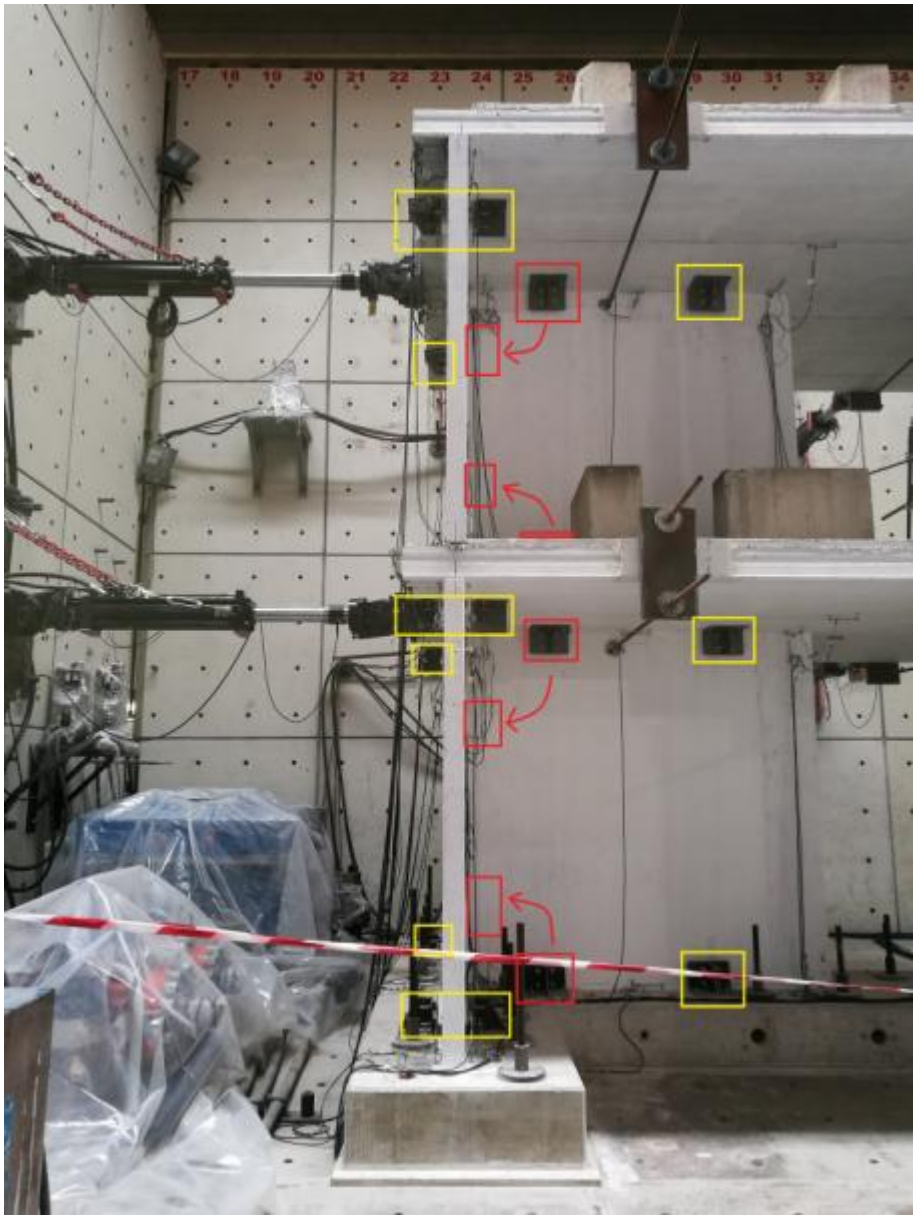

Figure 213. Rationale behind the implemented retrofitting strategy of EUC-BUILD4 specimen.

Figure 214. EUC-BUILD4 “retrofitted” specimen before test run.

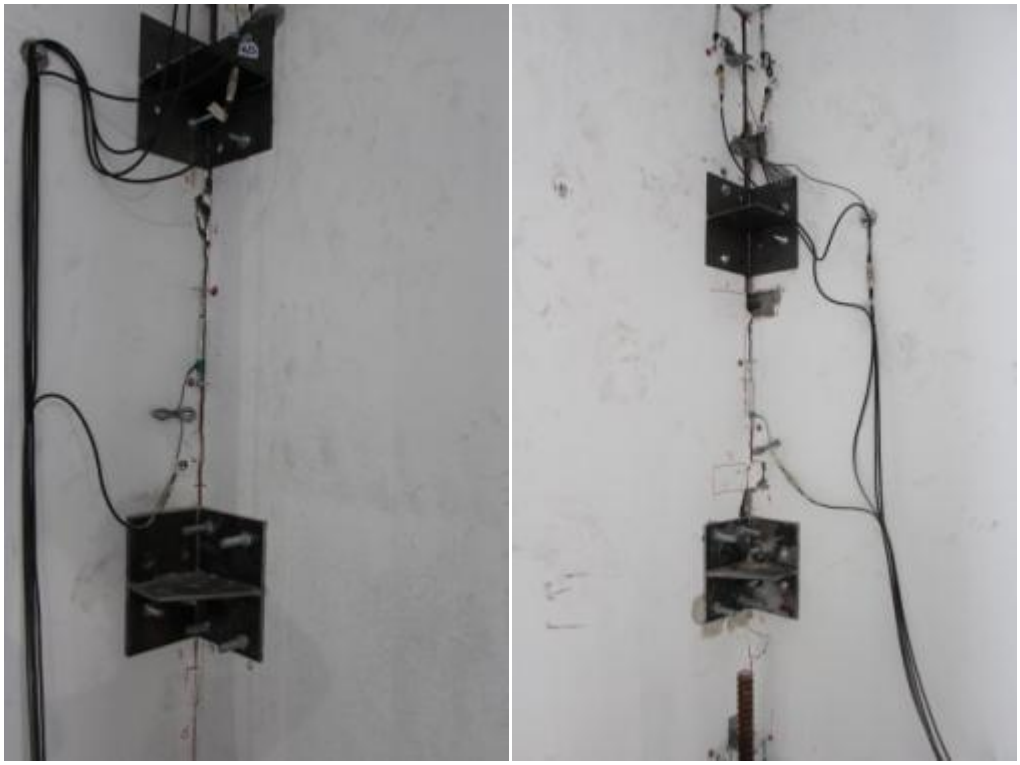

Figure 215. EUC-BUILD4 “retrofitted” specimen – Detail of steel angles, East and West side, first floor.

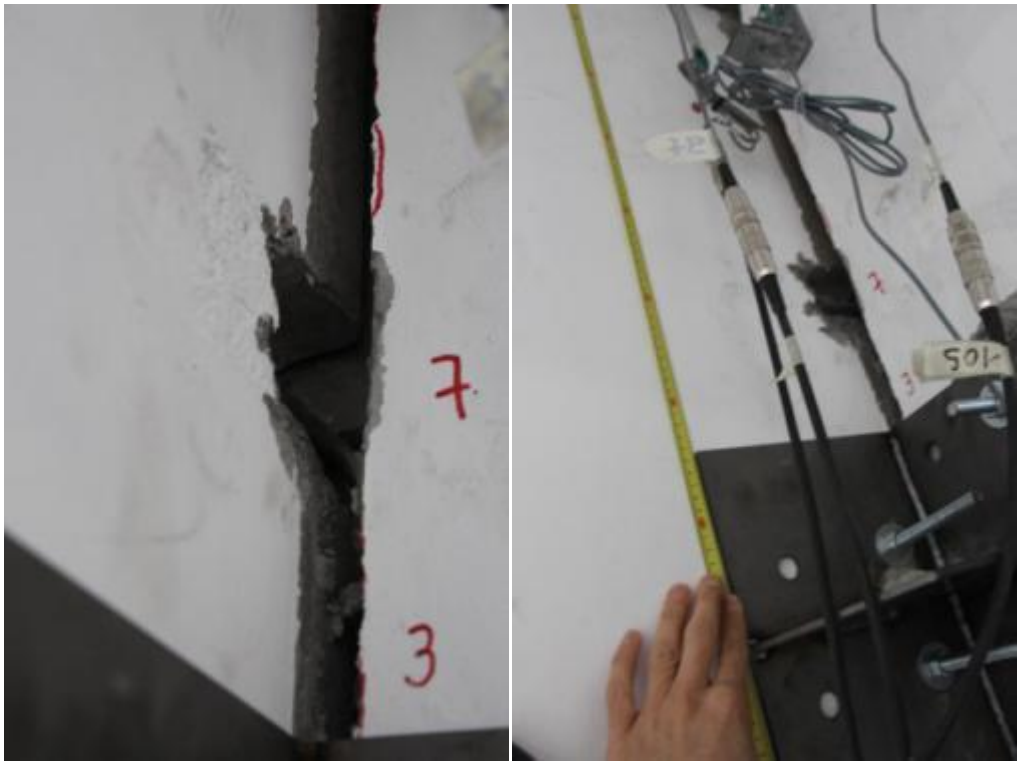

Figure 216. EUC-BUILD4 "retrofitted" specimen – Detail of the gap between stability and lateral walls.

Figure 217. EUC-BUILD4 "retrofitted" specimen – Number of bolts per angle and opposite wall face.

Figure 218. EUC-BUILD4 "retrofitted" specimen – Detail of bolts and washers, South lateral walls.

Figure 219. EUC-BUILD4 "retrofitted" specimen – Detail of the second-storey walls, South side.

6.3.1 Global response of the specimen

Once the cyclic inelastic tests of EUC-BUILD4 specimen in as-built configuration were completed, testing of EUC-BUILD4 "retrofitted" specimen was undertaken up to a top displacement of 33.7 mm (Table 19). In the following paragraphs, response plots are discussed to highlight the main characteristics of the specimen and the local behaviour of key precast walls. As done in the case of the response of EUC-BUILD4 specimen in its as-built configuration, significant care was also paid to deformed shapes of the structure as well as to the displacement profiles of its fundamental precast members. Moreover, the evolution of the damage pattern during different stages of the sequence of testing is examined in great detail. According to the framework considered for the presentation of results in the as-built configuration, sub-paragraphs were created to collect the aforementioned information/data, one per each field of interest.

Figure 220 shows the cyclic total base shear-roof top displacement response curve of EUC-BUILD4 specimen in the "retrofitted" configuration discussed above, whilst Figure 221 compares, in a clearer manner, the hysteresis loops of different displacement amplitudes with the envelope curve obtained from cyclic testing in pulling and pushing phases. As highlighted by Figure 222 to Figure 225, the response of each single storey was again decoupled to examine the behaviour observed for each one of them. Once again, the hysteretic responses of the first and second storey are presented in Figure 222 and Figure 223, respectively. The backbone curve of each one of them is then superimposed to the cyclic storey shear versus inter-storey displacement response in Figure 224 and Figure 225.

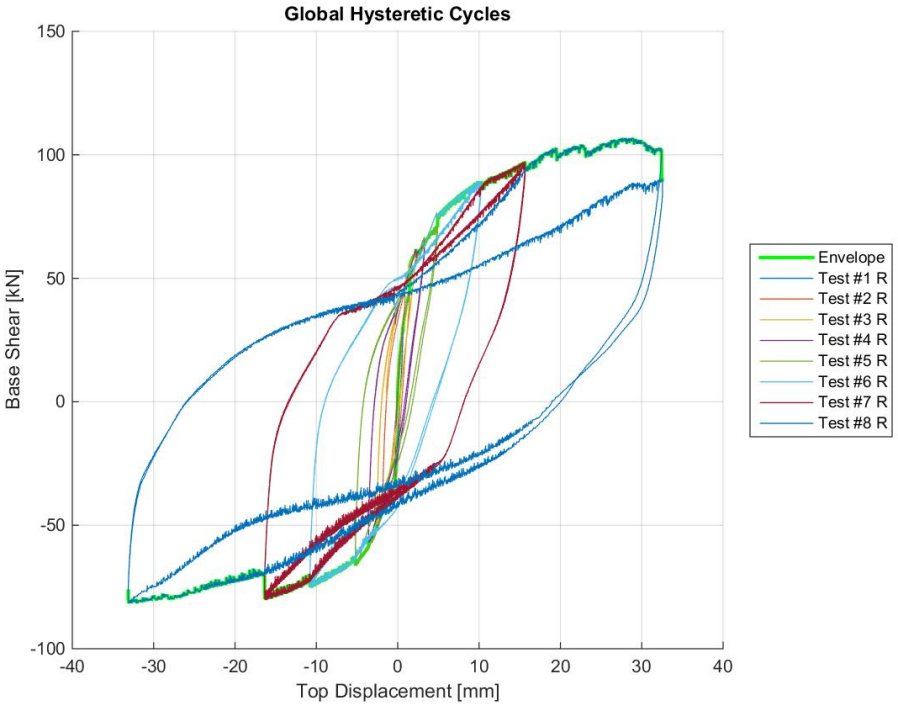

Figure 220. Cyclic total base shear-top displacement response of EUC-BUILD4 "retrofitted" specimen.

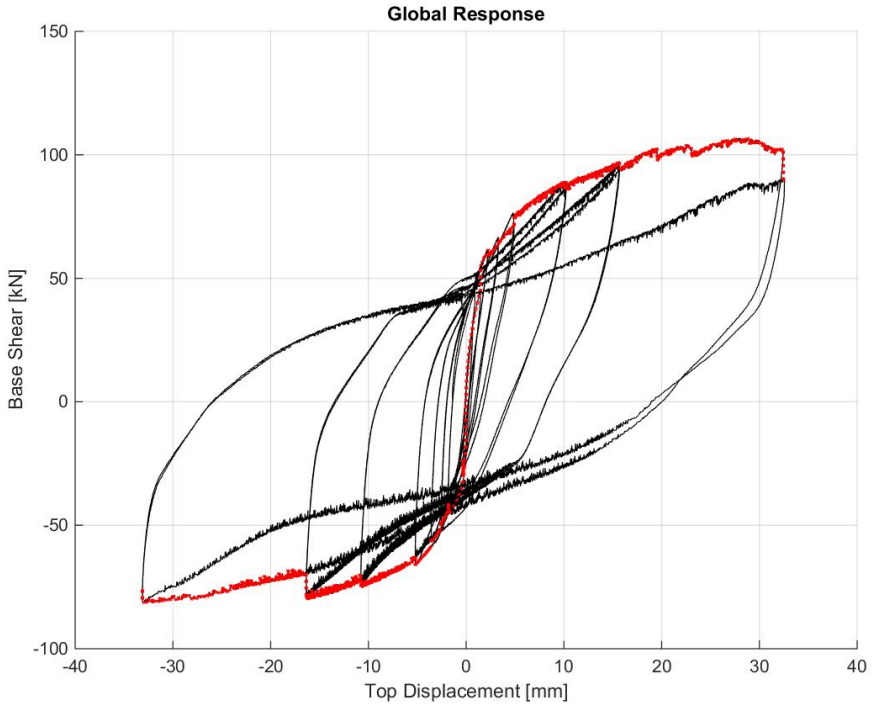

Figure 221. Base shear-top displacement response of retrofitted specimen – Backbone and cyclic curves.

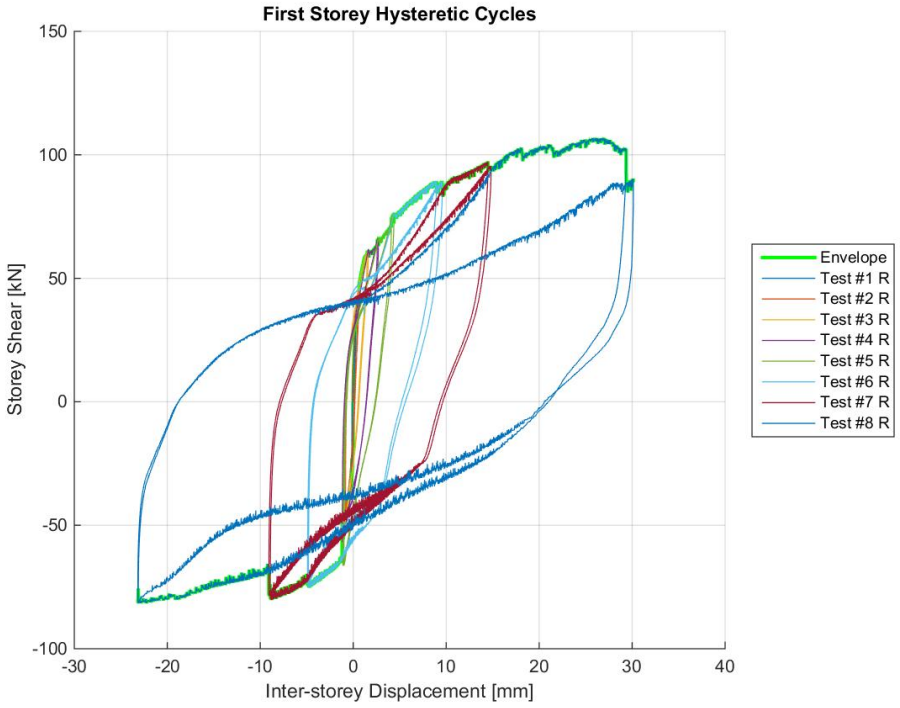

Figure 222. EUC-BUILD4 retrofitted specimen: storey shear vs. inter-storey displacement – First storey.

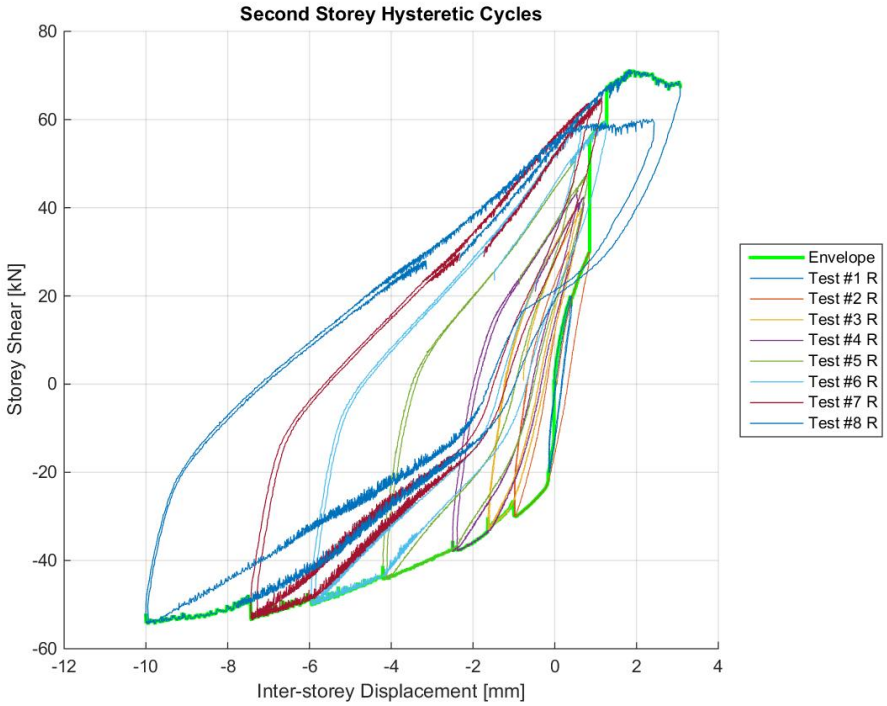

Figure 223. EUC-BUILD4 retrofitted specimen: storey shear vs. inter-storey displacement – Second storey.

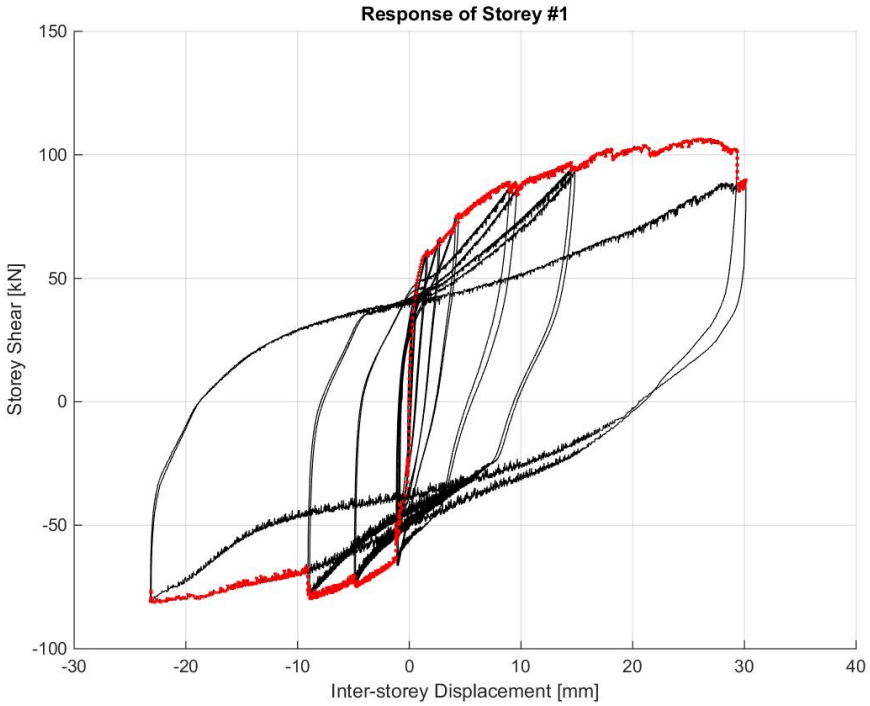

Figure 224. First storey shear vs. inter-storey displacement – retrofitted specimen, backbone and cyclic curves.

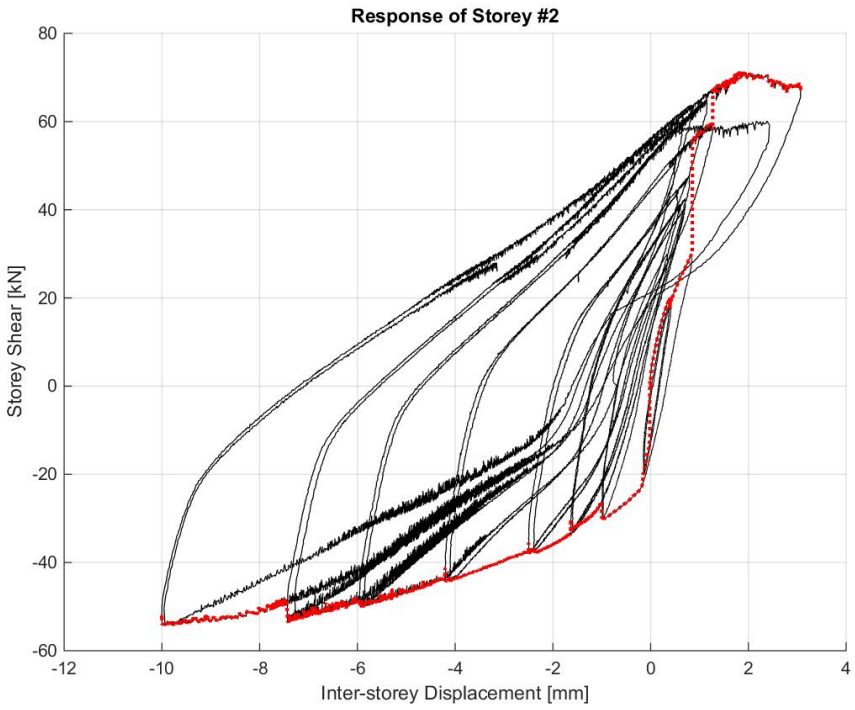

Figure 225. Second storey shear vs. inter-storey displacement – retrofitted specimen, backbone and cyclic curves.

As can be gathered from the results shown in Figure 220 and Figure 221, the "not-fully-effectively-retrofitted" damaged structure was able to undergo cyclic testing up to a roof top displacement level equal to 33.7 mm, which was double the displacement that had instead taken the original specimen EUC-BUILD4 to incipient collapse. Thus, although not all bolts that tie the steel angles to the walls could be screwed-in, the results of this final test run would make one think that a sturdier wall-slab connection was ensured by those steel clips. This in turn implies that sliding can be prevented from occurring and that a much more symmetric response of the specimen could be readily obtained, thus ensuing larger energy dissipation and equally higher seismic force resistance. In other words, one of the main conclusion that can be drawn by the set of response curves of the "retrofitted" specimen, in comparison with those obtained for the original structure in its as-built configuration, is that the lack of adequate connection between the stability walls and the slabs/transverse walls was the principle cause for the deficient response of the previously tested EUC-BUILD4 specimen.

Despite the improved behaviour, it is interesting to note that the response of the building mock-up is still not perfectly-symmetric in pulling and pushing directions. Indeed, the EUC-BUILD4 retrofitted specimen was able to sustain a maximum base shear of approximately 110 kN and 80 kN in the case of pulling and pushing, respectively. The peak base shear in pulling direction was experienced for a top displacement of about 27 mm, whilst the maximum lateral loadcarrying capacity in the opposite direction of testing (i.e. pushing – negative displacements/forces) was undergone for a displacement roughly equal to 16 mm. As shown in Figure 220, it is also noteworthy that the retrofitted specimen underwent no strength degradation in both pulling and pushing directions for top displacements of 16.8 mm (i.e. the ones that caused incipient collapse of the as-built EUC-BUILD4 specimen). Up to this level of displacement, also the in-cycle strength degradation was almost negligible. By contrast, in-cycle and hence between-cycle strength degradation started being

observed during the last cycle for a top displacement of up to 33.7 mm. In fact, for this stage of testing, very extensive damage could be seen spreading throughout the specimen, including a full-depth/full-width/mid-height horizontal crack in the lateral walls connected to the ground-floor stability wall.

As done before for the as-built specimen, the response curves (see Figure 220 and Figure 221) were not filtered, which in turn permits one to implicitly state that frictional transfer mechanisms evident from the noisy branch of the experimental response collected in Figure 132 and Figure 133 are now much less relevant. Such an observation, although preliminary, can be referred to as a confirmation of the fact that floor scratching on the precast wall-elements underneath, due to issues of sliding and friction, is relatively modest. Furthermore, it can be noticed, from Figure 222 or Figure 224, that the response of the first storey resembles very much like that of the specimen (see Figure 220 or Figure 221) in terms of shape and character. As presented in Figure 223 or Figure 225, the accumulation of residual displacements because of sliding of the precast hollow core slabs on the underneath felts is very moderate. The storey shear versus inter-storey displacement response of the second storey also confirms an asymmetric behaviour, but it is evident that neither in-cycle nor between-cycle strength degradation occurred there. This is in very close agreement with the fact that no other signs of "eye-catching" damage have been detected during the surveys undertaken at the end of each step of this further test sequence (see Sections 6.3.5 to 6.3.10).

Furthermore, as done for the as-built specimen and reported in Section 6.2.1, equivalent viscous damping ratios were computed by considering both the overall response of the structure, as well as that of each single storey separately. Computations were performed for each displacement amplitude and for each cycle at a constant displacement level as well; the aim is thus twofold, in the sense that track can be taken of the trends observed with respect to the lateral displacement and the number of cycles. The equivalent viscous damping-displacement relationships for the entire building in the retrofitted configuration are shown in Figure 226, whilst those obtained from the cyclic curves of the first and second storey can be observed in Figure 227 and Figure 228, respectively.

Figure 226 presents high levels of energy dissipation since the early stages of inelastic cyclic testing and a similar consideration can be drawn by the equivalent viscous damping ratios corresponding to the first and second storey. A comparison between Figure 227 and Figure 228 clarifies that the main sources of energy dissipation are again associated with the response of the first storey; regardless of the fact that reference is made to either global or local response curves, equivalent viscous damping ratio-displacement relationships are approximately characterised by two linear piecewise curves. As far as Figure 226 is concerned, values ranging between 17% and 25% can be computed for roof top displacements of up to 5 mm. Higher equivalent viscous damping ratios (i.e. 27-28%) were reached for higher displacement levels. Whilst the estimates obtained from the response curves of the second storey are smaller than those presented above, an opposite trend can be derived by considering those collected in Figure 228 and pertaining to the first storey of the building prototype.

As also observed for the as-built configuration, the last two steps of the testing sequence were the ones presenting the most significant degradation with the number of cycles (see e.g. Figure 226 and Figure 227). This is in close agreement with the fact that Test run #8R corresponds to the step of major damage observed in the specimen, as will be discussed later on in more details (see Section 6.3.10). On the other hand, it appears that no specific trends can be obtained, in terms of

degradation, from the equivalent viscous damping ratios computed by using the response of the second storey, which indeed remained almost undamaged during this second test run.

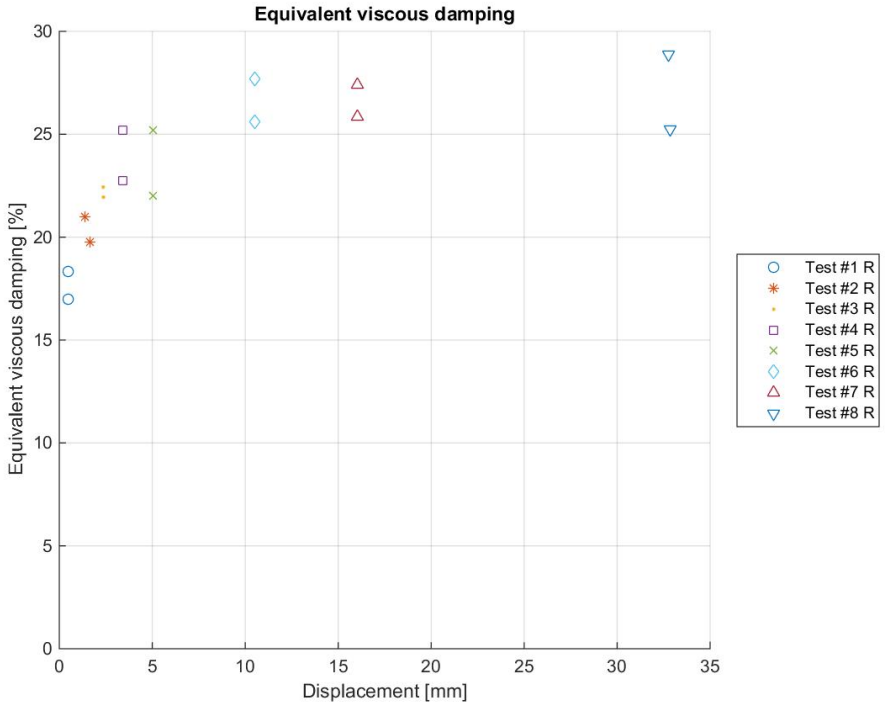

Figure 226. Equivalent viscous damping-displacement relationships – computed from overall response (retrofitted specimen).

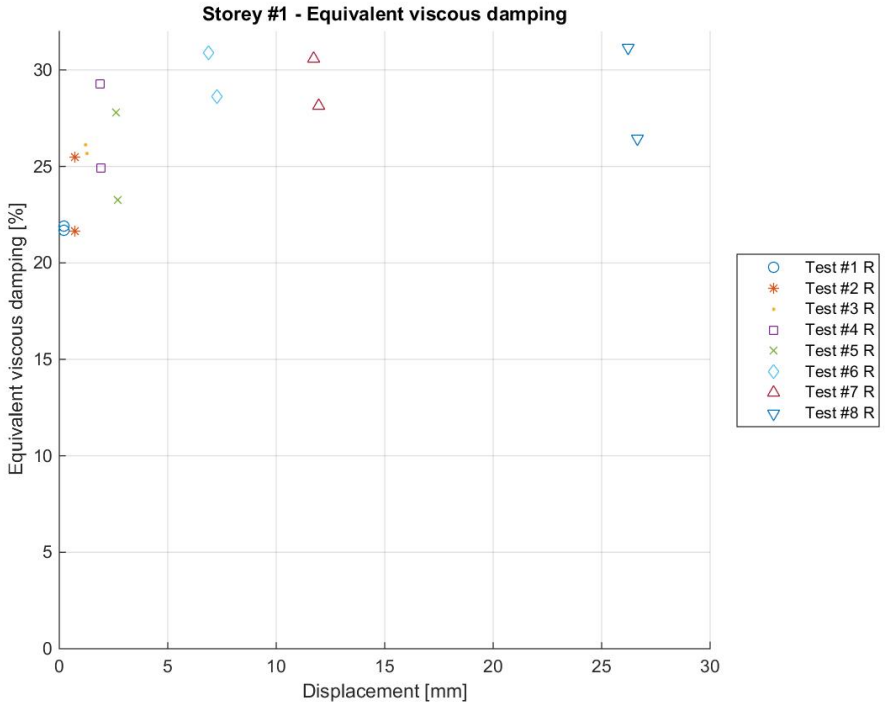

Figure 227. Equivalent viscous damping-displacement relationships – computed from first storey response (retrofitted specimen).

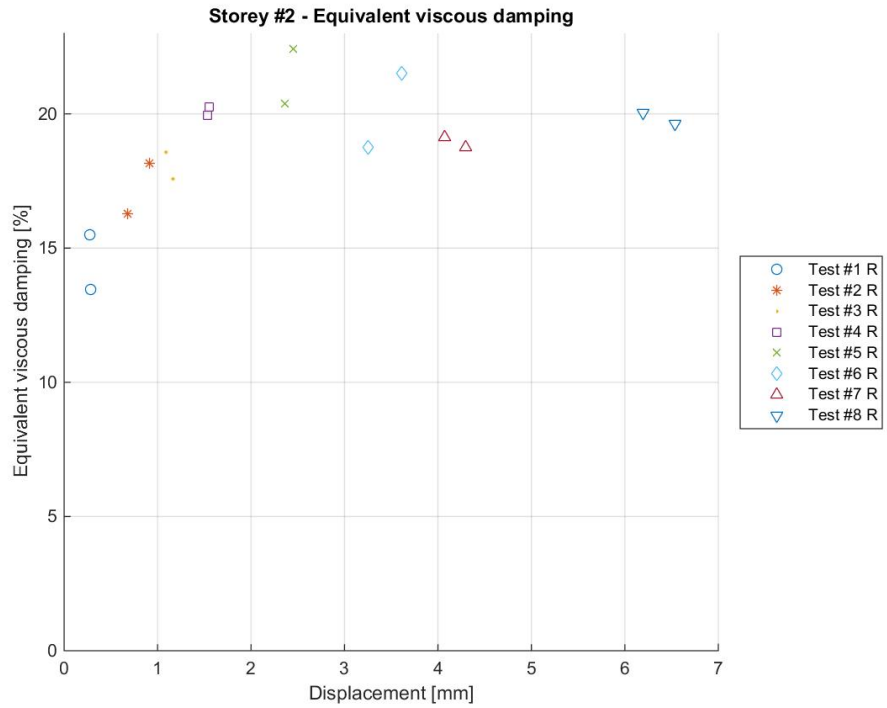

Figure 228. Equivalent viscous damping-displacement relationships – computed from second storey response (retrofitted specimen).

Response pseudo-time histories recorded during the different stages of testing are reported in Figure 229 to Figure 236. As done for EUC-BUILD4 specimen in the as-built configuration, all these plots show the horizontal forces applied to the two floors and the corresponding horizontal displacements measured in each one of them. Hysteretic curves were also presented for the first and second storey in terms of shear versus inter-storey displacement and applied force versus imposed displacement. It is evident from the series of response curves collected below (i.e. Figure 229 to Figure 236) that the response of the "not-fully-effectively-retrofitted" damaged specimen was considerably improved in comparison with that of the original structure, as a more symmetric behaviour was obtained for each drift amplitude. Sliding was confirmed to be relatively modest, as in turn was also the accumulation of residual displacements at the end of each stage of the testing sequence.

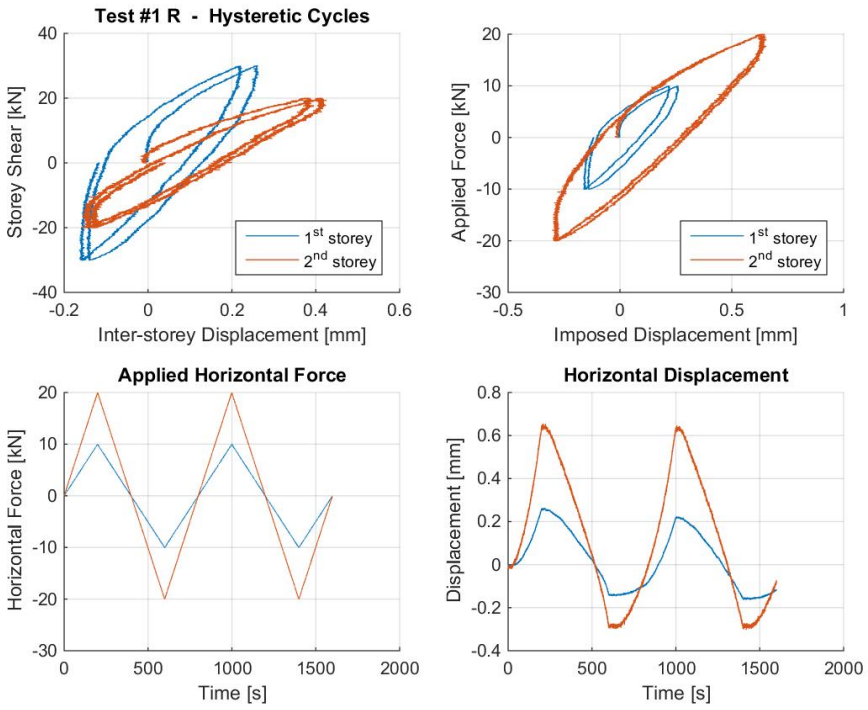

Figure 229. Response time histories: force, displacement and storey shear – Test run #1R (retrofitted specimen).

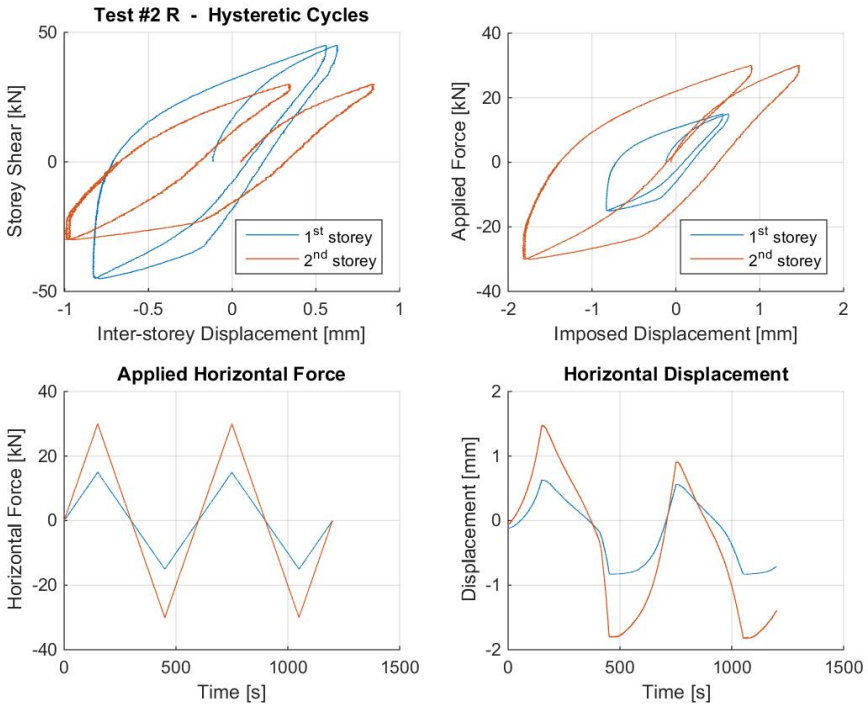

Figure 230. Response time histories: force, displacement and storey shear – Test run #2R (retrofitted specimen).

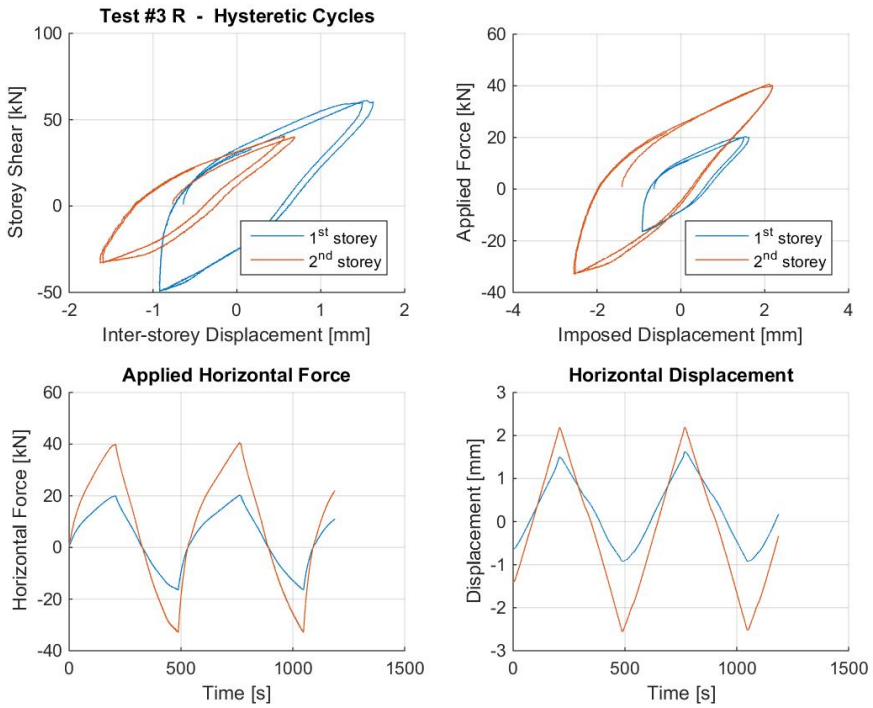

Figure 231. Response time histories: force, displacement and storey shear – Test run #3R (retrofitted specimen).

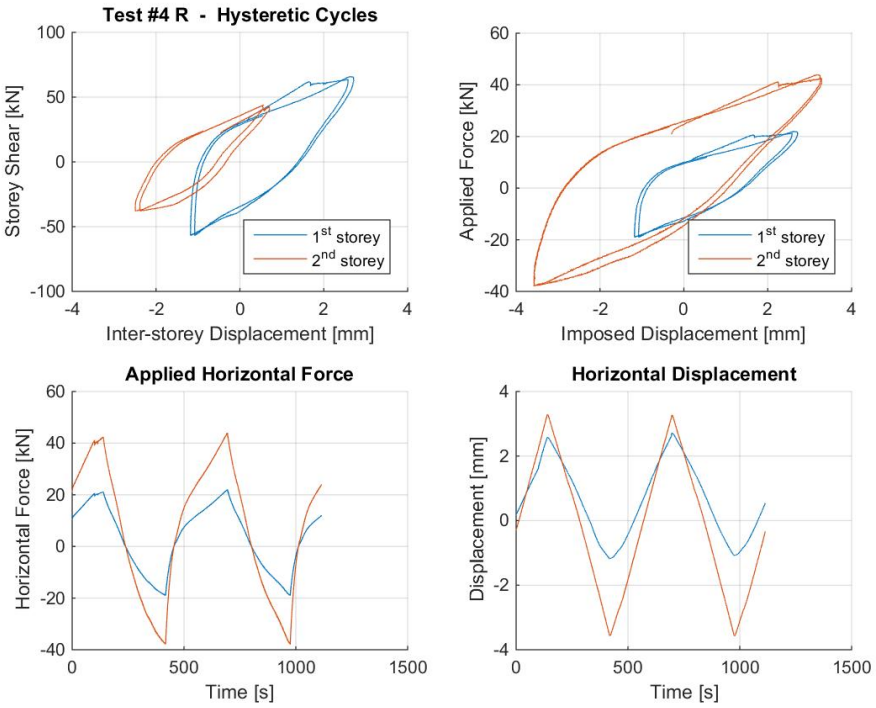

Figure 232. Response time histories: force, displacement and storey shear – Test run #4R (retrofitted specimen).

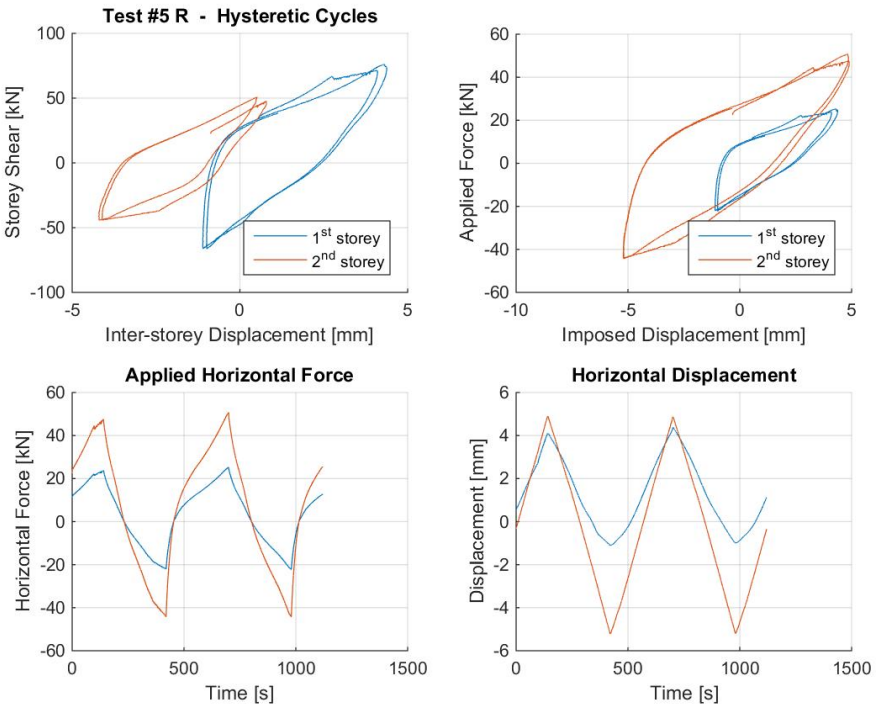

Figure 233. Response time histories: force, displacement and storey shear – Test run #5R (retrofitted specimen).

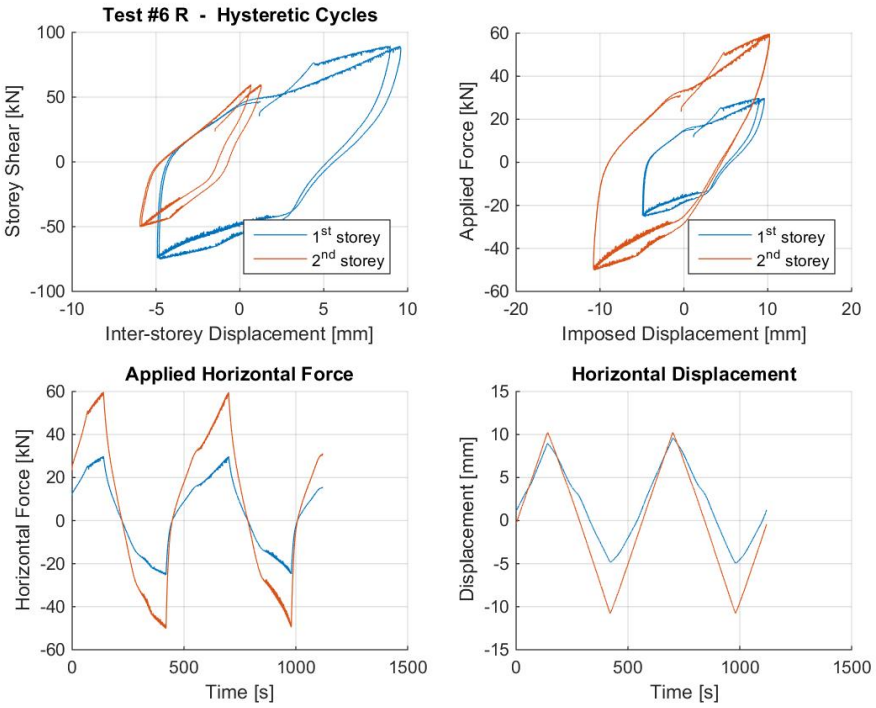

Figure 234. Response time histories: force, displacement and storey shear – Test run #6R (retrofitted specimen).

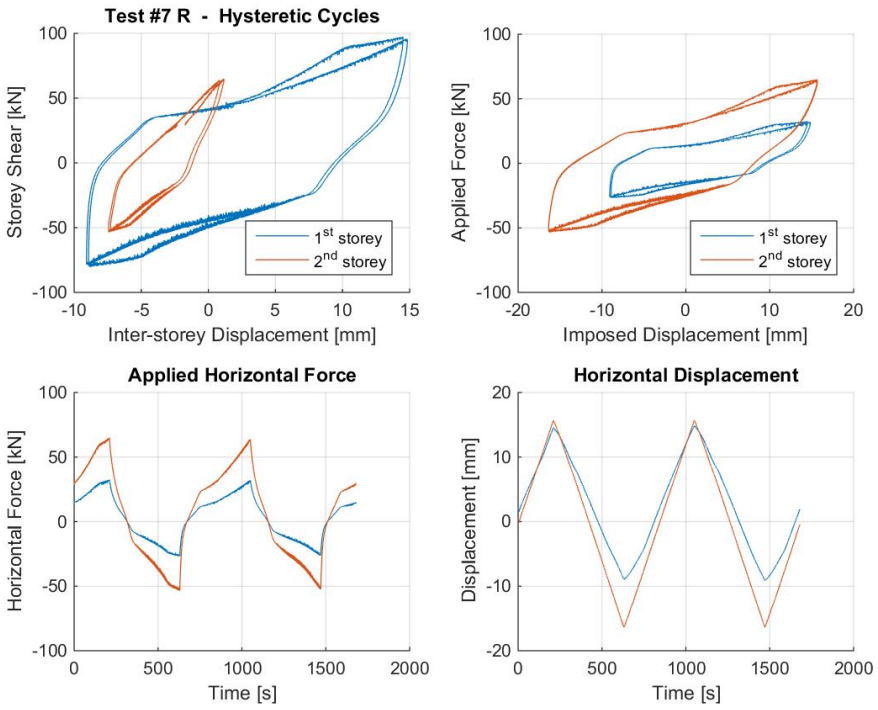

Figure 235. Response time histories: force, displacement and storey shear – Test run #7R (retrofitted specimen).

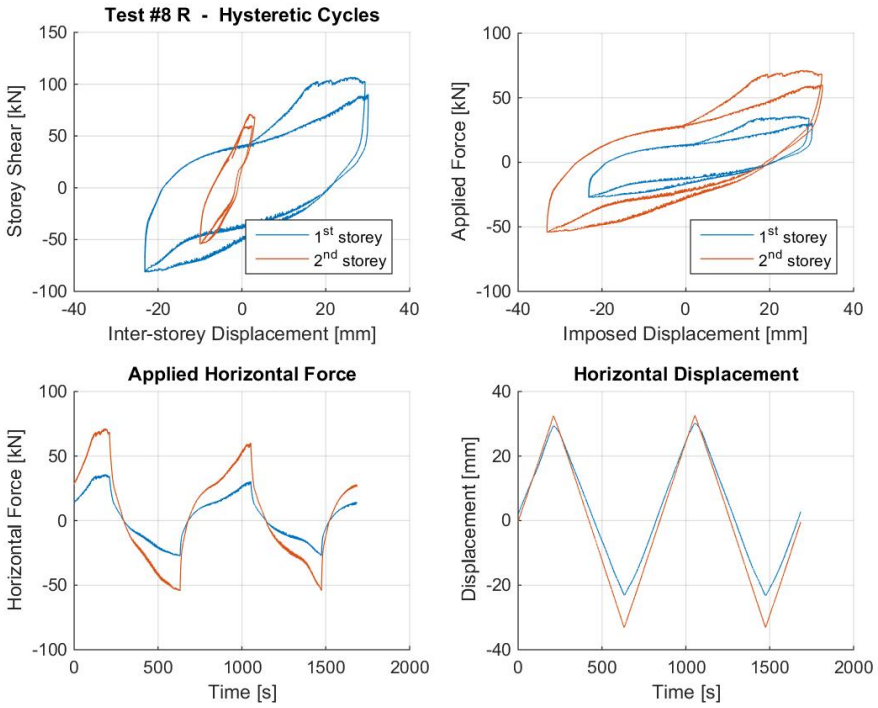

Figure 236. Response time histories: force, displacement and storey shear – Test run #8R (retrofitted specimen).

It can also be concluded that, last cycle apart (Figure 236), the response of EUC-BUILD4 retrofitted specimen was characterised by almost negligible in-cycle and between-cycle strength degradation,

which fits well with the damage patterns presented later on (see sub-Sections 6.3.5 to 6.3.10). Only minor concrete cracking was indeed observed for these steps of the testing sequence, whilst a full-depth/full-width/mid-height horizontal crack developed, during the last cycle, in the transversal walls connected to the ground-floor stability wall.

6.3.2 Qualitative deformed shapes

To shed some light on the reasons why the observed response was of the hardening type, sketches of the deformed shape of the retrofitted specimen during each step of testing have been produced using the readings from a number of instruments (after the application of required initial offsets). For each test, the maxima and minima of the acquired data allowed one to derive sketches of the two extreme positions of the specimen, which are systematically presented in Figure 237 to Figure 244.

The transducers fixed to the external reference permits positioning the two floor slabs. Out-of-plane transducers for the lateral walls and instruments that measure the sliding of stability walls indicate their position with respect to the floor slab. The series of deformed shapes do not include rocking of the stability walls that was always very limited. It is worth noting that displacements are magnified, which implies that sketches represent the observed mechanisms but displacement amplitudes cannot be derived from these plots (e.g. the South edge of the upper slab did not reach the South transversal walls). Furthermore, the interpenetration taking place between the stability wall and the lateral walls of the specimen indicates that those elements were moving one toward each other, partially closing the vertical crack present at the beginning of the second test run.

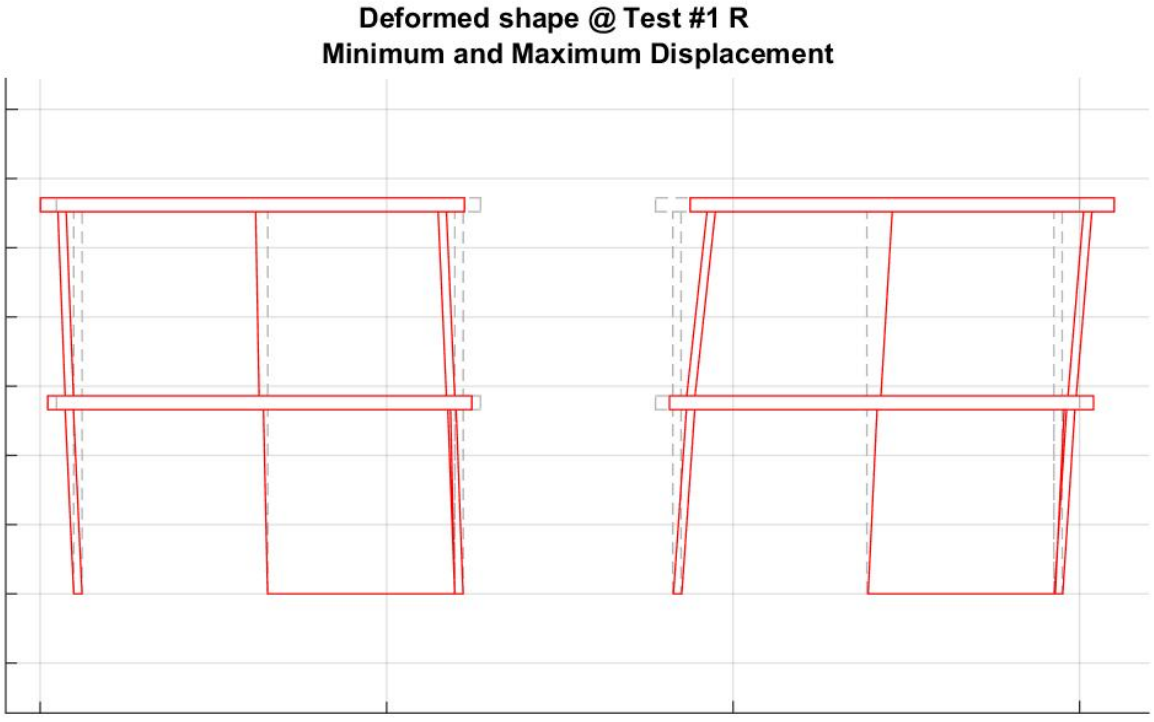

Figure 237. Deformed shape of EUC-BUILD4 retrofitted specimen (max and min) – Test run #1R.

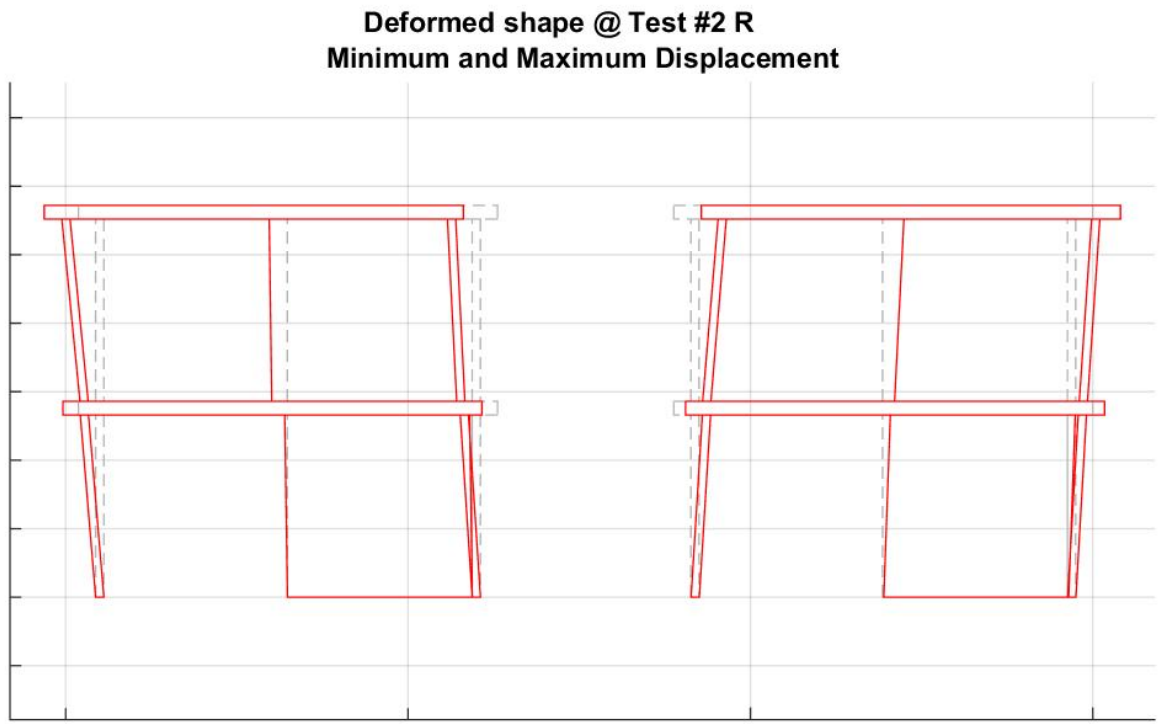

Figure 238. Deformed shape of EUC-BUILD4 retrofitted specimen (max and min) – Test run #2R.

Figure 239. Deformed shape of EUC-BUILD4 retrofitted specimen (max and min) – Test run #3R.

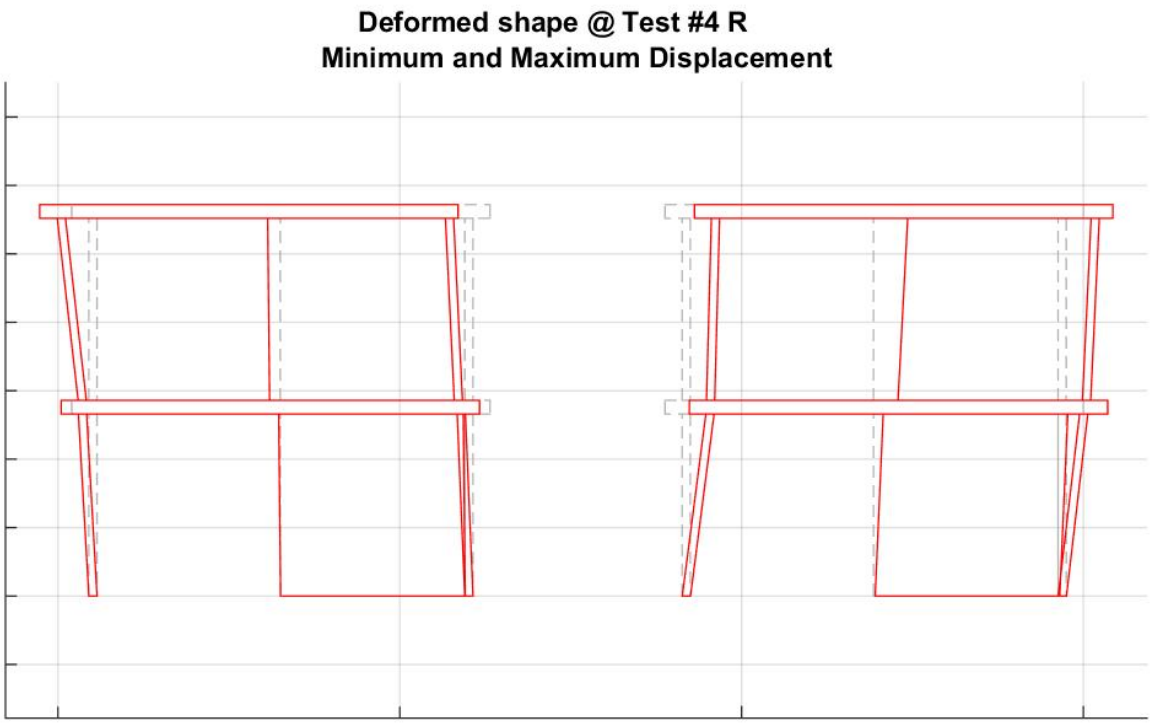

Figure 240. Deformed shape of EUC-BUILD4 retrofitted specimen (max and min) – Test run #4R.

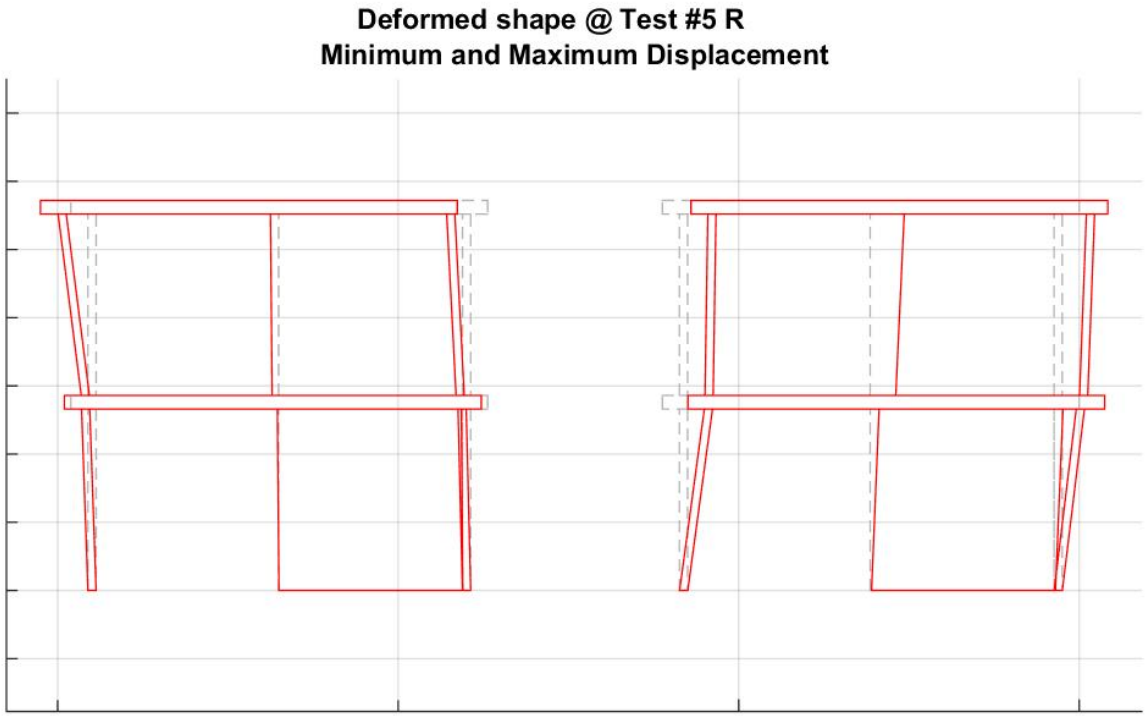

Figure 241. Deformed shape of EUC-BUILD4 retrofitted specimen (max and min) – Test run #5R.

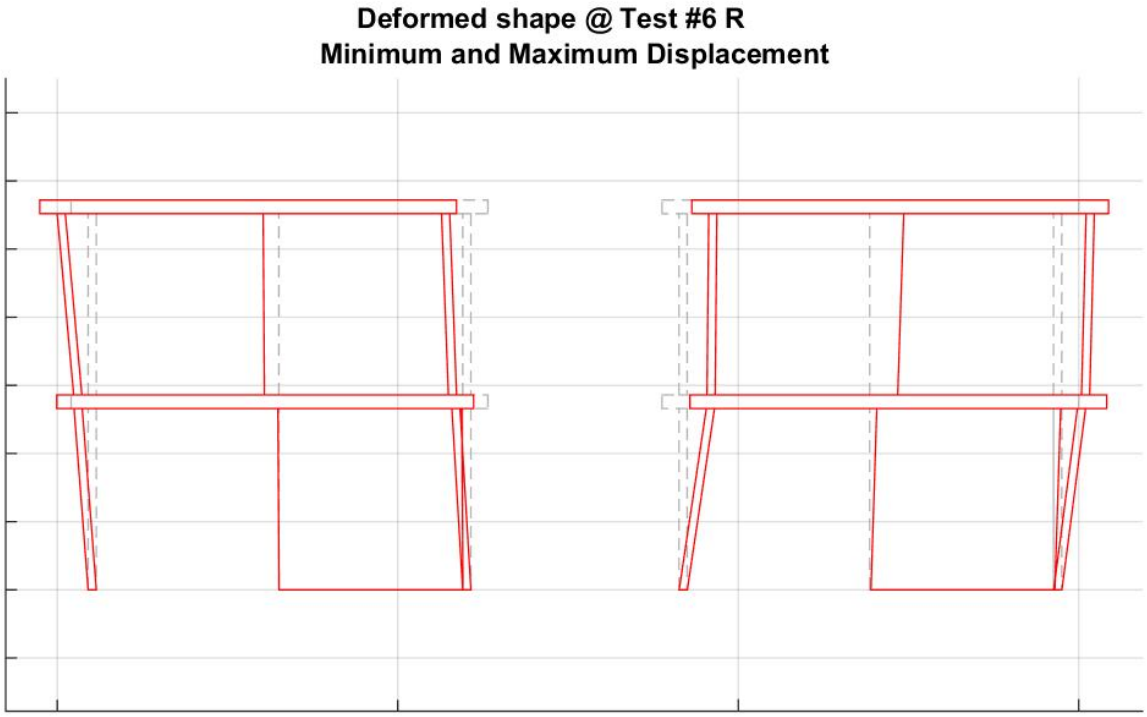

Figure 242. Deformed shape of EUC-BUILD4 retrofitted specimen (max and min) – Test run #6R.

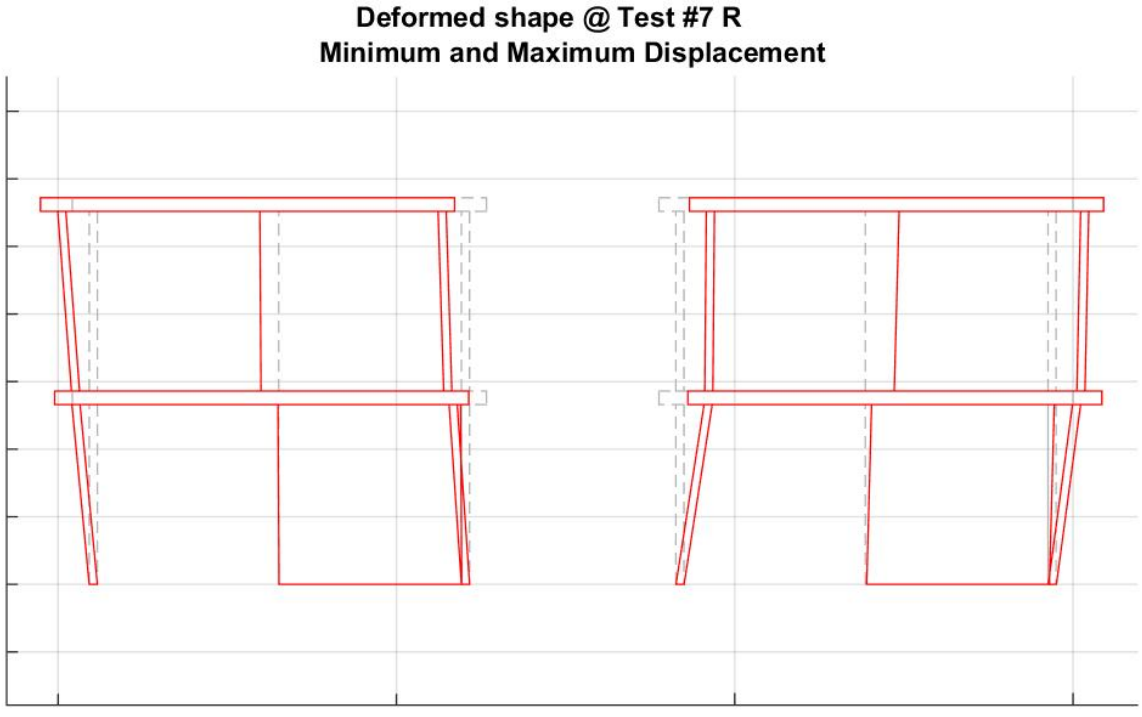

Figure 243. Deformed shape of EUC-BUILD4 retrofitted specimen (max and min) – Test run #7R.

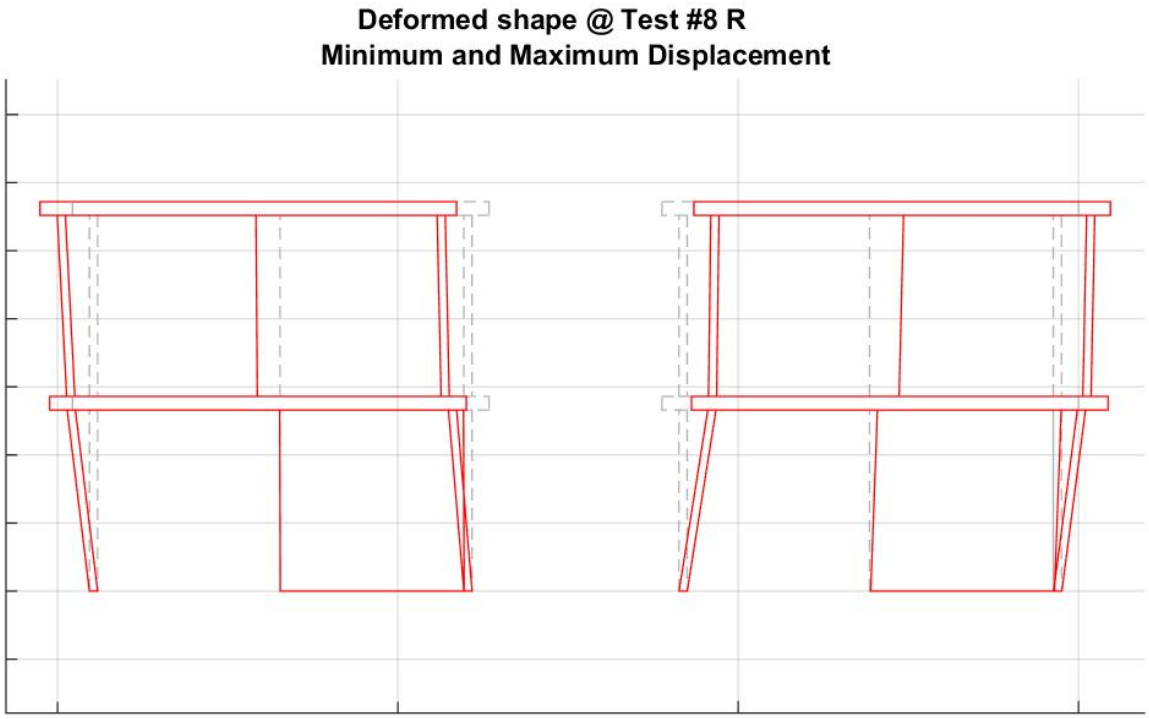

Figure 244. Deformed shape of EUC-BUILD4 retrofitted specimen (max and min) – Test run #8R.

Although the series of graphs collected above can only be considered to as "qualitative" sketches of the deformed shapes because of the reasons listed before, it is believed that they are still informative and that they reaffirm the mechanisms commented in the previous sub-Section, for what concerns the reduction of sliding and hence residual displacements. The comparison between deformed shapes at positive and negative displacement peaks also reveals improvements with regard to the symmetry of the response. By taking a look at Figure 237 to Figure 244, it becomes clear that the first-storey and second-storey transversal walls opposite to the stability walls (i.e. North side) were rocking out-of-plane toward the same direction, in-phase, during the pulling and pushing phases of each step of this second test run.

6.3.3 Displacement profiles

This paragraph is chiefly concerned with the analysis and discussion of the displacement profiles of both stability and lateral walls, which are systematically shown in Figure 245 to Figure 252. In accordance with the approach adopted to present the results of the counterpart specimen (see Paragraph 6.2.3), the displacement profiles of the North and South transversal walls, together with the ones of the stability wall, are shown in the following. The data recorded at both positive and negative displacement peaks of each stage of this testing sequence are plotted with the initial position of each element at the beginning of that stage.

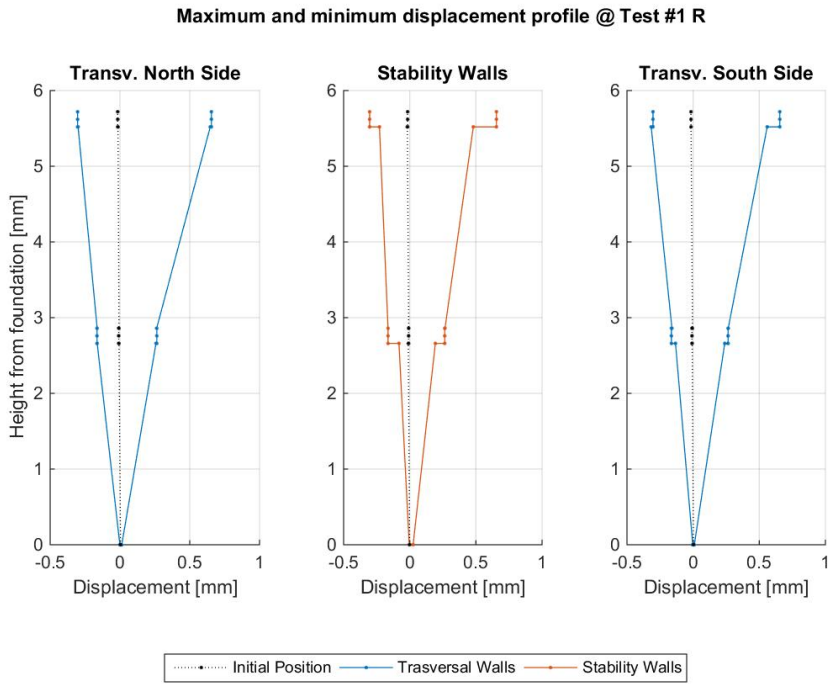

Figure 245. EUC-BUILD4 retrofitted specimen: displacement profiles of structural walls – Test run #1R.

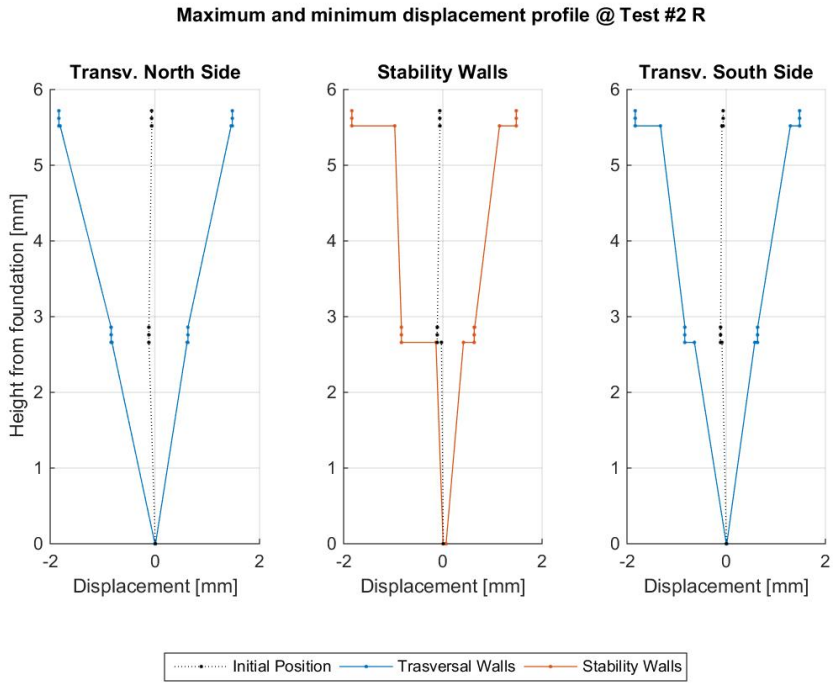

Figure 246. EUC-BUILD4 retrofitted specimen: displacement profiles of structural walls – Test run #2R.

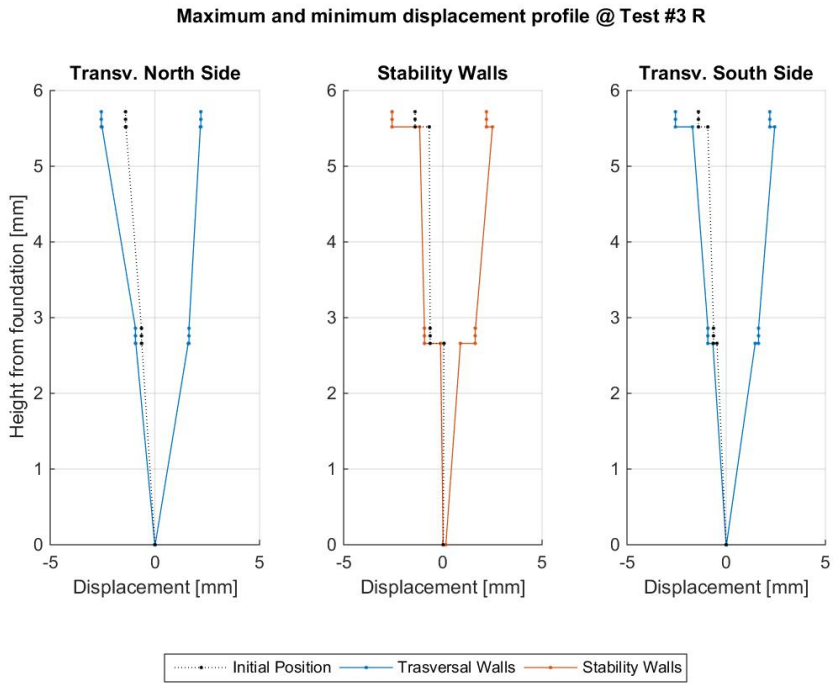

Figure 247. EUC-BUILD4 retrofitted specimen: displacement profiles of structural walls – Test run #3R.

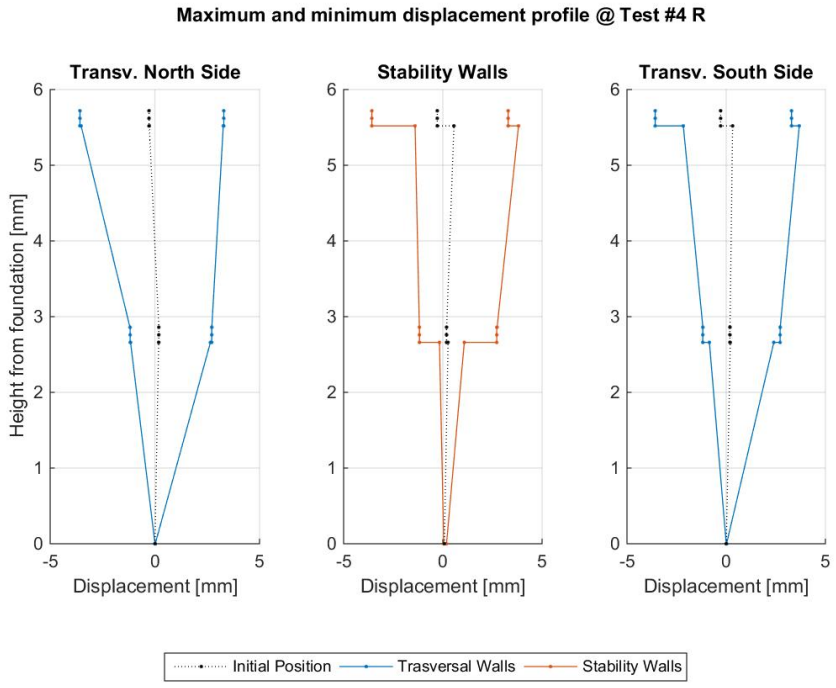

Figure 248. EUC-BUILD4 retrofitted specimen: displacement profiles of structural walls – Test run #4R.

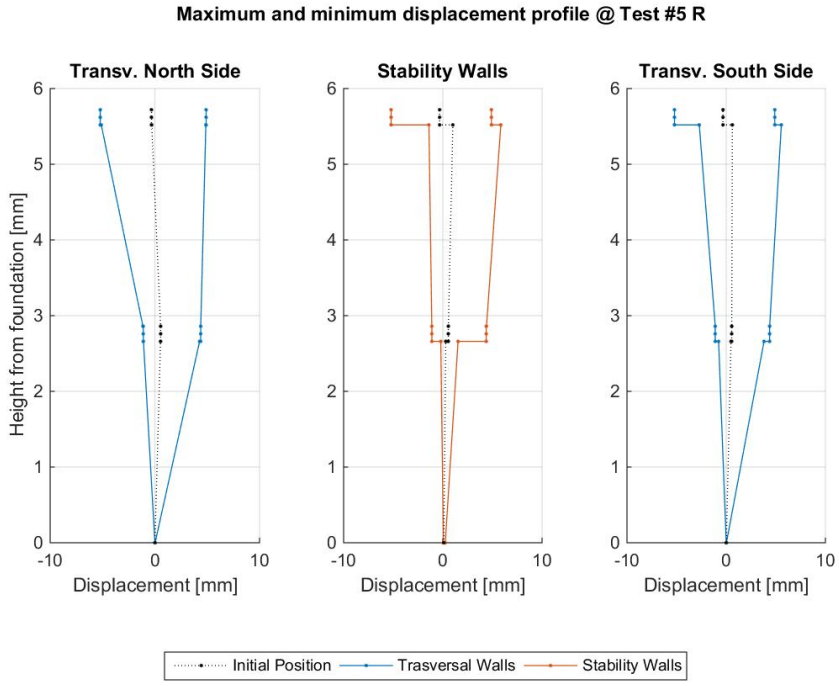

Figure 249. EUC-BUILD4 retrofitted specimen: displacement profiles of structural walls – Test run #5R.

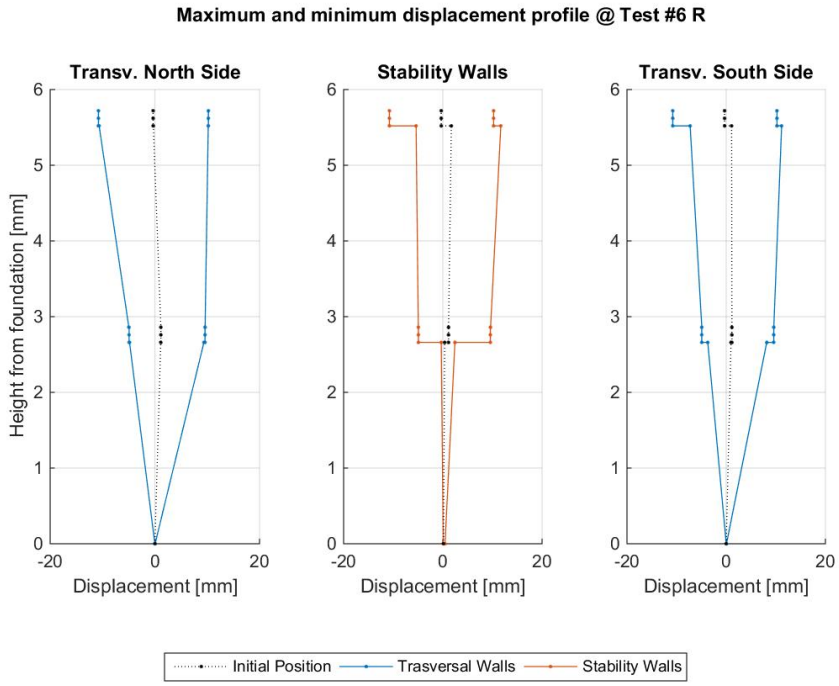

Figure 250. EUC-BUILD4 retrofitted specimen: displacement profiles of structural walls – Test run #6R.

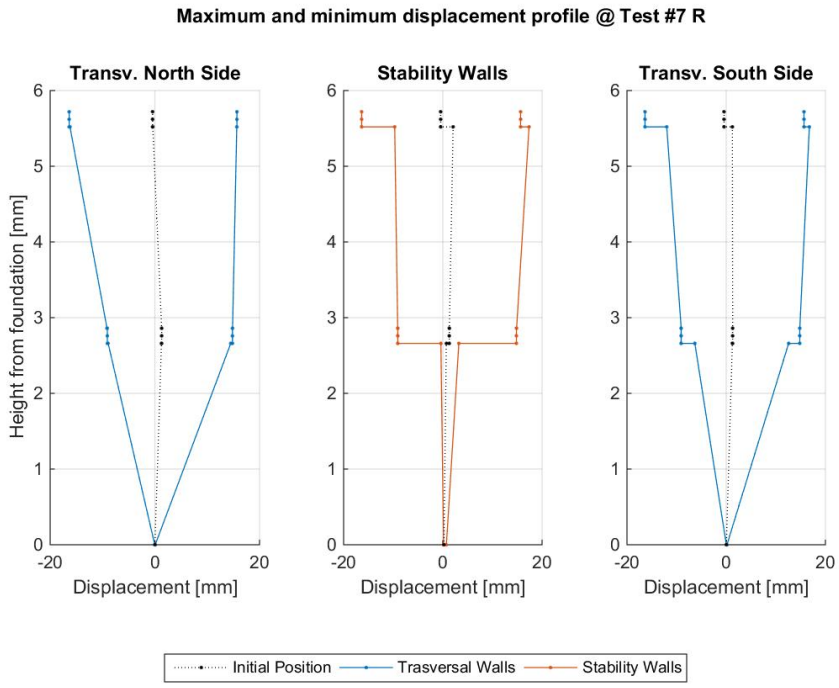

Figure 251. EUC-BUILD4 retrofitted specimen: displacement profiles of structural walls – Test run #7R.

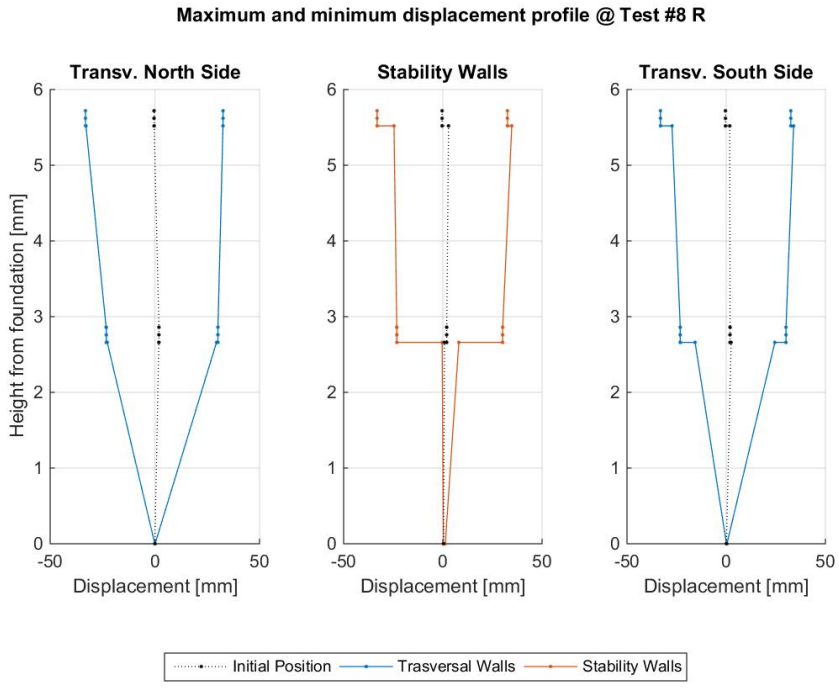

Figure 252. EUC-BUILD4 retrofitted specimen: displacement profiles of structural walls – Test run #8R.

Although some sort of sliding of precast slabs on the underneath walls is still present, particularly in the stability wall of both the first and second floors, such a mechanism was nonetheless found to be

relatively moderate. It is worth noticing that the profile of the three wall panels under consideration was plotted by assuming the same displacement limits, which means that a comparison can be thus derived between the three structural elements. As previously commented in terms of response curves and resisting mechanisms, it can be inferred that the behaviour of each structural element was fairly symmetric in pulling and pushing direction. This latter consideration refers to both the displacement profile of the wall-elements themselves as well as the sliding of floor slabs on them. It can be seen, from Figure 245 to Figure 252, that, during each stage of testing, the first-storey and second-storey transversal walls of the retrofitted structure were rocking out-of-plane toward the same direction in the case of both pulling and pushing. The same consideration can also be driven as far as the profile of the North and South lateral walls are compared together. The displacement profiles shown above confirm also that even if some moderate sliding was recorded, the accumulation of residuals was very limited or even almost negligible, depending on the wall-element under consideration.

6.3.4 Local response of key structural portions

The dataset pertaining to the behaviour of the first-storey and second-storey stability walls of EUC-BUILD4 retrofitted specimen was processed so as to examine and quantify base rocking and sliding of these crucial members. Results are presented in Figure 253 to Figure 260. As done for the case of the as-built configuration, the two mechanisms were evaluated by using the instruments of the West and East sides separately. Furthermore, the average of those measurements was also computed and presented.

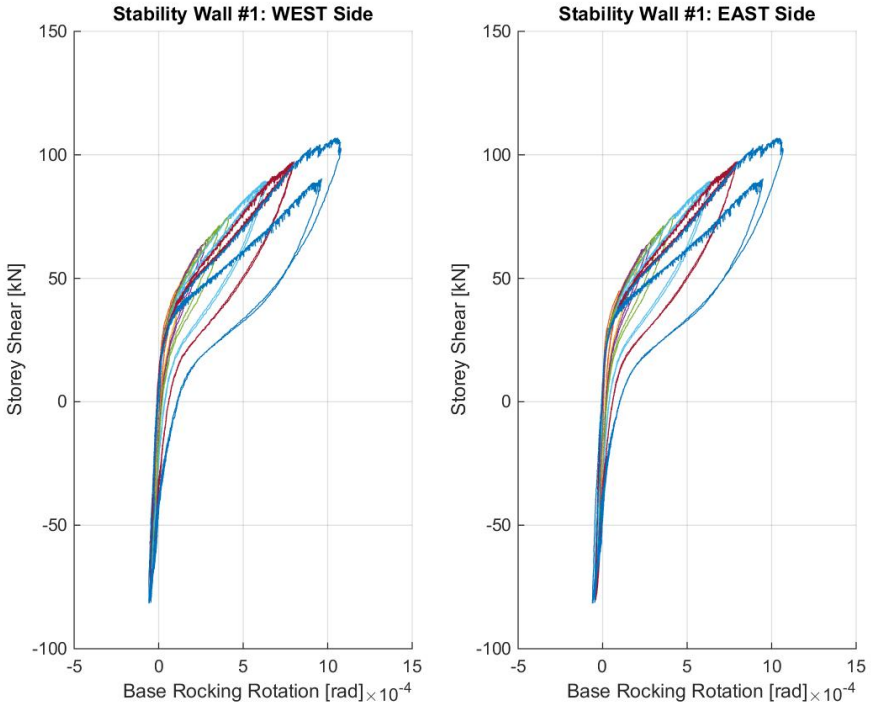

Figure 253. First-storey stability wall: base rotation due to rocking (retrofitted) – West and East sides.

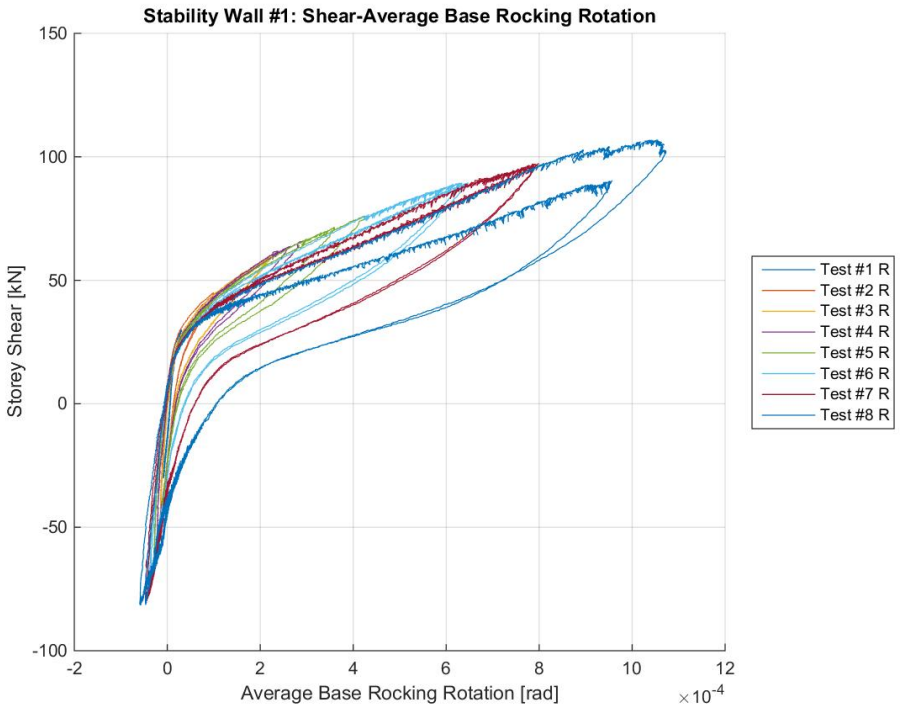

Figure 254. First-storey stability wall: base rotation due to rocking (retrofitted) – Average.

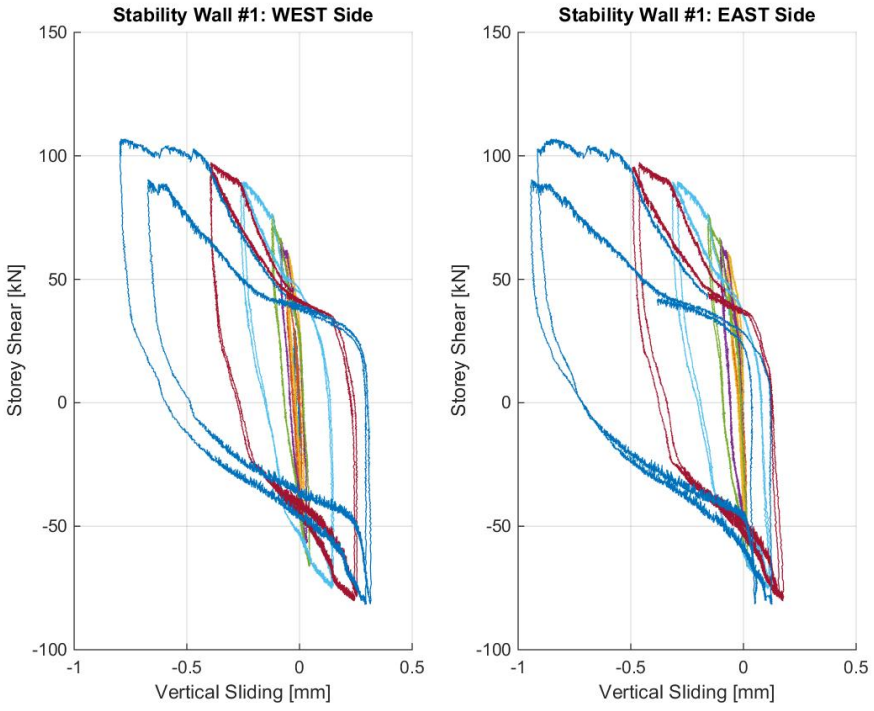

Figure 255. Vertical sliding of first-storey stability wall (retrofitted) – West and East sides.

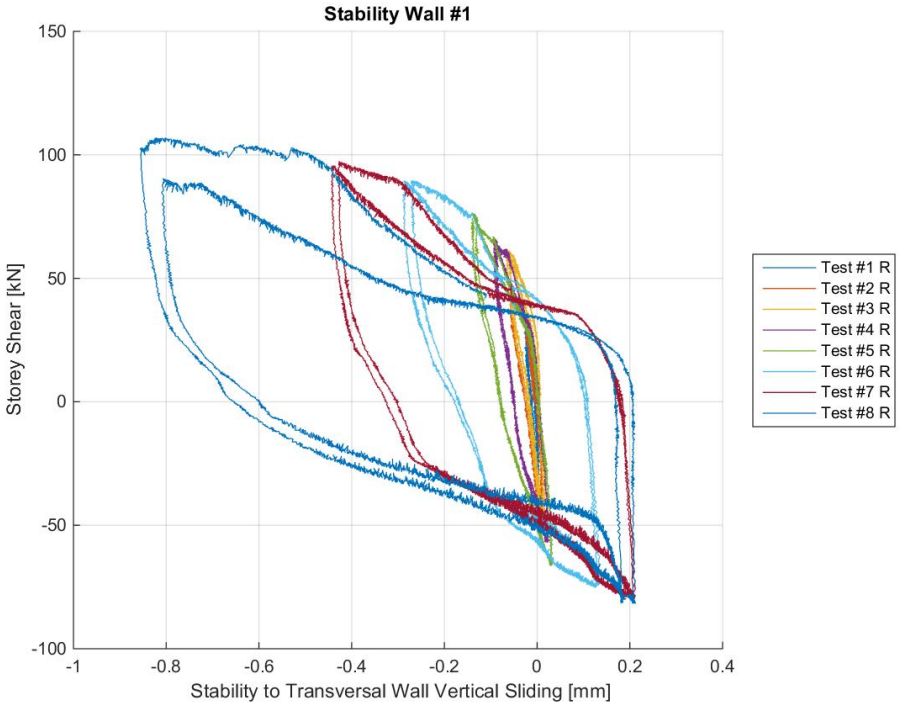

Figure 256. Vertical sliding of first-storey stability wall (retrofitted) – Average.

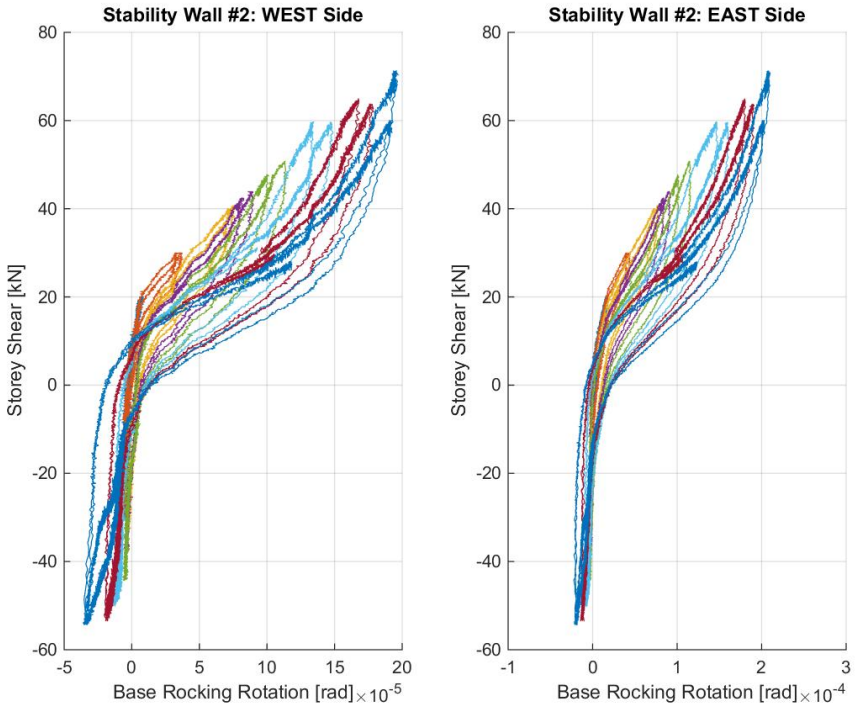

Figure 257. Second-storey stability wall: base rotation due to rocking (retrofitted) – West and East sides.

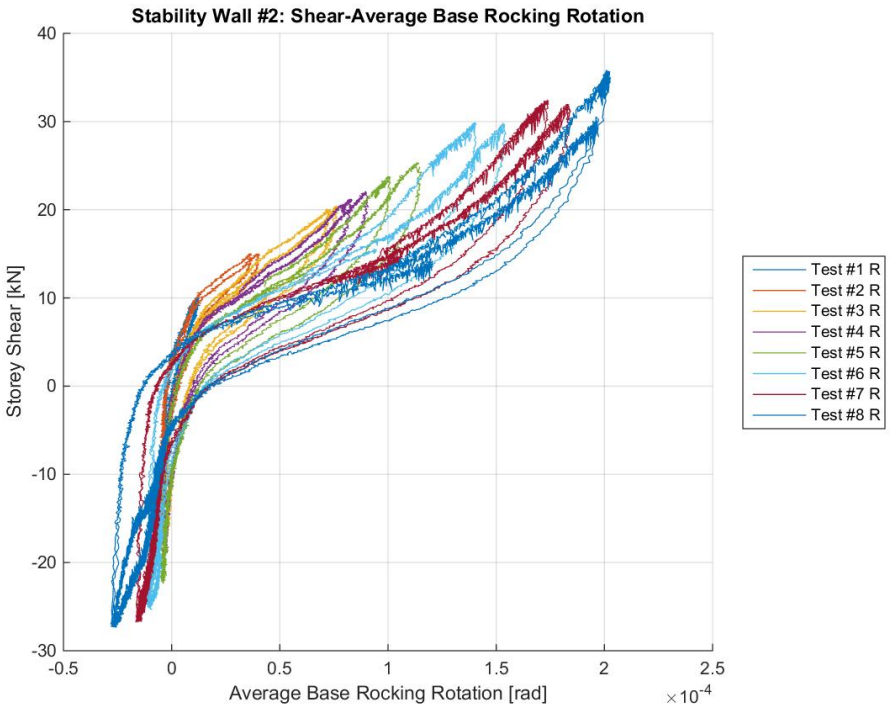

Figure 258. Second-storey stability wall: base rotation due to rocking (retrofitted) – Average.

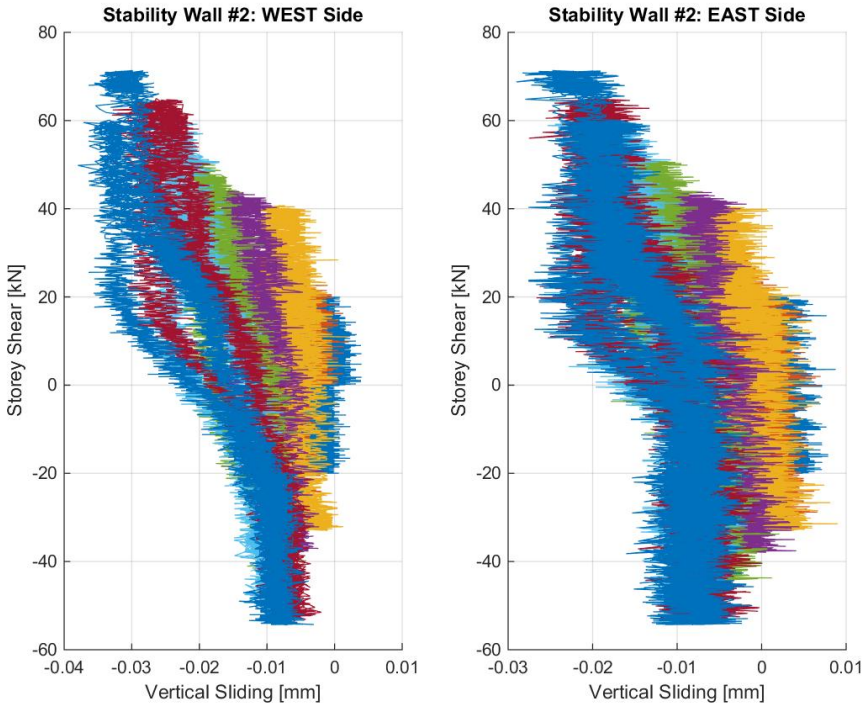

Figure 259. Vertical sliding of second-storey stability wall (retrofitted) – West and East sides.

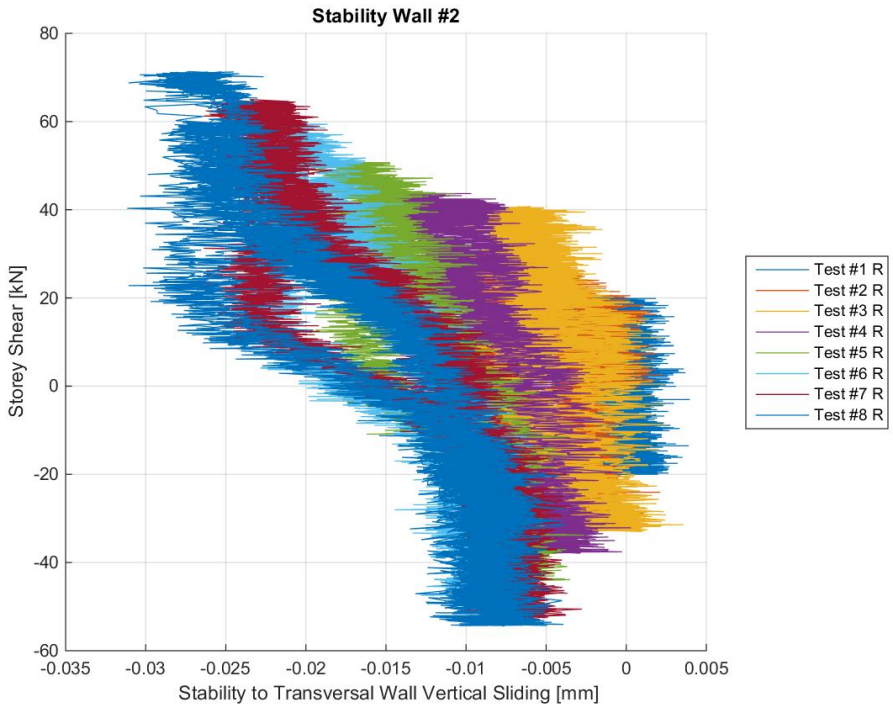

Figure 260. Vertical sliding of second-storey stability wall (retrofitted) – Average.

As shown above, rocking at the base of the first-storey and second-storey walls was not particularly pronounced, and the same applies to the vertical sliding of the two stability walls on the counterpart lateral walls (i.e. North side). As can be observed in Figure 253 and Figure 257, peak base rotations approximately equal to $10 \cdot 10^{-4}$ and $2 \cdot 10^{-4}$ rad were obtained for the ground-floor and second-storey stability walls, respectively. Similar trends and maxima were determined on average, as reported in Figure 254 and Figure 258. Thus, base rocking was again more evident in the ground-floor stability wall, and this mechanism was confirmed to be asymmetric in pulling and pushing directions. It can be nevertheless noticed that the storey shear-base rocking rotation curves of the retrofitted specimen are slightly smoother than those obtained for the as-built prototype. Hysteretic loops were also more regular and such an outcome confirms even further previous considerations regarding the improved response that can be obtained by guaranteeing through clipping angles a sturdier wall-slab and wall-wall connection. Considering that these steel angles are not as effective as they would have been if they had been properly designed as a structural upgrading measure for an intact/undamaged structure, it turns out that a minimal retrofitting intervention is nonetheless good enough to prevent sliding from occurring and also to readily mobilise higher lateral load-carrying capacity in this type of structures by appropriately connecting their structural precast elements together.

As far as vertical sliding of the stability wall on the corresponding transversal walls is concerned, it can be gathered from Figure 255 and Figure 259 that this mechanism is negligibly small, especially for the case of the second-storey stability wall. This applies to response graphs obtained from West- and East-sided instruments as well as to plots determined from the average of these measurements, as shown in Figure 260. Despite the fact that sliding of the ground-floor stability wall is slightly more visible, it can be in any case concluded that wall-to-wall clipping angle connections were sturdier enough to inhibit an actual mechanism from taking place during the testing. This is even

more so if one considers that the second test run started with a permanent gap of about 25 mm between the stability and transverse walls at the top of the ground floor. Maxima lower than 1 mm (0.8 mm) were indeed obtained at the first storey of the retrofitted specimen.

6.3.5 Observed damage after Test run #3R – Imposed top displacement = 2.8 mm (max storey drift of 0.05% measured)

Careful surveys of damage patterns, such as those undertaken when testing EUC-BUILD4 specimen in the as-built configuration, were carried out at the end of every stage of this second test sequence. It can be stated that the application of the first two force-controlled cycles (i.e. Test run #1R and #2R) did not produce any type of additional "eye-catching" damage in the retrofitted building, and this is why no observations were reported.

A detailed photographic sequence showing the primary observations collected after the first displacement-controlled step of the testing sequence (Test run #3R) is reported from Figure 261 to Figure 264. Needless to say that cyclic tests for a top displacement of 2.8 mm caused only very limited damage to the retrofitted specimen. A few minor cracks were observed to develop in the transversal walls close to the bolted steel angle clips. In more details, Figure 261 and Figure 262 present a view of the cracks above and below the bottom steel flanged angle connecting the ground-floor stability and lateral walls. The North face is shown therein, whereas the crack pattern of the external/South face can be observed in Figure 263 and Figure 264.

Figure 261. Development of new cracks in the transversal walls (internal face) – Below the steel angle.

Figure 262. Development of new cracks in the transversal walls (internal face) – Above the steel angle.

Figure 263. Crack pattern of the transversal walls (external/South face) – Below the high-strength rods.

Figure 264. Crack pattern of the transversal walls (external/South face) – Opposite wall panel.

The latter very minor cracks developed close to the washers and bolts that were used to tie the steel angles to the walls. Even though they are very short and narrow in width, these cracks might still be indicative of the fact that, as normally foreseen by proper retrofitting design (prevented in this case by the presence of existing rebars internal to the walls), four bolts per plate (instead of only two per each) would be a preferred solution.

6.3.6 Observed damage after Test run #4R – Imposed top displacement = 3.9 mm (max storey drift of 0.08% measured)

At this step of testing, only a new crack opened up at the base of the South ground-floor lateral wall and those already present in the specimen did not develop any further. Figure 265 shows this minor crack, which took place in the West corner of the South-East-sided transversal wall. Needless to say that it had moderate length and width.

Apart from the aforementioned occurrence, cyclic testing for a top displacement of 3.9 mm did not cause any other sign of "eye-catching" damage in the retrofitted specimen. Both the other lateral walls and the stability walls underwent Test run #4R without presenting any propagation of previously-developed cracks. It is noteworthy that such an observation fits well with the response curves discussed in Section 6.3.1, since, at this stage, they do not reveal any sort of even minor in-cycle and between-cycle strength degradation. To render the above consideration even clearer, it is worth noticing that those curves are still hardened in character for this level of imposed displacement, as can be clearly seen from the hysteretic loops of the structure and its first floor (Figure 220 and Figure 222).

Figure 265. Formation of new minor cracks at the base of the transversal walls – South side.

6.3.7 Observed damage after Test run #5R – Imposed top displacement = 5.6 mm (max storey drift of 0.14% measured)

EUC-BUILD4 specimen, in its retrofitted configuration, suffered other signs of damage during Test run #5R, which consisted of a series of two displacement-controlled cycles for top displacements of up to 5.6 mm. Whilst previous crack patterns commented in paragraphs 6.3.5 and 6.3.6 did not propagate any further, some new minor cracks were observed during the surveys undertaken at the end of this stage of testing. Figure 266 and Figure 267 collect the primary observations of damage pertaining to Test run #5R.

In particular, Figure 266 depicts a crack running around the grout injected in correspondence to the bottom steel angle used to tie the ground-floor stability wall to the South-East transversal one. Even though this crack is slightly more pronounced than those developed during Test run #3R, its width is, in any case, very moderate. However, cracks like that shown in Figure 266 propagate as a result of the "not-fully-effective" retrofitting intervention implemented in this case. If this is the likeliest reason for cracking close to the steel clipping angles, they can be obviously and easily avoided in the case that a proper retrofitting strategy/scheme would have been designed as a structural upgrading measure for an intact/undamaged structure. It can be concluded that the grout was still resistant enough to permit the imposed forces to be carried past it.

Finally, Figure 267 shows the crack pattern at the base of the ground-floor stability wall. Horizontal cracks due to the in-plane rocking of this precast wall-element propagated along its entire depth. It is worthwhile to mention that cracks developed only on the West face of the stability wall.

Figure 266. Development of crack pattern in correspondence to the implemented retrofitting intervention.

Figure 267. Propagation of crack pattern at the base of the ground-floor stability wall – West side.

Despite this, the application of a larger roof drift amplitude caused the crack/damage pattern at the base of the ground-floor stability wall to evolve in a remarkable manner on the East and West faces at once. Further and more specific details are presented in the following section.

6.3.8 Observed damage after Test run #6R – Imposed top displacement = 11.2 mm (max storey drift of 0.33% measured)

As shown in Figure 268 to Figure 273, cyclic testing for top displacement levels of up to 11.2 mm was observed to cause more damage than what had been discussed for previous steps of testing in sub-Sections 6.3.5, 6.3.6 and 6.3.7. As can be gathered by the photographic sequence reported below, the retrofitted specimen underwent further signs of damage that mainly developed at the base of the ground-floor stability wall as well as in correspondence to the top and bottom steel angles that were implemented to tie the stability wall to the transversal walls.

Figure 268 and Figure 272 present clear views of the evolution of crack pattern in the East and West face of the stability, thus confirming that the horizontal cracks at the base of this structural element propagated even further toward the South lateral wall panels. In accordance with the observations in Figure 268 and Figure 272, the base of the wall is almost completely cracked at this stage of testing, given that damage took place on both sides of the wall along its entire depth. Furthermore, it can be noticed that a new crack opened up in the North/internal face of one of the transversal wall panels, as pointed out by Figure 269. A careful survey of the South/external face of this wall also confirms that cracks previously-formed close to the steel angles evolved even further, as evidenced in Figure 270 and Figure 271. Also noteworthy is that the application of top displacements equal to 11.2 mm caused cracking of the injection grout in correspondence to both the top and bottom steel angles.

Figure 268. Propagation of crack pattern at the base of the ground-floor stability wall – East side.

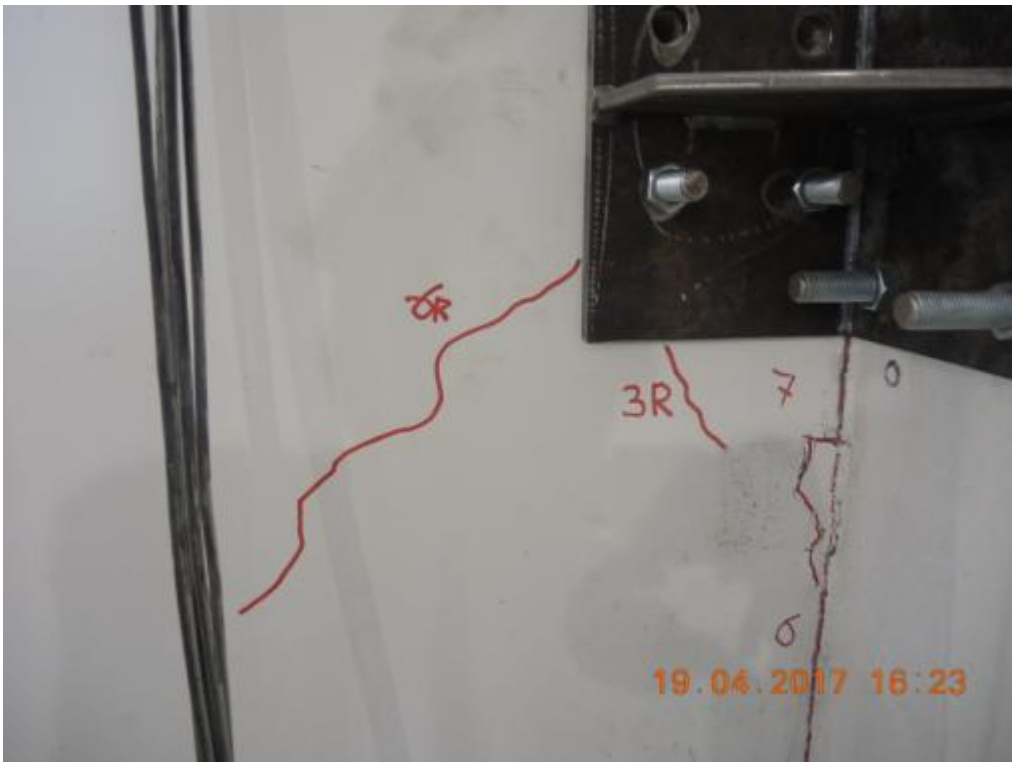

Figure 269. New crack in one of the transversal walls (internal face) – Below the steel angle.

Figure 270. Evolution of crack pattern in correspondence to the implemented retrofitting intervention – Bottom.

Figure 271. Evolution of crack pattern in correspondence to the implemented retrofitting intervention – Top.

Figure 272. Crack pattern at the base of the ground-floor stability wall – West side.

Figure 273. Crack pattern in correspondence to the bottom steel angle – Opposite/West side.

Finally, Figure 273 shows an incipient crack in correspondence to the bottom steel angle installed on the West face of the first-storey stability wall. Though this latter crack and abovementioned ones near the top and bottom clipping angles are still moderate in width, it becomes clear that the "retrofitted" specimen has experienced the first evident signs of damage in the walls (except for those previously detected at the base of the ground-floor stability wall).

6.3.9 Observed damage after Test run #7R – Imposed top displacement = 16.8 mm (max storey drift of 0.51% measured)

Test run #7R consisted of two displacement-controlled cycles for an imposed top displacement of 16.8 mm, which had caused the incipient collapse of EUC-BUILD4 specimen in its as-built configuration. By contrast, the "not-fully-effectively-retrofitted" prototype structure under investigation was able to withstand this drift amplitude, even if extensive damage was seen spreading throughout it. The photos shown in Figure 274 to Figure 285 present the main observations collected during the surveys undertaken at the end of this stage of testing.

As presented in Figure 274 and Figure 282, the South transversal walls of the first storey underwent further damage in correspondence to the steel angles. In particular, inclined cracks running from the bottom bolted clip angle to the base of the wall were found to develop in the North/internal face and also the opposite face revealed the propagation of a new crack near the installed clip angle. Finally, Figure 283 to Figure 285 present details of the damage pattern along the base of the other panel that compose the South transversal wall.

Figure 274. Propagation of inclined cracks running from the bottom steel angle to the lateral wall base.

Figure 275. Damage/crack pattern at the base of the ground-floor stability wall – South side.

Figure 276. Damage/crack pattern at the base of the ground-floor stability wall – Opposite (North) side.

Figure 277. Damage/crack pattern at the base of the ground-floor stability wall – North side, North face.

Figure 278. Minor friction-induced concrete chipping at the top of the first-storey stability wall.

Figure 279. Minor friction-induced concrete chipping at the top of the first-storey transversal wall.

Figure 280. Crack pattern at the base of the ground-floor stability wall – West side, edge.

Figure 281. Crack pattern at the base of the ground-floor stability wall – West side, opposite edge.

Figure 282. Formation of a new crack in one of the lateral walls close to steel angles and bolted rods.

Figure 283. Crack pattern at the base of one of the transversal wall – South side, first floor.

Figure 284. Crack pattern at the base of the other transversal wall – South side, first floor.

Figure 285. Detail of a minor crack close to one of the sliding restrainers – South side, lateral wall.

Nonetheless, it is noteworthy that, as expected, the ground-floor stability wall was clearly the most damaged element of the structure, at this stage of testing, as reported in Figure 275 to Figure 277

and also in Figure 280 and Figure 281; detailed views of the damage/crack pattern at the base of this element are collected there. Concrete spalling was pronounced, especially close to the corners of the panel wall, which were found to be completely cracked. Obviously, horizontal cracks were observed along the base on both sides of the first-storey stability wall. Figure 278 and Figure 279 also show a further secondary damage mechanism, which is minor concrete chipping at the top of the first-storey stability and transversal walls.

6.3.10 Observed damage after Test run #8R – Imposed top displacement = 33.7 mm (max storey drift of 1.04% measured)

The last step of the second test sequence, consisting of two displacement-controlled cycles for an imposed top displacement of 33.7 mm, was carried out and the main findings regarding the building surveys undertaken at the end of the test are collected in the following photographic sequence (see Figure 286 to Figure 316).

It is worthwhile to mention that both in-cycle and between-cycle strength degradation started being observed in the response curve of the retrofitted specimen (Figure 220 and Figure 221) for this stage of testing, which is in close correlation with the fact that very extensive damage was seen spreading throughout the structure (including a full-depth/full-width/mid-height horizontal crack in one of the transversal walls – see Figure 292 to Figure 295). As clarified in these photos, such a damage mode was observed in the South-West lateral wall, even if the corresponding South-East one presented a not-fully-developed similar mechanism (see Figure 288).

Figure 286. Crack pattern of transversal and stability walls – Bottom steel angle, East side.

Figure 287. Detail of cracks in the transversal and stability walls – Bottom steel angle, East side.

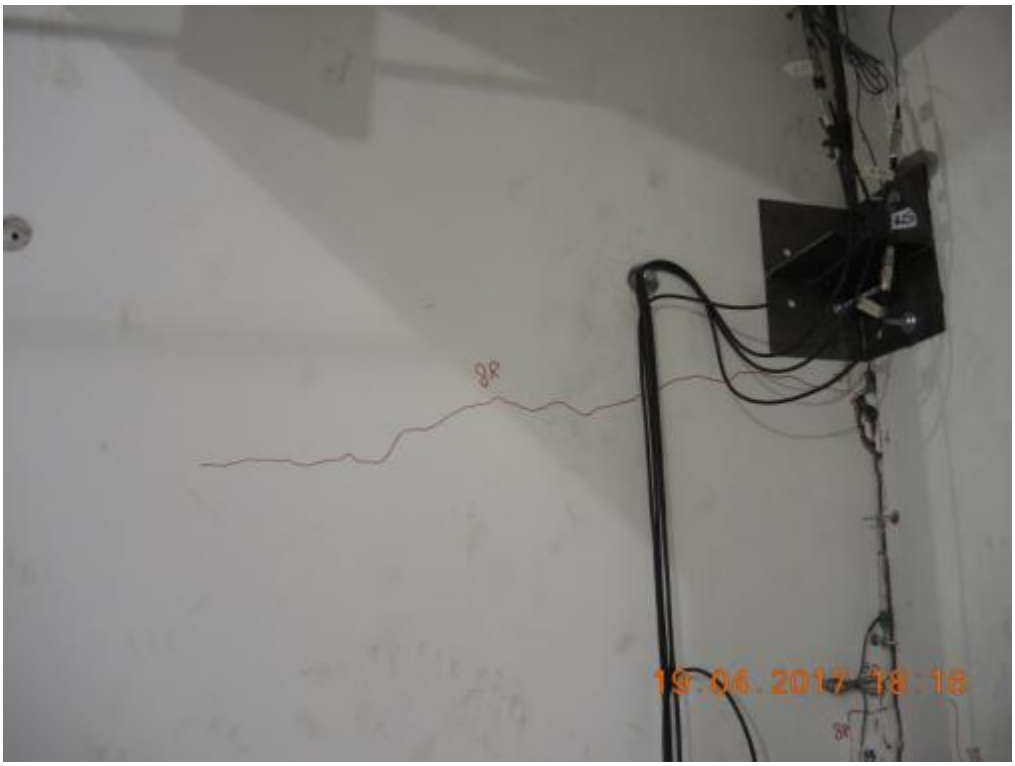

Figure 288. Full-width/mid-height horizontal crack in the transverse wall – Top steel angle, East side.

Figure 289. Detail of concrete crushing at the base of lateral wall W1L1 – East side.

Figure 290. Concrete crushing at the base of lateral wall W1L1 – East side, lateral face.

Figure 291. Damage at the base of lateral wall W1L2 – East side, first floor.

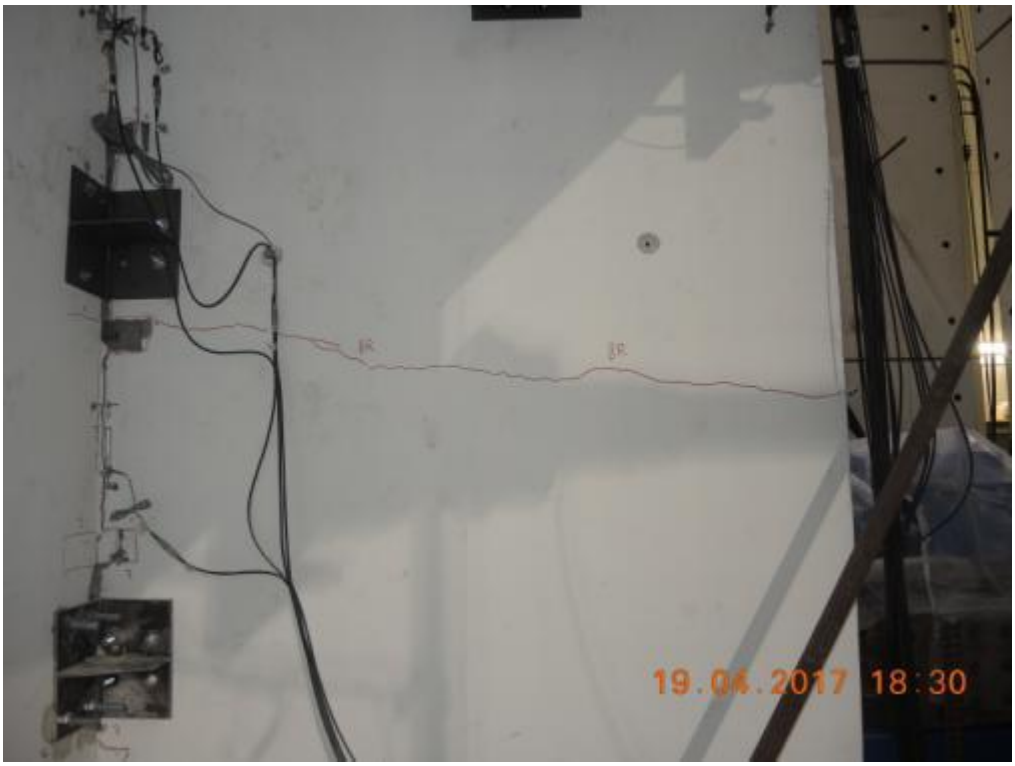

Figure 292. Full-depth/full-width/mid-height horizontal crack in lateral wall W1L2 – West side, North face.

Figure 293. Side view of the full-depth/full-width/mid-height horizontal crack in lateral wall W1L2.

Figure 294. Full-depth/full-width/mid-height horizontal crack in lateral wall W1L2 – West side, South face.

Figure 295. Front view of the full-depth/full-width/mid-height horizontal crack in lateral wall W1L2.

Figure 296. Crack pattern developed in the transversal wall W1L1 – West side, South face, mid-height.

Figure 297. Detail of inclined crack in the transversal wall W1L1 – West side, South face, mid-height.

Figure 298. Detail of inclined crack in the transversal wall W1L1 – West side, South face, base.

Figure 299. Detail of concrete crushing at the base of transversal wall W1L1 – West side, South face.

Figure 300. Formation and propagation of new cracks at the top of lateral wall W1L1 – West side, South face.

Figure 301. Detail of post-tensioned bar at the top of the second-storey stability wall – East side.

Figure 302. Detail of a three-way connection after test – West side, first storey.

Figure 303. Enlarged view of a three-way connection and bent/failed anchor – West side, first storey.

Figure 304. Enlarged view of flexural failure mechanism of a three-way anchor – West side, first storey.

Figure 305. Concrete chipping at the top of lateral wall W1L2 – West side, first storey.

Figure 306. Concrete chipping at the top of the ground-floor stability wall – West side, edge.

Figure 307. Concrete chipping at the top of the ground-floor stability wall – West side, mid-depth.

Figure 308. Detail of the base of lateral wall W1L1 after removal of crushed concrete – West side, South face.

Figure 309. Lateral wall W1L1 after removal of crushed concrete – West side, South face, edge.

Figure 310. Transversal wall W1L1 after removal of crushed concrete – West side, lateral face, edge.

Figure 311. Transversal wall W1L1 after removal of crushed concrete – West side, North face, edge.

Figure 312. Detail of a three-way joint after removal of crushed grout – West side, North face.

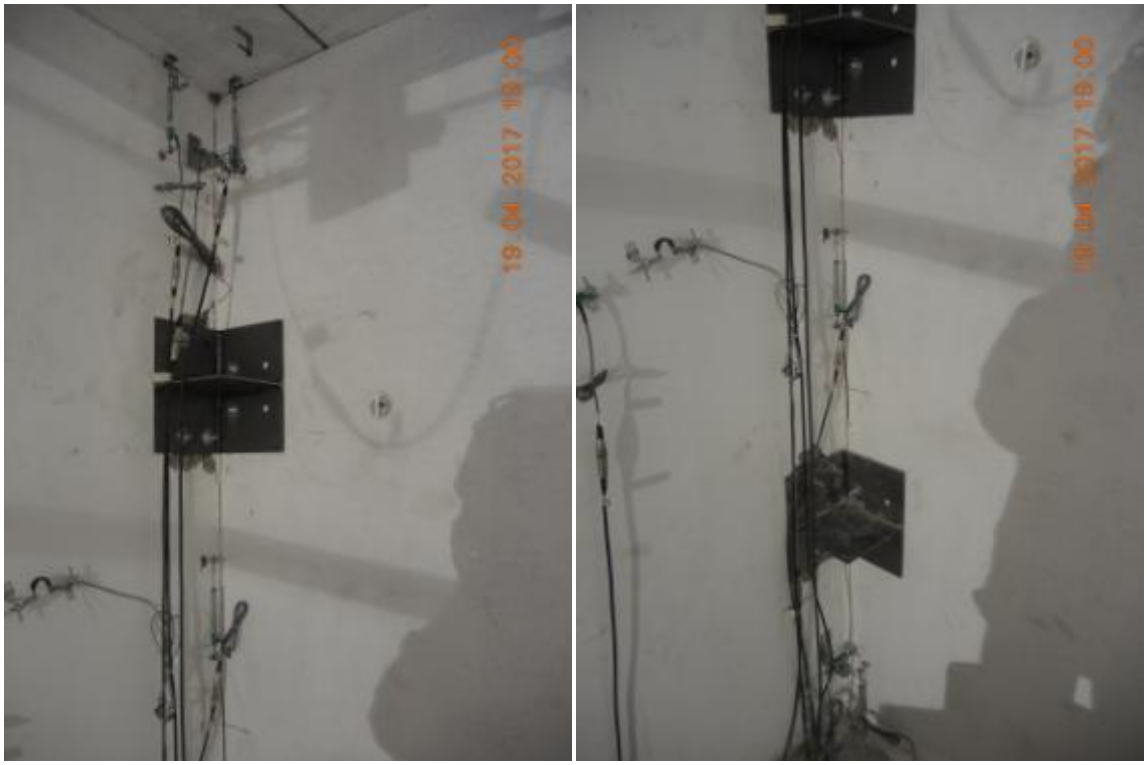

Figure 313. Damage pattern of retrofitted three-way connections – West side, North face, second storey.

Figure 314. Damage pattern of retrofitted three-way connections – East side, North face, second storey.

Figure 315. Chipping of concrete at the top of the second-storey stability wall – East side.

Figure 316. Detail of pre-existing full-depth/full-width/mid-height crack in the second-storey stability wall.

Figure 286 and Figure 287 point out that further cracks formed in the East face of the stability wall close to the bottom steel angle, thus confirming these elements to be part of the resisting mechanism

of the structure, despite the fact that their design was not optimised. The crack pattern at the base of the transversal walls was found to propagate, as presented in Figure 289 to Figure 291. In particular, Figure 289 and Figure 290 show some details of concrete crushing at the base of lateral wall W1L1, which was particularly significant at the corner of the panel. As one may notice by looking at Figure 291, the corresponding/opposite panel underwent extensive damage too. Indeed, damage was found at the base, especially in correspondence to the opposite corner of the panel.

Once the full-depth/full-width/mid-height horizontal crack observed in the South-West ground-floor lateral wall has been examined (Figure 292 to Figure 295), attention can be paid to the other cracks that opened up close to the bottom steel angle installed onto the South-East one. Some details of the inclined cracks developed in the South face of the transversal wall W1L1 are reported in Figure 296 to Figure 299. In this latter photo, concrete crushing at the base of this panel was presented as well. It is worth mentioning that, as far as that wall-element is concerned, new cracks were also observed to take place at the top of it, more precisely on the South face of this panel (i.e. wall W1L1). Figure 300 presents a bottom view of those cracks, which are nonetheless minor.

Because of the very extensive damage spread throughout the retrofitted specimen, in combination to the in-cycle and between-cycle strength degradation presented by its response curves, it was decided to stop this second test run and examine the damage patterns even further before dismantling. Thus, operations such as the removal of crushed concrete at the base of the walls and the removal of grout around the steel connectors of three-way joints were carried out, which in turn implies that the final configuration of the specimen at the end of testing was altered for more accurate inspection.

Details of the lateral wall W1L1 after the removal of crushed concrete are collected in Figure 308 to Figure 311, whereas enlarged views of three-way connections between the stability and transversal walls were provided in Figure 312. As shown therein and also in Figure 302 to Figure 304, this type of joint exhibited a flexural failure mechanism of the steel anchors embedded in the niches between the two lateral wall panels because of the tensile force exerted by the connectors of the stability wall and hence it is confirmed that no dislodgement was found to take place.

Furthermore, Figure 305 to Figure 307 point out another mechanism that was observed at the top of the first-storey stability and transversal walls, which indeed presented chipping of concrete in some zones close to the contact area between them and the bottom of the precast slab panels. As one may see in Figure 315, such a damage mechanism took place in the second-storey walls as well. Despite this type of damage is relatively moderate, it may be indicative of shear force transfer between the horizontal and vertical precast concrete elements of the specimen in its retrofitted scheme.

To conclude the analysis and discussion of the observed crack patterns, it is noteworthy that the pre-existing full-depth/full-width/mid-height crack in the second-storey stability wall was monitored by visual inspections at the end of each stage of testing and also by means of two instruments having a different accuracy (see Figure 316), to check any type of evolution in width and size that in any case did not occur during testing of EUC-BUILD4 specimen in both the as-built and the retrofitted configuration. Figure 316 shows a global view of the latter crack at the end of the two testing sequences.

6.4 Comparison between as-built and retrofitted configurations

As a further aim of this experimental research is to highlight how much of a weakness the original connections are in this type of precast buildings, and also how additional seismic resistance can be readily mobilised by properly connecting their structural elements, the cyclic response curves of the "not-fully-effectively-retrofitted" damaged structure are compared with those of the initial specimen in this section.

More in detail, the total base shear-roof displacement response of EUC-BUILD4 specimen in its as-built and retrofitted configurations are plotted together in Figure 317, whilst Figure 318 and Figure 319 present a similar comparison in terms of storey shear versus inter-storey displacement curve of the first and second floor, respectively.

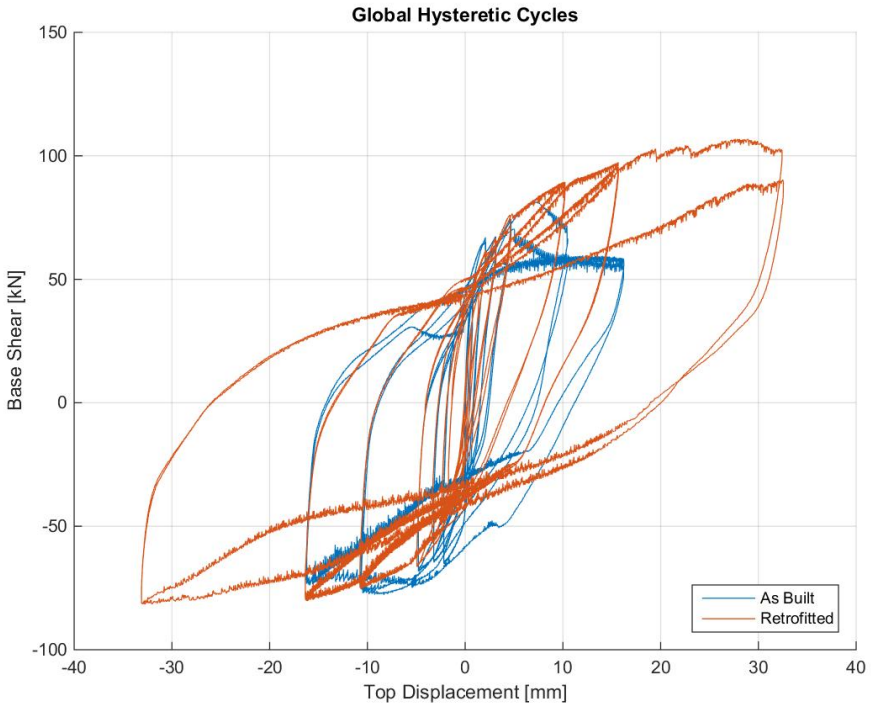

Figure 317. Retrofitted vs. as-built configuration: base shear-top displacement response of EUC-BUILD4.

Apart from the fact that the retrofitted structure was pushed up to a displacement level that doubles the one that had instead taken the as-built specimen to incipient collapse, which is itself a sign of an improved response, cyclic loops were more symmetric and stable. The response is also hardened in character, given that in-cycle and between-cycle strength degradation started being observed only at the last stage of testing. By contrast, post-peak softening was pronounced in the hysteretic response of the original specimen. The comparison also clarifies that, by guaranteeing through steel angles a sturdier wall-slab connection, sliding no longer occurred, ensuing larger energy dissipation and thus equally higher seismic force resistance. This in turn implies that issues regarding the accumulation of displacement residuals may be quite easily overcome, as clearly shown in Figure 319.

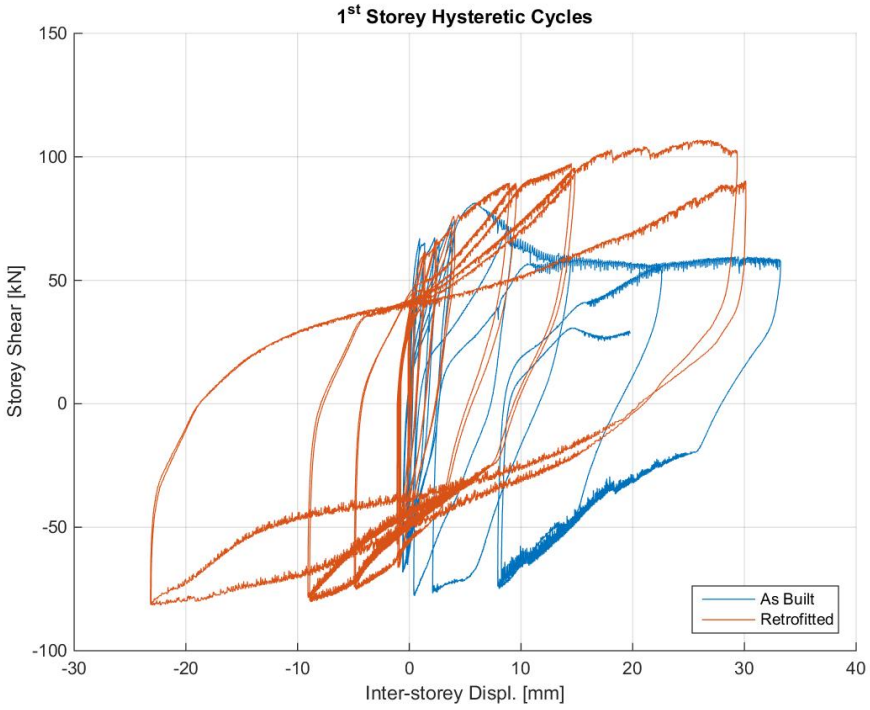

Figure 318. Retrofitted vs. as-built configuration: storey shear vs. inter-storey displacement – First storey.

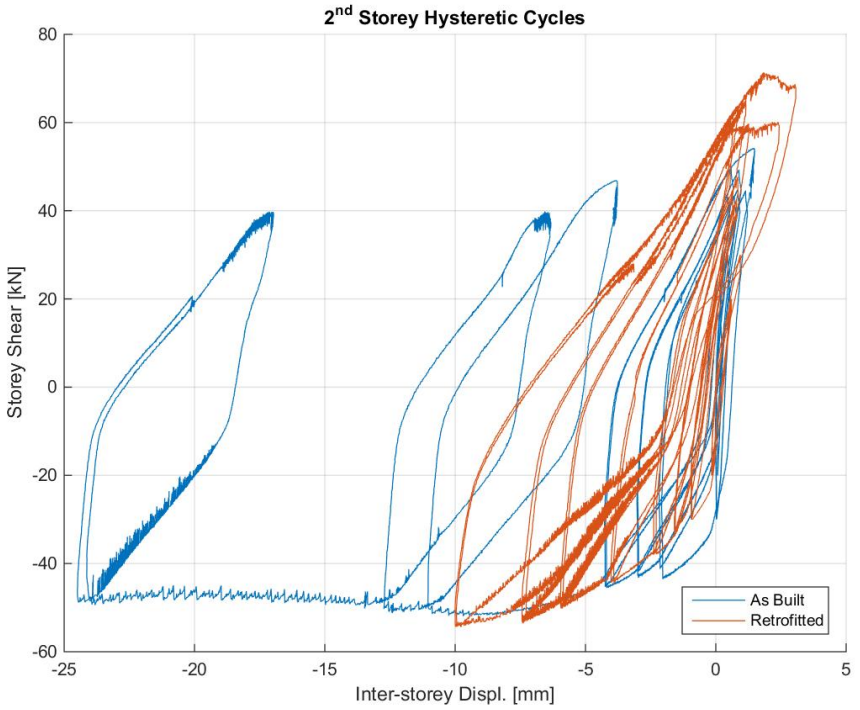

Figure 319. Retrofitted vs. as-built configuration: storey shear vs. inter-storey displacement – Second storey.

6.5 Further considerations

Even though the dataset presented and discussed in the previous sections could be considered itself as fully informative on the observed structural behaviour of EUC-BUILD4 as-built and "retrofitted" specimen, a few key aspects (emerging mainly from the first testing sequence) are recalled in the following, so as to point out specific information that might be beneficial for interested readers and helpful for what concerns the numerical efforts.

As far as the issue of sliding is regarded, some of the obtained response data are plotted below, for further insight into the occurrence of such a phenomenon in terms of structural elements involved as well as exact cycles corresponding to the activation of this mechanism. It is noteworthy that plotted data reported below feature initial offsets.

From the plots below (see Figure 320), it is possible to infer that the upper slab (F2) was sliding on the top of the transversal south walls (W2L1 and W2L2). It is clear that sliding was not symmetric and that the residual displacement was increasing cycle after cycle. Please note that the out-of-plane displacements of the transversal walls were measured relatively to the floor slabs.

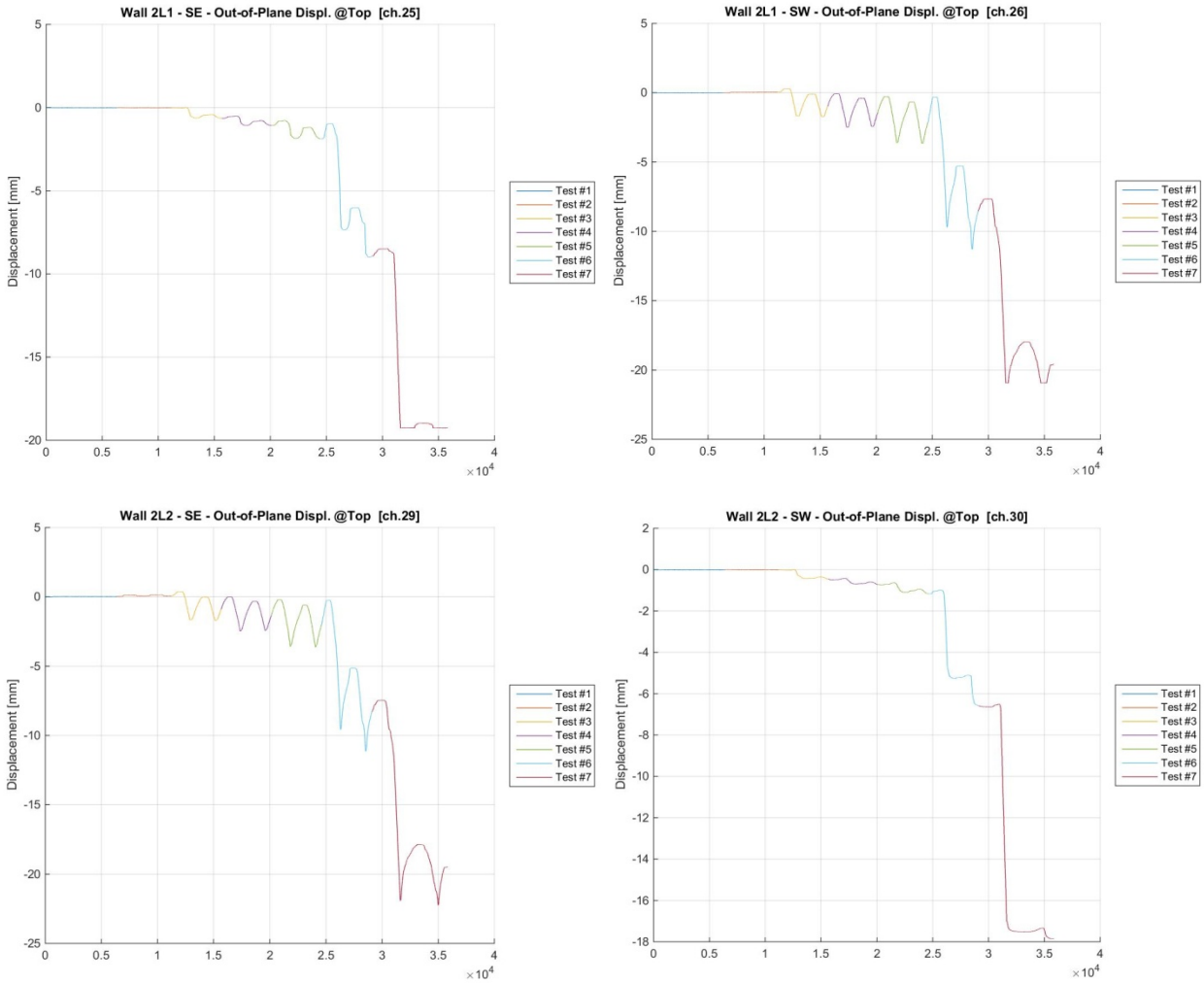

Figure 320. Out-of-plane displacement of transversal walls W2L1 and W2L2 – top, as-built.

It can also be noticed that the north side transversal walls (W2L3 and W2L4) were moving with the slab. As reported in Figure 321, the transducers recorded very small displacements, probably mainly connected with the out-of-plane rocking behaviour of these walls. Although not reported here, the north side transversal walls at the ground floor (W1L3 and W1L4) showed the same behaviour: out-of-plane rocking was taking place and no sliding occurred.

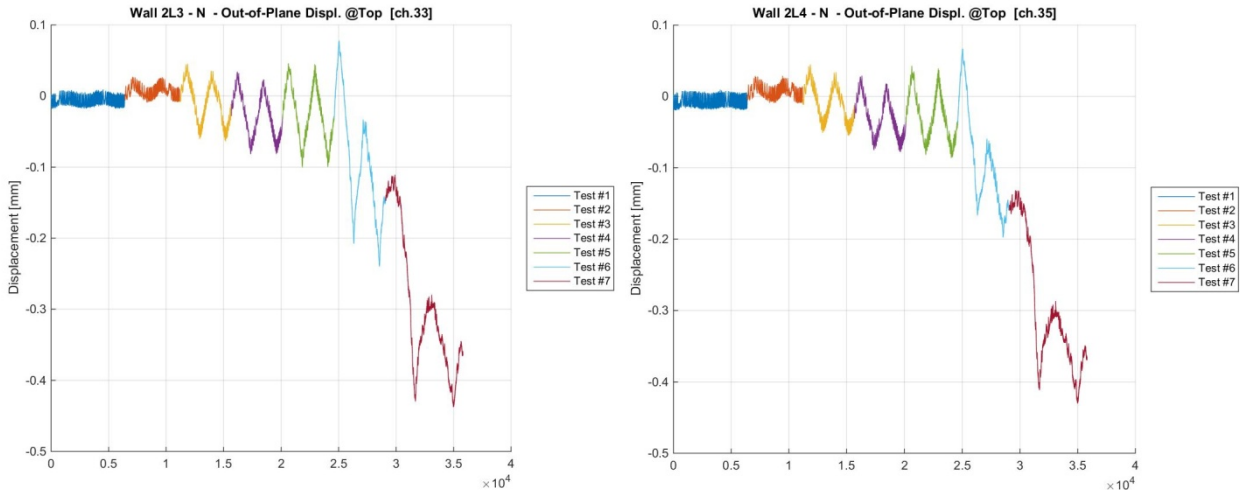

Figure 321. Out-of-plane displacement of transversal walls W2L3 and W2L4 – top, as-built.

At the ground floor, the vertical motion between the stability wall (W1S) and the transversal walls was very limited. During the last two test runs, this displacement increased probably because of the loss of efficiency of the steel connectors. An example of the above-mentioned behaviour is shown in Figure 322. At the upper floor, there was almost no vertical movement between the stability and the transversal walls, as presented in Figure 323.

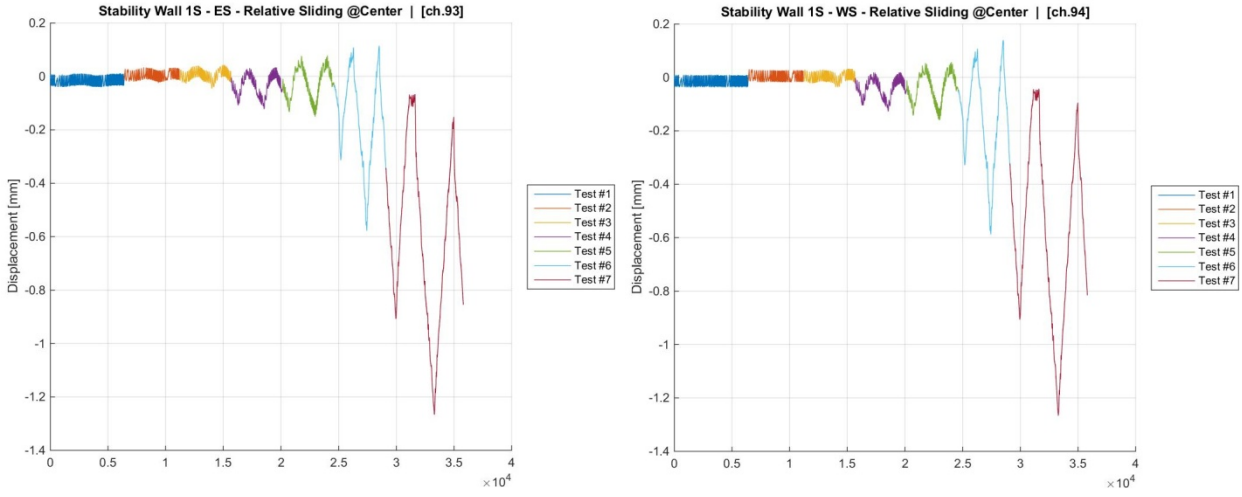

Figure 322. Relative sliding of the ground-floor stability wall – central zone, as-built.

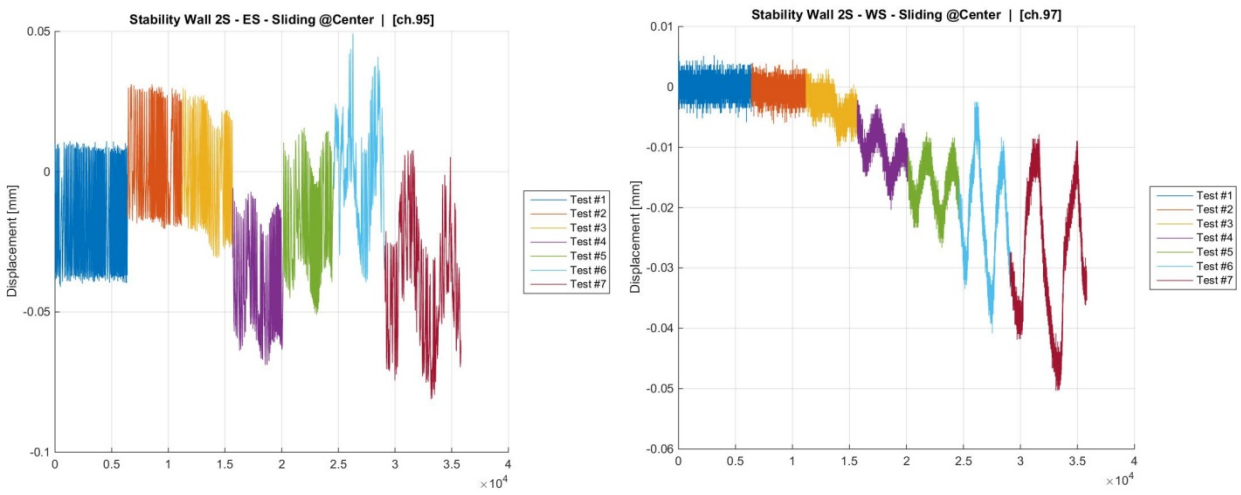

Figure 323. Relative sliding of the second-floor stability wall – central zone, as-built.

The stability wall at the ground floor (W1S) was "not moving" on the foundation, whilst the first slab was sliding on the top of the wall. The same applies to the upper stability wall, as it was resting on the first slab, whilst the second slab was sliding on its top; this type of behaviour appears evident from Figure 324 and Figure 325, which highlight the sliding response of the first-storey and second-storey stability walls, respectively.

The transversal walls at the ground floor (W1L1 and W1L2) were moving out-of-plane, detaching from the stability wall. The mechanism was something like a rotation about its base, and, hence, the crack was larger at the top of the wall and narrower at its base. Representative plots showing such a mechanism are given in Figure 326. Worthwhile to notice is that, at the upper floor, transversal and stability walls were stuck together and the transducers were recording relative deformations more than actual displacements (see Figure 327).

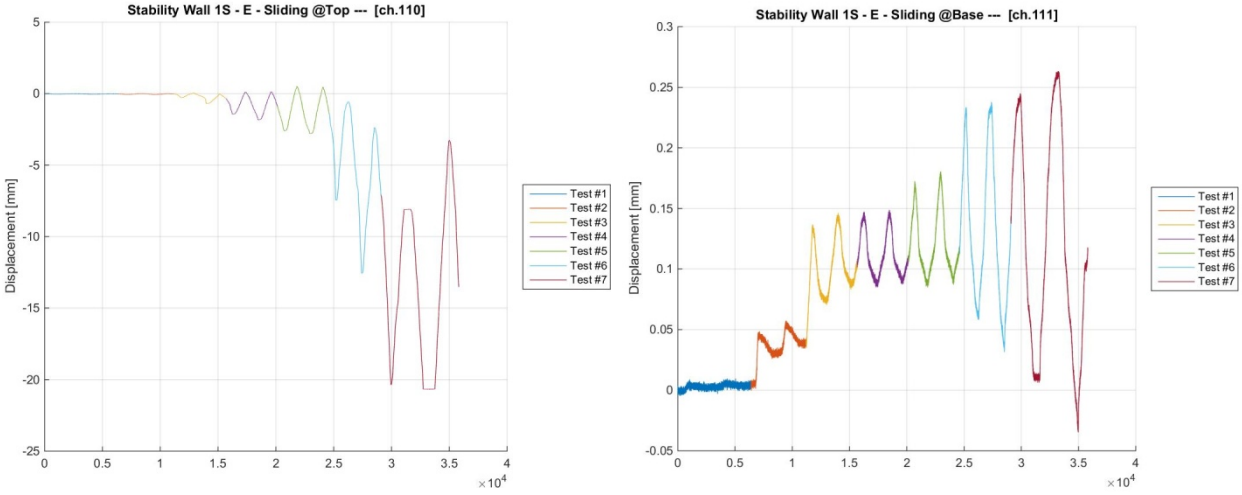

Figure 324. Sliding at the base and top of the ground-floor stability wall (W1S) – as-built specimen.

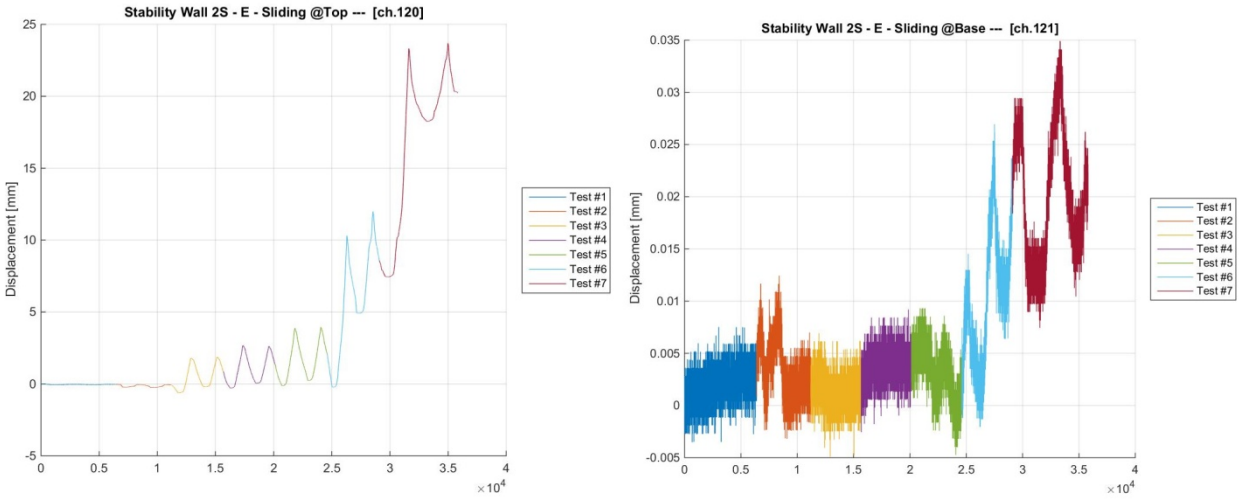

Figure 325. Sliding at the base and top of the second-floor stability wall (W2S) – as-built specimen.

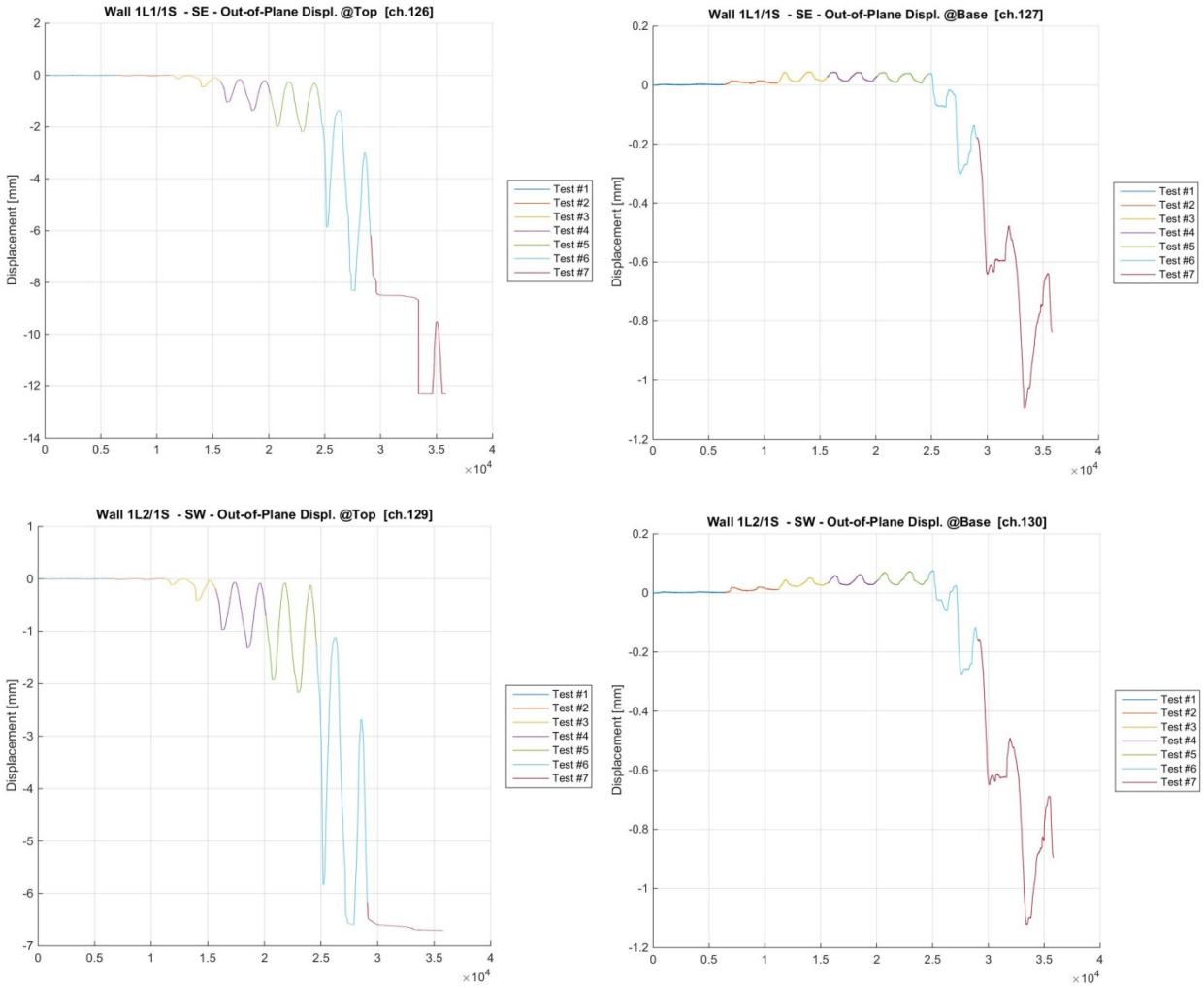

Figure 326. Out-of-plane displacements of lateral walls-to-stability wall – Base and top, first storey.

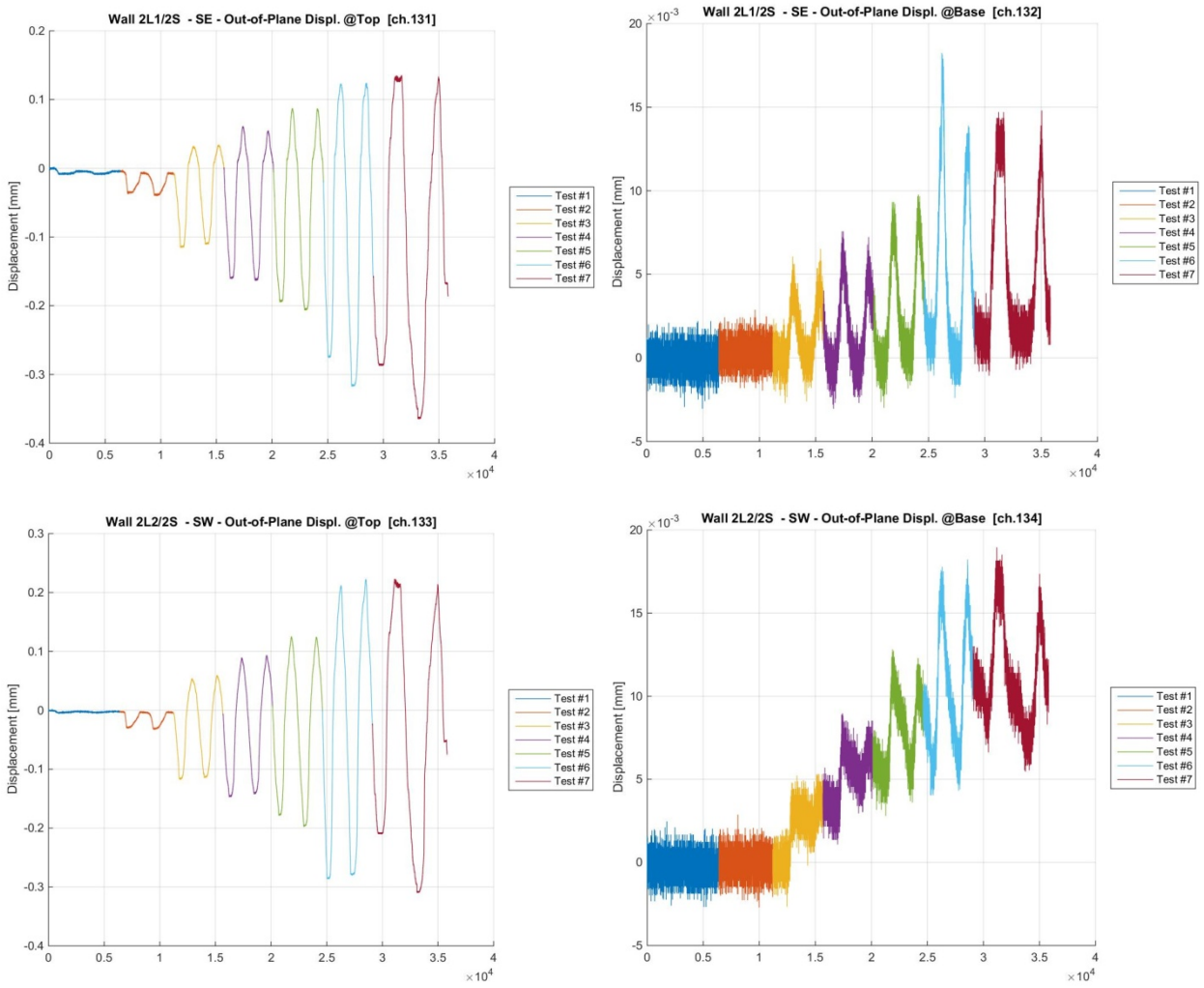

Figure 327. Out-of-plane displacements of lateral walls-to-stability wall – Base and top, second storey.

With respect to the flexural failure mode of the anchors in the first storey transverse walls, it could be evidenced that, during the testing of the original specimen, the connectors of the three-way-joint were deforming while the structure was pulled towards the reaction wall (i.e. positive displacement direction). The transversal walls (W1L1 and W1L2) were moving with the first slab, while the latter was sliding on the top of the stability wall (W1S) resulting in the opening of an approximately 3 cm wide vertical crack between these walls. When pushing the specimen, the crack width was reducing though plastic deformations were accumulated leading to a very wide, triangular, vertical crack with minimum width at the base and maximum at the top. Given that during "the pulling" the hook of the stability wall connector plastically bent the connector placed between the two transverse walls, it is reasonable to infer that the connectors were disengaged in the "pushing phase". On the other hand, because of their shape, the steel connectors work only when under tension, compression stresses are transferred by concrete and mortar.

Whilst Figure 244 presents the deformed shapes of the retrofitted specimen at positive and negative displacement peaks during Test run #8R, a picture of both the North and South faces of the South lateral walls at the ground floor (W1L1 and W1L2) are collected in Figure 328.

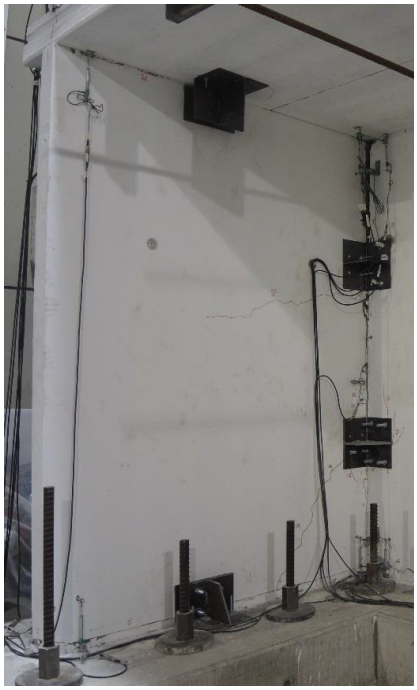

North face of W1L1

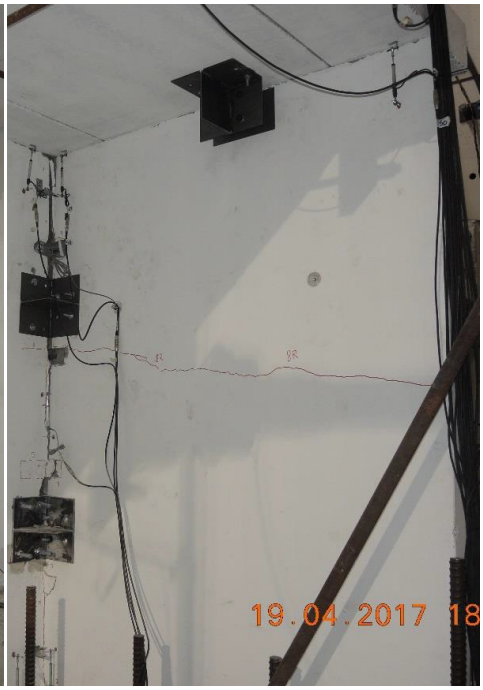

North face of W1L2

South face of W1L2

South face of W1L1

Figure 328. Retrofitted vs. as-built configuration: storey shear vs. inter-storey displacement – Second storey.

The precise time-step corresponding to the formation of these cracks (Figure 328) is obviously very hard to determine, also because safety precautions impose that visual inspection of the structure can be carried out only at the end of each test run. In any case, it is believed that the cracks on the North face of the walls formed when the specimen was displaced towards the reaction wall, which means positive direction. By contrast, the cracks on the South faces should have formed most likely during a negative displacement.

The following sketch (Figure 329) shows the deformed shape corresponding to the fifth test run on the "retrofitted" specimen, indicating what can be some of the likeliest sources of energy dissipation (i.e. cracking, sliding and rocking).

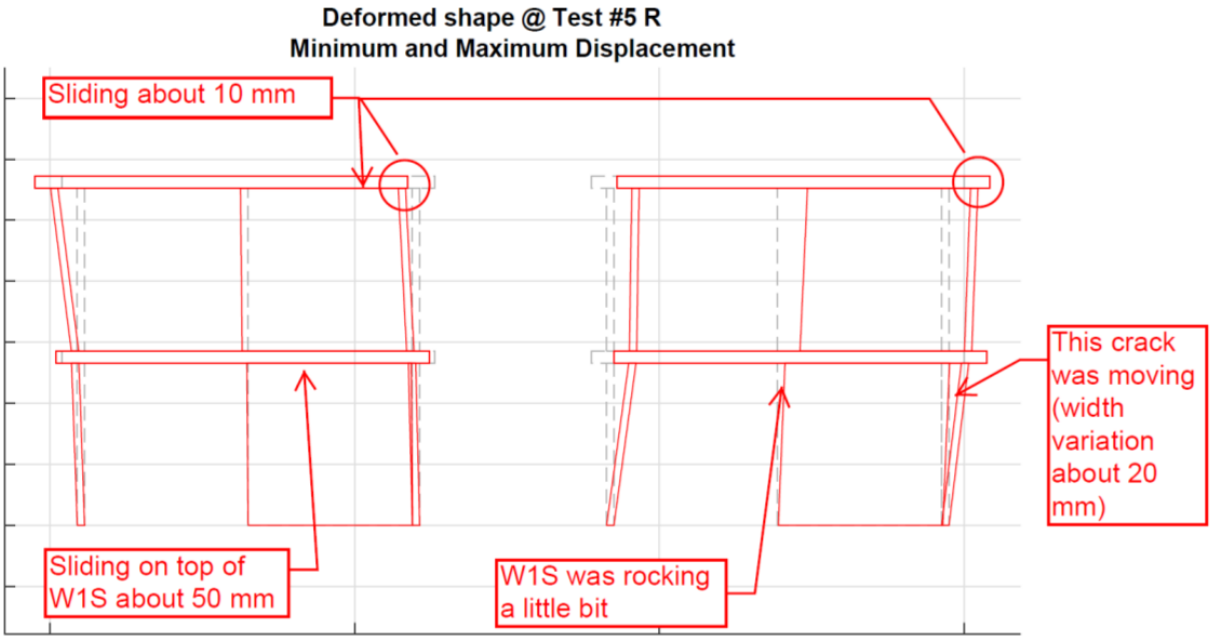

Figure 329. Retrofitted vs. as-built configuration: storey shear vs. inter-storey displacement – Second storey.

Moreover, the installed steel restrainers did not have grouted connectors, hence, relative movement between concrete elements induced small movements between the steel restrainers and the concrete underneath them. Most likely, this is another possible source of frictional energy dissipation, though probably very limited. Photographs collected in previous sections also show that a number of cracks formed across the concrete walls, mainly close to the steel restrainers installed on the ground-floor-South transverse walls (W1L1 and W1L2). The development of such cracks is another possible, and this time perhaps more meaningful (with respect to that indicated in the sentence above), source of energy dissipation.

7 Dismantling of EUC-BUILD4 specimen

A photographic sequence of the main phases related to the dismantling of EUC-BUILD4 specimen is provided in the following, with a view to further highlight some of the key aspects related to the observed damage after the execution of the mono-directional pseudostatic cyclic testing sequence. The "retrofitted" building was inspected during the dismounting of the experimental setup for unidirectional testing, and several photos were taken of the "naked" specimen. Particular care was, of course, paid to survey the zones that were mainly affected by cyclic inelastic testing up to a top displacement of 33.7 mm. Figure 330 to Figure 370 are presented to summarise the prevailing observations collected.

Whilst dismantling the test specimen, the flooring system composed of hollow core slab panels and concrete topping was carefully lifted without disassemblage of precast elements and concrete screed on top of them. As shown in Figure 330 to Figure 333, temporary steel diagonal members (the same used in the erection of the specimen) were first installed and then it was indeed possible to pull the first floor up from the precast walls underneath. The second-storey stability wall was dismantled, by removing the grout in the niches and cutting the hooked anchors embedded into them. Use was then made of a similar approach for dismantling the transversal walls, as reported in the photos collected in Figure 335 to Figure 340. As expected from the damage patterns of the two testing sequences, no particular considerations can be withdrawn, given that both anchors and panel reinforcement were actually still fully intact.

Figure 330. Uplift of second-storey flooring system without disassemblage of screed and precast panels.

Figure 331. Detail of props for the second-storey stability wall and transversal walls.

Figure 332. Detail of fabric felt underneath the second-floor slab – Transversal walls, North side.

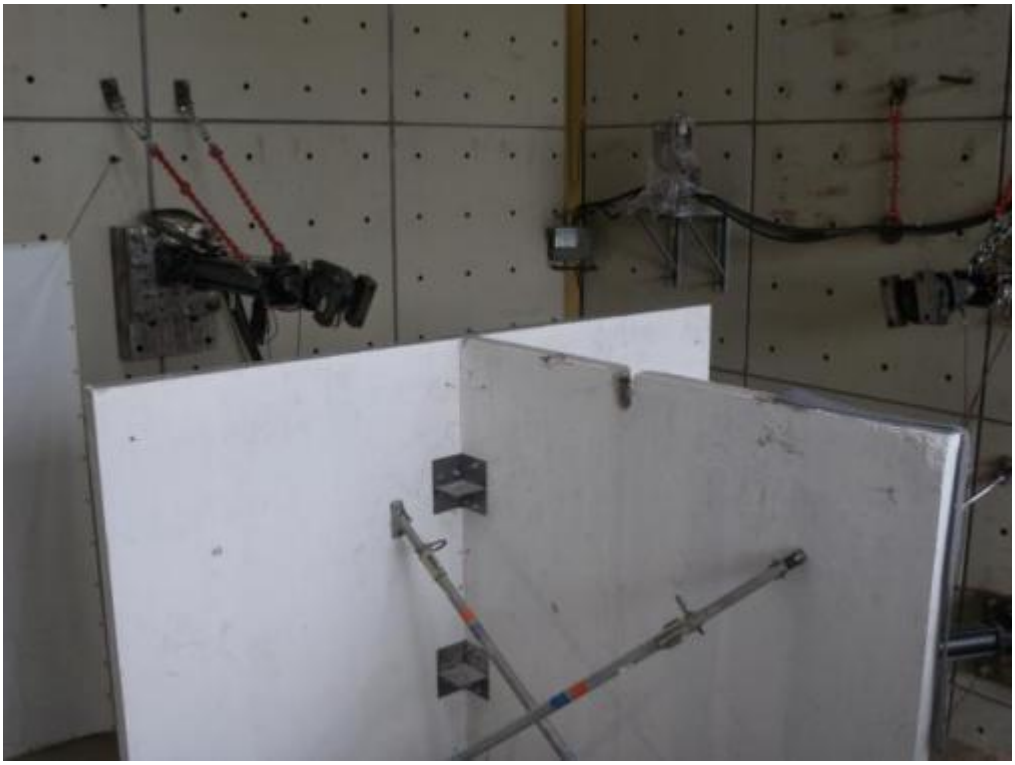

Figure 333. Detail of fabric felt underneath the second-floor slab – Stability wall, North side.

Figure 334. Detail of panel reinforcement in one of the second-storey transversal walls.

Figure 335. Detail of mortar in one of the niches for two-way panel-to-panel connection – Second-storey.

Figure 336. Transversal walls before dismantling – Second storey, South side.

Figure 337. Detail of a three-way joint between second-storey walls – Anchors and mortar.

Figure 338. Detail of anchors and grout in a three-way connection after dismantling of the stability wall.

Figure 339. Enlarged view of a three-way connection after dismantling of the stability wall – Second storey.

Figure 340. Detail of grout and wall panels after dismantling of steel angles – Second-storey walls.

Dismantling of the first storey started with the uplift of the flooring system that was carried out like before, without ruining the concrete topping and separating the slab panels apart. An example of the uplift process is shown in Figure 341. Details of both fabric felts underneath the first-floor slab and cut rebars in the stability wall are reported in Figure 342 to Figure 344. As far as dismantling of the ground-floor walls is concerned, the process started with the North transversal walls. Figure 345 to Figure 349 present the main steps also including a photo of the four intact anchors embedded in the niches of the North-sided transversal walls (Figure 346). As shown in Figure 350 to Figure 359, bolts were screwed-out and steel clip angles were disassembled so as to permit technicians to uplift the stability wall. Enlarged views of permanently-bent connectors before dismantling of wall panels are collected in Figure 351 to Figure 353, whereas details of the damage pattern in correspondence to the steel angles are given in Figure 354 to Figure 359.

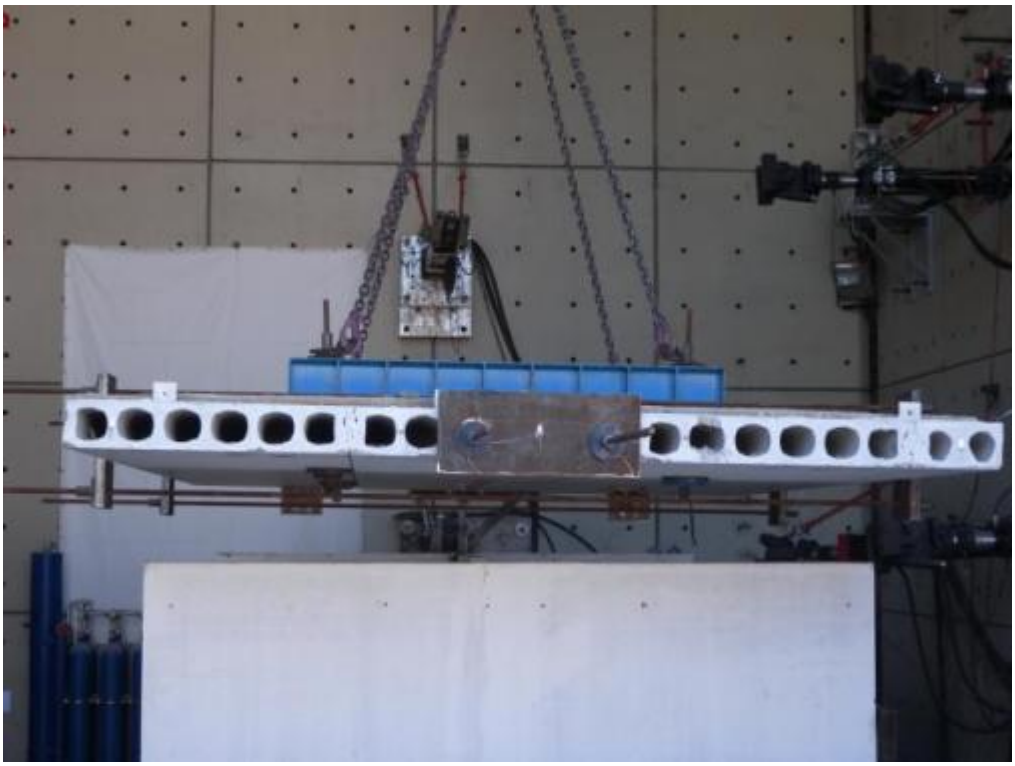

Figure 341. Uplift of first-storey flooring system without disassembling concrete screed and precast panels.

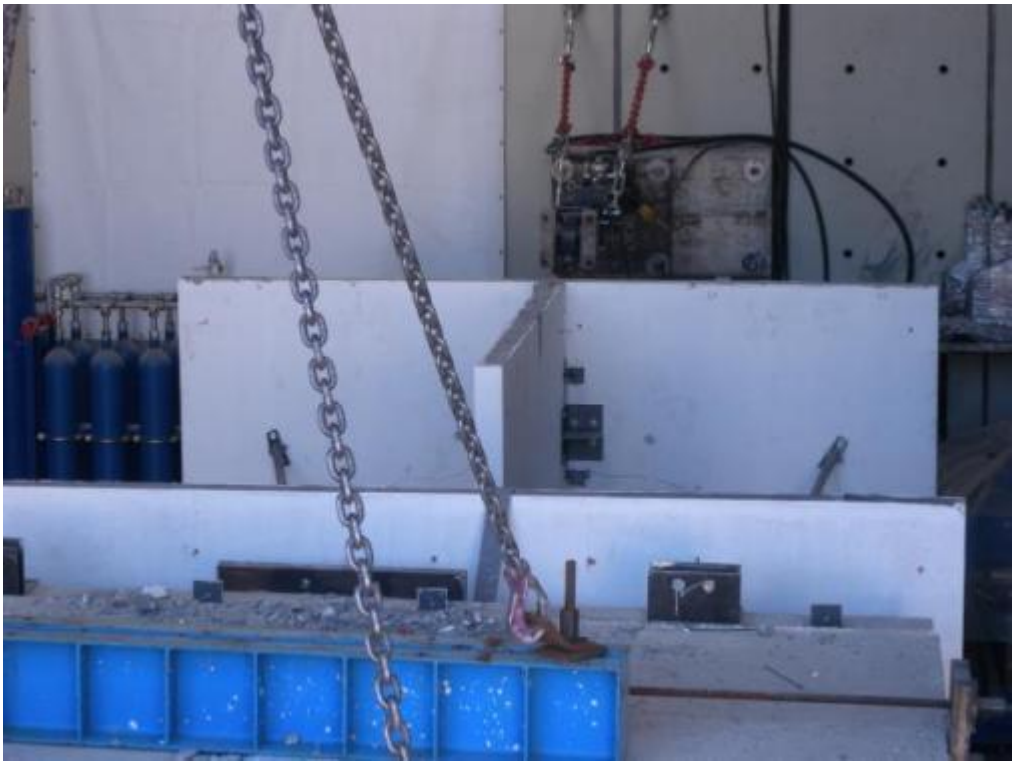

Figure 342. Fabric felts underneath the first-floor slab after completing its uplifting.

Figure 343. Detail of fabric felt underneath the first-floor slab – Stability wall, South side.

Figure 344. Detail of cut rebars in the ground-floor stability.

Figure 345. Detail of hook reinforcement after removal of grout around it – Lateral walls, first storey.

Figure 346. Detail of the four anchors for panel-to-panel connections – Lateral walls, first storey.

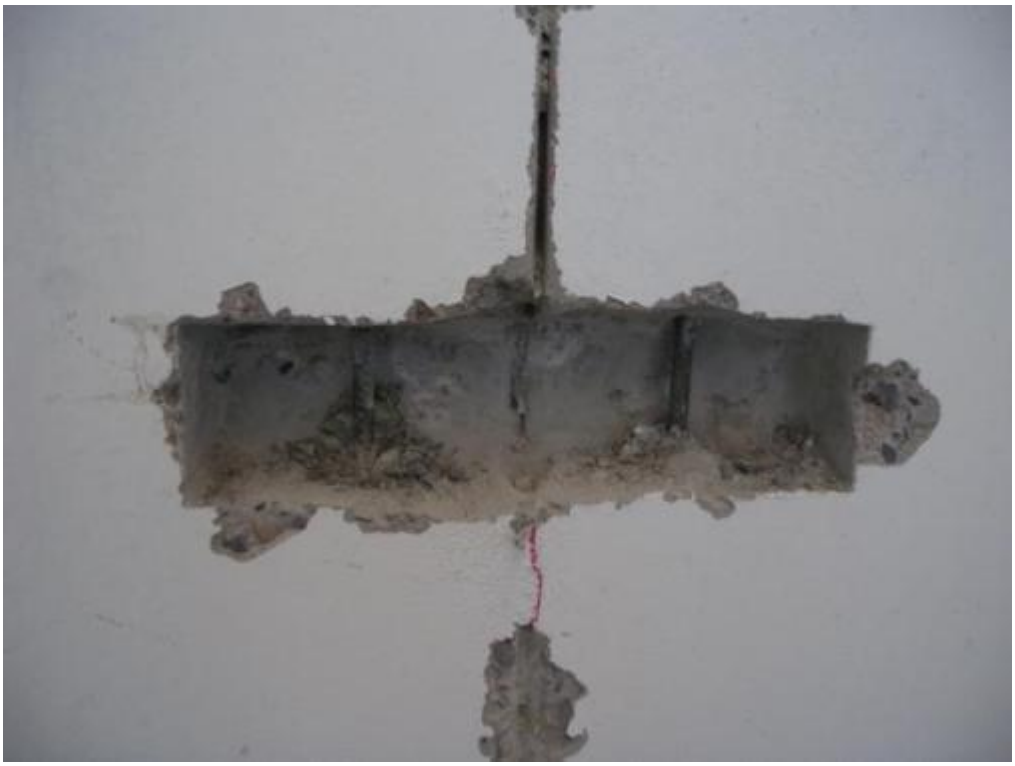

Figure 347. Panel reinforcement after removal of the hooked anchor – Lateral walls, first storey.

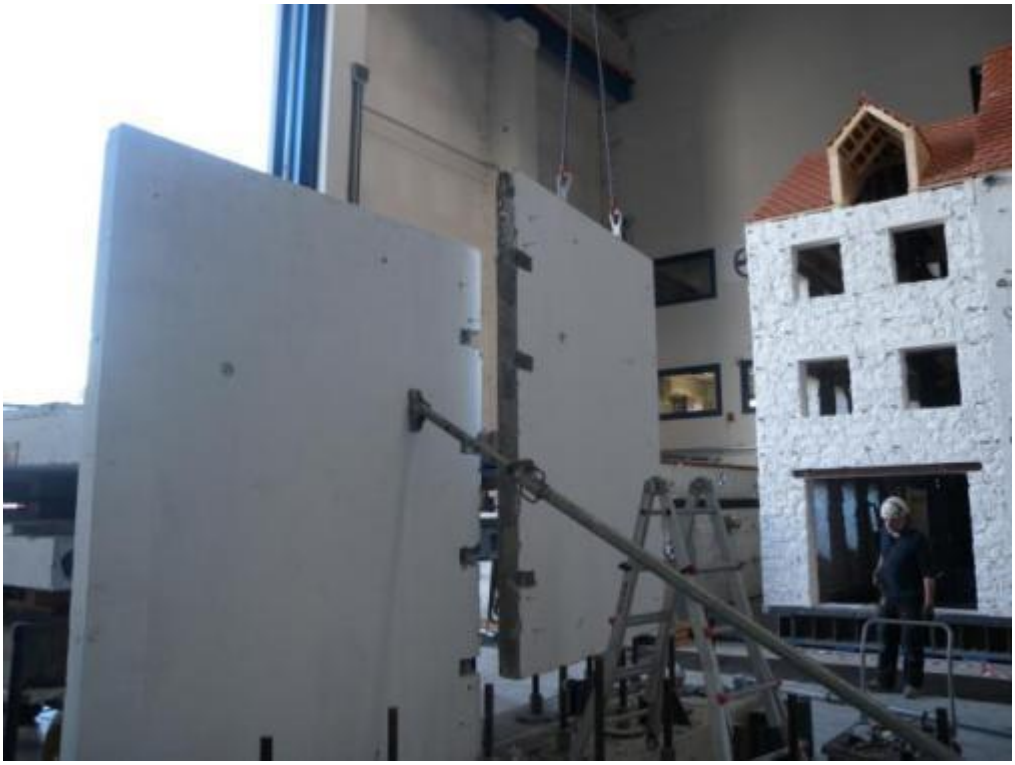

Figure 348. Uplifting of one of the ground-floor transversal walls – North side.

Figure 349. Detail of longitudinal rebar in one of the transversal walls – First storey, North side.

Figure 350. Ground-floor stability wall and corresponding lateral wall panel before dismantling of clip angles.

Figure 351. Detail of hooks and grout in a panel niche before dismounting of screwed steel angles.

Figure 352. Enlarged view of bent hook reinforcement before dismantling of wall panels – First storey.

Figure 353. Removal of screwed clip angles and detail of failed connector – First storey, South side.

Figure 354. Uplift of dismantled ground-floor stability wall panel.

Figure 355. Ground-floor stability wall panel – Detail of damage at the base, South edge/corner.

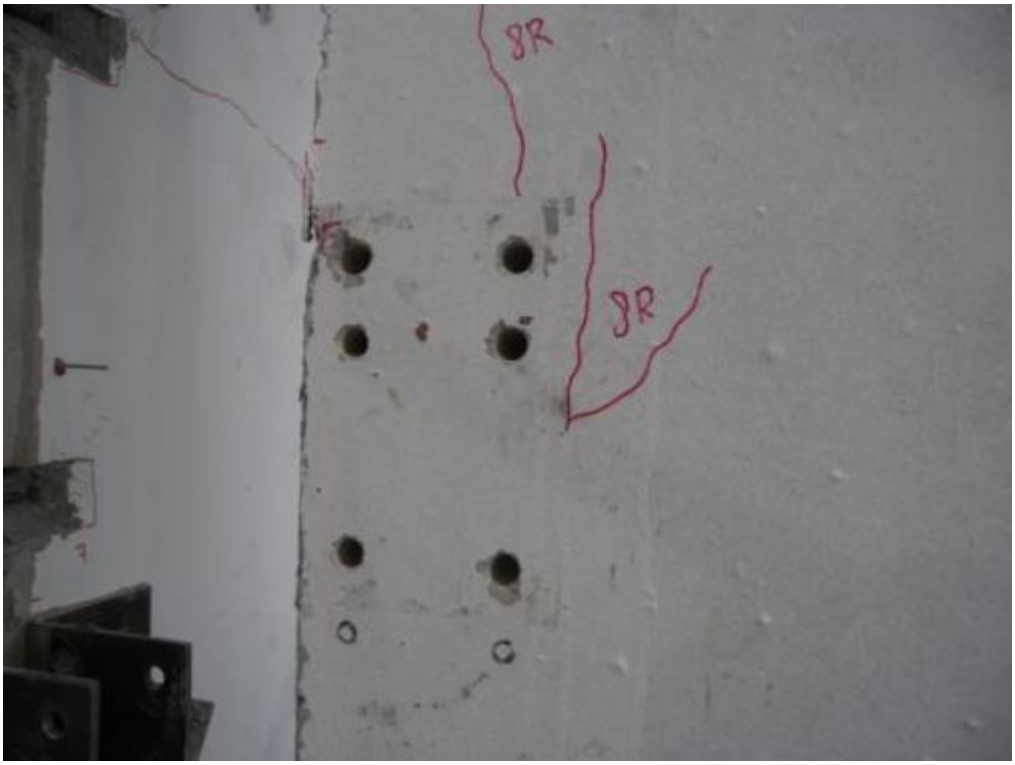

Figure 356. Ground-floor stability wall panel – Detail of cracks at approximately mid-height, South edge.

Figure 357. Detail of ground-floor stability wall panel after dismantling of steel clip angles.

Figure 358. Ground-floor stability wall panel – Detail of cut hooked anchors and chipping of panel concrete.

Figure 359. Damage pattern of the first-floor stability wall after dismantling of connections and setup.

As a result of this, it was possible to adamantly inspect the damaged anchors embedded in the South transversal walls of the first storey. A few photos of them are collected in Figure 360 to Figure 363,

and corroborate previous considerations regarding their failure mechanism. As also shown in Figure 370, permanent bending of them was caused by the orthogonal connectors embedded in the stability wall. The South transversal walls were finally dismantled as presented in Figure 364 to Figure 366, which also highlight the damage pattern at mid-height and close to the steel angles. Other examples of crack patterns produced by those clips are collected in Figure 368 and Figure 369. Noteworthy is that panel reinforcement did not exhibit any sign of damage (see for instance Figure 367).

Figure 360. Detail of flexural failure mechanism of a hooked connector – Below the bottom down clip.

Figure 361. Detail of flexural failure mechanism of a hooked connector – Above the bottom down clip.

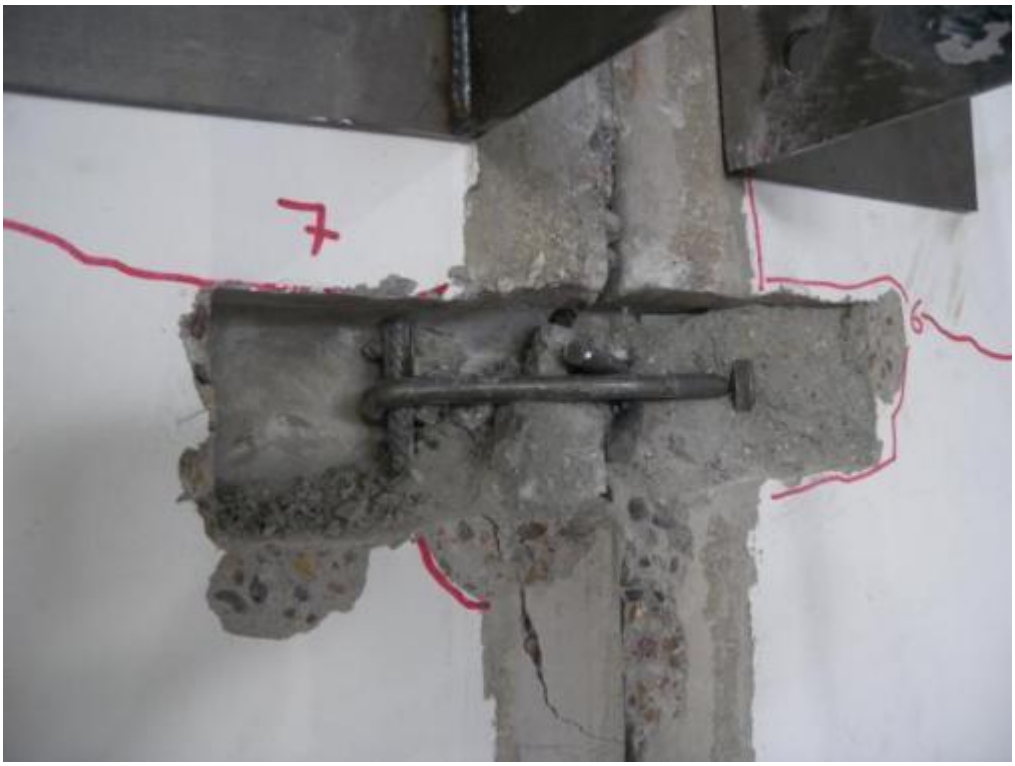

Figure 362. Detail of flexural failure mechanism of a hooked connector – Below the top clip.

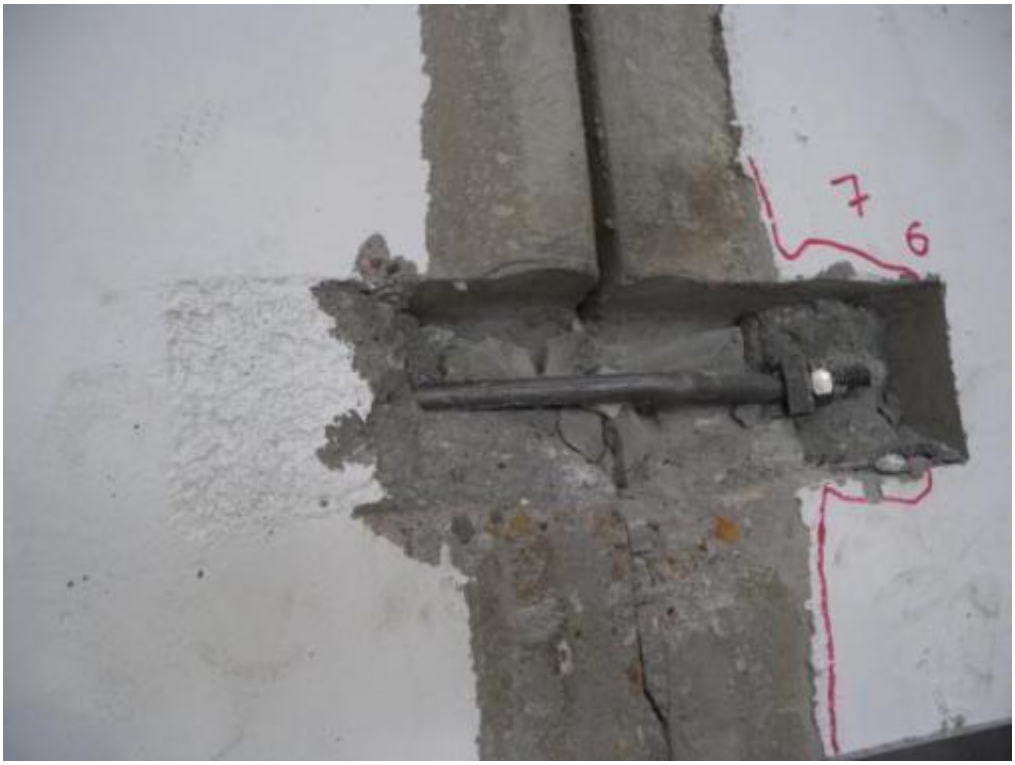

Figure 363. Detail of flexural failure mechanism of a hooked connector – Above the top clip.

Figure 364. Global view of South-sided transversal walls during their dismantling – First storey.

Figure 365. Removal of screwed clip angles and damage/crack pattern in the transversal wall panels.

Figure 366. Detail of panel reinforcement and top/bottom niches for panel-to-panel joint – First storey.

Figure 367. Detail of panel reinforcement passing through the niche of a panel-to-panel connection.

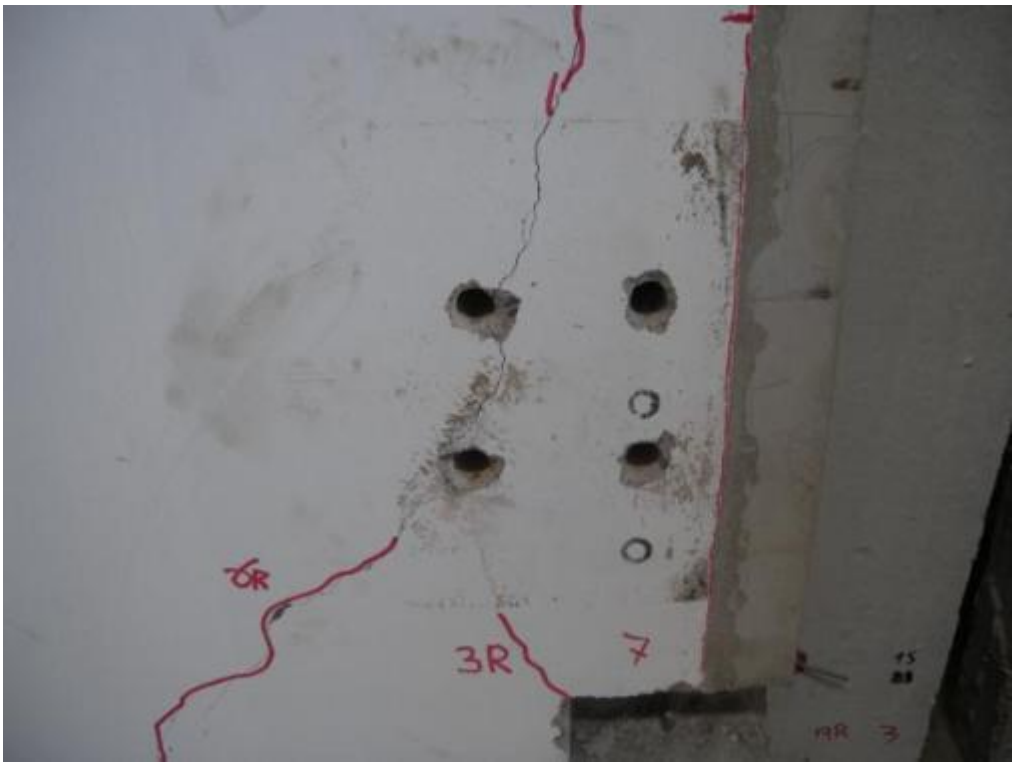

Figure 368. Detail of crack pattern after dismantling of steel angles.

Figure 369. Global and enlarged view of cracks beneath the steel plate of a clip angle.

Figure 370. Permanent bending of transversal connectors in each of the four three-way joints.

Once the operations of dismantling had been completed, the precast wall-panels were surveyed with a view to inspect construction details. A photographic sequence of this process is reported hereafter (i.e. Figure 371 to Figure 375). As shown in Figure 371, portions of concrete were demolished so as to examine the arrangement of reinforcing rebars close to the niches. Figure 372 presents a detail of 50 mm spacers that were used for the positioning of the steel net before concrete grouting, whereas Figure 373 shows the steel net itself and the position of the 10 mm diameter bar for the arrangement of the steel connectors. The steel mesh consisted of 5 mm diameter rebars, and the spacing between the horizontal and vertical bars was 25 and 18 cm, respectively, as can be gathered from Figure 374 and Figure 375. It is also worth noting that the steel net was not placed in the middle of the panel, as indicated by the fact that the embedment depth of the steel connectors was 40 mm.

Figure 371. Removal of concrete close to a panel niche.

Figure 372. Detail of a 50mm spacer for the arrangement of the steel net.

Figure 373. Detail of steel net and adjacent 10 mm diameter bar for the steel connectors.

Figure 374. Spacing between horizontal bars of the steel net.

Figure 375. Spacing between vertical bars of the steel net.

8 Additional remarks

The observations coming from the dismantling of the specimen, together with the set of damage patterns collected after each test run, confirmed that the response of the three-way connection between the stability and lateral walls is of paramount importance, since its cyclic behaviour affected the overall response of the test specimen at ultimate condition (i.e. max storey drifts of 0.50-1.15%). As such, further component tests aimed at testing this type of wet connections in cyclic pseudostatic fashion were planned and are the focus of the on-going research regarding characterisation/companion tests for EUC-BUILD5 specimen. Figure 376 shows a drawing of the experimental setup that will be adopted for testing them by applying cyclic loads through a displacement-controlled actuator. The specimen consists of two concrete blocks that resemble details of joint arrangement as well as typical concrete thickness of these precast panels.

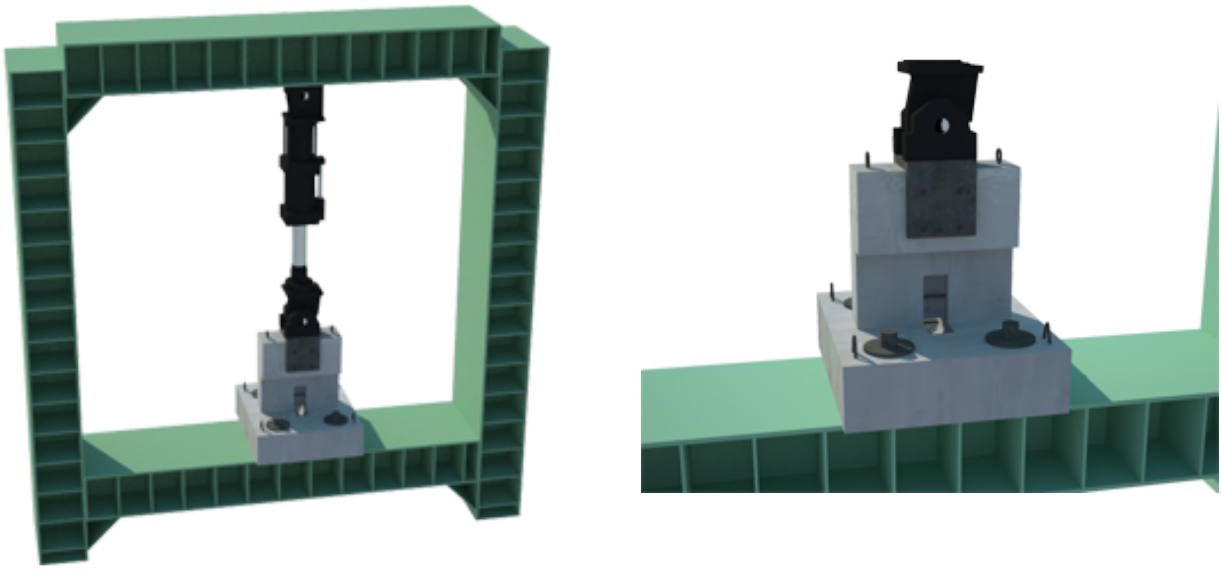

Figure 376. Testing apparatus for cyclic testing of three-way panel connections.

For the sake of completeness, it is herein noted also that an additional series of tests on fabric felts has also now been conceived, following the outcomes of this test series. Indeed, notwithstanding the fact that the set of triplet tests already performed and reported in this study had provided useful data on the frictional force transfer that can be exerted by this type of material, it was felt that it would be beneficial to try to obtain cyclic response curves that might capture any type of eventual in-cycle and between-cycle strength degradation of this response parameter. Therefore, a material characterisation cyclic test setup of the type shown in Figure 377 has been designed and scheduled to be undertaken as part of the characterisation/companion tests for EUC-BUILD5 specimen.

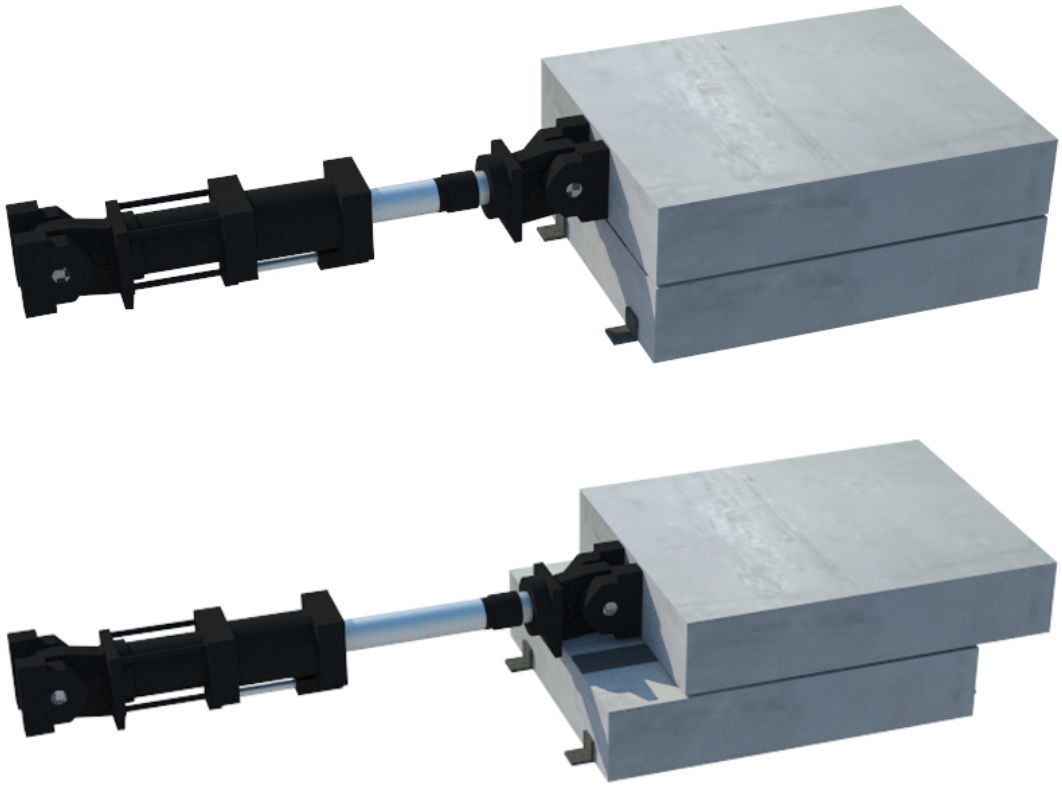

Figure 377. Setup for friction testing of felt material in cyclic fashion.

9 References

1. Arup [2017] 229746_031_NOT2008_Rev0.05_Issue EUC-BUILD-4 Prototype building description
2. Arup [2017] 229746_031.0_DRW2007_Rev0.05_Issue_EUC-BUILD-4_5 SWb Specimen drawings